ABSTRACT

Title of Dissertation:	CHARACTERIZATION OF SEPTIC SYSTEM WASTEWATER AND MUNICIPAL SOLID WASTE LANDFILL LEACHATE
	Katherine Robbins Martin, Doctor of Philosophy, 2021
Dissertation directed by:	Associate Professor, Dr. Michael Gonsior, University of Maryland Center for Environmental Science

The growing United States population means increasing waste production and a corresponding increase in the use and release of contaminants of emerging concern (CECs). The increasing volume and changing composition of waste poses new challenges for waste management and the protection of ecosystem, surface water, and groundwater resources. In the U.S., most domestic solid waste is disposed of in landfills, and domestic wastewater is treated by wastewater treatment plants (WWTPs) or onsite wastewater treatment systems (OWTSs). While OWTSs, the majority of which are conventional septic systems, account for the minority of wastewater treatment in the U.S., they present a significant pollution risk because they are not subject to the same treatment level or discharge regulatory standards as municipal WWTPs. Landfill leachate is also an important source of environmental contamination because most existing landfills in the U.S. are closed, unlined landfills

that lack engineered systems to enhance refuse degradation or collect leachate. To mitigate the pollution risks of these effluents, it is important to understand initial wastewater composition and how to identify and trace environmental contamination.

In this study, I generated background molecular composition data for landfill leachate and domestic wastewater effluents and developed chemical tracers for septic system impacted streams. I used ultrahigh resolution, Fourier-transform ion cyclotron resonance mass spectrometry, to molecularly characterize the dissolved organic matter (DOM) of septic system wastewater and septic system wastewater-impacted surface waters. I also analyzed traditional water quality markers such as CECs, chloride, nitrate isotopic signatures, and nutrients. Additionally, I molecularly characterized landfill leachate DOM and analyzed similar chemical markers to those used in the septic system study to understand composition.

The goals in the main septic system study were to better understand the composition and natural processing of septic system wastewater and to develop new chemical wastewater tracers while assessing traditionally used tracers. The landfill leachate study addressed the lack of nontargeted leachate composition data. Determining initial molecular composition is necessary to understand the consequences of discharge to the environment and to design leachate treatments.

CHARACTERIZATION OF SEPTIC SYSTEM WASTEWATER AND MUNICIPAL SOLID WASTE LANDFILL LEACHATE

by

Katherine Robbins Martin

Dissertation submitted to the Faculty of the Graduate School of the
University of Maryland, College Park, in partial fulfillment
of the requirements for the degree of
Doctor of Philosophy
2021

Advisory Committee:
Associate Professor Michael Gonsior, Chair
University of Maryland Center for Environmental Science

Associate Professor Lora Harris
University of Maryland Center for Environmental Science

Associate Research Professor Andrew Heyes
University of Maryland Center for Environmental Science

Senior Scientist Dr. Thomas Jordan
Smithsonian Environmental Research Center

Professor Philippe Schmitt-Kopplin
Helmholtz Zentrum München

https://doi.org/10.1039/D1EW00020A

Acknowledgements

Thank you so much to Dr. Michael Gonsior for taking me on as a graduate student, for always encouraging me to pursue my own questions, and for reigning in my ideas when necessary. Thank you for being so patient, understanding, and kind. I am so appreciative of your guidance in my development as a scientist. I am also deeply thankful to my committee members. Thank you to Dr. Andrew Heyes for encouraging me to attend grad school in the first place and for your mentorship as I have gone from an REU intern to a Ph.D. student. Thank you to Dr. Lora Harris for your support and scientific and field guidance and for sharing your statistical modelling knowledge. Thank you to Dr. Philippe Schmitt-Kopplin for sharing your analytical expertise and your assistance with data interpretation. Thank you also to Dr. Thomas Jordan. Your guidance has greatly improved my understanding of nutrient cycling. I am also grateful to Matthew Cumers, Steve Kullen, Dr. David Brownlee, and the Calvert County Department of Planning Zoning for septic system map data and assistance with study design.

Thank you to my wonderful labmates over the years—Jenna, Leanne, Alec, Mathapelo, Maddy, and Alex—for your support, question answering, lab assistance, and friendship. Thank you also to members of the Harris Lab—Mindy, Erin R., Zach, Isabel, and Kevin—for assistance with fieldwork and sample preparation. I would also like to thank my fellow CBL students in general, especially Erin C., Katie, and Alex, for being great housemates and friends. To Devin, Coco, and Kieres, thank you for all the laughs, adventures in NYC, and mystery solving, and to Sierra, for being

an incredible friend through it all. Thanks to the best cat, Domino Fuzzy-Crystal. I would also like to thank the members of the Southern Maryland Rock and Mineral Club for being a great source of camaraderie during my time here. Finally, I would like to thank Kevin for his unwavering encouragement and support. Also, a huge thank you to my family for always being there for me and pushing me forward.

I am very thankful for the financial support that made this work, my graduate studies, and presentation of this work at academic conferences, possible: Maryland Sea Grant's Research Fellowship and the University System of Maryland Dean's Fellowship, the Menzer Family and the MEES graduate program Reid Evans Menzer Research Fellowship, the Geological Society of America On To the Future Program, and Travel Awards from the CBL Graduate Education Committee.

Table of Contents

List of Tables

List of Figures

List of Abbreviations

AA	ammonium acetate
Ace-K	acesulfame potassium
ACM	acetaminophen
AOX	adsorbable organic halogen
ATS	atorvastatin
a.u.	arbitrary units
BAT	Best Available Technology
BOD	biological oxygen demand
BQL	below quantification limit
CAF	caffeine
CASIF	Central Appalachians Stable Isotope Facility
CAST	Chesapeake Assessment Scenario Tool
CAV	cell accelerator voltage
CBL	Chesapeake Biological Laboratory
CBZ	carbamazepine
CDD	construction and demolition debris
CE	collision energy
CEC	contaminant of emerging concern
CHO	formulas containing only carbon, hydrogen, and oxygen
CHOBr	formulas containing only carbon, hydrogen, oxygen, and bromine
CHON	formulas containing only carbon, hydrogen, oxygen, and nitrogen
CHONS	formulas containing only carbon, hydrogen, oxygen, nitrogen, and sulfur
CHOS	formulas containing only carbon, hydrogen, oxygen, and sulfur
CHOSCl	formulas containing only carbon, hydrogen, oxygen, sulfur, and chlorine
CID	collision-induced dissociation
COD	chemical oxygen demand
COT	cotinine
CSIA	compound specific isotope analysis
CSO	combined sewer overflow
DATS	dialkyl tetralin sulfonates
DATSI	dialkyl tetralin sulfonate intermediate
DBE	double bond equivalent
DCF	diclofenac
DCV	dichlorvos
DI	direct infusion
DL	detection limit
DO	dissolved oxygen
DOC	dissolved organic carbon
DOM	dissolved organic matter
DON	dissolved organic nitrogen
EA	elemental analyzer/analysis

EEM	excitation and emission matrix
EMV	electron multiplier voltage
ESI	electrospray ionization
EST	estrone
FA	formic acid
FTICR MS	Fourier-transform ion cyclotron resonance mass spectrometer/spectrometry
FV	fragmentor voltage
FWA	fluorescent whitening agent
GAM	generalized additive model
H/C	hydrogen to carbon ratio
HCD	higher-energy C-trap dissociation
HPLC	high performance liquid chromatograph/chromatography
IBU	ibuprofen
IC	ion chromatography/chromatography
ICP	inductively coupled plasma
IN	inorganic nitrogen
IPA	isopropanol
IRMS	isotope ratio mass spectrometer/spectrometry
ISTD	internal standard
LAS	linear alkyl benzene sulfonates
LC	liquid chromatograph/chromatography
LL	landfill leachate
LLOM	landfill leachate dissolved organic matter
LOD	limit of detection
MDL	method detection limit
MDS	multi-dimensional scaling
MeOH	methanol
MPB	methylparaben
MRM	multiple reaction monitoring
MS	mass spectrometer/spectrometry
MS/MS	tandem mass spectrometry
MSW	municipal solid waste
MW	megawords
m/z	mass to charge ratio
NANI	net anthropogenic nitrogen input
NASL	Nutrient Analytical Services Laboratory
ND	not detected
NDOM	natural dissolved organic matter
NMR	nuclear magnetic resonance
NSAID	nonsteroidal anti-inflammatory drug
O/C	oxygen to carbon ratio
OTC	over-the-counter
OWTS	onsite wastewater treatment systems
PARAFAC	parallel factor analysis
PC	particulate carbon

PFC	per- and poly-fluorinated compound
PFAC	perfluoroalkyl carboxylate
PFAS	perfluoroalkyl sulfonate
PFBuS	perfluorobutanesulfonic acid
PFHpA	perfluoroheptanoic acid
PFHpS	perfluoroheptanesulfonic acid
PFHxA	perfluorohexanoic acid
PFHxS	perfluorohexanesulfonic acid
PFOA	perfluorooctanoic acid
PFOS	perfluorooctanesulfonic acid
PFPeA	perfluoropentanoic acid
PFPeS	perfluoropentanesulfonic acid
PN	particulate nitrogen
POX	purgeable organic halogen
PP	particulate phosphorous
PPB	propylparaben
PXT	paraxanthine
QSU	quinine sulfate units
QqQ	triple quadrupole
RL	reporting limit
RO	reverse osmosis
RT	retention time
SCL	sucralose
SD	standard deviation
SIL	stable isotope-labelled
SMX	sulfamethoxazole
SPC	sulfophenyl carboxylic acid
SPE	solid-phase extract/extraction
SRM	selective reaction monitoring
SRNOM	Suwannee River natural organic matter
STE	septic tank effluent
STDOM	septic tank dissolved organic matter
TCD	Thermal Conduction Detector
TCS	triclosan
TDN	total dissolved nitrogen
TDP	total dissolved phosphorus
TFL	Terrestrial Fractionation Line
TIC	total ion counts
TIN	total inorganic nitrogen
TMDL	total maximum daily load
VPDB	Vienna Pee Dee Belemnite
VSMOW	Vienna Standard Mean Ocean Water
WAX	weak-anion exchange
WWTP	wastewater treatment plant

Chapter 1: Introduction

1.1 Septic Systems for Onsite Wastewater Treatment

Onsite wastewater treatment systems (OWTSs) treat domestic wastewater on or nearby the property where it is produced. These systems are generally used when municipal wastewater treatment is unavailable and allow for the disposal of effluent with some treatment to minimize public health risks. An estimated 23% of households in the United States use OWTSs, and they can be the predominant form of wastewater treatment in suburban and rural areas (U.S. EPA, 2002). Single household septic systems are the main form of OWTSs in the United States. In a septic system, domestic wastewater enters a tank, which may consist of one or two chambers. Within the septic tank, wastewater is treated through sedimentation, in which fats and oils float to the top of the tank, while solids settle to the bottom. Anaerobic microbial degradation within the tank chemically transforms effluent and decreases the volume of solids. Collected solids must be periodically pumped out for further treatment, usually at a wastewater treatment plant (WWTP). Liquid effluent flows or is pumped to a drain field for further treatment. A drainfield is usually an array of perforated tubing overlying trenches filled with a material that promotes water percolation, such as gravel. Effluent percolates through the tubing to slowly dose the drainfield material and underlying soil. Further treatment is accomplished by sorbing of contaminants to the drainfield or proximate sediment and through further aerobic or anaerobic microbial degradation. The effluent can then become soil water or enter groundwater.

Some septic systems, called advanced technology systems, have been engineered for greater wastewater treatment, often through aerobic or aerobic-anaerobic treatment (U.S. EPA, 2002). Advanced treatment enhances degradation of organic matter and promotes removal of nitrogen (Fig. 1.1), but even with advanced treatment, complete removal of all contaminants cannot be accomplished within the system, and advanced systems still do not meet the treatment level of most municipal WWTPs with enhanced nutrient removal (Oakley et al., 2010).

Septic system treatment relies on proper installation, performance, and maintenance of the system. Improper performance and especially failure can greatly increase the degree of environmental pollution from the system, but even a properly performing system pollutes soil water and groundwater by design. However, when centralized wastewater treatment is unavailable, septic system treatment is necessary to minimize sewage related health risks. Septic systems are not regulated or monitored as stringently as centralized wastewater treatment (U.S. EPA, 2002). Additionally, most regulation is only designed to address immediate pathogenic health risks, when contaminants present in domestic wastewater can cause both acute and chronic health risks for humans and other organisms. Contaminants present in initial domestic wastewater include bacteria, viruses, metals, nutrients like phosphorous and nitrogen, chloride, and organic chemicals originating from pharmaceuticals, household cleaners, personal care products, and diet. Extent of removal in a septic system depends on the level of treatment and individual properties of the contaminants. Effluent transformation and contaminant removal in the drainfield and beyond are controlled by numerous factors such as effluent

composition, sediment type, and soil water and groundwater properties. However, effluent transformation and movement are not monitored beyond the immediate drainfield region, so septic effluent can contaminate drinking water wells or be transported to surface waters, which is especially true for failed septic systems. To track septic effluent contamination, it is necessary to understand initial septic wastewater composition and what chemical features persist through environmental pathways.

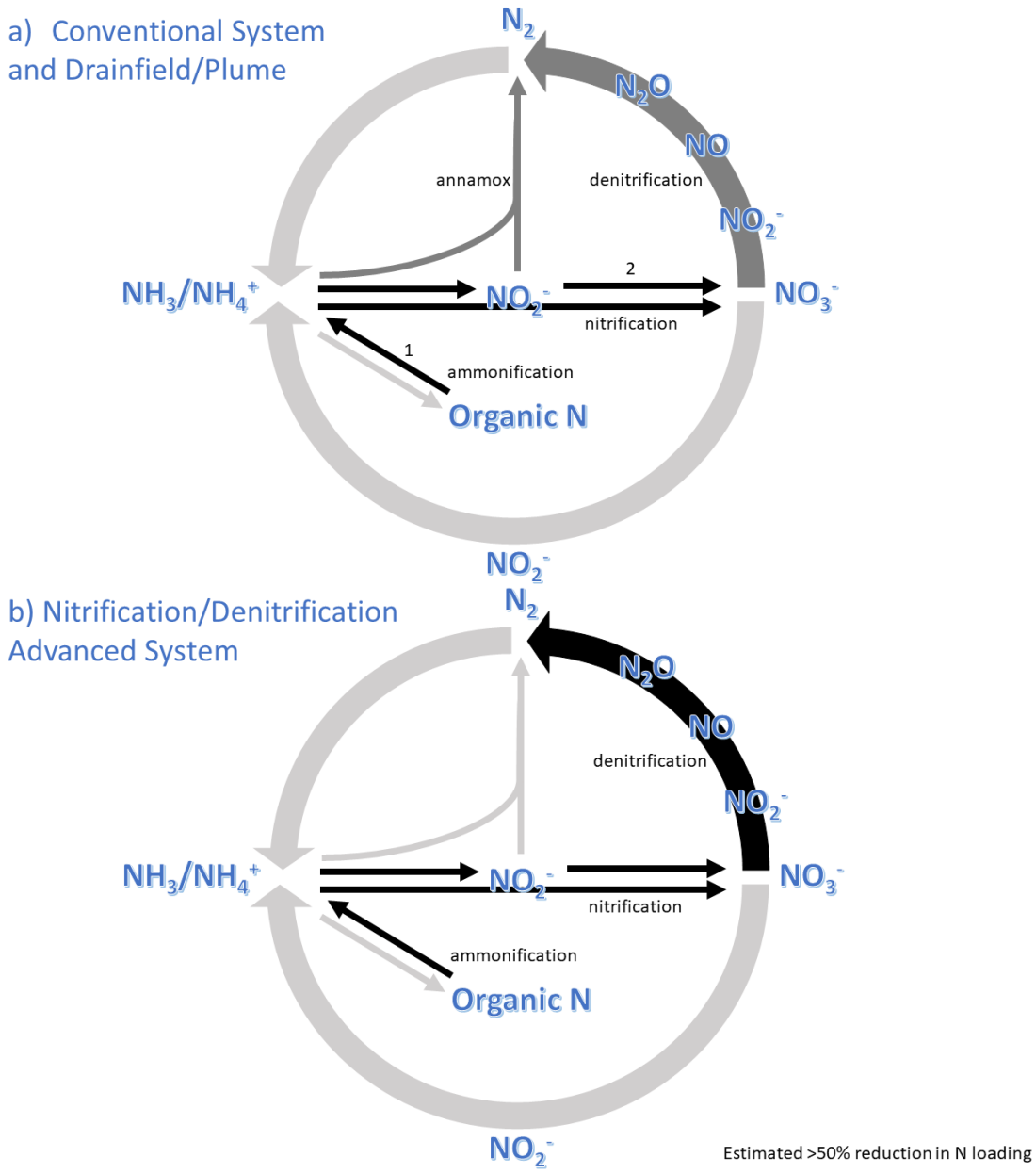

Figure 1.1 (a) Expected nitrogen transformations in a conventional septic tank (1) and the corresponding drainfield and plume (2) (Wilhelm et al., 1994; Wilhelm et al., 1996). Traditionally drainfields are installed to minimize water-table interactions, but in situations with a high, fluctuating water-table, annamox and denitrification can occur within the plume (Caschetto et al., 2018). (b) Expected pre-drainfield nitrogen transformations in a nitrification-denitrification advanced septic system. Estimated nitrogen reduction from Oakley et al. (2010).

1.2 Chemical and Microbial Tracers of Domestic Wastewater Contamination

Tracers of wastewater are chemical or microbial markers that can be detected or measured to identify contamination. Tracers are usually present in the initial wastewater source but can also be chemical transformation products found after initial treatment. Commonly used domestic wastewater tracers fit into four general categories: human or human-microbiome produced markers; organic contaminants of emerging concern (CECs); inorganic species; and isotopic signatures.

1.2.1 Human or Human-Microbiome Produced Markers

Total coliform has been measured as a marker of fecal contamination; however, coliform bacteria are not fecal specific, so fecal coliform is a better indicator for sewage contamination (Elmund et al., 1999). Fecal coliform also has the confounding issue that some contributing bacteria can thrive in the environment. Taking this a step further, *Escherichia coli*, or *E. coli*, is an even better indicator of sewage, but is still not human specific without genotyping (Elmund et al., 1999; Gomi et al., 2014). Recent work has moved towards human-specific fecal indicators such as *Bacteroides* HF183 or *Escherichia coli* H8 (Seurinck et al., 2005; Gomi et al., 2014; Hughes et al., 2017).

Steroids can be measured to trace sewage contamination in groundwaters and surface waters (Kolpin et al., 2002). Sterols, or steroid alcohols, are a type of lipid produced by plants and animals, the most familiar of which is probably the animal sterol, cholesterol. Sterols can be hydrogenated into stanols during digestion or plant stanols can be present in some foods. Coprostanol is an indicator of fecal contamination because its precursor sterol is cholesterol (Kanazawa and Teshima,

1978; LeBlanc et al., 1992). Furthermore, because sterols and stanols can be plant and animal specific or even species specific, other ratios can be used to delineate fecal contamination animal source. Lim et al. (2017) provide a literature review of sterols and stanols as wastewater tracers and previously used ratios for sewage source identification. Steroid hormones like estrogens and androgens, both naturally occurring and synthesized for medications, can also be indicators of sewage contamination (Kolpin et al., 2002; Standley et al., 2008; Singh et al., 2010; Phillips et al., 2012; Yang et al., 2016).

1.2.2 Organic Contaminants of Emerging Concern and DOM fluorescence

CECs are chemicals for which awareness of their existence, prevalence in the environment, or health effects is developing (Sauvé and Desrosiers, 2014). With some exceptions, CECs are mainly organic contaminants and human created, either through chemical discovery or mass production of naturally occurring chemicals. There are too many chemicals considered to be CECs to list and new CECs are constantly being identified and created, but common examples can be found in EPA Method 1694 (U.S. EPA, 2007) and the biennial reviews by Susan D. Richardson, the most recent of which is Richardson and Kimura (2020). CECs in domestic wastewater come from commonly used products such as pharmaceuticals, stimulants, household cleaning supplies, toiletries, makeup, food, and drinks. Recent studies have worked to identify CECs most suited for tracing domestic wastewater: namely those that are commonly used, that are less likely to be used industrially or in agriculture, that behave conservatively, or that are persistent through wastewater treatment or in the environment. Commonly named CECs for domestic wastewater tracing are the

artificial sweeteners, sucralose and acesulfame potassium (ace-K); the pharmaceuticals, atenolol, carbamazepine, sulfamethoxazole, ibuprofen, acetaminophen; caffeine and its metabolites; and the antimicrobials, methyl-, ethyl-, propyl-, and butyl- paraben, triclosan, and triclocarban (Kolpin et al., 2002; Loos et al., 2013; Subedi et al., 2015; James et al., 2016; Yang et al., 2016). Beyond simply identifying human wastewater contamination, researchers have also used CECs to determine wastewater age, level of treatment, and separate domestic wastewater sources. These techniques often capitalize on the widespread use, human specificity, persistence, and conservative behavior of the artificial sweetener sucralose (Oppenheimer et al., 2011).

Regulatory approval dates, usage trends, and production bans allow certain CECs to proxy wastewater age. For instance, Robertson et al. (2016) suggested the presence of the artificial sweetener sucralose to indicate wastewater from after the year 2000 in the U.S. and Canada. They additionally suggested the ratio of sucralose to ace-K as a more precise proxy of age based on market trends. Other trend-related ratios that have potential to proxy wastewater age are ratios of shorter chain to longer chain perfluoroalkyl sulfonates (PFASs) and perfluoroalkyl carboxylates (PFACs), as production has shifted to those with shorter human elimination half-lives (Bjerregaard-Olesen et al., 2016). This pattern has been observed in biological samples (Lam et al., 2016), but its application may be complicated by atmospheric precursors and unknown environmental pathways and degradation rates (Ellis et al., 2004; Liu and Avendaño, 2013). The 2017 ban of triclosan and triclocarban in antiseptic wash products in the U.S. (U.S. FDA, 2016) and related voluntary

phaseouts may also allow these compounds to become wastewater age proxies. Though the continued use of triclosan and triclocarban in hand sanitizers and wipes, dental products, non-FDA regulated household products, and medical settings (U.S. FDA, 2016); sorption capacity to sediments (Ying et al., 2007); and long-term persistence under anaerobic conditions must be considered (Singer et al., 2002).

Cantwell et al. (2018) used ratios of caffeine to sucralose to proxy levels of wastewater treatment, because caffeine has high removal efficiency during treatment. They were able to distinguish combined sewer overflow (CSO) input from WWTP effluent. While only speculative, ratios of sucralose to ace-K could perform similarly because microbial degradation pathways for ace-K are believed to have recently evolved (Castronovo et al., 2017; Kahl et al., 2018; Kleinsteuber et al., 2019). The same concepts may extend to distinguishing OWTS and WWTP effluent and effluent from WWTPs with different levels of treatment. Oppenheimer et al. (2012) suggested ratios of CECs with ubiquitous versus limited usage to distinguish septic system effluent from WWTP effluent. They were able to successfully distinguish the two using ratios of sucralose to the prescription medication, carbamazepine, and sucralose to gadolinium. They attributed the better performance of gadolinium ratios to its less widespread use.

Dissolved organic matter (DOM) fluorescence is a product of chemical composition, and fluorescence of domestic wastewater DOM is known to be different than natural waters (Yang et al., 2015), so optical properties (absorbance and fluorescence) of DOM have been used to trace wastewater. DOM fluorescence can be a powerful tool for monitoring transformation of wastewater during treatment

(Murphy et al., 2011). It has also been used to identify and monitor wastewater effluent in the immediate area of outflows (Baker, 2002; Dickerson Jr. et al., 2007). In the broader environment, protein-like fluorescence has been linked to detecting the presence of untreated sewage (Baker, 2001), and fluorescence features have been ascribed to specific emerging contaminant fluorophores (Carstea et al., 2016).

In particular, certain fluorescent properties of domestic wastewater have been linked to fluorescent whitening agents (FWAs) (Hudson et al., 2007; Carstea et al., 2016), also known as optical brighteners, which are compounds added to make white colors appear less yellow because they absorb ultraviolet light (360-365 nm) and re-emit blue light (400-440 nm) (Poiger et al., 1998; Assaad et al., 2014). FWAs are used in paper-making and in detergents to make fabrics appear brighter (Poiger et al., 1998). Commonly mentioned domestic wastewater tracer FWAs are DSBP and DAS 1, which are used in laundry detergents (Poiger et al., 1998; Chen et al., 2006; Dubber and Gill, 2017). Most wastewater tracer studies have identified presence/absence of FWAs by spectrofluorometry, even though natural dissolved organic matter (NDOM) is known to absorb and fluoresce in the same regions (Chen et al., 2006; Hudson et al., 2007; Dubber and Gill, 2017). Quantification of specific FWAs is rarely done to support detection (Chen et al., 2006). Quantification of total FWAs or detection of FWA presence/absence using photodecay rates is problematic, as all photolabile DOM, with or without FWAs, will undergo more rapid photodegradation than previously photoexposed DOM. While FWAs are produced and used in mass quantities, their purpose is to be retained on clothes, they have significant sorption to sewage sludge and sediment, and rapidly photodegrade (Poiger et al., 1998), so large

concentrations in surface waters are unlikely beyond immediate effluent outflow sources. FWA analysis should be done using conservative methods such as liquid chromatography (LC) with tandem mass spectrometry (MS/MS) to identify—and ideally quantify—specific chemicals.

Similarly, protein-like fluorescence is also observed in labile NDOM (Yang et al., 2015), and few studies have combined optics with nontargeted approaches to determine chemical composition (Stubbins et al., 2014). DOM fluorescence should not be used to assign source solely based on the correlations with the wide variety of features that have been connected to wastewater (Murphy et al., 2011). DOM Fluorescence may not be solely the product of specific compounds or classes of compounds, but instead a product of charge transfer (Sharpless and Blough, 2014). Temperature, pH, and metal presence and speciation can also affect detected DOM absorbance and fluorescence (Carstea et al., 2016). While identifying wastewater contamination by optical properties is an appealing notion because of the speed and cost of analysis, any application in most natural waters should be done with extreme caution. As shown later in this study, natural waters with significant domestic wastewater impacts shown using unambiguous wastewater tracers were not optically distinctive from low-impact and no-impact natural water samples (Section 4.3.2).

1.2.3 Inorganic Species

Nitrogen and phosphorus, metals, boron, and halogens are frequently used inorganic constituents for wastewater tracing. Inorganic nitrogen and phosphorous species are likely some of the most familiar wastewater tracers. These nutrients are nonspecific to domestic wastewater and can come from agricultural and household

fertilizer use, so their role as wastewater tracers by concentration is limited to use in combination with other tracers or basins with limited nutrient sources. Additionally, nitrogen deposition can influence measured nitrogen concentration. While it is known that anthropogenic nitrogen inputs are well-attenuated in most rivers and streams (~75%) (Boyer et al., 2002; Swaney et al., 2012), domestic wastewater, particularly septic systems, can be a significant source of nitrogen loading and elevated nitrogen concentrations in surface waters (Iverson et al., 2015).

The phosphorous cycle does not have a gas phase, so phosphorous deposition is unlikely to be an important source (Anderson and Downing, 2006; Hale et al., 2013). Domestic wastewater is still elevated in phosphorous from diet and household products, even after widespread bans and phase outs of detergent phosphates (de-Bashan and Bashan, 2004; Robertson, 2008; Van Drecht et al., 2009). Phosphorous is more likely to be immobilized in sediments than nitrogen, so it is less often measured when trying to identify wastewater contamination (Benitez-Nelson, 2000; Robertson, 2008). Anaerobic sewage contains high concentrations of ammonia, which is transformed to nitrate during treatment or in aerobic environments following release. Organic nitrogen is also elevated in wastewater but historically has been rarely measured for water quality monitoring (Pehlivanoglu-Mantas and Sedlak, 2006).

Metals are present in many household products, so wastewaters often have elevated concentrations. However, studies have shown that measuring most metals to trace wastewater input in groundwater and surface waters is unlikely to be successful because of heterogeneous natural background levels and sorbing to and exchange with sediment during transport (Robertson, 2008; Richards et al., 2016). The metal,

gadolinium, and metalloid, boron, perform well as wastewater tracers because they have low natural abundances in the Earth's continental crust and more limited geological occurrences than other metals and metalloids elevated in initial wastewater (Vengosh et al., 1994; Vengosh, 1998; Kümmerer and Helmers, 2000; Oppenheimer et al., 2012). Gadolinium is a rare-earth metal used in a chelated form as a contrast agent in magnetic resonance imaging (MRI). It is particularly elevated in effluent from WWTPs also receiving medical wastewater but is also present in all sewage inputs from larger combined populations because of the prevalence of MRI scans (Kümmerer and Helmers, 2000; Oppenheimer et al., 2012). The metalloid boron is also a wastewater tracer because it is used in household detergents (Vengosh et al., 1994). Use of gadolinium as a wastewater tracer is complicated by the fact that the anthropogenic gadolinium anomaly is a recent occurrence and because of gadolinium's toxicity as a free ion, it is strongly chelated with various ligands for medical imaging use, therefore much is still unknown about gadolinium environmental cycling and sinks (Kümmerer and Helmers, 2000). Likewise, understanding of boron cycling is still limited, partly because of early analytical challenges (Marschall and Foster, 2018).

The halide ion, chloride, is elevated in domestic wastewater due to salt in human diet, its presence in household products, and from the use of water softening units (Davis et al., 1998; Panno et al., 2006). While, in many situations elevated chloride concentration alone can indicate wastewater contamination, it can also derive from local geology, agricultural wastewater, natural saltwater intrusion, or road salt application; therefore, ratios of chloride to other ions have also been used for source-

tracking. For example, chloride to bromide ratio can be used to identify domestic wastewater, likely because of the more extensive use of chlorine in household products and an overall evaporite chlorine and bromine source (Davis et al., 1998). Ratios of chloride to bromide in combination with chloride concentrations have been used to distinguish septic system wastewater from animal wastewater (Showers et al., 2008), septic system wastewater from animal wastewater and landfill leachate (Panno et al., 2006), and to recognize potential septic system effluent impact on groundwater (Katz et al., 2011). However, signal distinction may be location specific, as Panno et al. (2006) found septic effluent to have higher Cl^-/Br^- than animal waste, while Showers et al. (2008) used the opposite trend to separate the two sources. Another caveat is that domestic wastewater can have a signature overlap with other evaporative sources such as road salt (Vengosh and Pankratov, 1998; Panno et al., 2006). Pastén-Zapata et al. (2014) found greater source separation for groundwater samples in an area of Northeastern Mexico containing evaporite deposits by additionally using iodide to sodium ion ratios in combination with bromide concentrations. See Davis et al. (1998) for a detailed description of processes that control chloride and bromide concentration and Katz et al. (2011), for a review of their ratio for tracking septic effluent and possible source signature overlaps. The radioisotope iodine-131, used to treat thyroid conditions and in some medical imaging, has been used as a wastewater tracer (Smith et al., 2008), but its use is limited compared to stable gadolinium because of its short half-life. This is different from stable isotope iodinated organic contrast agents, such as diatrizoic acid, which have also been used as wastewater tracers (Wolf et al., 2012; Ribbers et al., 2019).

1.2.4 Isotopic Signatures

Various stable isotope ratios have been successfully used to identify domestic wastewater contamination, but this description will focus on two of the most commonly used ones: stable boron and stable nitrogen isotope signatures.

$$\delta(‰) = \frac{R_{sample} - R_{standard}}{R_{standard}} \cdot 1000 \quad (1)$$

All mentioned values are in delta notation and expressed in permil (‰) (Eq. 1), where R is the ratio of the heavy to light isotope, in this discussion $^{15}N/^{14}N$, $^{18}O/^{16}O$, $^{17}O/^{16}O$, and $^{11}B/^{10}B$, and values are relative to the standards atmospheric nitrogen (N), Vienna Standard Mean Ocean Water (VSMOW) (O), and NIST-SRM951 (B).

Nitrogen stable isotope ratios have been extensively used to trace wastewater inputs because biological assimilation generally produces tissues and solid waste enriched in ^{15}N (Kendall et al., 2007). This is thought to be because of deamination preferentially removing isotopically light amine groups, making urea, uric acid, and ammonia in waste enriched in ^{14}N and leaving ^{15}N enriched amino acids (Gannes et al., 1998). Nitrogen, therefore, undergoes a predictable "trophic fractionation" of approximately 3-5 ‰ relative to diet (Gannes et al., 1998). While waste nitrogen is isotopically light compared to respective tissue, waste nitrogen follows the same trophic-associated signature, as organisms with isotopically heavier tissue and diet will produce isotopically heavier waste products. Volatilization of ^{15}N depleted ammonia can subsequently make waste even heavier isotopically (Kendall et al., 2007). Ammonia and dissolved organic nitrogen (DON) from waste can be

microbially transformed to other nitrogen species which will show similar isotopic signatures.

Heterotrophs must obtain essential amino acids from diet, so these processes have allowed particulate organic nitrogen, nitrate, bulk tissues, and compound specific analysis of tissue to be successfully used to identify animal wastewater input (Evershed et al., 2007; Hadwen and Arthington, 2007; Kendall et al., 2007; Montoya, 2007). Of these species, nitrate is extensively used to trace wastewater contamination because of ease of analysis and greater specificity. A dual-isotope approach of $\delta^{15}N_{NO3}$ and $\delta^{18}O_{NO3}$ can help identify mixing effects or fractionation. For example, negative correlation between $\delta^{15}N_{NO3}$ and $\delta^{18}O_{NO3}$ can indicate mixing with atmospheric nitrate, while a positive correlation between $\delta^{15}N_{NO3}$ and $\delta^{18}O_{NO3}$ within a specific slope range can indicate isotopic signature alteration from denitrification or assimilation (Kendall et al., 2007; Kaushal et al., 2011; Duan et al., 2021). As discussed more extensively in *Chapter 4* (4.2.6), measuring both $\delta^{18}O_{NO3}$ and $\delta^{17}O_{NO3}$ can allow for unambiguous identification of atmospheric-sourced nitrate (Michalski et al., 2003). Different sources of nitrate have typical isotopic signatures (Fig. 1.2), and in absence of evidence of significant effects of denitrification or other signature alteration (Kendall et al., 2007; Venkiteswaran et al., 2019), a $\delta^{15}N_{NO3}$ value greater than 8.6 ‰ can be a marker of animal, including human, wastewater contamination (Kendall et al., 2007).

As previously described, boron can be elevated in domestic wastewaters, but $\delta^{11}B$ with boron concentration is a more source specific tracer that can distinguish if high boron concentration is from a natural saline source or sewage. This distinction is

because wastewater boron is from sodium borates used in detergents, which are depleted in ^{11}B compared to seawater (Vengosh et al., 1994). Seawater enrichment in ^{11}B is thought to be due to preferential adsorption of ^{10}B onto clay minerals (Palmer et al., 1987). Measurements of $\delta^{11}B$ between 0-13‰ in combination with elevated boron concentrations relative to local, unimpacted freshwaters, can therefore, signify domestic wastewater contamination (Vengosh et al., 1994; Vengosh, 1998; Seiler, 2005).

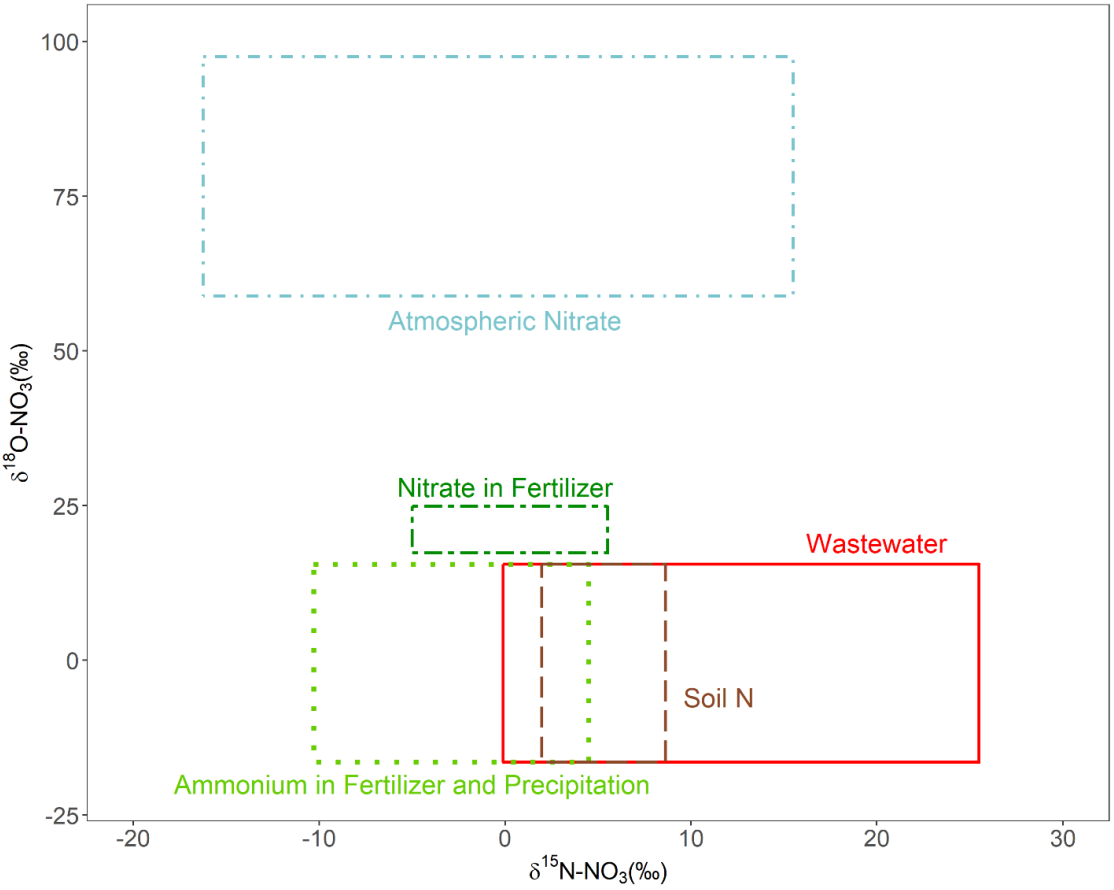

Figure 1.2 Typical nitrate $\delta^{15}N$ and $\delta^{18}O$ ($^{18}O/^{16}O$, relative to the Vienna Standard Mean Ocean Water standard) isotopic signatures (adapted from Kendall et al., 2007).

1.3 Landfill Leachate

In a similar way to septic systems, landfill wastewater, or leachate, can be a source of effluent contamination to groundwater and surface waters and pose a public health risk. In the United States, while MSW production has increased, the number of active landfills accepting waste has decreased because MSW is increasingly sent to larger landfills (U.S. EPA, 2008a). It is unknown how many landfills exist in the United States. The U.S. Environmental Protection Agency's Landfill and Landfill Gas Energy Project Database lists 1,289 operational landfills (U.S. EPA, 2020b), but it is estimated that there are thousands of closed and unlined landfills (U.S. EPA, 2008a). Landfills closed within the past decades are more likely to be accounted for and monitored for environmental impact, but there are also many historic landfills with unknown sizes, waste types, owners, and sometimes even locations that have water impact risks (Maryland Department of the Environment, 2009; Colorado Department of Public Health and Environment, 2019). Likewise, the volume of leachate generated in the U.S. is still poorly constrained due to factors such as the existence of historic landfills, the role of climate in leachate generation, and lack of understanding of long-term waste degradation. Lang et al. (2017) estimated the generation of leachate for 2013 at 61.1 million m^3, but more research is needed to better understand leachate volume and to account for leachate generation from historic, unlined landfills.

Landfill leachate is a product of slow percolation and leaching of garbage, so it can contain extreme concentrations of metals, organic pollutants, dissolved organic carbon (DOC), and ammonia in comparison to domestic wastewaters (Kjeldsen et al.,

2002; Masoner et al., 2016). A major factor in the toxicity of landfill leachate is ammonia (Berge et al., 2005). One form of leachate treatment is re-injection, where leachate is collected and re-circulated through the landfill, sometimes with an air addition or supplementation with other water, to promote degradation of organic matter. Landfills using this treatment are called bioreactor landfills, and while leachate recirculation accelerates organic matter degradation, it also accelerates ammonia production (Berge et al., 2005). Leachate can be collected and treated *ex-situ* using biological treatment systems like those used in WWTPs, but this can be complicated by the intrinsic microbial toxicity of highly concentrated leachate. Leachate can also be treated *ex-situ* at WWTPs, but because of the levels of contaminants, particularly ammonia, WWTP operators may limit or refuse leachate for treatment. Solutions to better treat landfill leachate are needed, but to engineer new leachate treatments, it is necessary to understand leachate composition.

1.4 Study Purpose and Design

1.4.1 Rationale

The principal objectives of this study were to (1) molecularly characterize DOM of septic effluent and through this (2) develop novel organic tracers of septic wastewater and assess existing tracers, while (3) generating data that could aid in understanding nitrogen loading by septic systems. I also (4) applied many of the same tools to the study of landfill leachate, to understand the similarities and differences between septic and landfill domestic wastewater. I addressed these objectives by combining targeted analyses of traditional water quality parameters, quantification of

specific emerging contaminants, measurements of DOM optical properties, and nontargeted, ultrahigh resolution MS to study septic system wastewater, reference streams, streams impacted by septic system wastewater, and landfill leachate. Ultrahigh resolution MS, like electrospray ionization Fourier transform ion cyclotron resonance MS (ESI FTICR MS), is a technique that identifies the presence of thousands of molecular masses. The high resolution and mass accuracy of ESI FTICR MS allows for the assignment of exact molecular formulae to masses.

Total dissolved nitrogen (TDN) is present in watersheds as both inorganic nitrogen, including nitrate, nitrite, ammonia, and ammonium, and organic nitrogen; however, the majority of past research has focused on the source and fate of only inorganic nitrogen and mostly nitrate. Organic nitrogen is rarely measured, despite work showing it to be a significant component of dissolved nitrogen in freshwaters (Jones et al., 2004), it being the dominant form of dissolved nitrogen in nitrification-denitrification wastewater effluent (Pehlivanoglu-Mantas and Sedlak, 2006), and a major component of nitrogen in waste entering septic systems (Wilhelm et al., 1994). DON is active in nitrogen transformation pathways and is both a potential nutrient and a precursor to a variety of toxic disinfection by-product (Jones et al., 2004; Pehlivanoglu-Mantas and Sedlak, 2006). Lack of information on the structure and properties of DON has made it hard to target for removal in WWTPs (Pehlivanoglu-Mantas and Sedlak, 2006). This study contributes to the knowledge of domestic wastewater DON composition.

Studying domestic wastewater DOM is equally important as understanding wastewater DON because it will allow for the identification of metabolites and

product-sourced chemicals that comprise domestic wastewater. By studying the DOM at both wastewater sources and contaminated sites, it is possible to identify possible DOM transformations. Traditionally, wastewater tracers have been developed based on what is already known to be present in wastewater; whereas, a nontargeted approach identifies the presence of thousands of chemicals, and can identify previously unknown or unconsidered manufacturing products, by-products, and co-products; transformation products; or human metabolites. These previously unidentified or ignored wastewater components have the potential to be wastewater tracers, and their performance can be assessed by combining wastewater source and surface water data.

While many wastewater tracers already exist, that does not preclude a need for more tracers or a better understanding of existing tracers. Currently, the best source-identification results are generally reached through a combination of tracers to surmount the shortcomings of individual tracers. Many tracers are not human wastewater source specific; for instance, high chloride can come from road salt, saltwater intrusion, human sewage, or animal sewage. Tracers, such as *E. coli*, certain antibiotics and hormones, or $\delta^{15}N_{NO3}$, likewise, cannot distinguish between human and animal waste. Many of the more human-specific tracers, like human-specific gut markers (*Bacteroides* HF183, *Escherichia coli* H8, sterol/stanol ratios), $\delta^{11}B$, or CECs like sucralose or carbamazepine, require highly specialized sample preparation and method development or prohibitively expensive analytical equipment. While many studies have used multiple tracers to better constrain sources, allowing them to compare tracers, few studies have performed long-term sampling to temporally assess

tracer performance. Another issue, which has only recently been addressed, is the need for wastewater tracer proxies that can be applied to questions and problems beyond domestic source identification. For example, wastewater tracers can potentially be a proxy for treatment level, degradation, and age, or distinguish specific domestic wastewater sources like WWTP effluent, CSOs, or septic system effluent. This study addresses these issues, as newly identified tracers may be more human-specific, easier to quickly assess, or more informative of transformation pathways. The large dataset produced is important background knowledge to support the development of more specific tracer proxies.

Another advantage of this extensive sampling operation is that beyond just combining nontargeted characterization and targeted chemical analyses, this study also combines analyses of source wastewater and impacted surface waters. Most septic system wastewater studies have only looked at environmental data, with measurements in soil, groundwater, or surface waters. Comparatively few studies have also measured the same parameters in septic system tank wastewater itself to better understand source composition.

Landfill leachate is also a high contamination risk to groundwater and surface waters, so chemical composition information is necessary for leachate treatment, to understand health risks, and to identify which chemicals could be leachate contamination tracers. Landfill leachate is like domestic wastewater in that it contains metals, CECs, chloride, and ammonia, but different in that concentrations of these contaminants are generally orders of magnitude more extreme than domestic wastewater because leachate is the product of slow, continuous leaching of mass

amounts of garbage. Leachate contains CECs like commonly used pharmaceuticals and artificial sweeteners, but with different sources. Unless biosolids are being collected, there should be minimal human waste in landfills, so most domestic CECs are coming from wrappers and containers or discarded food and medications. In contrast to septic system wastewater, landfill leachate is less likely to be pathogenic and is likely to contain industrially associated CECs or chemicals derived from disposal of construction debris. Leachate can contain ammonia-N and DOC in the thousands of mg/L (Kjeldsen et al., 2002). For comparison, Richards et al. (2016) studied effluent from 32 septic tanks and measured maximum ammonia-N of 144 mg/L and DOC of 179 mg/L. Correspondingly, the organic CECs contributing to leachate DOC have high concentrations, with individual compounds measuring in the mg/L range (Masoner et al., 2016). Despite these differences, both septic systems and landfills are anaerobic systems that are the product of society, and many of the same analytical techniques can be used to determine DOM composition.

1.4.2 Relevance of Septic System Tracer Study Area

This study was primarily conducted in Calvert County, Maryland, a county in the Southern Maryland Region on the western shore of the Chesapeake Bay. Calvert County has seen rapid population growth, and with this, a shift from agricultural to residential land-use. Between 1990 and 2010, the population increased from 51,372 to 88,737, a 72.7% increase, making Calvert County the fastest growing county during this period in the state of Maryland (U.S. Census Bureau, 1992, 2012). Septic systems are the primary method of wastewater treatment in the county. Concerns about excess nitrogen reaching the Chesapeake Bay and targeted legislation have led to installation

of denitrifying septic systems. The Bay Restoration Fund, established by Maryland Senate Bill 320 (2004), provides financial support for the installation of denitrifying septic systems through fees collected from septic system users. The Sustainable Growth and Agricultural Preservation Act of 2012 (Maryland Senate Bill 236, 2012), designed to limit septic nitrogen contribution and residential growth on conventional septic systems, mandated the installation of denitrifying septic systems for all new development requiring on-site wastewater treatment. In response to concerns surrounding limits on economic development, increased financial strain on the Bay Restoration Fund, and limited data on the effectiveness of denitrifying septic systems, the requirement was reformed in 2016 to only apply to new development in the "Chesapeake Bay Critical Area" (Baltimore Sun, 2016), land within 1,000 feet of tidal waters and wetlands (COMAR 26.04.02.07, 2004). This legislative and development history makes Calvert County highly suitable for a field and direct sampling study to evaluate existing domestic wastewater tracers, assess performance of denitrifying septic systems, and develop new methods of identifying wastewater contamination.

1.4.3 Sampling Design

We sampled eight streams in Calvert County, MD and one stream in Anne Arundel County, MD, approximately monthly over a year between 2016-2017. All streams were small, first order streams with little to no agricultural land-use, no WWTP effluent input, and minimal sewer infrastructure in their catchments. Catchments ranged in size from approximately 0.02-4.8 sq mi (USGS, 2017). Three streams were forested, reference streams draining areas with zero to low septic

system density (<60 systems/sq mi) and six drained areas with high septic system density (>80 systems/sq mi). One of the six high septic system density sites had primarily advanced septic systems in the catchment. Parameters measured include discharge, pH, conductivity, Cl^-, temperature, DO, TDN, total dissolved phosphorus (TDP), PO_4^{3-}, SO_4^{2-}, NH_4^+, NO_3^--NO_2^-, particulate P, N, and C, DOC, optical properties of DOM (excitation and emission matrix fluorescence and UV-vis absorption), and CECs. CECs measured include the artificial sweeteners sucralose and ace-K; caffeine and the caffeine metabolite paraxanthine; the nicotine metabolite cotinine; NSAIDs ibuprofen, acetaminophen, and diclofenac; antimicrobials methylparaben, propylparaben, and triclosan; the insecticide dichlorvos; the prescription medications sulfamethoxazole, carbamazepine, and atorvastatin; and estrone. DOM was molecularly characterized by ESI FTICR MS. Additionally, $\delta^{15}N$, $\delta^{18}O$, and $\delta^{17}O$ of NO_3^- were seasonally measured, and $\delta^{13}C$ and $\delta^{15}N$ of extractable DOM was measured at one time point. In 2018, additional measurements were made for dissolved Zn and dissolved and particulate Mn, Fe, Cd, Pb, Cr, Cu, As, Se, and Hg.

Conventional septic tank effluent was sampled in 2018 in Calvert County, MD from six systems. Septic tanks sampled served households of 2-6 people, were made of various materials, and included both one and two chambered tanks. One system had an aerobic chamber, and both chambers were sampled when possible. Parameters analyzed include molecular composition, pH, TDN, TDP, PO_4^{3-}, NH_4^+, NO_3^--NO_2^-, DOC, optical properties of DOM, sucralose, ace-K, caffeine, paraxanthine, and triclosan.

Leachate samples from two lined landfills in Florida were collected and sent to us by Nicole Robey and Dr. Timothy Townsend, collaborators at University of Florida, who also measured initial pH, BOD, and COD. DOM was molecularly characterized by ESI FTICR MS. Measured properties include DOM optical properties, DOC, TDN, NH_4^+, NO_3^--NO_2^-, Cl^-, V, Cr, Mn, Fe, Cu, Zn, As, Cd, Pb, sucralose, ace-K, triclosan, methylparaben, propylparaben, paraxanthine, cotinine, ibuprofen, acetaminophen, carbamazepine, and sulfamethoxazole. Additionally, C:N, $\delta^{13}C$ and $\delta^{15}N$ of extractable DOM were measured.

1.4.4 Mass Spectrometric Analytical Techniques

In this study I used electrospray ionization (ESI) triple quadrupole (QqQ) tandem mass spectrometry (MS/MS), and the ultrahigh resolution techniques, ESI Orbitrap MS and MS/MS, as well as ESI FTICR MS. Ionization is used to produce positively or negatively charged ions which can be detected by MS. ESI is a soft ionization technique, designed to produce predominantly in-tact and singly charged ions. High performance liquid chromatography (HPLC) was paired with ESI QqQMS/MS (Agilent 6420) for quantification of emerging contaminants. This technique can be used to quantify many targeted chemicals simultaneously because of its high scan speed. HPLC is used to separate the components of the complex mixture. As chemical components arrive at the MS, precursor ions are mass filtered in the first quadrupole mass analyzer (Q1), fragmented in the collision cell (q2), and then product ions are detected in the final quadrupole mass analyzer (Q3). Detecting ion transitions, instead of just the precursor ion mass, is used to more reliably select the chemical of interest.

This technique was additionally used to fragment certain molecular ions of interest in landfill leachate samples. The molecular identities of product ions can provide structural information or be used to help confirm suspected molecular structure. Despite the lower mass resolution, this was done because collision-induced dissociation (CID) in QqQMS/MS is a non-resonant fragmentation technique which can produce more and smaller fragments (de Graaf et al., 2011; Ichou et al., 2014), and non-resonant fragmentation data was available for the suspected chemical structure identity.

Ultrahigh resolution ESI FTICR MS is used to identify the chemical composition of complex mixtures, for example, natural DOM (Stenson et al., 2003; Powers et al., 2018), wastewaters (Gonsior et al., 2011; Tseng et al., 2013), petroleum (Liu and Kujawinski, 2015), or even extraterrestrial matter in meteorites (Schmitt-Kopplin et al., 2010). Here, a 12 Tesla ultrahigh resolution Bruker solariX ESI FTICR MS was used for nontargeted, full scan, molecular characterization of natural waters, domestic wastewater, and landfill leachate DOM, and to identify novel chemical tracers of septic system impact in natural waters. The high mass resolution, typically >400,000 at 400 *m/z* for the FTICR MS used here, allows for the assignment of exact molecular formulas to *m/z* ions. This technique is not quantitative or structural but allows for thousands of chemical formulas to be identified in samples.

The lower, but still ultrahigh, mass resolution technique, Orbitrap MS, was used in direct infusion, full scan mode (DI/ESI Orbitrap MS) to look at sucralose adduct formation, first identified by FTICR MS, in a different instrument. DI/ESI Orbitrap MS/MS using resonant CID was used to fragment sucralose adduct ions and

specific ions in landfill leachate to help confirm suspected identities. The Orbitrap MS was also paired with HPLC (HPLC/Orbitrap MS) to show sucralose adduct formation also occurring under these conditions. The Orbitrap MS used in this study, a Thermo LTQ Orbitrap XL Hybrid, can operate at mass resolutions from approximately 15,000 to 100,000. Orbitrap MS has much higher mass resolution than QqQMS, but comparatively, very slow scanning speed, so the specific Orbitrap system available to me is not typically used for quantitative analysis. For this reason, it was used for exploratory analysis in this study.

Chapter 2: Evidence for adduct generation of sucralose in electrospray ionization

Abstract

The artificial sweetener, sucralose ($C_{12}H_{19}Cl_3O_8$), is gaining more attention as a human-derived wastewater tracer, making it important to accurately detect and measure. Most analyses of sucralose are focused on quantification. Through nontargeted analyses, we identified extensive adduct formation in negative mode electrospray ionization (ESI) and in-source fragmentation with implications for quantification.

Dissolved organic matter in water samples from natural systems, septic tanks, and wastewater treatment plants were concentrated and de-salted by solid-phase extraction. Extracts were analyzed by ESI Fourier transform ion cyclotron resonance mass spectrometry (FTICR MS) in negative ion mode. Sucralose quantification was by high performance liquid chromatography (HPLC) triple quadrupole (QqQ) tandem mass spectrometry (MS/MS). Fragmentation of certain adducts was by Orbitrap MS/MS using collision-induced dissociation.

We identified sucralose $[M - H]^-$, formation of chloride $[M + Cl]^-$, formate $[M + CHOO]^-$, nitrate $[M + NO_3]^-$, bromide $[M + Br]^-$, iodide $[M + I]^-$, and other tentatively identified adducts, along with the apparent in-source fragmentation product, $[M - H - HCl]^-$. The in-source fragmentation product ion, and nitrate, bromide, and iodide adducts of sucralose do not appear to be previously described.

Sucralose appears to have similar adduct formation behavior as natural saccharides under soft-ionization techniques in negative ion mode. This has the potential to improve sucralose ionization and detection limits but may also complicate targeted quantification. Additionally, sucralose has 3 chlorine atoms, which increases numbers and relative abundances of isotopologues. This, in combination with extensive adduct ion formation, complicates the interpretation of high and ultrahigh resolution nontargeted MS spectra. For example, FTICR MS spectra of certain wastewater samples can have more than 50 *m/z* ions attributable to sucralose.

2.1 Introduction

Sucralose (SCL) (1,6-Dichloro-1,6-dideoxy-β-D-fructofuranosyl-4-chloro-4-deoxy-α-D-galactopyranoside, $C_{12}H_{19}Cl_3O_8$), is an artificial sweetener made by the chlorination of the natural, non-reducing disaccharide, sucrose (β-D-fructofuranosyl α-D-glucopyranoside). SCL is used in foods, beverages, and dental hygiene products, among other uses, and is highly resistant to degradation (Meyer et al., 1993; Roberts et al., 2000; Oppenheimer et al., 2011). This resistance to degradation has led to its commercial popularity as a noncaloric sweetener that is excreted almost unmetabolized, mainly in feces (Roberts et al., 2000). It has also been historically considered to have high thermal stability which has led to use in product formulation that involves heating, cooking, and recently e-cigarette liquid; however, recent studies have questioned its stability at high temperatures (de Oliveira et al., 2015; El-Hage et al., 2019; Eisenreich et al., 2020). SCL is used as an effluent source-tracer because of its specificity to human-derived wastewater, persistence through conventional wastewater treatment, and resistance to environmental degradation pathways

(Oppenheimer et al., 2011; Van Stempvoort et al., 2011). In regions where SCL is used, it is almost ubiquitously detected in septic system wastewater (Oppenheimer et al., 2011; Snider et al., 2017) and in WWTP inflow and treated outflow at similar concentrations (Buerge et al., 2009; Torres et al., 2011; Subedi and Kannan, 2014; Li et al., 2020). This detection extends to treated wastewater reuse-sourced reservoirs and drinking water (Mawhinney et al., 2011), as well as in all types of natural waters receiving wastewater impact; including groundwater (Van Stempvoort et al., 2011), streams and rivers (Loos et al., 2009; Cantwell et al., 2018), lakes and ponds (Oppenheimer et al., 2012; Wang et al., 2020), and coastal and marine waters (Mead et al., 2009; Cantwell et al., 2018). Additionally, SCL regulatory approval and usage patterns in combination with conservative tracer behavior mean the presence of SCL can be a temporal marker in waters, and it has been used this way in a septic system effluent plume (Robertson et al., 2016) and landfill leachates (Roy et al., 2014; Stefania et al., 2019).

SCL has been measured in complex matrices using a wide range of instrument techniques, some examples being gas chromatography/MS (GC/MS) (Mead et al., 2009), ion chromatography/MS/MS (IC/MS/MS) (Van Stempvoort et al., 2011; Snider et al., 2017), LC/evaporative light scattering detection (LC/ELSD) (Wasik et al., 2007), LC/quadrupole time-of-flight MS (LC/QTOFMS) (Ferrer et al., 2013), and LC/MS/MS (Ferrer et al., 2013). Predictably, different sample concentration and cleanup methods as well as quantification methods are also described in the literature. One of the most popular analytical methods for quantifying SCL is sample preparation using online or offline polymeric sorbent solid-phase extraction (SPE)

and subsequent quantification by LC/MS/MS using negative ion mode electrospray ionization (ESI) as the ion source (Buerge et al., 2009; Loos et al., 2009; Scheurer et al., 2009; Mawhinney et al., 2011; Torres et al., 2011; Kokotou and Thomaidis, 2013; Cantwell et al., 2018; Stefania et al., 2019). Note that in this text, we use LC to universally refer to traditional LC, HPLC, and ultrahigh performance LC (UHPLC).

High and ultrahigh resolution MS and MS/MS can also be used for quantitative (Batchu et al., 2015; Wang et al., 2020) and non-quantitative (Smirnov, 2018; Fu et al., 2020) detection of SCL based on mass accuracy, a characteristic three chlorine isotopic pattern, and/or indicative fragmentation pathways in positive or negative ion mode. The characteristic isotopic pattern visible in mass spectrometric data is due to the high relative natural abundances of the two stable chorine isotopes, ^{35}Cl (76%) and ^{37}Cl (24%), and the three chlorine atoms in SCL. The three highest abundance isotopologues of SCL, $^{12}C_{12}{}^{1}H_{19}{}^{35}Cl_{3}{}^{16}O_{8}$, $^{12}C_{12}{}^{1}H_{19}{}^{35}Cl_{2}{}^{37}Cl_{1}{}^{16}O_{8}$, and $^{12}C_{12}{}^{1}H_{19}{}^{35}Cl_{1}{}^{37}Cl_{2}{}^{16}O_{8}$, therefore, have relative abundances of 100:96:31 (Loos et al., 2015), assuming SCL atomic composition reflects natural abundance (Fig. 2.1).

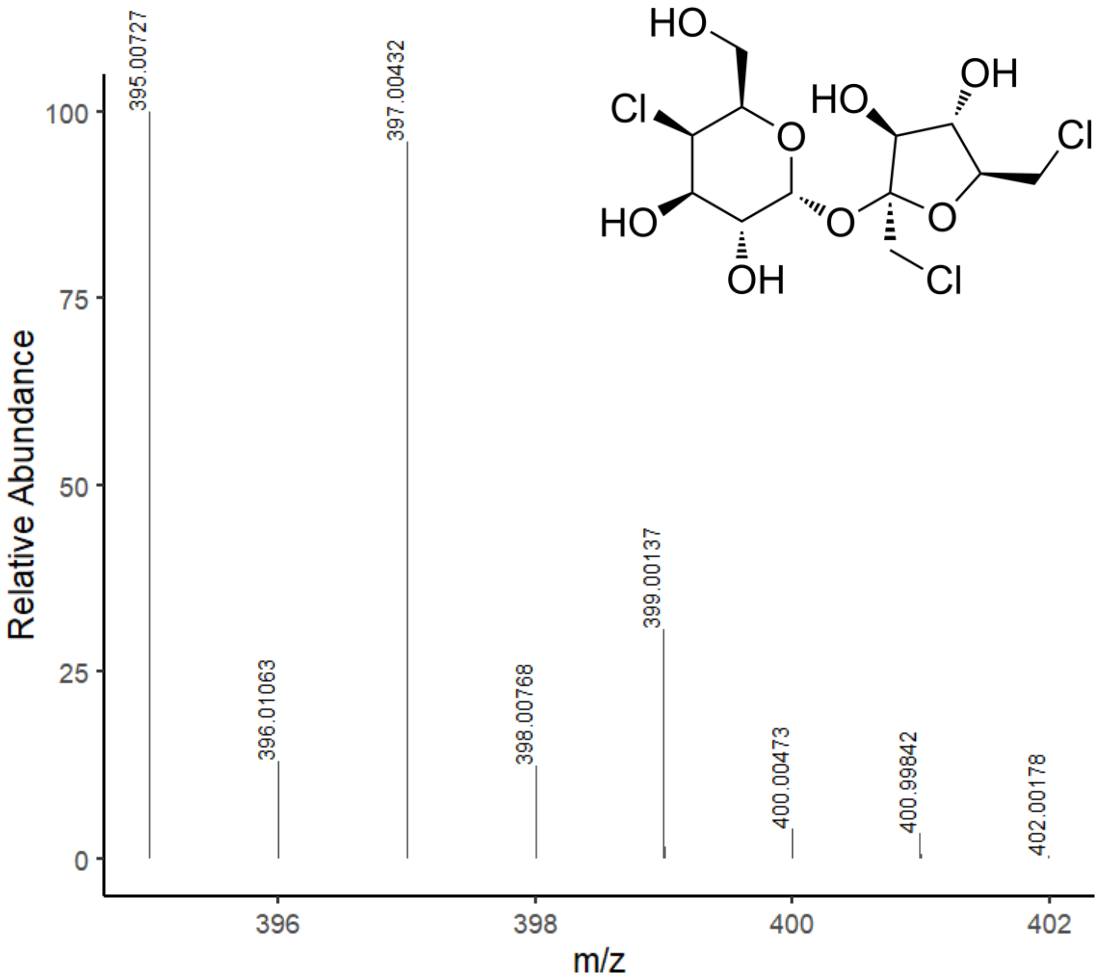

Figure 2.1 Chemical structure of SCL and theoretical $[M - H]^-$ mass spectrometric isotopic pattern simulated by Bruker IsotopePattern software at 650,000 resolution at 400 *m/z* with a 0.3 relative abundance threshold and labelling of the highest abundance isotopologues per subcluster.

Domestic wastewater source-tracing, food and product analysis, and metabolomics studies rely on accurate detection and quantification of SCL. A complicating factor of saccharide detection and quantification is extensive adduct ion formation when using soft ionization techniques in both positive and negative ion modes (Harvey, 2005; Jiang and Cole, 2005; Guan and Cole, 2008; Boutegrabet et al., 2012; Ruf, 2013). Saccharide adduct formation behavior has been more extensively

studied with lower energy, soft ionization like matrix-assisted laser desorption/ionization (MALDI) and ESI ion sources (Cai et al., 2002; Harvey, 2005; Jiang and Cole, 2005; Guan and Cole, 2008) but may also be relevant to other soft ionization techniques. Adduct ions form when one or more atoms or molecules interact with the analyte of interest, forming an ion that contains all atoms of the original analyte as well as the associated adducted atoms or molecules. Many factors are considered to contribute to analyte adduct formation including the presence of specific functional groups, stereochemistry, acidity, polarity, molecular size, solvent composition and purity, background ions in the matrix, and instrument parameters, particularly that affect analyte internal energy (Zhu and Cole, 2000; Cai et al., 2002; Harvey, 2005; Guan and Cole, 2008). Adduct formation can be undesirable because adduct ions can deflect signal from the desired ion and decrease analytical reproducibility.

Complicating matters is the intertwinement of adduct formation and fragmentation. In-source fragmentation, here referring to non-induced dissociation during soft ionization, not to be confused with source-induced dissociation (SID), is the unintended dissociation of ions into fragmentation product ions in the ion source. While in-source fragmentation or other dissociation before the detector can prevent the detection of adducts, adducting atoms or molecules can also promote decomposition of the adduct to the $[M - H]^-$ ion or other product ions before the detector (Harvey, 2005). The adducting atoms or molecules can also affect adduct ion fragmentation products in MS/MS, a behavior particularly seen for adduct ions of saccharides, meaning saccharide adduct ions can have different fragments than the

molecular $[M - H]^-$ ion under the same instrument parameters and dissociation techniques and energies (Harvey, 2005; Jiang and Cole, 2005).

Anion adduction can occur at electrophilic hydrogens (Zhu and Cole, 2000), and hydroxyl groups are common features to most saccharides. However, the fundamental structural influences of saccharides on adduct formation, particularly in consideration of the complex isomerism of reducing saccharides, are still poorly understood. Cai et al. (2002) demonstrated that for certain small saccharides, including sucrose, multiple hydrogen bonding plays a role in the formation and high stability of some anionic adducts in ESI MS. Many methods benefit from this adduct forming behavior and force adduct generation (e.g. addition of a dopant) (Bayer et al., 1999; Koch et al., 2014) to improve or allow ionization of neutral saccharides either through detection of the adduct or the decomposition product of the adduct (Harvey, 2005; Jiang and Cole, 2005; Guan and Cole, 2008). Adduct ions of saccharides are also used to gain structural information based on adduct formation trends and fragmentation product ions (Harvey, 2005; Jiang and Cole, 2005; Guan and Cole, 2008).

As a chlorine substituted disaccharide, SCL appears to show similar adduct formation behavior as natural saccharides, and has been previously found to produce adducts with chloride (Wu et al., 2014; Batchu et al., 2015; Cantwell et al., 2018), formate (Batchu et al., 2013; Wu et al., 2014; Batchu et al., 2015), and acetate (Ordoñez et al., 2013; Wu et al., 2014) in negative-mode soft ionization and adducts with sodium (Ferrer and Thurman, 2010; Batchu et al., 2013; Ferrer et al., 2013; Wu et al., 2014), ammonium (Ferrer and Thurman, 2010), and sodium chloride (Wood et

al., 2000) in positive-mode soft ionization MS. The formate (Wu et al., 2014; Wang et al., 2020), acetate (Ordoñez et al., 2013), and chloride (Wu et al., 2014; Cantwell et al., 2018) adducts of SCL have been used to improve analytical sensitivity. In contrast to natural saccharides, SCL adduct formation is largely unstudied. Most previously known adducts observed in LC/MS and LC/MS/MS were formed intentionally or directly related to mobile phase additives or background sodium contamination. While chloride can be a common contaminant in mass spectrometry, Wu et al. (2014) observed the chloride adduct with low consistency after cleanup of the ionization source and with no known source in the mobile phase, and suggested the source of chloride could be SCL in-source fragmentation or impurities in SCL standards.

When dealing with a high potential for adduct formation it is necessary to identify possible adduct ions, consider contributing factors to adduct formation, and to use quantification methods that account for this behavior. As part of a larger project molecularly characterizing natural freshwaters impacted by septic system wastewater, we conducted nontargeted ultrahigh resolution ESI FTICR MS on a sample from an artificial lake and a large seasonal set of samples from nine small, nontidal streams. In this dataset we happened to identify extensive adduct ions of SCL. We then assessed ESI FTICR MS data from untreated septic system wastewater and WWTPs for adducts of SCL to better understand adduct formation. In these datasets we identified the $[M - H]^-$ SCL ions; chloride $[M + Cl]^-$, formate $[M + CHOO]^-$, nitrate $[M + NO_3]^-$, bromide $[M + Br]^-$, and iodide $[M + I]^-$ SCL adducts; and the apparent in-source fragmentation ions $[M - H - HCl]^-$. Tentatively, other potential SCL adducts, such as with trifluoroacetate, bisulfate, and benzenesulfonates,

may also be present in spectra. To our best knowledge, the in-source fragmentation ion and nitrate, bromide, and iodide adducts have not been previously described. Possible determining factors for adduct formation considering sample matrices and analytical techniques is discussed. We demonstrate the same adduct formation in ESI Orbitrap MS and that the chloride and bromide adducts can be readily observed in HPLC/ESI Orbitrap MS. We performed fragmentation experiments by Orbitrap MS/MS on the chloride, formate, and bromide adducts.

Identified adducting ions are previously known for natural oligosaccharides (Cai et al., 2002; Harvey, 2005; Jiang and Cole, 2005; Guan and Cole, 2008; Gabbanini et al., 2010). The current study shows that SCL has similar adduct formation potential. This understanding opens many possibilities to improve the notoriously poor ionization of SCL. These conclusions have relevance to sample preparation, mobile phase selection, and method development, and internal standard (ISTD) selection. These results have especially significant implications to nontargeted, full scan, high resolution and ultrahigh resolution MS analyses. This adduct formation behavior could make SCL appear absent in spectra. Additionally, this adduct formation for a molecule with 3 chlorine atoms creates an unprecedented number of *m/z* ions that can be related to one chemical in FTICR MS spectra of real-world samples. For example, in a wastewater treatment sample analyzed by standard methods, we found at least 50 *m/z* ions to be attributable to SCL. These ions have mass decimals characteristic of more chlorinated organohalogens and have a high potential for misidentification during formula assignment. Even more extensive

anionic adduct formation is suggested by these samples and should be further explored.

2.2 Experimental

2.2.1 Materials

Hydrochloric acid for sample acidification was pure grade 32% solutions from Acros Organics. All methanol (MeOH), 0.1% (v/v) formic acid (FA) water, and isopropanol (IPA), used in SPE and instrument analyses was LC/MS grade. Ultrapure water used in SPE and instrument analysis had a resistivity of 18.2 MΩ·cm and was from in-lab systems. Ammonium acetate (AA) was purchased from Sigma-Aldrich and was ≥99.0% purity. The SCL analytical standard used in the SPE recovery experiment and quantification standard curves was purchased from Sigma-Aldrich and is ≥98.0% purity. The SCL-d6 ISTD used in quantification was obtained from Toronto Research Chemicals and has an isotopic purity of ≥98.0%.

2.2.2 Sample collection and solid-phase extraction of water samples

Duplicate 2 L grab water samples were collected from eight streams and one lake in Calvert County, MD, USA and one stream in Anne Arundel County, MD, USA. Stream samples were taken approximately monthly, at baseflow hydrological conditions between October 2016 and November 2017. Lake samples were taken in February 2017. A total of 198 samples were collected, for twelve months of sampling from eight stream sites in duplicate, two months of sampling from one stream site because of no flow conditions most of the year, and one month of sampling from the lake site. Glass bottles were pre-combusted (500 °C) and sample rinsed three times in

the field before sample collection. In the lab, samples were vacuum filtered through pre-ashed 0.7 µm glass microfiber filters (Whatman GF/F) into combusted glass bottles, acidified to pH 2 using hydrochloric acid, and desalted and concentrated by solid-phase extraction using Agilent Bond Elut PPL cartridges (1 g, 3 mL) generally following the previously described procedure (Dittmar et al., 2008). Cartridges were activated with 5 mL MeOH, rinsed with 5 mL 0.1% FA water, then loaded with the filtered and acidified sample by gravity or a peristaltic pump as necessary. After sample loading, cartridge exteriors were rinsed with ultrapure water and the sorbent was rinsed with 5 mL 0.1% FA water to remove salts. Cartridges were dried, and eluted with 10 mL MeOH into new, trace contaminant certified or acid-washed and combusted 40 mL amber vials. None of the sites in our study receive drainage with potential sources of WWTP effluent.

Septic system wastewater was sampled from traditional, one or two chambered systems serving single households in MD, USA. Water samples were collected from below the grease layer in the tank chambers using acid washed tubing lowered through the access lid and a peristaltic pump. Duplicate samples were collected in combusted glass bottles after sample rinsing three times. Six septic tanks were sampled in total, and in two of these six systems, samples were taken from the first and second chamber. In one of these systems the second chamber was oxygenated by an aeration system. In the lab, samples were filtered and subsampled to approximately 500 mL if one chamber was sampled or to 250 mL for the first chamber and 500 mL for the second if both were sampled. They were then acidified and extracted as previously described, but the 0.1% formic acid water rinse after

sample loading was increased to 30 mL to account for the higher salt content in wastewater.

Tertiary treated final effluent samples from a WWTP in the United States (Effluent-A) were 1 L samples extracted in triplicate using Bond Elut PPL cartridges (1 g, 6 mL) which were activated with 10 mL MeOH, rinsed with 10 mL 0.1% FA water, loaded with the acidified sample, rinsed with 10 mL 0.1% FA water to remove salts, then dried and eluted as described. Samples from a second WWTP in the United States, including two different influent samples (Influent-B1 and Influent-B2) that join together for an unsampled final influent and an effluent sample (Effluent-B), were 300 mL samples extracted using the same method as described for Effluent-A. All extracts were stored at -20 °C between analyses.

2.2.3 ESI FTICR MS analysis

Natural water sample SPEs were diluted in MeOH with a 1:40 dilution factor and analyzed on a 12 Tesla Bruker solariX FTICR MS with an Apollo II ESI source operated in negative ion mode. Samples were introduced to the ESI source using an autosampler at a flow rate of 120 µL/h. MeOH blanks were run after every 20 samples. Spectra were acquired with a time-domain transient of 4 megawords and a 500 scan accumulation over an *m/z* range of 147-1000. Spectra were then lightly smoothed and calibrated with a mass list of molecular formulae consistently found in natural organic matter using the Bruker DataAnalysis software. Peak lists were exported with a signal-to-noise ratio cutoff of ≥10. A peak aligned matrix of the 198 samples was generated using a matrix generator software (Lucio, 2009) with a window width of 1.2 ppm.

Septic system wastewater SPEs were analyzed similarly but were manually injected using a syringe and syringe pump at a flow rate of 120 µL/h and acquired with a 300 scan accumulation over an *m/z* range of 130-1000. Spectra were then smoothed and calibrated using a mass list of molecular formulae typically found in wastewater, including common surfactants. A data matrix was produced as described, with a 1 ppm window width, containing 16 samples, representing 8 chambers in sample duplicates.

Effluent-A SPEs were diluted in MeOH with a 1:40 dilution factor and introduced by autosampler and analyzed as described for natural water samples over an *m/z* range of 130-1000. Influent-B and Effluent-B SPEs were diluted with a 1:40 dilution factor, introduced by autosampler, and analyzed over an *m/z* range of 100-1200. Spectra processing was the same as septic system wastewater. Data matrices were produced separately for the mass lists from the two WWTPs, with Influent-B and Effluent-B as part of a larger sample matrix, and both matrices were made with a 1 ppm window width.

2.2.4 Adduct Identification

SCL was identified in FT data by exact matching of *m/z* values and intensities to the distinctive three chlorine isotopic pattern of $[M - H]^-$ SCL. This was further confirmed by corresponding quantitative measurements. The chloride and bromide adducts were initially identified in the extensive natural waters dataset based on correlation with the intensities of the $[M - H]^-$ SCL ions, exact matching to expected masses, and a four chlorine isotopic pattern and three chlorine, one bromine, isotopic pattern.

This and other wastewater datasets were then checked for other adducts of SCL by searching for masses corresponding to other commonly occurring adducting anions (Huang et al., 1999) and those known to occur for saccharides (Harvey, 2005; Guan and Cole, 2008) and SCL. A script that filtered for an approximate chlorine isotopic spacing (1.997 *m/z*) was used to further check mass lists. These results could then be further filtered for features such as accuracy to exact isotopic spacing, signal intensity ratios between potential isotopic *m/z* ions, mass decimals, or signal correlations with the already identified SCL related *m/z* ions. Determinations were undertaken in consideration of quantified SCL concentrations in the samples. The adduct and potential adduct ions were molecularly assigned using the SmartFormula feature of Bruker DataAnalysis with isotopic pattern matching using the Bruker IsotopePattern software and enviPat by Loos et al. (2015). While the FTICR MS instrument used in this study only has a typical mass resolution slightly above 400,000 at 400 *m/z*, a much higher 650,000 mass resolution input was used in isotopic pattern modelling programs to better match the observed fine isotope patterns in spectra, particularly for the bromide adduct.

2.2.5 SCL and other chemical quantification

SCL was quantified in all samples by HPLC/QqQMS/MS using an Agilent 1260 Infinity II LC and an Agilent 6420 Triple Quadrupole MS. Instrument control and data processing was carried out using the Agilent MassHunter software suite. An Agilent 1260 Infinity II Vialsampler autosampler was used to inject 7 µL of samples with an isopropanol needle wash step between injection. The LC columns were an ACE Excel C18-PFP (3.0 mm i.d. × 100 mm, 2 µm particle size) connected to an

ACE HILIC-B (2.1 mm i.d. × 50 mm, 1.7 µm particle size) with a MAC-MOD UltraShield pre-column filter, and the thermostatted column oven was set to 50 °C. Mobile phase A was MeOH and B was 0.1% FA water. The flow rate was 250 µL/min with the separation gradient beginning at 50% mobile phase A, increasing to 97% mobile phase A for 0.3-9.5 min, and 98% mobile phase A until 10.0 min, and then returning to 50% mobile phase A. For MS settings, the carrier gas was high purity nitrogen from a Peak Scientific Genius NM32LA nitrogen generator and the collision gas was ultrahigh purity nitrogen. Capillary voltage was 5000 V in positive mode, gas temperature was 350 °C, gas flow was 10 L/min, nebulizer gas pressure was 35 psi, and delta electron multiplier voltage (+) was 400 V.

An ISTD quantification method was used to account for fluctuations in instrument performance, analyte behavior, and matrix ion suppression. A target SCL transition and a stable isotope-labelled (SIL), here SCL-d6, ISTD transition were used for standard curve quantification. A second SCL transition was monitored as a qualifier to further confirm identity. The SIL ISTD spike was added at 30 µg/L to all blanks, calibration standards, quality control standards, and samples before instrument analysis. An injection standard method was used, instead of a pre-SPE spike, to not conflate the effects of extraction recovery with analytical performance.

Other analytes were quantified with SCL, so the MS/MS method used ESI polarity switching, dynamic selective reaction monitoring (SRM) mode, and non-resonant CID, monitoring the positive mode transitions 419 $[M + Na]^+ \rightarrow 221$ *m/z* $[C_6H_{11}ClO_5 + Na]^+$, 419 → 239 *m/z* $[C_6H_{10}Cl_2O_4 + Na]^+$, and 425 $[M\text{-}d6 + Na]^+ \rightarrow$ 243 *m/z* $[C_6H_{10}Cl_2O_4\text{-}d4 + Na]^+$ as the target, qualifier, and ISTD transitions,

respectively. For all SCL-related monitored transitions, fragmentor voltage was 120 V, collision energy was 15 V for the target transition and 19 V for the other transitions, and cell accelerator voltage was 7 V. Positive ion mode and monitored transitions were selected using the Agilent MassHunter Workstation software optimization feature and are also previously described (Ferrer et al., 2013). Quantification was done in triplicate and averaged. Results were corrected for SPE concentration factors and analysis dilution factors. Results were not corrected for SPE recovery as our previous PPL SPE SCL recovery experiments show ≥100% recovery (Table A4.12).

Chloride was quantified in stream whole water samples by a standard calibration curve, IC method in selected whole waters using a Dionex AS40 Autosampler and Dionex ICS-1000 IC with a Dionex IonPac AG22 (4 × 50 mm) guard column, IonPac AS22 (4 × 250 mm) column, and an ASRS 300 (4 mm) suppressor. A sodium bicarbonate/carbonate eluent was used at a 1.2 mL/min flow rate with a 50 mA suppressor current. Combined nitrate-nitrite (hereafter referred to as nitrate) was quantified in stream and septic system whole waters by the Nutrient Analytical Services Laboratory, CBL (MD, USA), referencing standard method ASTM D7781-14 (ASTM International, 2014).

2.2.6 ESI Orbitrap MS and MS/MS experiments

We used a Thermo LTQ Orbitrap XL Hybrid Ion Trap-Orbitrap Mass Spectrometer with an ESI ion source in negative ion mode and the FTMS (Orbitrap) detector for all analyses. The carrier gas was high purity nitrogen generated as previously described and the collision gas was ultrahigh purity helium. An Eksigent

Nano LC Ultra was used as a direct pump for MeOH to the Orbitrap and flow was 10 µL/min. The Thermo Tune Plus software was used for instrument control and Thermo Xcalibur 2.1 for data processing. A duplicate SPE from the freshwater stream with the highest SCL concentrations was diluted 1:40 with MeOH and directly injected by syringe and loop injection. For MS/MS, fragments were generated for the monoisotopic and highest signal intensity isotopic *m/z* peaks for the chloride (430.98, 432.98) and bromide (474.93, 476.93 *m/z*) adducts at a 1 *m/z* window width. Note that both the 432.98 and 476.93 *m/z* targets include two isotopologues of signal relevancy. For the source settings the heater temp was 60 °C, sheath gas flow rate was 7, auxiliary gas flow rate was 2, sweep gas flow rate was 0, spray voltage was 3.8 kV, capillary temperature was 275 °C, capillary voltage was −45 V, and tube lens was −129.0 V. The mass resolution was 15,000 and scan time was 2 microscans with a maximum inject time of 40 ms. Fragmentation was by resonant CID at collision energies of approximately 15 and 40 eV in full scan mode, recording approximately 150 scan averages.

The Effluent-B SPE was diluted 1:10 with MeOH and directly injected at 4 µL/min. The heater temp was 98 °C, sheath gas flow rate was 12, auxiliary gas flow rate was 1, capillary voltage was −50 V, and tube lens was −98.3 V. Other settings were the same. We performed full scan MS analysis at 60,000 resolution with a scan range of 80-700 *m/z*, recording a 50 scan average, to show adduct formation in ESI Orbitrap MS. The same sample was diluted 1:2 and a full scan was undertaken at 15,000 resolution, with a scan range of 500-600 *m/z*, and recording 40 scans for iodide adduct ions. For MS/MS, fragments were generated for the monoisotopic and

second highest signal intensity isotopic *m/z* peaks for the formate (441.01, 443.01 *m/z*) adduct at these same settings and 0, 15, 40, and 60 eV CID, recording approximately 33 scan averages. Scan ranges were set to the minimum allowed *m/z* to slightly beyond the precursor *m/z* ions for all MS/MS experiments. While the nitrate, iodide, and tentative trifluoroacetate SCL adducts were visible by Orbitrap MS, fragmentation was not possible because of low signal intensity.

The same effluent sample was analyzed undiluted by HPLC/Orbitrap MS to test if the chloride and bromide, the two generally highest signal intensity, adducts could be observed. The LC/MS experiments were carried out using an Agilent 1260 Infinity II LC system coupled to the Orbitrap MS. An Agilent 1260 Infinity II Multisampler autosampler was used to inject 2 µL of sample per test. The sample was spiked with SCL-d6 at 35 µg/L. Separation was performed on an ACE Excel 5 SuperC18 column at isocratic conditions of 90% 0.01 % w/v AA in MeOH, 10% 0.01% w/v AA in water for 10 min. Column temperature was 50 °C, and flow rate was 0.1 mL/min until 5 min, increasing to 0.6 mL/min at 6 to 9 min for cleanup, then returning to 0.1 mL/min at 10 min. For ESI source settings the heater temp was 280 °C, sheath gas flow rate was 20, auxiliary gas flow rate was 8, sweep gas flow rate was 8, spray voltage was 3.8 kV, capillary temperature was 375 °C, capillary voltage was −10 V, and tube lens was −51.0 V. Detection was using selected ion monitoring (SIM) at 7500 resolution where the first test monitored the first isotopic peak of SCL (395 *m/z*) and the second major isotopic peak of SCL-d6 (403 *m/z*) as two scan events, a second test monitored only the second major isotopic peak of the chloride

adduct (433 *m/z*), and a third test monitored only the second major isotopic peak of the bromide adduct (477 *m/z*). All had a 1 *m/z* window width.

2.3 Results and Discussion

2.3.1 Evidence for Adduct Ions and Other Sucralose Related Ions

The ESI FTICR MS datasets clearly show the presence of SCL $[M - H]^-$ ions; in-source fragment $[M - H - HCl]^-$ ions; and chloride $[M + Cl]^-$, formate $[M + CHOO]^-$, nitrate $[M + NO_3]^-$, bromide $[M + Br]^-$, and iodide $[M + I]^-$ adduct ions (Figs. 2.2, 2.3). Of these, the chloride and formate adducts are previously known for SCL (Wu et al., 2014; Batchu et al., 2015). To our best knowledge, the in-source fragmentation behavior and nitrate, bromide, and iodide adducts have not been previously described; however, these adducting anions have all been previously observed to form stable adducts with other saccharides (Cai et al., 2002; Harvey, 2005; Jiang and Cole, 2005; Guan and Cole, 2008; Gabbanini et al., 2010). Additionally, saccharide in-source fragmentation behavior in relation to adduct formation is well-known (Harvey, 2005), and the in-source fragment is the same as the major known SCL negative ion mode MS/MS product ion (Ferrer et al., 2013). While exact ion *m/z* values, isotopic pattern matching, formula assignment and signal trends across samples from the FTICR MS data in context of SCL concentrations in samples provide very strong evidence for the related ions, Orbitrap MS/MS experiments show even more definite SCL relation, and will therefore, be described first.

2.3.2 Orbitrap MS/MS for Adduct Ions

Negative ion mode ESI Orbitrap MS/MS experiments are presented in Table 2.1. The chloride adduct shows the loss of a chlorine and a hydrogen atom, forming the deprotonated SCL $[M - H]^-$ ion, as well as a loss of two chlorine and hydrogen atoms, likely forming the major known negative ion mode fragment ion of SCL $[M - HCl - H]^-$. Similar consecutive dissociation of saccharide chloride adducts has been demonstrated using other ionization and dissociation techniques (Zhu and Cole, 2001; Jiang and Cole, 2005; Guan and Cole, 2008). and may suggest an association between chloride adduct formation and in-source fragmentation. Fragmentation of the formate adduct only shows the loss of formate and a hydrogen atom, producing the deprotonated SCL $[M - H]^-$ ion. Fragmentation of the bromide adduct shows the loss of a bromine and hydrogen atom, or the deprotonated SCL $[M - H]^-$ ion, but also another apparent product ion requiring rearrangement that may be a chloride or bromide adduct of a neutral product or a deprotonated ion.

Table 2.1 Results from Orbitrap CID MS/MS experiments, where precursor ions are from the lowest eV CID analyses, and product ions are from the 40 eV CID analyses. Most product ion identities assume loss of adducting ion first, neutral loss, and no rearrangement, and may not reflect true dissociation pathways. Only isotopologues of relevant abundance are considered.

Precursor Ions				**Product Ions**			
Adducting Anion	**Observed *m/z***	**Exact *m/z***	**Proposed Identity**	**Observed *m/z***	**Exact *m/z***	**Formula**	**Proposed Identity**
Chloride	430.98220	430.98395	$[C_{12}H_{19}{}^{35}Cl_3O_8 + {}^{35}Cl]^-$	395.00555	395.00727	$C_{12}H_{18}{}^{35}Cl_3O_8^-$	$[C_{12}H_{19}{}^{35}Cl_3O_8 + {}^{35}Cl - H^{35}Cl]^-$
				359.02860	359.03060	$C_{12}H_{17}{}^{35}Cl_2O_8^-$	$[C_{12}H_{19}{}^{35}Cl_3O_8 + {}^{35}Cl - H^{35}Cl - H^{35}Cl]^-$
	432.97926	432.98100	$[C_{12}H_{19}{}^{35}Cl_3O_8 + {}^{37}Cl]^-$	397.00241	397.00432	$C_{12}H_{18}{}^{35}Cl_2{}^{37}ClO_8^-$	$[C_{12}H_{19}{}^{35}Cl_2{}^{37}ClO_8 + {}^{35}Cl - H^{35}Cl]^-$
			$[C_{12}H_{19}{}^{35}Cl_2{}^{37}ClO_8 + {}^{35}Cl]^-$	395.00555	395.00727	$C_{12}H_{18}{}^{35}Cl_3O_8^-$	$[C_{12}H_{19}{}^{35}Cl_3O_8 + {}^{37}Cl - H^{37}Cl]^-$
				361.02553	361.02765	$C_{12}H_{17}{}^{35}Cl^{37}ClO_8^-$	$[C_{12}H_{19}{}^{35}Cl_2{}^{37}ClO_8 + {}^{35}Cl - H^{35}Cl - H^{35}Cl]^-$
				359.02846	359.03060	$C_{12}H_{17}{}^{35}Cl_2O_8^-$	$[C_{12}H_{19}{}^{35}Cl_2{}^{37}ClO_8 + {}^{35}Cl - H^{35}Cl - H^{37}Cl]^-$ and $[C_{12}H_{19}{}^{35}Cl_3O_8 + {}^{37}Cl - H^{37}Cl - H^{35}Cl]^-$
Formate	441.01255	441.01275	$[C_{12}H_{19}{}^{35}Cl_3O_8 + HCO_2]^-$	395.00628	395.00727	$C_{12}H_{18}{}^{35}Cl_3O_8^-$	$[C_{12}H_{19}{}^{35}Cl_3O_8 + HCO_2 - H_2CO_2]^-$
	443.00871	443.00980	$[C_{12}H_{19}{}^{35}Cl_2{}^{37}ClO_8 + HCO_2]^-$	397.00303	397.00432	$C_{12}H_{18}{}^{35}Cl_2{}^{37}ClO_8^-$	$[C_{12}H_{19}{}^{35}Cl_2{}^{37}ClO_8 + HCO_2 - H_2CO_2]^-$
Bromide	474.93178	474.93344	$[C_{12}H_{19}{}^{35}Cl_3O_8 + {}^{79}Br]^-$	438.95552	438.95676	$C_{12}H_{18}{}^{35}Cl_2{}^{79}BrO_8^-$	rearrangement, simplified identity may be $[C_{12}H_{18}{}^{35}Cl_2O_8 + {}^{79}Br]^-$, $[C_{12}H_{18}{}^{35}Cl^{79}BrO_8 + {}^{35}Cl]^-$, and/or $[C_{12}H_{19}{}^{35}Cl_2{}^{79}BrO_8 - H]^-$
				395.00565	395.00727	$C_{12}H_{18}{}^{35}Cl_3O_8^-$	$[C_{12}H_{19}{}^{35}Cl_3O_8 + {}^{79}Br - H^{79}Br]^-$
	476.93011	476.93049	$[C_{12}H_{19}{}^{35}Cl_2{}^{37}ClO_8 + {}^{79}Br]^-$	440.95247	440.95381	$C_{12}H_{18}{}^{35}Cl^{37}Cl^{79}BrO_8^-$	rearrangement, simplified identity may be $[C_{12}H_{18}{}^{35}Cl^{37}ClO_8 + {}^{79}Br]^-$, $[C_{12}H_{18}{}^{35}Cl^{79}BrO_8 + {}^{37}Cl]^-$, $[C_{12}H_{18}{}^{37}Cl^{79}BrO_8 + {}^{35}Cl]^-$, and/or $[C_{12}H_{19}{}^{35}Cl^{37}Cl^{79}BrO_8 - H]^-$
		476.93139	$[C_{12}H_{19}{}^{35}Cl_3O_8 + {}^{81}Br]^-$		440.95471	$C_{12}H_{18}{}^{35}Cl_2{}^{81}BrO_8^-$	rearrangement, simplified identity may be $[C_{12}H_{18}{}^{35}Cl_2O_8 + {}^{81}Br]^-$, $[C_{12}H_{18}{}^{35}Cl^{81}BrO_8 + {}^{35}Cl]^-$, and/or $[C_{12}H_{19}{}^{35}Cl_2{}^{81}BrO_8 - H]^-$
				397.00184	397.00432	$C_{12}H_{18}{}^{35}Cl_2{}^{37}ClO_8^-$	$[C_{12}H_{19}{}^{35}Cl_2{}^{37}ClO_8 + {}^{79}Br - H^{79}Br]^-$
				395.00288	395.00727	$C_{12}H_{18}{}^{35}Cl_3O_8^-$	$[C_{12}H_{19}{}^{35}Cl_3O_8 + {}^{81}Br - H^{81}Br]^-$

Results across experiments followed expected isotopic patterns. Product ions are described using neutral losses for clarity, but this does not necessarily reflect the identities or final charge states of the losses, all of which are below mass range using CID MS/MS on this model of Orbitrap (≤ 115 *m/z* for these experiments). Others have observed Cl^- as a SCL MS/MS product ion using analytical techniques with lower *m/z* cutoffs (Berset and Ochsenbein, 2012; Ferrer et al., 2013; Gan et al., 2013). Additionally, anionic saccharide adducts, $[M + A]^-$, have been described as having competing dissociation pathways, as neutral loss, producing $[M - H]^-$ and [HA] fragments or as loss of the adducting anion, producing [M] and $[A]^-$ fragments (Cai et al., 2002), the latter of which would not be detectable with this Orbitrap *m/z* cutoff. Additionally, MS/MS was done on SPEs with complex dissolved organic matter (DOM) matrices, and therefore background ions, so data was assessed by considering known SCL dissociation patterns, *m/z* decimals characteristic of organochlorines, isotopic patterns, and known background ions or ions present at 0 eV CID, as applicable. This may bias conclusions against lower signal intensity fragment ions and more complex fragmentation behavior. Future work is recommended to perform fragmentation experiments on adducts generated using dopants and SCL analytical standards as well as using other dissociation techniques.

2.3.3 Sucralose Related Ion Formation in FTICR MS

Relevant FTICR MS and other corresponding data are available in a data repository (https://figshare.com/s/3352e8215764b8c102d3). Extensive adduct formation is shown in samples with generally increasing observable adducts with SCL concentrations (Fig. A1.16).

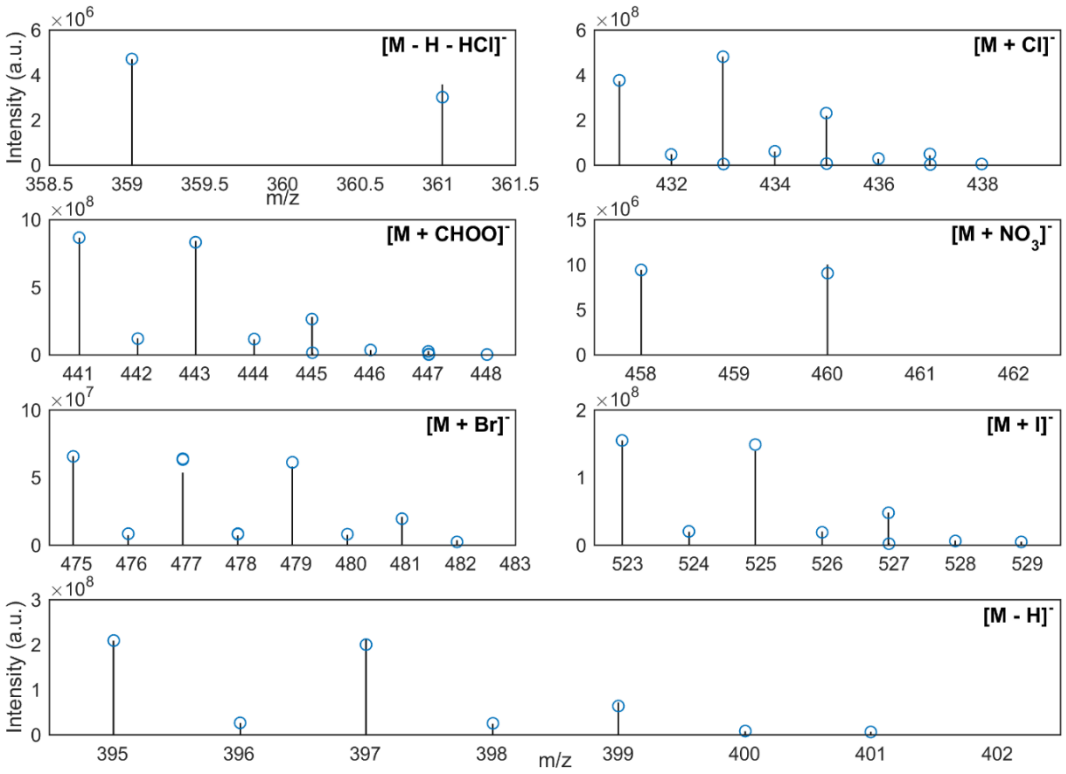

Figure 2.2 SCL related *m/z* ions (black bars), as observed in the Influent-B2 SPE by FTICR MS, compared to scaled corresponding theoretical isotopic patterns (blue circles) at 650,000 resolution at 400 *m/z*. Note, background ions are not shown for optimized visualization. All matched ions had mass errors ≤ 0.74 ppm, with mass error typically < 0.10 ppm. Please see Figures A1.1-A1.7 for larger, detailed figures with exact mass error labels.

In the stream dataset, the in-source fragment, SCL, and chloride, formate, nitrate, bromide, and iodide adducts are observed, though most can only be seen in the spectra of the highest SCL stream site (13 µg/L average SCL concentration as measured by targeted LC/QqQMS/MS). This large dataset shows a fairly consistent pattern of relative signal intensities of ions for these samples, where the signal intensity generally ranks from higher to lower: molecular $[M - H]^-$, $[M + Br]^-$, $[M + CHOO]^-$, $[M + Cl]^-$, for the four higher and more consistently appearing species (Fig. A1.16).

The septic system wastewater (maximum 109 µg/L SCL) and WWTP Effluent-A (21 µg/L SCL) FTICR MS datasets contained ions corresponding to all conclusive species, except the iodide adduct. The WWTP Influent-B1 (61 µg/L SCL), Influent-B2 (134 µg/L SCL), and Effluent-B (76 µg/L SCL) had ions corresponding to all species, except the nitrate adduct which was only observed in the Influent-B2 and Effluent-B, and the in-source fragment which was only observed in Influent-B2. Across all samples, in-source fragmentation was only seen in higher sucralose concentration (≥5 µg/L) samples.

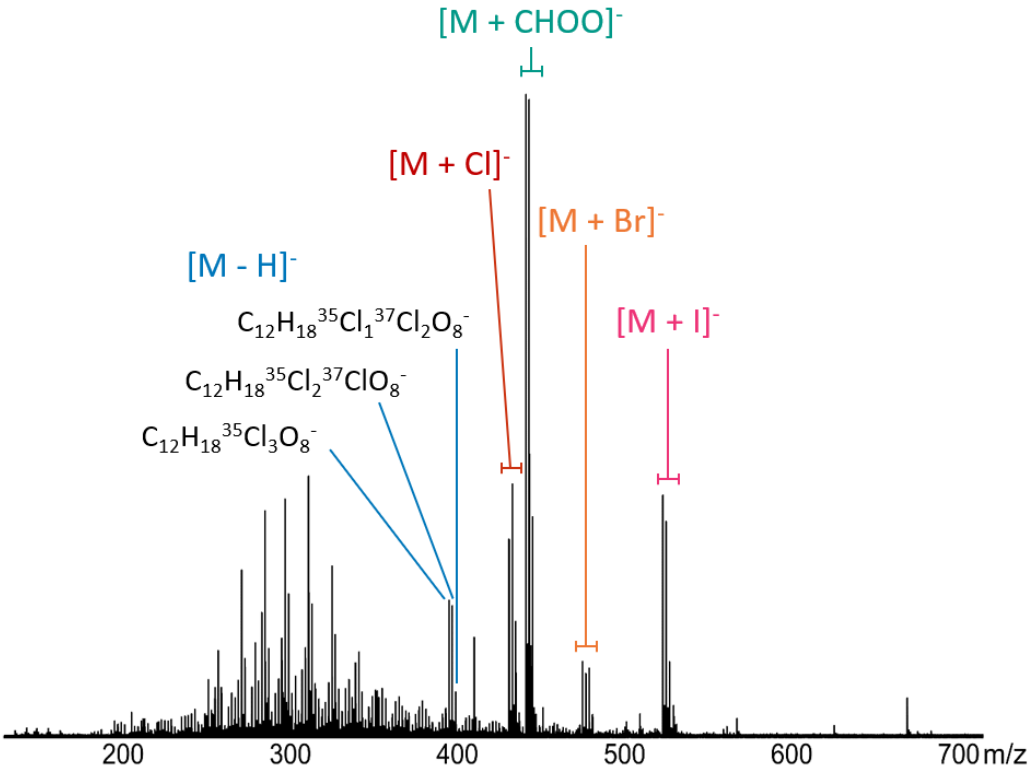

Figure 2.3 Mass spectrum of the Effluent-B wastewater SPE by FTICR MS showing prominence of certain sucralose related ions.

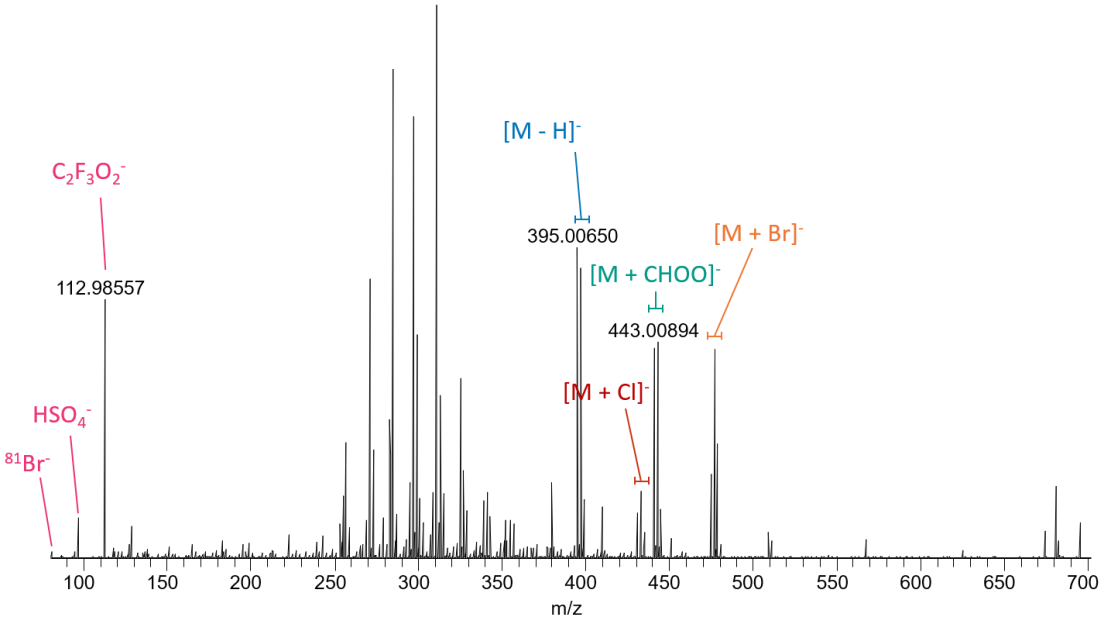

Figure 2.4 Mass spectrum of the Effluent-B wastewater SPE by flow-injection Orbitrap MS. See Figures A1.17-1.22 for magnified figures and A1.23 for the iodide adduct.

These described SCL associated species are confidently identified for the reasons mentioned, such as the exact matching of experimental mass and isotopic patterns and the correlations between ion signals, but also based on the lack of more reasonable alternatives during assignment. Considering the observed adduct formation, in-source fragmentation is a common co-occurrence (Harvey, 2005). All adducting anions are known for saccharides (Cai et al., 2002; Harvey, 2005; Jiang and Cole, 2005; Guan and Cole, 2008; Gabbanini et al., 2010), and while similar extensive formation of reasonably stable adducts has not been described for the chlorinated saccharide, SCL, it is also not surprising. As described in the following section, some adducting anions can be observed unattached by lower mass cutoff Orbitrap MS.

We additionally propose the possibility of more, tentative but supported, SCL adducts with trifluoroacetate (TFA−H), bisulfate (HSO_4), and certain benzenesulfonates. Corresponding data are available (https://figshare.com/s/3352e8215764b8c102d3, Figs. A1.9-A1.15) and also include further *m/z* ions that could fit sucralose adduct patterns. These are observed in fewer samples and may be lower signal intensity with less isotopologues visible but have exact masses and isotopic patterns for the proposed identities. The possibility of trifluoroacetate and bisulfate adducts is supported because they are known stable adducting anions of saccharides (Cai et al., 2002; Harvey, 2005; Jiang and Cole, 2005). The *m/z* ions that may be the bisulfate adduct were only observed in a single duplicate of the sampled lake (average 4 μg/L SCL) and a duplicate of a sample from the highest sucralose stream site in the freshwater dataset. The *m/z* ions that may be trifluoroacetate adducts are visible in FTICR MS spectra of the highest sucralose concentration samples, Influent-B2 and Effluent-B, as well as in the Orbitrap MS full scan spectrum of Effluent-B along with the unassociated trifluoroacetate ion (Fig. 2.4). The unassociated bisulfate ion is also visible in this Orbitrap MS spectrum.

The highest signal intensity potential benzenesulfonate adduct is with a $C_8H_9SO_3^-$ associated anion, though other likely benzenesulfonate adducts are also suggested. Similar benzene sulfonates have been shown to be very stable adducting ions of oligosaccharides, including disaccharides (Wong et al., 2000). These potential adduct signals all follow expected patterns of correspondence of both known high presence of sucralose and presence of the unassociated anion at higher intensity. For example, if sucralose is present at high concentration, but the *m/z* ion of the

associated surfactant is not visible or is at lower signal intensity in the FTICR MS spectra, the potential SCL adduct *m/z* ions are also absent. The potential benzenesulfonate SCL adducts are seen in the FTICR MS spectra of the Influent-B1 and Influent-B2, as well as some septic system wastewater samples, all of which are untreated, higher sucralose concentration wastewaters. One, which may be a sulfophenyl carboxylic acid-type anion (Gonsior et al., 2011), is also seen in Effluent-A. Any potential formation in freshwater samples could not be discerned among the complex DOM background.

2.3.4 Sucralose Related Ion Formation in LC Orbitrap MS and Orbitrap MS

Analysis of the Effluent-B sample by nontargeted high resolution Orbitrap MS shows similar adduct formation as the corresponding FT-ICR-MS spectrum (Figs. 2.3, 2.4). Differences include decreased signal intensity of the chloride, formate, and iodide adduct ions and increased signal intensity of the potential trifluoroacetate adduct ions relative to the molecular sucralose ions. Differences in the bromide adduct isotopic pattern reflect the lower resolving power of an Orbitrap MS. Unassociated anions corresponding to the masses of trifluoroacetate, bisulfate, bromide, and iodide can be seen in the lower *m/z* cutoff, Orbitrap MS spectrum (Figs. 2.4, A1.21, A1.22). HPLC/Orbitrap MS experiments show that at least the chloride and bromide SCL adducts are also observable by LC/MS (Figs. A1.24-26).

2.3.5 Factors for Adduct Formation

There are multiple possible sources of adducting anions to form these SCL adducts, including instrument or mobile phase contamination, unintended SPE salt

extraction or contamination, or in-source fragmentation of other molecules in the complex samples. For the chloride adduct, sucralose in-source fragmentation itself could provide chloride anions, as previously suggested (Wu et al., 2014). Intended SPE DOM extraction would likely be the factor for some described tentative adducting surfactant anions. Investigating the roles of these potential sources is a subject of further study.

As shown, sucralose concentration can determine whether less ionizing or favorable sucralose adducts are formed to an observable extent. Some data used in this study appears to demonstrate competing formation based on instrument or SPE parameters. For example, in the Effluent-A FTICR MS spectra, the triplicate with the lowest signal intensity for the major chloride and bromide adduct ions has more extensive adduct formation with other anions. The differences between the FTICR MS spectrum and Orbitrap MS spectrum for the same sample may demonstrate how differences in instrumentation, instrument settings, or background contamination affect adduct formation.

The Orbitrap MS used in this study undergoes regular skimmer cone cleaning and vacuum system bakeouts. One of the reasons for SPE sample preparation is salt removal before instrument analysis. SPE by Agilent Bond Elut PPL sorbent, used in this study, has been suggested to be capable of completely desalting marine samples (Dittmar et al., 2008); however, salt recovery by PPL SPE has not been extensively studied. Rinsing of cartridges in this study is believed to be reasonable for cartridge size and sample type. Septic system wastewater extraction was done with cartridge rinsing in excess of recommendations (Dittmar et al., 2008) and still shows similar

SCL adduct formation. While salt extraction is possibly a factor in adduct formation, sample preparation in this study is comparable to typically used methods in DOM LC/MS and high and ultrahigh resolution MS analyses.

In the large freshwater dataset, chloride adduct formation appears less consistent than other major species, largely because of an unexpectedly high formation of the chloride adduct in samples from the second month of stream sampling (Fig. A1.16). This does not correspond to analysis order or higher chloride concentrations in whole water and appears to represent an unknown contaminating factor during SPE. While the results of the MS/MS analyses in this study and other saccharide chloride adduct studies suggest that the adducting chloride can promote consecutive dissociation (Zhu and Cole, 2001; Jiang and Cole, 2005; Guan and Cole, 2008), we saw no clear correlation between chloride adduct formation and in-source fragmentation (Fig. A1.16). In-source fragmentation of SCL has been proposed to contribute chloride anions for adduct formation (Wu et al., 2014), but this lack of correlation, likewise, limits any conclusions about this potential opposite association. Considering adduct formation, the in-source fragmentation of SCL seen in this study seems unlikely to be caused by high source voltage settings causing dissociation.

Interestingly, a clear pattern was seen between nitrate adduct formation and matrix characteristics, as the nitrate adduct was only observed in certain WWTP SPEs, SPEs from the highest sucralose stream site, and SPEs from the oxygenated septic tank chamber. These are all wastewater or higher wastewater impacted samples that are likely oxygenated or partially oxygenated. Limited measurements show high relative nitrate concentrations in whole waters from the stream site (5 mg N/L

average) and septic chamber (36 mg N/L). The adducting anion source is unclear, but it may be unintended extraction of nitrate or dissociation of oxidized DOM before the source. See provided data for a summary of chloride and nitrate whole water measurements (https://figshare.com/s/3352e8215764b8c102d3).

2.3.6 Relevance to Analytical Methodologies

This adduct forming behavior has not been previously described, possibly due to the less frequent use of nontargeted analyses in studies of wastewater tracers. Another factor may be that sucralose was first proposed as a wastewater tracer based on extensive data from studies in Europe (Buerge et al., 2009; Loos et al., 2009; Scheurer et al., 2009; Neset et al., 2010) but it has been approved commercially for longer and consumption is higher in the United States (Oppenheimer et al., 2011; Oppenheimer et al., 2012). Consequently, much higher concentrations can be measured in wastewaters and natural waters in the United States (Mawhinney et al., 2011; Oppenheimer et al., 2011; Oppenheimer et al., 2012; Subedi and Kannan, 2014), and most adducts seen in this study are only apparent in high sucralose concentration samples. Additionally, most natural saccharides are not significantly extractable by the polymeric SPE methods (e.g. Agilent Bond Elut PPL, Waters Oasis HLB, and C18 cartridges) that are popular in quantification of organic contaminants by LC/MS techniques and nontargeted high and ultrahigh resolution MS molecular characterizations (Raeke et al., 2016). The 3 chlorine atoms of SCL are likely why it is well-extracted by these polymeric SPE methods, in comparison (Ordóñez et al., 2012).

These chlorine atoms in combination with in-source fragmentation and extensive adduct formation, including adducts with chloride and bromide, allow for complex isotopic patterns in MS and so many *m/z* ions to be sucralose related. Like chlorine, bromine has high relative natural abundances of the major stable isotopes: ^{79}Br (51%) and ^{81}Br (49%). In this study the Influent-B2 and Effluent-B FTICR MS spectra are found to have at least 50 and 46 SCL related *m/z* ions, respectively. Tentatively identified adducting anions suggest even more ions could be SCL related in these samples. This kind of behavior in nontargeted MS of a molecule common in DOM is, to our knowledge, unprecedented.

The use of FTICR MS in the molecular characterization of natural and anthropogenic DOM is rapidly increasing (Gonsior, 2019), and polymeric SPE for sample preparation and negative mode ESI for the ion source are some of the most popular techniques with FTICR MS (Kim et al., 2021). This behavior in MS could lead to misidentification of sucralose related ions, as the multitude of SCL adduct *m/z* ions could be misidentified as molecular ions or other incorrect organohalogens based on characteristic mass decimals. For instance, Fu et al. (2020) describe first misidentifying $C_{12}H_{20}Cl_4O_8$ as the highest signal organochlorine in a Tokyo Bay seawater sample, assuming deprotonation, before further FTICR MS/MS identifying it as the SCL chloride adduct, $[C_{12}H_{19}Cl_3O_8 + Cl]^-$. In a spectrum with low molecular *m/z* ion signals but high adduct *m/z* ion signals, SCL could be misinterpreted as absent. Similarly, LC-Orbitrap MS in full scan mode (Neset et al., 2010; Batchu et al., 2015), sometimes with subsequent data-dependent MS/MS acquisition (Wang et al., 2020), is also gaining popularity for SCL quantification because high resolution MS

can offer increased specificity and less reliance on chromatographic separation. Ionization that is not as expected could lead to the false conclusion that sucralose is absent.

Most SCL quantification is by negative mode ESI LC/MS/MS on samples prepared using polymeric SPE techniques. The results of this study highlight the value of using a SCL SIL-ISTD that can control for this adduct formation and in-source fragmentation behavior during quantification, as it is assumed that SIL-SCL would have similar adduct formation. We would discourage the use of sodium warfarin as an internal standard for SCL during targeted quantification, as has been used in food research, as it is very unlikely to emulate this complex in-instrument behavior.

Another factor of concern to SCL research is that in-source fragmentation *m/z* ions could be mistaken as degradation products, as the unintended $[M - H - HCl]^-$ fragment appears to be the same as one of the previously identified high pH, hydrolysis degradation products (Soh et al., 2011).

While our results highlight how unexpected MS behavior could affect analysis, the fact that sucralose appears to have similar adduct formation to saccharides may open new possibilities for quantification. In this study, without dopants and no intention of forming adducts, the chloride, formate, and bromide SCL adducts had similar or sometimes greater intensity signals than molecular sucralose. Chloride and formate SCL adducts have been used to improve detection, but the bromide adduct has, to our knowledge, not been previously described. Intentional formation of the bromide adduct using a dopant could potentially improve SCL

ionization. The other identified and tentative SCL adducts could also be explored for improving ionization, as lower ionization in this study may only be due to lack of adducting anions, adduct competition, or instrument setting settings, and in studies of adducting anions of natural oligosaccharides, the *m/z* ions of the chloride, bromide, nitrate, iodide, bisulfate, and trifluoroacetate adducts have been shown capable of having higher signal intensity than molecular $[M - H]^-$ ions (Jiang and Cole, 2005; Guan and Cole, 2008). Future work could also explore if other known saccharide adducting anions can form adducts with SCL. In consideration of the tentative surfactant SCL adducts, future studies should also consider whether other small molecules in DOM could be adducting anions of SCL. This work also suggests that there may be more adducting cations of SCL than previously described which could have better ionization or behavior during dissociation that may improve sucralose detection in positive mode (Wong et al., 2000; Zhu and Cole, 2001). Sucralose and sucralose fragment ions are considered to be poorly ionizing (Loos et al., 2009; Scheurer et al., 2009; Berset and Ochsenbein, 2012), leading to detection limits often higher than other commonly measured organic wastewater tracers. All of these newly described or potential SCL adducts may provide better signals by themselves $[M + A]^-$, by dissociating to molecular ions in-source $[M - H]^-$, by producing other dissociation products in-source, or by improved collision cell fragment generation.

A further consideration of the known connection between in-source fragmentation and adduct formation, reveals that currently popular mobile phase additives in sucralose analysis may be working to improve molecular ionization by forming sucralose adducts that are dissociating before the detector. Harvey (2005)

theorized that ammonium hydroxide improves molecular ion formation of larger polysaccharides by initially forming a $[M + OH]^-$ adduct which rapidly loses H_2O to form $[M - H]^-$. Likewise, the acetate adduct of saccharides has been described as unstable and undergoing the same unintended dissociation to improve $[M - H]^-$ formation (Jiang and Cole, 2005). Ammonium hydroxide (Oppenheimer et al., 2011; Batchu et al., 2015) and ammonium acetate (Torres et al., 2011) are popular mobile phase additives in sucralose quantification. In-source fragmentation of SCL adducts could be investigated as a factor for improved sucralose detection. Following this, the fluoride adduct of saccharides can behave the same way and may imply that fluoride dopants would improve molecular ionization of SCL (Jiang and Cole, 2005).

It is unclear how a chlorine substituted saccharide has such extensive adduct formation. Where adducting anions attach and where dissociation occurs structurally and the interactions behind adduct formation should be a topic of future research.

2.4 Conclusions

The artificial sweetener sucralose forms $[M - H]^-$ molecular SCL ions; chloride $[M + Cl]^-$, formate $[M + CHOO]^-$, nitrate $[M + NO_3]^-$, bromide $[M + Br]^-$, and iodide $[M + I]^-$ SCL adducts; and the apparent in-source fragmentation ions $[M - H - HCl]^-$ in ESI MS. More tentatively, it may also form adducts with trifluoroacetate and certain benzene sulfonates, with some suggestion of even more extensive adducting anion possibilities. The three chlorine atoms of SCL, the high relative natural abundances of the two stable chorine isotopes, and this behavior in MS allows an unprecedented number of ions to be related to the same chemical in nontargeted high and ultrahigh resolution MS.

Sucralose is a human metabolite and domestic wastewater tracer, and quantifying sucralose in the environment and molecular characterization of DOM are increasingly popular topics of research. Awareness of this adduct formation and dissociation behavior is important for analytical methods. These SCL related ions were all observed with no intention to form them and following typical sample preparation and analysis. This behavior could lead to misinterpretation of nontargeted MS data and has significance to analytical methodology for SCL quantification, such as by LC/MS or LC/MS/MS. While this adduct formation can complicate SCL analysis, it may also lead to method development that would improve SCL ionization and detection limits, as adduct ions could provide better signals themselves or have improved fragment generation.

2.5 Acknowledgements

We thank Colman Welles for assistance in sample acquisition and preparation and Dr. Mourad Harir for assistance in FTICR MS analyses. We would also like to thank Dr. Laura Lapham for allowing use of her IC system. Thank you to Maryland Sea Grant (NA14OAR4170090 and SA75281450-K) for supporting this work.

Chapter 3: Septic system wastewater tracer identification using ultrahigh resolution mass spectrometry

Abstract

Septic systems can contribute contaminants such as bacteria, viruses, nutrients, metals, and organic contaminants of emerging concern (CECs) to surface and groundwaters. A better understanding of septic tank effluent (STE) composition and ways to recognize STE impact in the environment could aid in avoiding STE pollution. We used ultrahigh resolution Fourier transform ion cyclotron resonance mass spectrometry (FTICR MS) to molecularly characterize dissolved organic matter (DOM) in streams with high septic system density (>80 systems/sq mi), forested reference streams, and septic tank wastewater itself. FTICR MS is qualitative, but normalized signals of sulfophenyl carboxylic acids (SPC) and dialkyl tetralin sulfonate intermediates (DATSI) were found to function as semi-quantitative indicators of septic system impact in stream samples, also supported by the Gaussian distribution of CH_2 homologues.

The molecular composition of higher STE impacted stream sites was found to have differences in mainly sulfur containing, but also nitrogen and nitrogen with sulfur containing molecular formulas. We identified 137 septic system wastewater tracers, or specific molecular formulas based on accurate mass that were present in higher STE impacted sites, but absent in lower to unimpacted sites. We also assessed which tracer signatures may be better performing for STE source tracing. Signals of

presumed perfluoroalkyl carboxylates (PFACs) and sulfonates (PFASs) also appeared to be appropriate tracers for STE impact.

Septic tank dissolved organic matter (STDOM) was found to have a high presence of sulfur and nitrogen with sulfur containing molecular formulas, and 108/137 of identified chemical tracer formulas from impacted streams were also found in STDOM. These various techniques could function as quick nontargeted analytical approaches for distinguishing domestic wastewater impact or in the case of specific molecular tracers, may lead to new targeted and quantitative wastewater tracers, if the structures can be determined and synthesized.

3.1 Introduction

Septic systems are an important source of pollution to surface and groundwaters. In the United States, an estimated 20% of households use septic systems for onsite domestic wastewater treatment (U.S. EPA, 2008b), and septic systems can be the dominant form of wastewater treatment in rural and suburban areas where connection to municipal wastewater treatment is unavailable (U.S. EPA, 2002; U.S. EPA, 2008b). In these regions, businesses and municipal buildings may also be served by septic systems. Onsite wastewater treatment systems, like septic systems, are not subject to the same treatment or discharge regulatory standards as municipal wastewater treatment plants (WWTPs) in the United States, and an estimated 10-20% of septic systems are in performance failure status (U.S. EPA, 2002). Septic tank effluent (STE) can contain elevated levels of bacteria, viruses, metals, phosphorous, nitrogen, carbon, and chloride, as well as contaminants of emerging concern (CECs) from personal care products, human diet, pharmaceuticals,

and other household chemicals. Removal of contaminants in septic system treatment depends on the system design and performance, adjacent sediment, soil water, and groundwater properties, and individual properties of the contaminants. STE transport and transformation is typically not monitored beyond the drainfield region. Septic systems contaminate groundwater by design and can contaminate shallow drinking water wells and surface waters. Therefore, it is necessary to better understand STE composition and which chemical features might persist during transport to better track STE contamination.

Previous targeted work on metals (Robertson and Blowes, 1995; Ptacek, 1998; Richards et al., 2016; Richards et al., 2017), phosphorous (Robertson et al., 1998; Zanini et al., 1998; Robertson, 2008; Robertson et al., 2019; Robertson and Garda, 2020), nitrogen (Oakley et al., 2010; Robertson et al., 2012; Robertson et al., 2013; Caschetto et al., 2018), chloride (Katz et al., 2011; Robertson et al., 2013), and CECs (Carrara et al., 2008; James et al., 2016; Yang et al., 2016) has greatly improved our understanding of STE composition and contamination risks and the efficacies of these and related species as tracers of septic system impact. However, the composition of septic system dissolved organic matter (DOM) is still minimally characterized. Nontargeted analytical approaches have been used to improve our understanding of complex mixtures. Nontargeted ultrahigh resolution electrospray ionization Fourier-transform ion cyclotron resonance MS (ESI FTICR MS) is a powerful tool for studying complex molecular composition because it allows for exact molecular formula assignment to detected mass-to-charge ratios (*m/z*). Previous work has molecularly characterized WWTP wastewaters (Gonsior et al., 2011; Tseng et al.,

2013), STE impacted groundwaters (Longnecker and Kujawinski, 2011; Arnold et al., 2014), and urban streams with multiple impact sources, including STE (Lusk and Toor, 2016). FTICR MS has been used to effectively fingerprint organic signatures, with applicability to source tracking. Through comparison to more pristine natural waters, specific potential tracer compounds can be identified, as has been shown for hydraulic fracturing wastewaters (Luek, 2017).

To contribute to the understanding of STE and its impact, we used FTICR MS to molecular characterize DOM in forested reference streams and streams draining areas with high septic system density to identify novel potential chemical tracers for STE impact. We molecularly characterized STE from septic tank chambers to better understand initial composition and assess identified tracer compounds. We also assess ways certain homologous series may function as semi-quantitative tracers of STE volume in impacted streams.

In this study, we used sucralose concentration in combination with septic system density to better rank STE contribution at stream sites. Sucralose is particularly effective as a quantitative tracer of STE impact. It is in significant use in the United States, hydrophilic, essentially unmetabolized, and highly resistant to degradation, so it can function as a conservative tracer of domestic wastewater (Oppenheimer et al., 2011; James et al., 2016). Sucralose is persistent and can outlast septic-related bacterial, nutrient, or other removable chemical signals during water transport, and has been found to be one of the most frequently detected CECs in STE impacted waters (James et al., 2016).

3.2 Materials and Methods

3.2.1 Stream Study Sites and Sampling

We sampled 9 streams, 12 times, or approximately monthly, at baseflow conditions, for a year between October 2016 and November 2017 (Fig. 3.1). Of these 9 stream sites, 6 were considered to have high septic system density in their drainage basins, and 3 stream sites were forested reference streams. Here, high septic system density was defined as >80 septic systems/sq mi. This definition is an adaption from a previous suggestion of >40 systems/sq mi as high density (Canter and Knox, 1984) because of the predominance of septic system use in this study area. Reference streams were significantly less developed than high septic density sites, but 2/3 reference streams did still have septic systems in their drainage basins (Table 3.1). Almost all sites were in Calvert County, MD, USA. The 1 reference site with no septic systems, SERC, is the study watershed SERC-110 at the Smithsonian Environmental Research Center in Anne Arundel County, MD, USA. This site was only sampled 2/12 expected times due to low flow conditions.

Site drainage basins ranged from 0.02-4.84 sq mi. Sites had a mix of advanced nitrogen-removing septic systems, referred to as “Best Available Technology” (BAT) systems, and traditional septic systems. None of these sites have input from WWTPs, though some drainage basins do contain sewered areas. All sites have very low to no agricultural land use, including crop and animal agriculture (Table 3.1). Traditional and BAT septic system number data were calculated from maps produced by Calvert County Department of Planning and Zoning. Drainage Basin size was calculated using the United States Geological Survey (USGS) StreamStats Application (USGS,

2017). Basin land use is from the USGS Chesapeake Bay Phase 6, 1 m Land Use Datasets (USGS, 2019), where land use categories have been simplified to *Developed* (Impervious Road, Impervious Non-Road, Fractional Impervious, Mixed Open, and Tree Canopy Over Impervious), *Semi-developed* (Tree Canopy Over Turf, Turf Grass, Fractional Turf Small, Fractional Turf Medium, and Fractional Turf Large), *Undeveloped* (Water, Tidal Wetlands, Floodplain Wetlands, Other Wetlands, and Forest), and *Agriculture*. Basin size and land use for the SERC site is from previous studies (Jordan et al., 1997a; Correll et al., 1999; Weller et al., 2003).

Stream discharge was calculated during sample collection by measuring stream width and depth and flow with an electromagnetic flow meter (Marsh McBirney Flo-Mate Model 2000). At SERC, flow was measured by volume collection at a v-notch weir. We collected duplicate 2L grab samples in combusted (500 °C) glass bottles, sample rinsing bottles 3 times before water collection, for solid-phase extraction in the lab. A nearby lake with high expected septic system input was also sampled in this same manner in February 2017, which while not included in this study, was included in FTICR MS data processing. In the field, we also used sterile syringes, which were first sample rinsed 3 times, to syringe filter (0.2 µm, Whatman GD/X cellulose acetate) 30 mL samples of stream water for dissolved organic carbon (DOC) analysis. A brief rinse was sent through filters before sample collection to minimize potential leaching. These samples were stored in the lab at -20 °C until analysis.

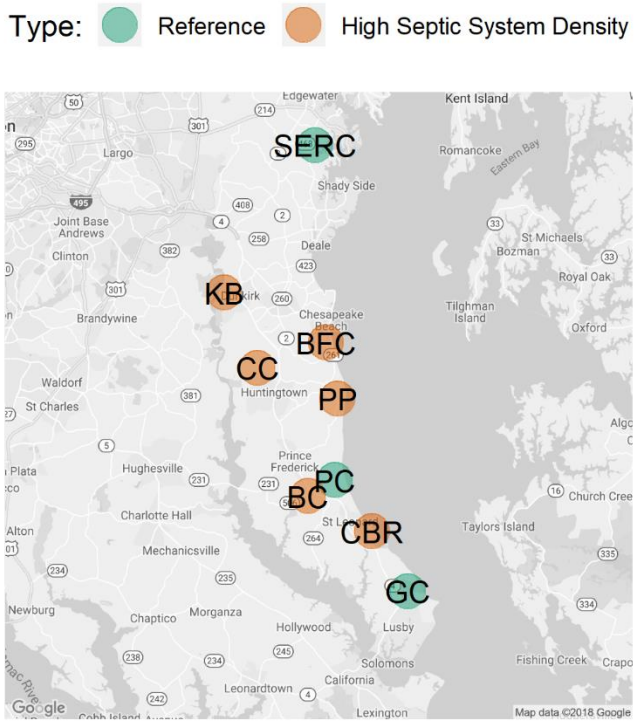

Figure 3.1 Map of stream sampling sites in Calvert and Anne Arundel County, MD.

3.2.2 Septic Tank Chamber Sampling

We additionally sampled wastewater from 6 different traditional septic systems in Calvert County, MD, USA. In 2/6 systems, samples were collected from both a first and second chamber, and in 1 of these systems, the second chamber was continuously aerated by an installed oxygen pump system. All systems served single households with 2-6 household members and septic tanks were of a variety of ages. Samples were collected from below the grease layer with acid-washed tubing and a peristaltic pump, collecting duplicate samples in combusted bottles after sample rinsing bottles 3 times. At the lab, duplicates were subsampled to volumes of ~500 mL for systems where a single chamber was sampled and to 250 mL for the first and 500 mL for the second if two chambers were sampled.

3.2.3 Sample Processing

In the lab, samples were vacuum filtered through combusted 0.7 µm Whatman GF/F glass microfiber filters into combusted glass bottles. Samples were acidified to pH=2 with pure grade, 32% hydrochloric acid (Acros Organics). Samples were then solid-phase extracted for sample concentration and desalting using Bond Elut PPL cartridges (1 g, 3 mL, Agilent). Cartridges were activated with 5 mL of LC/MS grade methanol (MeOH) then rinsed with 5 mL of LC/MS grade 0.1% formic acid (FA) water. Samples were gravity-loaded onto cartridges with some peristaltic-pump loading as necessary. The inside reservoir and outside of cartridges were then rinsed with ultrapure water, and the sorbent was rinsed with 5 mL or 30 mL of 0.1% FA water for stream samples or septic system wastewater samples, respectively, to remove remaining salts. Cartridges were dried under vacuum and eluted with 10 mL MeOH into new, trace contaminate certified or cleaned and combusted amber vials.

Sucralose quantification was by high performance liquid chromatography triple quadrupole tandem mass spectrometry (HPLC/QqQMS/MS) using an Agilent 1260 Infinity II LC and an Agilent 6420 Triple Quadrupole MS. Exact sucralose analytical methods are described in detail in *Chapter 2* (Section 2.2.5). Samples for DOC analysis were acidified with hydrochloric acid to pH 2 and quantification was done using a Shimadzu total organic carbon analyzer (TOC-VCPH).

3.2.4 FTICR MS Analysis

Solid-phase extracts were analyzed in negative ion mode ionization on a 12 Tesla Bruker solariX FTICR MS with an Apollo II ESI source at the Helmholtz Zentrum München, Munich, Germany. Samples were diluted 1:40 in MeOH and

introduced at 120 µL/h into the ion source. Spectra acquisition was with a time-domain transient of 4 megawords (MW) and a 500 scan accumulation over a range of 147-1,000 *m/z* for the stream samples and a 300 scan accumulation over 130-1,000 *m/z* for the septic system wastewater samples. Spectra were calibrated using lists of known common molecules in DOM and wastewater. Lists of *m/z* ions were exported with a signal-to-noise ratio cutoff of 10, and *m/z* aligned matrices were generated for the stream samples with a 1.2 ppm window width and a 1.0 ppm window width for the septic system wastewater samples.

The stream sample matrix contained 198 samples, representing 8 streams sampled 12 times in duplicate, 1 stream sampled 2 times in duplicate, and the lake sampled in duplicate. This matrix was reduced to only include *m/z* ions detected in more than 20 samples to limit the contribution of rare *m/z* ions that are likely individual sample contamination, adducts, or instrument contaminations. Formula assignment was undertaken using NetCalc, which utilizes common chemical transitions and a network assignment approach. Allowed formula assignments included the elements C, H, O, N, S, ^{35}Cl, ^{79}Br, and ^{81}Br. Assignments containing Br were only considered valid if both isotopic assignments were found and were secondly confirmed by isotopic pattern matching, and the ^{81}Br assignments were then removed from subsequent data analysis to not account for the same molecular formula twice. Assignments with implausible atomic ratios were also removed, and assignments were further filtered to only include those with mass error $\leq$ 0.60 ppm and molecular weight < 660 *m/z*. The higher mass error allowed in this data set was necessary because of introduced error from the large number of samples within the

alignment matrix. Additional formula assignments containing F were assigned manually in the pre-filtered matrix based on distinctive mass decimals and homologous series but are not considered in the general molecular characterization discussion.

The septic system wastewater matrix contained 18 samples, for 8 chamber duplicates from 6 septic systems. The matrix was filtered for *m/z* ions present in both duplicates, as applicable. Formula assignment was carried out as discussed above, but without ^{81}Br as it led to assignment issues and no valid Br containing formulas were assigned. Assignments were filtered to only include those with mass error ≤ 0.50 ppm and < 660 *m/z*.

Visualization in this text was using the R packages ggmap (Kahle and Wickham, 2013) and ggplot2 (Wickham, 2016).

3.3 Results and Discussion

3.3.1 Stream DOM Molecular Characterizations

Sucralose concentrations ranged from not detected (ND) to 13.3 μg/L and correlated well with septic system density and combined % Developed and Semi-developed land use (Tables 3.1,3.2). Sucralose is likely a much better ranking of septic system impact for these streams as septic system density does not factor in age of installation. For example, septic system counts for site BC were heavily weighted by a large newly developed region where many systems were not in use, or recently began operation and any septic impacted groundwater may not yet have reached surface waters. For this reason, in referring to apparent STE impact, the sites are now

ranked from most to least impacted in order of highest to lowest sucralose concentrations: BFC, CBR, KB, CC, PP, PC, GC, BC, SERC. Where BFC, CBR, KB, CC, and PP are higher STE impact and PC, GC, BC, and SERC are lower to no STE impact (Table 3.2), superseding original classifications (Fig. 3.1, Table 3.1).

Table 3.1 Stream site characteristics, land use, and drainage septic system density.

Sites	Drainage Area (sq mi)	Width (in)	Flow (f^3/s)	% Developed	% Semi-developed	% Undeveloped	% Agriculture	Traditional/ BAT Systems	Traditional/ BAT Septic System Density (systems/sq mi)
High Septic System Density									
BFC	0.04	21	0.02	42	48	10	0	76/3	2053/81
CBR	0.25	37	0.11	28	47	24	0	209/7	836/28
KB	0.53	44	0.32	13	32	48	8	78/1	148/2
CC	3.91	89	1.97	13	33	52	3	773/6	198/2
PP	4.84	119	2.45	8	16	70	6	650/6	134/1
BC	0.53	33	0.18	5	3	90	2	26/41	49/77
Original Reference									
PC	0.53	43	0.32	4	10	75	11	29/0	55/0
GC	0.35	41	0.41	7	11	82	0	5/0	14/0
SERC	0.02	-	0.0008	0	0	100	0	0/0	0/0

Table 3.2 Stream site average DOC, average sucralose, and molecular characterization characteristics. For sucralose, not detected (ND), is presumed absent or less than method detection limits (~5 ng/L), while below quantification limit (BQL) signifies occasional detection at concentrations below method quantification limits (40-190 ng/L).

Sites	Total Septic System Density (systems/sq mi)	DOC ± SD (mg C/L)	Sucralose ± SD (µg/L)	Total Formulas	% CHO	% CHON	% CHOS	% CHONS
Higher STE Impact								
BFC	2134	3.4±1.1	13.3±1.2	4704	47	30	17	6
CBR	864	4.0±0.8	4.9±0.6	4777	47	29	17	6
KB	150	2.3±1.4	1.8±0.2	4816	46	29	17	6
CC	199	3.4±1.2	1.0±0.2	4765	47	30	17	6
PP	135	5.6±1.1	0.5±0.1	4770	47	30	16	6
Lower to No STE Impact								
PC	55	3.2±0.8	0.5±0.1	4661	49	29	16	5
GC	14	2.9±0.8	0.3±0.1	4594	49	28	16	4
BC	127	2.6±1.2	BQL	4255	52	28	15	3
SERC	0	5.3±0.0	ND	3691	54	27	14	3

A total of 4,932/11,854 formulas were assigned to *m/z* ions in the stream sample matrix. Of these, the majority, or 45.9% were formulas containing only carbon, hydrogen, and oxygen (CHO). The second highest class was CHON, or only containing carbon, hydrogen, oxygen, and nitrogen, which was 28.9% of formula assignments. The remaining formula classes were 17.4% CHOS, 6.1% CHONS, 1.3% CHOCl, 0.3% CHOBr, and 0.1% CHOSCl.

Higher STE impacted streams had higher % of assigned formulas in the CHON, CHOS, and CHONS formula classes (Table 3.2). No overall trends were observed between STE impact and intensity weighted average H/C, O/C, or double bond equivalent (DBE). All CHOBr formulas were similar (Table A2.1), had low corresponding signal intensity, and their presence was not related to STE impact but was common at KB, PC, GC, and BC, suggesting these could be naturally occurring. The presence of CHOCl formulas also appeared more site specific and unrelated to STE impact. The CHOSCl class included only 3 formulas (Table A2.2) and essentially only appeared at the highest STE impacted site, BFC, at low signal intensities.

There were clear differences in molecular composition between sites with higher and lower STE impact. Here, for visualization, we use Van Krevelen diagrams (van Krevelen, 1950), plotting hydrogen to carbon ratio (H/C) versus oxygen to carbon ratio (O/C) for formula assignments. Multiple formulas may have the same H/C and O/C values and overlay each other in plots. Van Krevelen diagrams are helpful for distinguishing differences in molecular composition. To understand differences, comparisons were made to the reference site PC to minimize any

potential bias from differences in DOC or number of formulas assigned. Though a reference site, the PC drainage basin did contain septic systems and the site had the fourth lowest average sucralose concentration (Table 3.2). Comparisons to other likely lower impacted sites such as BC and SERC showed similar patterns.

For the various sites, CHO formula assignments were very similar (Fig. A2.1). In comparison to PC, for all sites <3 CHO formulas were unique per site. Though these data are non-structural and differences between structural isomers would not be distinguishable. In contrast, molecular differences were seen for CHOS, CHON, and CHONS formulas between sites in relation to STE impact. For CHOS formulas, in comparison with PC, a higher % unique formulas were assigned to more impacted sites in exact ranked order (Table 3.3). These formulas associated with higher STE impact generally had higher H/C and lower O/C values (Fig. 3.2), as well as lower *m/z* (Fig. A2.2). They also fell into clusters of similar formulas (Fig. A2.2).

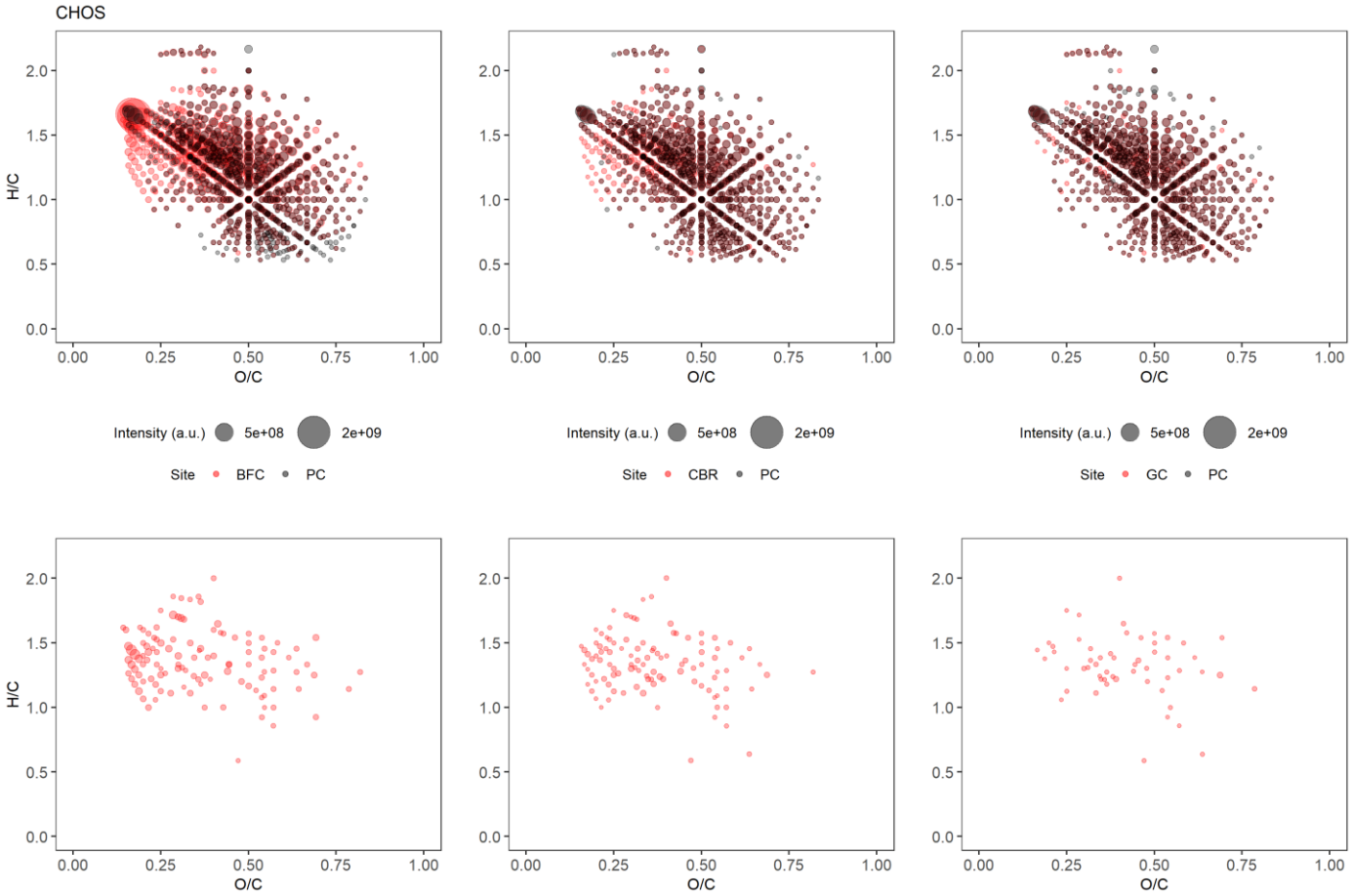

Figure 3.2 Van Krevelen diagrams showing intensity averaged CHOS formula assignments for sites BFC (2134 septic systems/sq mi) (left), CBR (864 septic systems/sq mi) (middle), and GC (14 septic systems/sq mi) (right) versus PC (55 septic systems/sq mi) (top) and corresponding unique formula assignments (bottom).

For CHON and CHONS formulas, generally a higher % of unique formulas were assigned to more impacted sites (Table 3.3). CHON formulas had similar H/C and O/C values across both higher and lower STE impact sites (Figs. A2.3, A2.4). In contrast to CHOS, the highest signal intensity unique formulas at the highest impacted site often had *m/z* >400 (Fig A2.5). Unique CHONS formulas for higher STE impacted sites generally had 0.75-1.5 H/C and 0.5-0.75 O/C (Fig A2.6, A2.7). These had similar formulas and 250-375 *m/z* values, with a small secondary cluster at approximately 470 *m/z* (Fig A2.8).

Differences in CHOS assignments may be related to surfactants in household products, either manufactured surfactants, co-products, or degradation products (Gonsior et al., 2011). While CHON and CHONS differences may reflect greater DON loading from STE and microbial activity (Arnold et al., 2014). It is unclear what these general higher STP impact molecular differences signify structurally, and this should be further explored by tandem mass spectrometry (MS/MS).

Table 3.3 Unique formula assignments in comparison to site PC for sites ranking from presumed highest to lowest STE impact based on sucralose concentration.

Site	% Unique CHOS	% Unique CHON	% Unique CHONS
BFC	14	3	22
CBR	13	3	18
KB	12	3	23
CC	9	3	19
PP	8	3	22
GC	7	2	9
SMB	4	1	6
SERC	3	1	7

3.3.2 Potential Specific Molecular Tracers for Septic System Wastewater

To identify specific potential tracers for STE impact we identified molecular formulas that were only present in the higher STE impact samples and absent in the

lower impact samples (Table 3.2). We identified 137 molecular formulas that were exclusive to the higher impact sites (Table A2.3). Of these, 46% (n=63) were CHOS, 36% (n=49) were CHONS, 16% (n=22) were CHON, and 2% (n=3) were CHOSCl type formulas. This list was narrowed to the top 10 by highest maximum signal intensity, highest average signal intensity, and highest frequency of detection (Table 3.4). The highest maximum intensity list consisted of only $CHOS_1$ formulas. The highest average intensity list contained 8/10 of the same formulas from the maximum intensity list, with 2 additional $CHON_1S_1$ formulas. The highest frequency list consisted of mainly $CHON_1S_1$ formulas (9/10) as well as 1 $CHOS_2$ formula. The 2 highest detection frequency formulas (n = 111/120 and 110/120) were shared with the average intensity list.

Table 3.4 Top 10 potential STE tracers by highest maximum signal intensity, highest average signal intensity, and highest frequency of detection. Asterisks mark shared formulas across lists.

Top Potential Tracer Ions by:					
Maximum Intensity		**Average Intensity**		**Frequency**	
Exact *m/z*	**Formula**	**Exact *m/z***	**Formula**	**Exact *m/z***	**Formula**
307.13734	$C_{17}H_{24}O_3S$*	307.13734	$C_{17}H_{24}O_3S$*	354.02891	$C_{14}H_{13}NO_8S$**
335.16864	$C_{19}H_{28}O_3S$*	335.16864	$C_{19}H_{28}O_3S$*	356.04456	$C_{14}H_{15}NO_8S$**
185.02779	$C_8H_{10}O_3S$*	319.13734	$C_{18}H_{24}O_3S$*	324.01835	$C_{13}H_{11}NO_7S$
289.09039	$C_{16}H_{18}O_3S$*	289.09039	$C_{16}H_{18}O_3S$*	372.03948	$C_{14}H_{15}NO_9S$
305.12169	$C_{17}H_{22}O_3S$*	356.04456	$C_{14}H_{15}NO_8S$**	330.06530	$C_{13}H_{17}NO_7S$
319.13734	$C_{18}H_{24}O_3S$*	333.15299	$C_{19}H_{26}O_3S$*	340.01326	$C_{13}H_{11}NO_8S$
333.15299	$C_{19}H_{26}O_3S$*	305.12169	$C_{17}H_{22}O_3S$*	398.01874	$C_{15}H_{13}NO_{10}S$
241.09039	$C_{12}H_{18}O_3S$*	354.02891	$C_{14}H_{13}NO_8S$**	375.02138	$C_{14}H_{16}O_8S_2$
291.10604	$C_{16}H_{20}O_3S$	185.02779	$C_8H_{10}O_3S$*	342.02891	$C_{13}H_{13}NO_8S$
213.05909	$C_{10}H_{14}O_3S$	241.09039	$C_{12}H_{18}O_3S$*	344.04456	$C_{13}H_{15}NO_8S$

The maximum intensity list formulas may be easier to detect, but mainly only appeared at the highest and second highest impact STE sites, so may indicate higher septic impact or a less degraded STE signal. These may also be less universal signals. The average intensity list is still largely driven by signals at the highest impact sites,

but with some influence of detection frequency. The frequency list included many lower signal intensity formulas, but interestingly, was dominated by CHONS formulas. We believe CHOS tracers to likely be related to sulfonated surfactants and their degradation products, which can be highly ionizing in ESI, while CHONS tracers may be microbially derived. While generally of much lower signal intensity, CHONS tracers may be a better indicator for lesser STE impact or a more environmentally degraded signal. The CHON tracers could be related to human diet or waste or degradation products of initial STE DON, but generally had lower signal intensity or were of less frequent detection (Table A2.3).

This presence/absence approach was done to identify tracers that might be more STE specific, but ignores other potential indicator formulas that may still be present at low intensities in the low impact sites, such as those that may be present due to instrument carry-over, those that may be structural isomers with natural DOM molecules, or those that are also naturally occurring molecules. Therefore, we also identified formulas which were only present in lower impact samples with <5,000,000 total ion counts (TIC), but that were present in higher impact samples at TIC ≥5,000,000 at least 24 times. Within the higher impact samples, we selected those with the 10 highest average signal intensities. These were all $CHOS_1$ formulas and included 2 molecular formulas matching dialkyl tetralin sulfonate intermediates (DATSI) and 1 matching a sulfophenyl carboxylic acid (SPC) (Table A2.4).

As a final check, in looking for potential unassigned tracer ions, 99/6,553 unassigned *m/z* ions were exclusive to the higher impact samples. The list of the 10 formulas with the highest average signal intensities in the higher impact samples was

found to contain 2 *m/z* values related to sucralose adducts (see *Chapter 2*), 4 related to perfluorinated assignments (described in the following section), 1 that was an isotopic peak of a CHOS assignment, and 2 that appear to be negative mode sodium adducts ($[M - 2H + Na]^-$). The 1 remaining ion, 469.92099 *m/z*, could not be confidently identified, but appears to contain 2 chlorine atoms. This suggests many of these were not ions that were intended to be assigned, such as isotopic peaks and adducts, and these overall had low signal intensities, but future work could better assess the unassigned fraction in these samples.

3.3.3 Perfluorinated Compounds as Tracers of STE Impact

While considered separately from the bulk molecular characterization, per- and poly- fluorinated compounds (PFCs) were identified almost exclusively in the higher STE impact sites (Fig. 3.3). We identified what appeared to be perfluoroalkyl carboxylates (PFACs), perfluoroalkyl sulfonates (PFASs), as well as other PFCs (Table A2.6.). While FTICR MS is nonstructural, these assignments represent expected homologous series and are structurally limited.

PFASs included likely perfluorobutanesulfonic acid (PFBuS), perfluoropentanesulfonic acid (PFPeS), perfluorohexanesulfonic acid (PFHxS), perfluoroheptanesulfonic acid (PFHpS), and perfluorooctanesulfonic acid (PFOS). While PFACs included likely perfluoropentanoic acid (PFPeA), perfluorohexanoic acid (PFHxA), perfluoroheptanoic acid (PFHpA), and perfluorooctanoic acid (PFOA). The other PFCs were C_4HF_9, C_5HF_{11}, C_6HF_{13}, and C_7HF_{15} (Table A2.5), and these signals were highly correlated to those of corresponding $+CO_2$, PFAC assignments (Figs. 3.3, A2.9). We suspect that these are likely in-source

fragmentation products, fragment ions forming during analysis, of PFACs and match known fragmentation products (Loos et al., 2008), but this connection should be better explored. These signals were often of equal of higher intensity than those of corresponding PFACs (Figs. 3.3, A2.9).

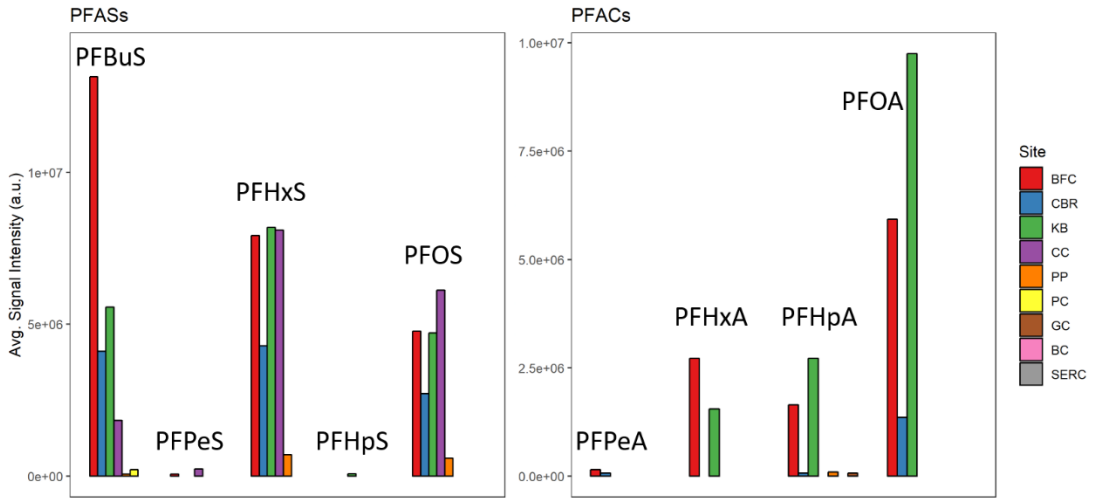

Figure 3.3 Grouped bar plot of PFAS (left) and PFAC (right) signal intensities for stream sites, in order of decreasing STE impact. Groups show $+CF_2$ homologous series related to chain length.

Previous work has identified PFCs in septic system wastewater (Subedi et al., 2015) and that STE is a source of PFCs to surface and groundwater (Subedi et al., 2015; Schaider et al., 2016). These compounds can be found in public and well water, common household products, food packaging, and human waste (Trudel et al., 2008; Zhang et al., 2015; Schaider et al., 2017) which would all chemically contribute to STE. Exposure sources to humans before excretion include household textile sources, household products, food, workplace exposure, and drinking water (Trudel et al., 2008; Schaider et al., 2017). FTICR MS data are non-quantitative, but the correlation of these signals with STE impact based on septic system density and sucralose

concentrations does suggest PFASs and PFACs are coming from an STE source (Fig. 3.3).

Results in this study do not necessarily reflect the extent of PFCs in streams, as PPL solid-phase extraction may have a chain-length bias, but this data supports that PFASs and PFACs can be quantified as STE chemical tracers. These compounds might also work for age dating STE impact, similar to the way artificial sweeteners have been used as temporal markers in septic system wastewaters (Robertson et al., 2016). These compounds are persistent in the environment and shorter chain length PFASs and PFACs are used in modern formulations which has allowed chain length to be related to time (Lam et al., 2016).

3.3.4 Semi-Quantitative Indicators of STE Impact

Surfactants, or surface-active agents, are often used in soaps and detergents. Linear alkyl benzene sulfonates (LAS) are some of the most used surfactants, and they are used both as detergents in household products themselves as well as in the production of other surfactants. Dialkyl tetralin sulfonates (DATS) are surfactant co-products of LAS production. Both these classes of surfactants degrade, and SPC are degradation products of LAS and DATSI are degradation products of DATS. SPC and DATSI signal intensity normalization was done by dividing signal intensities by average CHO formula signal intensity for each sample. These CH_2-spaced, surfactant degradation product homologous series have been previously described in WWTP effluent (Gonsior et al., 2011), and normalized SPC signatures were shown to function well as semi-quantitative indicators of domestic wastewater in FTICR MS data of Hawaii coastal waters (Mitchelmore et al., 2019).

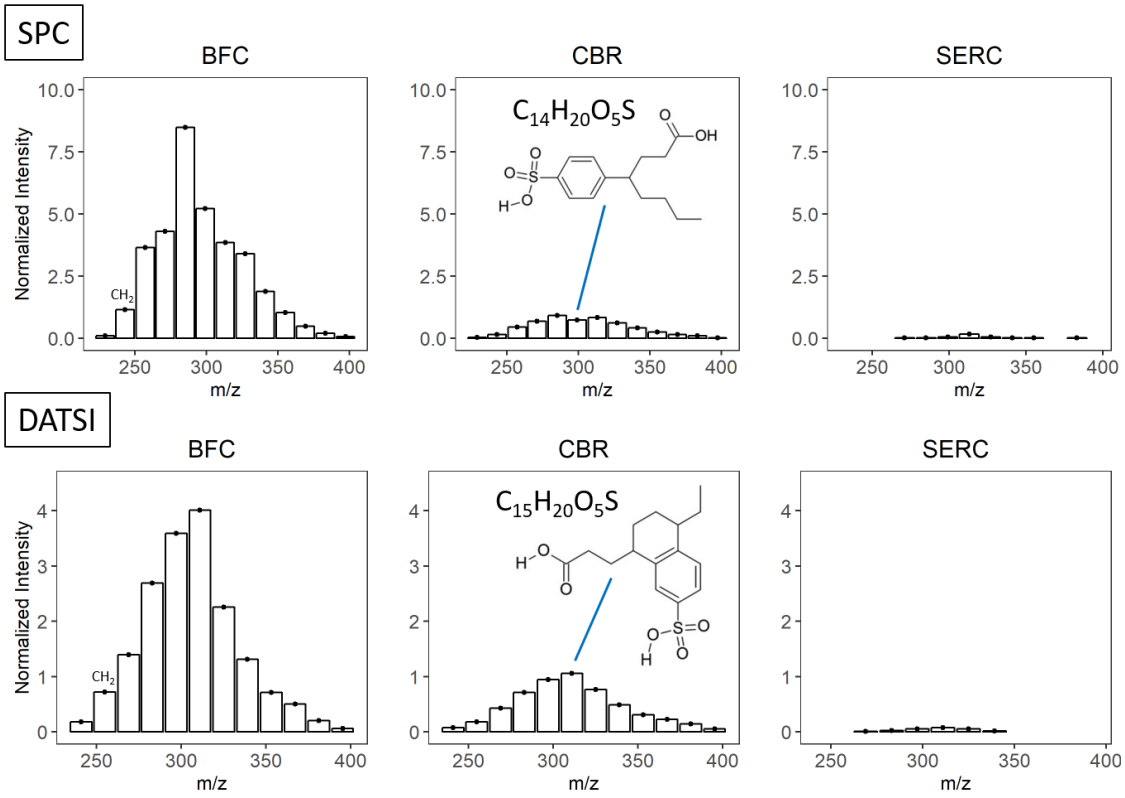

Figure 3.4 SPC (top) and DATSI (bottom) signal intensities for stream sites BFC (2134 septic systems/sq mi) (left), CBR (864 septic systems/sq mi) (middle), and SERC (0 septic systems/sq mi) (right). Points are at measured *m/z* values and show $+CH_2$ homologous series related to chain length. Signal intensity (a.u.) was normalized to the average intensity (a.u.) of all CHO signals in each sample, and then averaged by site.

While LAS and DATS type formulas were present in stream DOM, this mainly was only as higher signal intensity in the highest STE impacted site (BFC) and low, but similar signal intensities in other sites. In contrast to this, normalized SPC and DATSI signals could be strongly related to STE impact, consistent with degraded STE source (Figs. 3.4, A2.10, A2.11, Table A2.6).

3.3.5 Septic System Wastewater Molecular Characterization and Assessment of Tracers

FTICR MS spectra of septic tank DOM (STDOM) were visually distinct from stream DOM, though had similarities to high STE impact stream spectra. Spectra were dominated by CHOS surfactant *m/z* ions and contained fewer identified *m/z* ions, likely due to signal suppression by highly ionizing surfactants (Fig. 3.5).

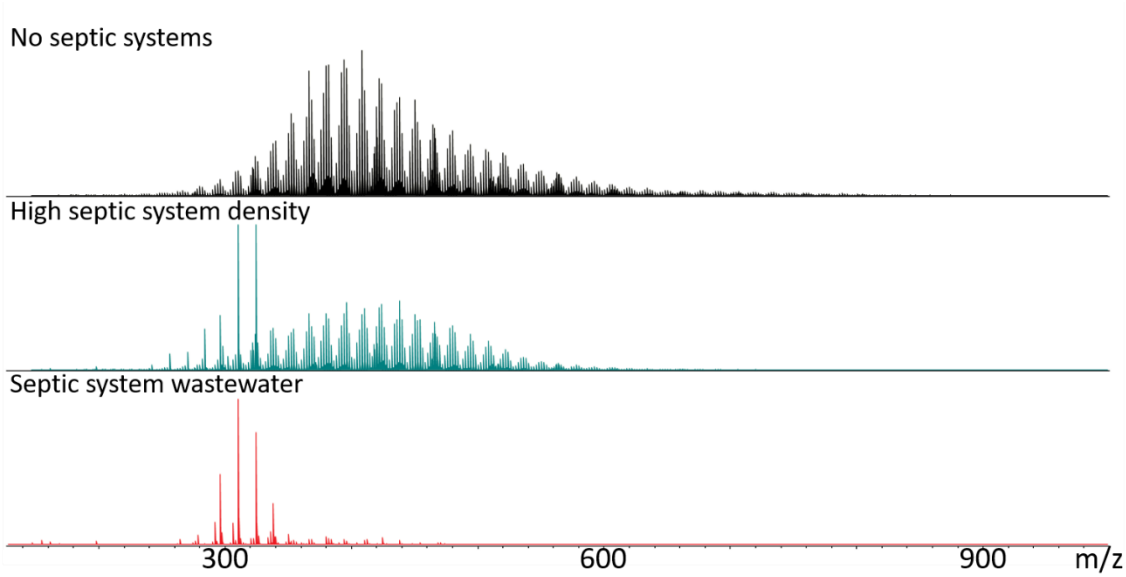

Figure 3.5 FTICR MS spectral comparison between SERC (top) and BFC (middle) stream DOM samples and STDOM (bottom), showing high intensity CHOS surfactant peaks in STE impacted stream DOM and the dominance and signal suppression of the same *m/z* ions in septic system wastewater. Signal height has been scaled to base peak.

STDOM had higher presence of CHOS and CHONS formulas relative to stream DOM (Table 3.5), consistent with described STE impact indicators. Other formula classes besides the major classes included CHOCl (2% of total) and a minor fraction of CHONCl and CHOSCl. Septic tanks had diverse molecular signatures, and only 699 formulas were found in all samples, but 2,899 were found in 5 or more

samples. Individual tanks had generally similar formula class distributions. Tank A had a higher % CHOS formulas and much lower total assigned formulas, suggesting higher surfactant signal suppression. While tank chamber B2, the aerated chamber, had a higher % CHON and lower % CHOS, likely representing the degradation of signal suppressing CHOS molecules (Table 3.5).

Table 3.5 Molecular characterization summary for the 6 sampled septic tanks. For tanks B and C, 2 chambers were sampled. B2 had an oxygen pump system. Total is for the STDOM dataset.

Septic Tank	Total Formulas	%CHO	%CHON	%CHOS	%CHONS
A	1422	29	22	43	5
B1	3769	30	36	24	8
B2	3683	29	41	19	11
C1	4171	32	31	25	11
C2	3379	32	30	29	9
D	3921	29	30	28	12
E	3705	30	27	30	12
F	2504	32	29	30	8
Total	**6532**	**27**	**34**	**24**	**13**

STDOM had higher H/C, particularly higher H/C and O/C, CHOS assignments than stream DOM (Figs. 3.2, 3.6, A2.15). This more aliphatic signature included homologous series of likely alkoxylated surfactants, seen at higher signal intensity with H/C $\geq$ 2.1 and O/C $\geq$ 0.6. These three series had 44.0262 *m/z* spacing, likely ethylene oxide (CH_2CH_2O) units. The 6 ion long, higher intensity series began with $C_{12}H_{26}O_{10}S$, and appears to be a sulfonated polyethylene glycol (Fig. 3.6). CHO, CHON, and CHONS classes also had higher H/C formula assignments than stream DOM (Figs. A2.1, A2.3, A2.6, A2.12-15). STDOM appears to overall have a more aliphatic molecular signature, which may reflect presence of lipids and linear detergents.

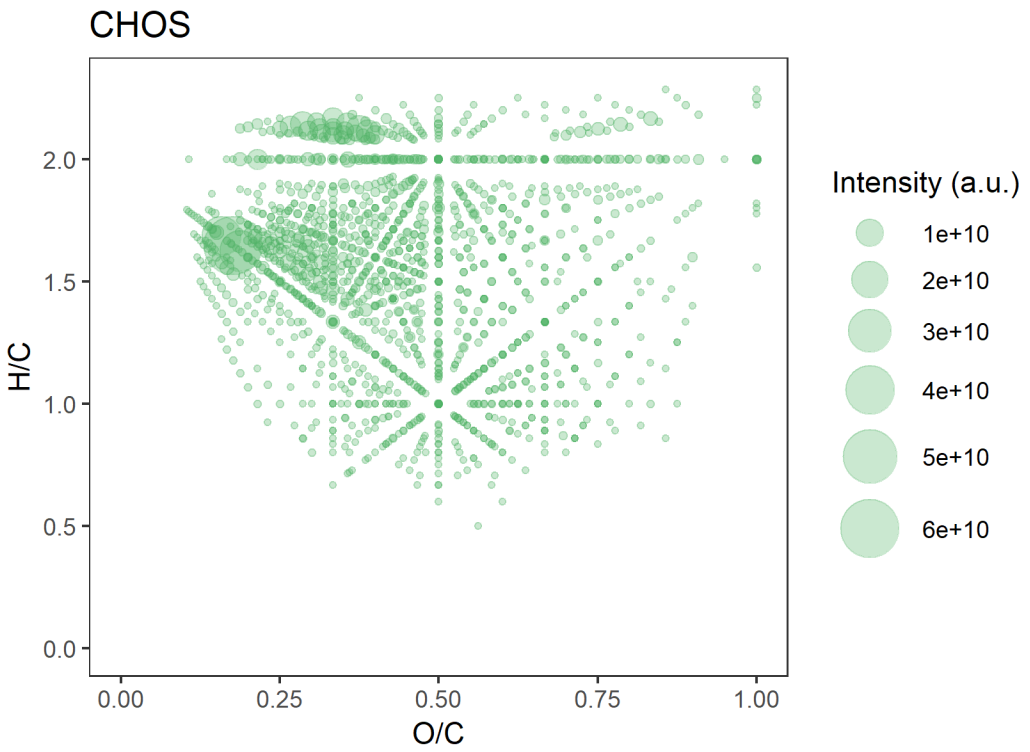

Figure 3.6 Van Krevelen diagram showing intensity averaged CHOS formula assignments in STDOM.

Of the 137 identified potential STE molecular tracers in the stream portion of this study, 108 of the same formulas were also identified in STDOM (Table A2.3). While FTICR MS is nonstructural, this supports an STE source, and that these or similar molecules may be present in initial septic system wastewater. Not matched formulas were not of a specific formula class and may be suppressed by highly ionizing sulfonates. Tracers that were not also found in STDOM included all CHOSCl tracers. Molecular tracers with >380 *m/z* were less commonly also detected in STDOM (Table A2.3), which also may reflect signal suppression in STDOM samples. Not found signals could also be due to the small septic tank sample size in this study (n=6) or they could reflect transformation products or metabolites being produced later in the drainfield or groundwater.

3.3.6 Identification of STE Impact

General molecular STE source indicators such as a higher presence of CHOS, CHON, and CHONS formulas, particularly with similar H/C and O/C ratios as those seen in higher septic impact stream DOM could be used to assess if surface water DOM molecular signatures may be STE impacted. This could be done quickly by nontargeted, full scan MS analysis such as with an FTICR MS, Orbitrap MS, or other ultrahigh resolution instruments, and avoids more time-intensive organic CEC quantification methods to assess likelihood of wastewater impact. Specific homologous series signatures related to STE impact, such as those of SPC, DATSI, PFASs, and PFACs, could also be used similarly in nontargeted analysis. Normalized SPC and DATSI signals may be able to perform as more quantitative indicators of STE impact. Commercial standards, if available, can also be purchased for chemicals in these series, so they can be quantified for true quantitative measures of STE impact or contributing STE water volume, although quantification of amphiphilic compounds is challenging.

The 137 identified molecular tracer ions which were only present at higher STE impacted streams may serve as more STE source specific markers. Most of these are previously undescribed as domestic wastewater tracers. Detection of these exact *m/z* values using ultrahigh mass resolution techniques could be used for quick nontargeted assessment of surface waters, with the higher % detected indicating a higher likelihood of domestic wastewater impact. “Top 10” lists of tracers may be more powerful indicators of STE impact. While certain CHOS formulas indicate

more STE impacted waters, CHONS formulas appear to be more ubiquitous and consistent source indicators of even moderate STE impact.

Tools for preliminary, nontargeted assessment of domestic wastewater impact could be used to decide sites of interest for further quantitative study using known CEC chemical tracers of domestic wastewater, saving analysis time and money. However, another goal of nontargeted tracer identification is to ultimately identify the molecular structures of tracers. Techniques like tandem MS (MS/MS) or nuclear magnetic resonance (NMR) spectroscopy can reveal structural information or even be used to identify the specific molecular structures of formulas, if sufficient separation (MS/MS) or isolation (NMR) is achievable. Some of these 137 potential tracers may be known chemicals with purchasable analytical standards, so they could be quantified by targeted analytical techniques. Standards could also be developed for structurally identified novel tracers. These chemical tracers could improve the toolbox for identifying domestic wastewater impact and source, as they could be more human or even STE specific or perform better than some commonly used CEC tracers.

3.3.7 Considerations and Future Research

This study was a preliminary step to identifying new indicators for STE impact. Future goals are to identify the molecular structures of the apparent best potential tracers by MS/MS for possible quantitative analysis. Similar molecular signature assessment should be undertaken in a wider variety of samples, such as groundwater, rivers, lakes, and marine waters, as well as in more regions with differing environments and geologies. This would provide a better understanding of

the performance, representativeness, and applicability of STE indicator tools used in this study. Developed tracers in this study are related to STE in these waters without significant other sources of wastewater impact but are not source specific and are likely also indicators of domestic wastewater and other wastewaters. Future work should try to better separate a more septic system source-specific signature through comparison to WWTP wastewaters. Future work could also explore potential health and ecosystem level effects of molecules related to STE impact.

Expected future analyses could use this year-long, seasonal stream DOM dataset to assess temporal trends in molecular composition. The septic system dataset, particularly the aerobic STDOM data, can be used to better understand degradation and molecular transformations, particularly through comparison with the oxygenated, and more degraded stream DOM STE signature. FTICR MS could be used to molecularly characterize transformation of septic system wastewater through different treatment technologies or through drainfields or groundwater plumes. We hope to perform similar assessment of positive ion mode stream and septic system data in the future. This would identify additional molecular tracers, and positive mode analysis is expected to improve detection of nitrogen containing molecules for a better understanding of septic system DON. Alkoxylated surfactant homologous series, like polyethylene and polypropylene glycols and potential degradation products, should be further studied as wastewater source indicators in stream data. Future studies should also better explore the likely microbial source of the septic system wastewater CHONS molecular signature.

3.4 Conclusions

STE impacts surface and groundwaters, and a septic system sourced wastewater signature is detectable in surface water in ways that well correlate with expected impact based on sucralose concentrations and septic system density. Streams with higher STE impact had higher presence of CHOS, CHON, and CHONS molecular formulas. These signatures are likely related to human diet and product use and are either from initial wastewater or are transformation products from before water parcels reach streams. Certain homologous series like PFCs and surfactant degradation products like SPC and DATSI can be STE indicators. Normalized FTICR MS signal intensities of SPC and DATSI can perform as semi-quantitative tracers for levels of STE impact.

We identified 137 molecular tracers that were unique to streams with higher STE impact, as well as additional potential molecular tracers. Most of these tracers were CHOS formulas and likely are surfactants or related to surfactants found in household cleaning and personal care products. CHOS tracers generally had much higher signal intensity, but CHONS tracers, which are thought to be microbially related, were more frequently detected and even present in more moderately STE impacted sites. We found 108/137 molecular tracer formulas were also present in STDOM, further supporting that these are indicators for STE. While there are many domestic wastewater chemical tracers, developed from known or expected compounds in waste, nontargeted tracer development allows for the identification of unknown or unconsidered molecular tracers. These molecules may be more commonly present, in higher concentrations, and/or resistant to removal in

comparison to currently used targeted STE tracers. These novel tracers may better indicate wastewater treatment level, degradation, age, or more human or septic system specific source.

Molecular characterization and tracer development in this study offer tools for researchers and managers to identify domestic wastewater contamination of surface and drinking waters and groundwaters. Improved detection of domestic wastewater impact through nontargeted methods may be a quicker and cheaper method for identifying contamination. While, future MS/MS analyses of specific molecular tracers could lead to molecular structure information or identification. Some of these compounds may be known or standards could be developed for targeted quantification. Results of this study are also of interest for understanding transformations of STDOM in the environment, particularly DON, and its bioavailability.

3.5 Acknowledgements

Thank you to members of the Harris Lab: Mindy Forsyth, Erin Reilly, and Isabel Sanchez-Viruet for assistance with sample collection, and to Jessica Flester for GIS assistance. We thank the septic system homeowners. We would also like to thank Steve Kullen, Dr. David Brownlee, Matthew Cumers, and the Calvert County Department of Planning and Zoning, for septic system location data and assistance with site selection. Thank you to Maryland Sea Grant for funding this work.

Chapter 4: Evaluating domestic wastewater tracers: nutrients, chloride, organic matter fluorescence, nitrate isotopic signatures, and contaminants of emerging concern (CECs)

Abstract

Septic systems can pollute groundwaters and surface waters, so it is important to be able to identify the presence of septic system wastewater contamination. In *Chapter 3* we developed septic system wastewater chemical tracers through nontargeted mass spectrometric analyses. In this study we assessed the performance of traditional chemical tracers through targeted analyses. We measured an extensive suite of commonly measured wastewater tracers, including nutrients, Cl, NO_3 isotopic signatures, and organic contaminants of emerging concern (CECs), as well as other chemical parameters in the same Maryland stream waters. We found total dissolved nitrogen (TDN), NO_3-NO_2, NH_4/NH_3, $\delta^{15}N_{NO3}$, Cl, and the artificial sweeteners, sucralose (SCL) and acesulfame-K (ace-K) to be the best performing of assessed tracers for identifying level of septic tank effluent (STE) impact. This work can help improve understanding and tracing of septic system contamination in the Chesapeake Bay region.

4.1 Introduction

Onsite wastewater treatment systems (OWTSs), the majority of which, in the U.S., are septic systems, are a source of pollution to surface and groundwaters. Therefore, it is important to identify chemicals that can be detected to track the

presence of septic system wastewater in the environment. There are many different "wastewater tracers" commonly measured or detected to identify septic system wastewater. These chemical markers are often in the general categories of human or human-microbiome produced markers, organic contaminants of emerging concern (CECs), inorganic constituents, or isotopic signatures. A summary of commonly used domestic wastewater tracers is provided in *Chapter 1*. All wastewater tracers are of varying efficacies and have various shortcomings, for example source specificity, analytical costs, seasonal effects, or detection limit (DL) restrictions, and it is often concluded that a suite of tracers provides the best information on wastewater presence, level of impact, and source (Oppenheimer et al., 2012; James et al., 2016).

Over the last few decades, organic CECs that are, or are related to, chemicals in human food and drinks, pharmaceuticals, personal care products, and household cleaners, have been increasingly measured as wastewater tracers. This is because of the increasing availability and resolving power of analytical techniques like tandem mass spectrometry and the fact that many of these chemicals are more human-sewage specific. Certain CEC tracers may be better performing because of factors such as common and/or high-volume use, high mobility, and persistence. Tracers are mainly selected based on the end goal of detection, whether that is to identify source, pathogenesis, signal age, nutrient loading, or the presence of persistent pollutants. Selection must also be made in consideration of overlapping signals of other potential wastewater sources such as those from direct watershed runoff or manufacturing or agricultural wastewaters. Separating signals of domestic wastewater types, such as

wastewater treatment plant (WWTP) effluent versus OWTS effluent can be an additional concern.

In this study we wanted to develop novel septic system wastewater tracers, the results of which are presented in *Chapter 3*; however, another goal was to assess the performance of existing commonly used wastewater tracers in these same watersheds. There have been few studies relating domestic wastewater tracers to septic system effluent loading in comparison to studies tracing WWTP effluent. Additionally, fewer wastewater tracer studies have been conducted for small, headwater streams despite headwaters playing an important role in pollutant removal. There is also a lack of temporal data for wastewater tracers, as longer-term sampling studies are less common.

A better understanding of tracer performance and the presence of septic system wastewater in surface waters is of special interest in the Chesapeake Bay watershed region. Lowering nutrient loading to the Bay is necessary to meet U.S. Environmental Protection Agency (EPA) Total Maximum Daily Load (TMDL) requirements as well as to improve Bay health. Nitrogen is removed in both traditional and advanced nitrogen-removing septic systems, drainfields, and groundwater (Oakley et al., 2010; Iverson et al., 2015). However, septic systems do cause elevated nitrogen concentrations in groundwater and surface waters (Iverson et al., 2015). Most rivers and streams have been shown capable of attenuating ~75% of net anthropogenic nitrogen input (NANI) before export (Boyer et al., 2002; Swaney et al., 2012). Attenuation of septic system nitrogen is likely to vary for different types of watersheds. This has been shown regionally for watersheds with differing geology

(Jordan et al., 1997b; Weller et al., 2011), contributions by groundwater versus surface water flow (Jordan et al., 1997b), and amounts of riparian forests (Weller et al., 2011). Improved knowledge of septic system effluent loading in the region will aid understanding of septic system nutrient loading and CEC contamination levels.

This study was conducted to compare contaminant presence in headwater streams with actual septic system wastewater, examine correlations between tracers and environmental variables such as septic system density, watershed size and type, and whether tracer performance was impacted by season. We measured an extensive suite of traditional wastewater tracers, other water quality parameters, and CECs in 9 small streams in Maryland, U.S. Almost all associated stream sampling was conducted approximately monthly over a year-long study. We additionally sampled wastewater from 6 septic tanks in the region to better understand concentrations of some of the same chemical species and parameters in initial wastewaters.

4.2 Materials and Methods

4.2.1 Study Sites and Collected Data

The region of the study is described in *Chapter 1* (Section 1.4.2) and the stream sites themselves are described in detail in *Chapter 3* (Section 3.2.1, Fig. 3.1). Namely, we sampled 8 streams in Calvert County, MD and 1 stream in Anne Arundel County, MD approximately monthly (n=12) for a year between October 2016 and November 2017. Streams were sampled at baseflow conditions. These streams drained regions of a variety of sizes (0.02-4.84 sq mi), a variety of septic system densities (0-2134 systems/sq mi), and land uses (10-100% undeveloped land use).

None of the catchments contained any treated WWTP effluent input and all had low to no agricultural land use (0-11%). Basin characteristics are from the USGS StreamStats Application (USGS, 2017) and USGS Chesapeake Bay Phase 6 1 m Land Use Datasets (USGS, 2019), and the septic system data was provided by Calvert County Department of Planning and Zoning. Basin characteristics for site SERC are from previous studies (Jordan et al., 1997a; Correll et al., 1999; Weller et al., 2003). The reference site SERC was only sampled 2/12 times during the main study period due to low flow conditions. Land use category simplification is described in *Chapter 3* (Section 3.2.1).

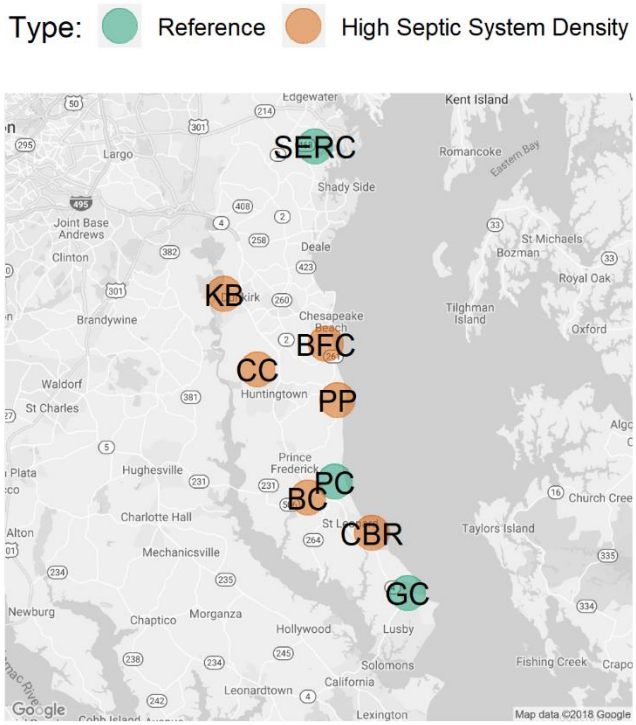

Figure 4.1 Map of stream sampling sites and initial division as high septic system density (>80 systems/sq mi) or forested reference sites (<60 systems/sq mi).

In the stream portion of the study, measurements were made for **pH**, **conductivity**, dissolved oxygen (**DO**), **temperature**, **stream width**, **flow**, **optical**

properties of dissolved organic matter (DOM), **$\delta^{15}N_{NO3}$**, **$\delta^{17}O_{NO3}$**, **$\delta^{18}O_{NO3}$**, **$\Delta^{17}O_{NO3}$**, **$\delta^{15}N_{DOM}$**, **$\delta^{13}C_{DOM}$**, total dissolved nitrogen (**TDN**), **NH_4/NH_3**, **NO_3-NO_2**, dissolved organic nitrogen (**DON**), total dissolved phosphorous (**TDP**), **PO_4**, **SO_4**, **Cl**, dissolved organic carbon (**DOC**), particulate phosphorous (**PP**), particulate nitrogen (**PN**), and particulate carbon (**PC**), dissolved **Zn** and **Hg**, and dissolved and particulate **Mn**, **Fe**, **Cd**, **Pb**, **Cr**, **Cu**, **As**, and **Se**. We additionally measured 16 CECs: the artificial sweeteners, **acesulfame-K** (ace-K) and **sucralose** (SCL); the antimicrobials, **triclosan** (TCS), and **methyl-** and **propylparaben** (MPB and PPB); the prescription drugs, **sulfamethoxazole** (SMX), **carbamazepine** (CBZ), and **atorvastatin** (ATS); the prescription and over-the-counter (OTC) drug, **diclofenac** (DCF); the non-steroidal anti-inflammatory drugs (NSAIDs), **ibuprofen** (IBU) and **acetaminophen** (ACM); **caffeine** (CAF) and its major metabolite **paraxanthine** (PXT); the nicotine metabolite, **cotinine** (COT); the insecticide, **dichlorvos** (DCV); and the hormone **estrone** (EST).

The compounds cover a range of human applications. ATS is a prescription statin medication. DCV is an insecticide with restricted household use. DCF is a prescription NSAID that was exclusively available as a prescription medication during the time of this study. Ace-K and SCL are artificial sweeteners found in food and drink products as well as personal care products. SMX is a prescription antibiotic. Carbamazepine CBZ is a prescription anticonvulsant that is used in the treatment of epilepsy, bipolar disorder, and other conditions.

In the septic tank portion of the study, we sampled septic tank wastewater from 6 traditional septic tanks in Calvert County, MD. Samples were collected one

time per system between August and October 2018. In 2 of these systems, samples were collected from both first and second chambers. One of these systems, the second chamber was continuously oxygenated by an oxygen pump. Septic systems were single household systems of various ages. Measurements were made for **pH**, **optical properties of DOM**, **TDN**, **NH_4/NH_3**, **NO_3-NO_2**, **DON**, **TDP**, **PO_4**, **DOC**, **SCL**, **CAF**, **PXT**, and **TCS.**

4.2.2 Stream Sampling Design

Measurements for pH, conductivity, dissolved oxygen (DO), and temperature were made in the field at each sampling with a multiparameter sonde. Stream width and flow data were also collected at sampling, with flow measured using a Marsh McBirney Flo-Mate Model 2000 electromagnetic flow meter. For optical measurements, DOC, TDN, SO_4, Cl, and NO_3 specific isotope analysis, approximately four 30 mL samples were collected at each site per sampling in trace contaminant certified or acid-washed and combusted 40 mL amber glass vials or base- or acid-washed HDPE bottles. These samples were filtered in the field using sterile syringes and syringe filters (0.2 µm, Whatman GD/X cellulose acetate). Syringes were sample rinsed 3 times and a small rinse was sent through filters before sample collection to minimize potential leaching. Samples for optical properties were stored in the lab at 0 °C, while other samples were stored at -20 °C until analysis. Approximately 200 mL samples were collected in acid-washed, and sample-rinsed HDPE bottles for NH_4/NH_3, NO_3-NO_2, TDP, PO_4, PP, PN, PC, and secondary analysis of TDN. These samples were vacuum filtered in the lab using provided filters

and subsampled into provided bottles for measurements by the Nutrient Analytical Services Laboratory (NASL), Chesapeake Biological Laboratory (CBL), MD.

Duplicate 2 L grab samples were collected in combusted (500 °C) glass bottles, after sample rinsing bottles 3 times, for Agilent Bond Elut PPL solid-phase extraction (SPE) in the laboratory. These SPEs were used for all CEC analysis except ace-K. In September 2017, single large volume additional samples (20 L for the low DOC sites, KB and BC, 10 L for all other sites) were collected for all sites besides SERC, while a 6.5 L additional sample was collected for SERC in February 2018. These large volume samples were collected in base-washed, HDPE cubitainers for SPE for $\delta^{15}N_{DOM}$ and $\delta^{13}C_{DOM}$. Additional duplicate 300 mL grab samples were collected in December 2018, after the main study period, for Waters Oasis reversed-phase/weak-anion exchange (WAX) SPE for analysis of ace-K, which was found to have poor recovery by PPL SPE. Samples were also taken at this time for analysis of dissolved and particulate metals in acid-washed PTFE bottles. In the laboratory, these were vacuum filtered through combusted 0.7 µm Whatman GF/F filters, with the filtrate used for dissolved species and the filters microwave digested in concentrated ultrapure nitric acid for particulates. The filters used are known to contain Zn, so particulate Zn was not measured.

4.2.3 Septic Tank Sampling Design

Acid-washed peristaltic tubing and a peristaltic pump was used to collect samples from below the grease layer. Duplicate samples were collected in combusted glass bottles, after sample rinsing bottles 3 times. In the lab, duplicates were separated into volumes of approximately 500 mL, if a single chamber was sampled, and to 250

mL for the first and 500 mL for the second, if two chambers were sampled for PPL SPE and for CEC quantifications. We measured pH using a pH meter. Subsamples were taken for optical measurements and DOC as well as for NH_4/NH_3, NO_3-NO_2, secondary measurement of TDN, TDP, and PO_4 which was measured after sample filtration by NASL.

4.2.4 Filtering and Solid-Phase Extraction of DOM

SPE was used to concentrate and desalt samples for measurements of CECs and isotopic analyses of extractable DOM. The 2 L duplicate stream grab samples and septic tank wastewater samples were extracted, also in duplicate, as described in Chapters 2 (2.2.2) and 3 (3.2.3). The additional WAX SPE used to recover ace-K in streams was undertaken using Waters Oasis WAX (150 mg, 6 mL, 30 µm particle size) cartridges. These cartridges were activated with 5 mL of a ~2% NH_3, NH_4OH methanol (MeOH) solution, which was made with reagent grade, ~20% NH_4OH water solutions diluted in LC/MS grade MeOH. Cartridges were rinsed with 5 mL LC/MS grade MeOH and 5 mL ultrapure water. Samples were then gravity-loaded onto the cartridges. The outside and inside reservoir of cartridges was briefly rinsed with ultrapure water then the cartridge sorbent was rinsed with 10 mL ultrapure water and dried under vacuum. Samples were eluted with 3 mL LC/MS grade MeOH for a reverse-phase fraction and then 3 mL of the NH_4OH MeOH solution for an anion exchange fraction. The anion exchange fraction was used for ace-K measurements.

The large volume (6.5-20 L) SPE to recover enough stream DOM for isotopic analyses was carried out with cleaned 5g of PPL packed into 60 mL cartridges. PPL was cleaned using a 24-hour Soxhlet extraction method with 50:50, high purity

acetone and hexane. Previous in-lab tests have shown recovery and background equivalent to new PPL. Samples were extracted as described for PPL extractions except all steps were at 25 mL volumes and extracts were eluted in 30 mL MeOH.

4.2.5 Analytical Methods

Optical properties, excitation-emission matrix (EEM) fluorescence and UV-vis absorption, were measured simultaneously using a Horiba Aqualog spectrofluorometer as described in *Chapter 5* (Section 5.2.2, Text A4.6). Raman, first-order Rayleigh, and second-order Rayleigh scatter was corrected and EEMs were smoothed. Septic tank DOM (STDOM) was diluted for analysis and EEMs have been corrected for dilution. Stream DOM EEMs were analyzed using statistical parallel factor analysis (PARAFAC) modeling using the MATLAB DrEEM toolbox (Murphy et al., 2013). We removed 2 outliers (n=96) as well as excitation scans <250 nm because of high leverages. A five-component model was generated to explain the data, which was split-half validated using four random splits and met other validation requirements (Murphy et al., 2013). Unit normalization was reversed to report components. The maximum fluorescence values of components, Fmax01-Fmax05, were summed for each sample and the relative contribution in % of each Fmax value were calculated to explain representation by these statistical components.

DOC and stream TDN were measured using a Shimadzu total organic carbon analyzer (TOC-VCPH) with a total nitrogen unit (TNM-1). SO_4 and Cl were measured with a Dionex ICS-1000 Ion Chromatograph (IC) as described in *Chapter 2* (Section 2.2.5). Dissolved Hg was measured using a Tekran 2600 mercury analyzer using EPA Method 1631. All other metals were measured using an Agilent 7500 ICP-

MS. Filters were frozen and microwave digested in concentrated nitric acid and diluted for analysis. All measured values were blank corrected, and standards and the digestion procedure is described in *Appendix 4* (Text A4.4).

TDN, NH_4/NH_3, NO_3-NO_2, TDP, PO_4, PP, PN, PC were measured by NASL using standard methods. As reported by NASL, TDN and TDP were undertaken with an alkaline persulfate digestion and then measured using EPA Methods 353.2 and 365.1, respectively. Combined NO_3-NO_2 was determined using ASTM D7781-14 with occasional use of EPA 353.2 for low values. NH_4/NH_3 was at different points measured by SM 4500-NH_3 F and G and EPA Method 350.1. PP was measured using the methods described in Aspila et al. (1976) and EPA Method 365.1. PO_4 was determined using EPA Method 365.1. PN and PC were measured using EPA Method 440.0.

NASL TDN measurements used a colorimetric method that is believed to be more accurate at higher values than the TOC analyzer catalytic combustion method (ASTM D8083), so NASL measurements are used with some missing values substituted with data from the catalytic combustion method where a correction factor has been applied. This correction factor was developed using regression analysis, assuming an intercept of zero. The regression was statistically significant ($p<0.01$) and the slope of the relationship was 1.18. We calculated DON by subtracting total inorganic nitrogen (TIN) (NH_4/NH_3 and NO_3-NO_2) from TDN, with small negative values, likely due to combined error, set to 0.

4.2.6 Stable Isotope Analyses

Nitrate specific isotopic analysis, $\delta^{15}N_{NO3}$, $\delta^{17}O_{NO3}$, $\delta^{18}O_{NO3}$, was done by the Central Appalachians Stable Isotope Facility (CASIF, Appalachian Laboratory of the University of Maryland Center for Environmental Science, MD). NO_2 was included in these measurements but was expected to be at negligible concentrations relative to NO_3. These data were only collected seasonally (Fall, Winter, Spring, Summer) during the main study period, as possible by nitrate minimum concentration requirements. Some samples were concentrated by evaporation or freeze-drying to concentrate nitrate for analysis. Analysis was done using the bacterial denitrifier method with N_2O thermally decomposed (800 °C) into N_2 and O_2 to allow additional measurement of $\delta^{17}O_{NO3}$, and therefore, $\Delta^{17}O_{NO3}$. Slight negative $\Delta^{17}O_{NO3}$ values, likely due to compounded precision error, were set to 0 for site averages and % atmospheric NO_3 calculations. Measurements were made on a ThermoFisher Delta V+ Isotope Ratio Mass Spectrometer (IRMS). Isotope ratios were normalized using reference materials USGS34 and USGS35 for O and USGS32 and USGS34 for N isotopes.

Complex cycling, alterations to NO_3 isotopic composition, and mixing of NO_3 from multiple sources can complicate tracing. Atmospheric NO_3 is highly enriched in ^{18}O relative to other NO_3 sources such as soil, fertilizer, and wastewater; however, $\delta^{18}O_{NO3}$ is subject to numerous biogeochemical alterations (Kendall et al., 2007). The use of photosynthetically produced, ^{18}O depleted O_2, in nitrification would produce ^{18}O depleted NO_3, whereas, denitrification produces ^{15}N and ^{18}O enrichments in remaining NO_3 (Kendall et al., 2007). Consequently, mixing models using source

specific mean $\delta^{18}O$ as end members to estimate % atmospheric nitrate are limited by uncertainties in signature alteration. A triple oxygen isotope (^{16}O,^{17}O, ^{18}O) method, as used here, can be used to address fractionations altering $\delta^{18}O$. Through $\delta^{17}O_{NO3}$ and the triple oxygen isotope tracer $\Delta^{17}O_{NO3}$, the contribution of atmospheric NO_3 can be unambiguously measured. The triple stable oxygen isotope method eliminates $\delta^{18}O$ alteration uncertainties by controlling for kinetic and equilibrium, or mass-dependent, fractionation which effects $\delta^{18}O$ and $\delta^{17}O$ in an expected ratio, $\delta^{17}O \cong 0.52 \times \delta^{18}O$.

This linear mass-dependent fractionation, also known as the Terrestrial Fractionation Line (TFL), has an approximate slope of 0.52 (Michalski et al., 2004). The oxygen isotope signature of atmospheric NO_3 deviates from this mass-dependent relationship and is enriched in ^{17}O relative to ^{18}O. This is believed to be because of oxygen sourced from ozone which is known to have a mass-independent isotopic composition ($\delta^{17}O \cong 1 \times \delta^{18}O$) (Thiemens and Heidenreich, 1983; Michalski et al., 2004). A difference from the isotopic signature expected from the TFL is measured as $\Delta^{17}O$, where $\Delta^{17}O \cong \delta^{17}O - 0.52 \times \delta^{18}O$ (Michalski et al., 2004).

Non-atmospheric sources of NO_3, such as nitrification and synthetic fertilizers, do not have mass independent isotopic fractionation signatures, so have a $\Delta^{17}O$ of 0‰ and fall on the TFL (Michalski et al., 2004). Seasonal and global differences in $\Delta^{17}O_{NO3atm}$ are well understood, with values typically between 20 and 30 ‰ in the mid-latitudes (Michalski et al., 2003; Alexander et al., 2009). Proportion of atmospheric nitrate can be estimated using a mixing model based on this range of expected values, so % atmospheric NO_3 was estimated as $(\Delta^{17}O_{NO3} / 25) \times 100$.

Isotopic analyses on extractable DOM, $\delta^{15}N_{DOM}$ and $\delta^{13}C_{DOM}$, were performed by the Stable Isotopes Laboratory, CBL, MD, also using a ThermoFisher Delta V+ IRMS. Aliquots of PPL SPE material were dried in tin capsules at 45 °C prior to analysis. The larger volume SPE aliquots needed for $\delta^{15}N_{DOM}$ (12-23 mL SPE versus 0.8 mL for $\delta^{13}C_{DOM}$) were first concentrated by freeze-drying before transfer to tin capsules. Standards were acetanilide and bass protein lab standards which were calibrated against USGS40 and USGS41a. Isotopic values are reported using delta notation and expressed in permil (‰) relative to Vienna Pee Dee Belemnite (VPDB) (C), atmospheric nitrogen (N), and Vienna Standard Mean Ocean Water (VSMOW) (O).

4.2.7 HPLC/QqQMS/MS Quantification of CECs

High performance liquid chromatography (HPLC) triple quadrupole (QqQ) tandem mass spectrometry (MS/MS) was used to quantify the 16 CECs. This was undertaken using an Agilent 1260 Infinity II LC interfaced with an Agilent 6420 Triple Quadrupole MS, generally following the methods described in *Chapter 5* (Section 5.2.2) for both quantification of ace-K and all other CECs (the "Main CEC Method"). A MAC-MOD UltraShield pre-column filter was used for both methods. The Main CEC Method used an ACE Excel C18-PFP (3.0 mm i.d. × 100 mm, 2 µm particle size) column connected to an ACE HILIC-B (2.1 mm i.d. × 50 mm, 1.7 µm particle size) column, while the ace-K method used only the C18 column. Other differences in injection volume and LC gradient for the Main CEC Method are described in *Chapter 2* (Section 2.2.5). Analytical standards and SIL-ISTDs for additional CECs that were not measured in *Chapter 5* (Table A4.2) are described in

Appendix 3 (Table A3.1). Monitored transitions for ace-K are in *Appendix 4* (Table A4.6) and other CECs are described in *Appendix 3* (Table A3.2). Please see *Appendix 3* (Text A3.1) for discussion of SPE recovery. Because of compound carryover/contamination, cotinine was only measured as detected/not detected (ND) based on blank subtraction of the maximum value blank in the instrument run.

4.2.8 Multivariate Statistics

One goal of evaluating environmental forensic tracers for septic system wastewater is to determine how they align with environmental characteristics and measurements. We were particularly interested in environmental factors such as septic system density, land use, stream chemistry, and local nutrient concentrations for carbon, phosphorus, and especially nitrogen. We applied multivariate statistical technique to the tracer and environmental data collected from each of our drainage basins. This required some reduction in the dataset due to missing values so that the total number of samples for this analysis was n=94 and only a critical subset of variables were evaluated (Tables 4.1-4.5). These included cluster analysis and a non-parametric approach for visualizing these data using multi-dimensional scaling (MDS) plots, all using Primer-E version 6 software. A key step in these analyses is computing a resemblance matrix using Euclidean distances. The environmental data were first log transformed (log(x+1)) and then normalized. The resemblance matrix and cluster analysis relied on a similarity profile routine (SIMPROF; Clarke 2008) to test data groupings. The resemblance matrix was also used to create non-metric multi-dimensional scaling plots and overlain with groupings developed with the cluster

analysis. The visualization produced from this for the MDS plot had reported 2D stress levels less than 0.20.

4.2.9 Data Handling and Missing Data

For data below reporting limits but above detection limits, measured values are reported and included in site summary data. For CECs, instrument detection limits fluctuated day to day during analysis, the higher STE impacted sites, KB, CBR, and BFC, were run at higher dilution levels, and there is minor varying in SPE concentration factors. For these reasons, reported method detection limits (MDLs) are representative approximations calculated as described (Text A3.2, Table A3.3), and there are remaining values in the dataset that are smaller than approximate MDLs.

In this large dataset, some data are missing due to factors such as instrument malfunction, sample loss, or variables that were added later in the sampling plan. For example, Cl and SO_4 were not measured for the first month of the year-long study and 2 sites were not measured for Hg. While only analyzed seasonally, some expected NO_3 specific isotope measurements were not possible due to minimum NO_3 concentration requirements for the triple oxygen isotope method. For multivariate statistics some missing data were corrected and ND values and NASL <MDL measurements were substituted to allow for data transformation. CECs that were never detected in any samples, data that were not measured as part of the monthly year-long study, and confounding similar or repeated variables were excluded. Missing TDN measurements were corrected as described. NASL values that were <MDL and ND CECs were set as (1/3 × MDL) or (1/3 × the minimum detected value) if a smaller value.

4.3 Results and Discussion

4.3.1 Stream Data and STE Impact Tracing

For understanding of data, apparent stream STE impact was ranked based on the agreement of the artificial sweetener CECs, sucralose and acesulfame-K. Both are very persistent and hydrophilic wastewater tracers (Buerge et al., 2009; Oppenheimer et al., 2011). Data tables are, therefore, displayed in this site ranking order: BFC, CBR, KB, CC, PP, PC, GC, BC, SERC. This is a better representation of the level of STE impact rather than septic system density, which does not account for actual system use or fully control for basin size. For example, the high septic system density site, BC, was mainly new home development with septic systems not in use during the sampling period. Higher apparent impact was also found at the small drainage basin site, KB, despite similar septic system density to large basin sites, CC and PP, which may be due to improved treatment potential or increased groundwater storage potential. However, septic system density ranking did generally agree with the rankings of other traditional wastewater tracers. Results were not related to differences in septic system types as advanced, nitrogen-removing septic systems, known as “Best Available Technology” (BAT) systems had only a small contribution to septic system density. As stated, the highest BAT site, BC, was mainly new development where systems were not in-use or possible groundwater impact had not yet reached surface waters.

Table 4.1 Stream site characteristics, land use, and septic system density. Asterisks (*) denote parameters included in multivariate statistical analyses.

Sites	Drainage Area (sq mi)*	Width (in)	Flow (f^3/s)*	% Developed*	% Semi-developed	% Undeveloped*	% Agriculture*	Traditional/ BAT Systems	Traditional/ BAT Septic System Density (systems/sq mi)*	Total Septic System Density (systems/sq mi)
BFC	0.04	21	0.02	42	48	10	0	76/3	2053/81	2134
CBR	0.25	37	0.11	28	47	24	0	209/7	836/28	864
KB	0.53	44	0.32	13	32	48	8	78/1	148/2	150
CC	3.91	89	1.97	13	33	52	3	773/6	198/2	199
PP	4.84	119	2.45	8	16	70	6	650/6	134/1	135
PC	0.53	43	0.32	4	10	75	11	29/0	55/0	55
GC	0.35	41	0.41	7	11	82	0	5/0	14/0	14
BC	0.53	33	0.18	5	3	90	2	26/41	49/77	127
SERC	0.02	-	0.0008	0	0	100	0	0/0	0/0	0

Table 4.2 Stream site characteristics, particulate nutrients, and phosphorus. Asterisks (*) denote parameters included in multivariate statistical analyses.

Sites	pH*	Temperature (°C)*	DO (mg O_2/L)	Conductivity (mS/cm)*	DOC (mg C/L)*	PP (mg P/L)*	PN (mg N/L)*	PC (mg C/L)*	TDP (mg P/L)*	PO_4^{3-} (mg P/L)*
BFC	6.9	14	7.4	0.49	3.4	0.021	0.042	0.511	0.006	0.003
CBR	6.8	13	8.1	0.44	4.0	0.016	0.039	0.865	0.018	0.010
KB	5.8	12	9.6	0.26	2.3	0.084	0.035	0.583	0.065	0.039
CC	6.9	12	10.2	0.30	3.4	0.069	0.052	0.874	0.049	0.020
PP	6.9	14	10.0	0.26	5.6	0.044	0.064	0.865	0.052	0.026
PC	7.4	13	9.9	0.27	3.2	0.076	0.139	2.736	0.036	0.019
GC	6.2	13	9.8	0.15	2.9	0.004	0.027	0.642	0.006	0.002
BC	7.1	14	10.1	0.17	2.6	0.014	0.026	0.710	0.034	0.024
SERC	4.8	-	-	0.10	5.3	0.028	0.093	1.020	0.021	0.016

Table 4.3 Stream nitrogen and isotopic signatures. Asterisks (*) denote parameters included in multivariate statistical analyses.

Sites	TDN (mg N/L)*	NO_3^--NO_2^- (mg N/L)*	NH_4^+/NH_3 (mg N/L)*	DON (mg N/L)	$\delta^{15}N_{NO3}$ (‰)	$\delta^{18}O_{NO3}$ (‰)	$\delta^{17}O_{NO3}$ (‰)	$\Delta^{17}O_{NO3}$ (‰)	$\delta^{13}C_{DOM}$ (‰)	$\delta^{15}N_{DOM}$ (‰)
BFC	6.0	5.03	0.80	0.50	11.6	5.5	3.0	0.4	−27.5	1.1
CBR	2.5	2.14	0.08	0.37	11.3	5.2	2.9	0.3	−28.6	2.7
KB	2.2	1.88	0.10	0.20	7.4	3.7	2.3	0.6	−27.6	1.5
CC	0.8	0.45	0.10	0.28	7.6	5.9	3.3	0.3	−28.3	1.2
PP	0.5	0.13	0.04	0.28	5.8	0.5	1.4	1.1	−29.3	2.9
PC	0.4	0.21	0.06	0.16	5.7	3.4	2.4	0.6	−29.0	0.1
GC	0.5	0.35	0.04	0.14	5.4	4.5	2.9	0.6	−28.8	0.6
BC	0.2	0.05	0.02	0.08	-	-	-	-	−29.5	0.1
SERC	0.4	0.15	0.02	0.14	5.5	1.7	2.7	1.8	−28.3	0.3

Table 4.4 Stream Cl, SO_4, and dissolved (D) and particulate (P) metals.

Sites	Cl^- (mg/L)	SO_4^{2-} (mg/L)	Cr (µg/L)		Mn (µg/L)		Fe (µg/L)		Cu (µg/L)		Zn (µg/L)	As (µg/L)		Se (µg/L)		Cd (µg/L)		Hg (ng/L)	Pb (µg/L)	
			D	P	D	P	D	P	D	P	D	D	P	D	P	D	P	D	D	P
BFC	81	21	0.7	ND	909	0.5	2850	1190	ND	ND	46	1.9	ND	0.3	ND	0.44	ND	-	0.08	ND
CBR	79	17	ND	ND	131	0.2	415	379	0.2	ND	32	2.2	ND	0.7	0.07	ND	0.04	2.4	0.42	ND
KB	47	27	ND	ND	52	0.2	347	105	0.1	0.19	86	1.8	ND	2.3	ND	9.02	0.68	1.8	0.12	ND
CC	44	18	ND	ND	87	0.3	379	743	ND	ND	29	1.7	ND	0.4	0.11	0.34	0.40	-	0.09	ND
PP	38	14	ND	ND	132	1.2	313	642	ND	ND	13	1.9	ND	0.3	ND	0.01	0.04	1.9	0.06	ND
PC	21	16	ND	0.16	57	0.4	282	613	ND	ND	14	1.6	ND	ND	0.14	ND	0.15	1.6	0.49	ND
GC	32	10	ND	ND	40	0.2	358	450	ND	ND	22	1.7	ND	0.4	0.05	ND	ND	1.9	0.14	ND
BC	15	11	ND	ND	43	0.3	194	256	ND	ND	17	1.7	ND	0.4	0.05	ND	0.06	1.2	0.10	ND
SERC	8	27	ND	ND	80	0.2	663	481	0.2	ND	26	3.6	ND	1.8	ND	0.30	0.01	3.5	0.20	ND

Table 4.5 Stream CECs. Asterisks (*) denote parameters included in multivariate statistical analyses.

Sites	Ace-K (µg/L)	SCL (µg/L)*	CBZ (ng/L)*	COT (# Detects)	IBU (ng/L)*	TCS (ng/L)*	DCF (ng/L)*	SMX (ng/L)*	CAF (ng/L)*	PXT (ng/L)*	ACM (ng/L)	ATS (ng/L)	EST (ng/L)	DCV (ng/L)	MPB (ng/L)	PPB (ng/L)
BFC	4.26	13.3	1	10/12	160	15	1	ND	49	46	ND	ND	ND	ND	ND	ND
CBR	1.32	4.9	83	7/12	20	ND	ND	ND	69	20	ND	ND	ND	ND	ND	ND
KB	0.77	1.8	28	5/12	ND	ND	ND	7	65	40	ND	ND	ND	ND	ND	ND
CC	0.28	1.0	1	5/12	ND	ND	ND	ND	ND	ND	ND	ND	ND	ND	ND	ND
PP	0.20	0.5	1	5/12	ND	ND	ND	ND	ND	13	ND	ND	ND	ND	ND	ND
PC	0.07	0.5	2	3/12	ND	ND	ND	ND	25	ND	ND	ND	ND	ND	ND	ND
GC	0.07	0.3	7	0/12	ND	ND	ND	ND	48	27	ND	ND	ND	ND	ND	ND
BC	0.02	0.1	ND	0/12	ND	ND	ND	ND	15	9	ND	ND	ND	ND	ND	ND
SERC	ND	ND	ND	0/2	ND	ND	ND	ND	ND	ND	ND	ND	ND	ND	ND	ND

Land use trends matched septic system density data and site STE impact ranking. Note, land use for BC does not reflect new development. Higher % developed and % semi-developed land-use had higher septic system density, as expected, as there is very minimal sewer infrastructure in the study basins.

Traditionally used chemical wastewater tracers were found to be performing well and in good agreement for apparent levels of STE impact. TDN, and its components NH_4/NH_3, NO_3-NO_2, and DON, $\delta^{15}N_{NO3}$, conductivity and the major contributing species, Cl, and presence and concentrations of CECs all showed general trend agreement and were higher at sites with higher expected STE impact. An in-depth discussion of measured parameters follows.

4.3.2 Stream DOM Fluorescence

In contrast to specific chemical wastewater tracers, DOM fluorescence was not found to perform as a wastewater tracer in these streams. Protein-like (275-300/340-355) (Murphy et al., 2014) or fluorescent whitening agent (FWA) (360-365/400-440 nm ex/em) (Assaad et al., 2014) characteristic fluorescence have been suggested as tracers of domestic wastewater impact (Baker, 2001; Assaad et al., 2014). PARAFAC analysis showed no clear trends between DOM fluorescence signatures and STE impact evidenced by numerous chemical tracers. Component 1, which has sometimes been referred to as a "humic-like" signature, includes the FWA region. Component 5 best fit what has been referred to as a "protein-like" signature. Fmax values of components, Fmax01-05, and % relative abundances did not show clear trends between sites but reflected shared seasonal fluorescence trends. Overall fluorescence was lower in winter and Fmax04, and therefore, its relative abundance,

increased in May-June, coinciding with spring onset (Fig. A3.1). DOM fluorescence was not a useful wastewater tracer and we caution the use of DOM fluorescence as a tracer beyond at immediate wastewater outflows.

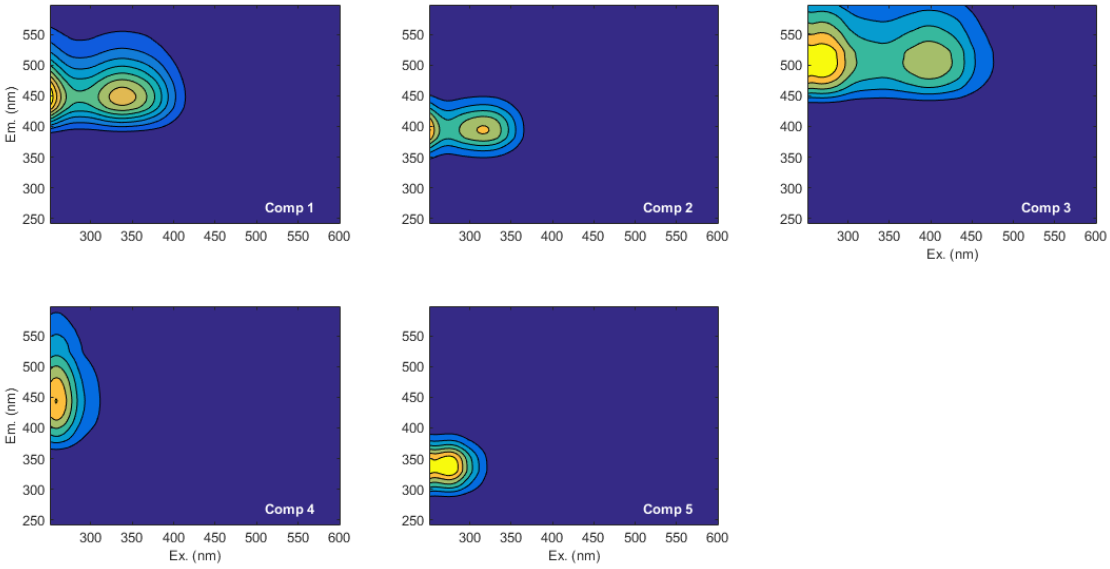

Figure 4.2 PARAFAC components in stream DOM EEM spectra.

4.3.3 Stream Metals

There were no clear trends between metal concentrations and STE impact (Tables 4.1-4.5). This matches the conclusions of previous septic system studies which have shown low mobility of most metals (Robertson, 2008; Richards et al., 2016). Iron and manganese concentrations were high (~3 mg/L dissolved, 1 mg/L particulate Fe; 1 mg/L dissolved Mn) at the highest STE impact site (BFC) which matches field observations of iron flocculates and apparent presence of iron-oxidizing bacteria and lab observations of iron precipitation during handling. This stream is believed to be mainly fed by a highly STE impacted, anaerobic groundwater seep and has the highest average concentrations of nitrogen species, particularly NH_4/NH_3 (Table 4.3). While high iron concentrations are likely natural, in combination with

STE-sourced contaminants (Table 4.5), this could lead to worse stream health effects. A connection between STE impact and iron could be interesting to explore as iron-oxidizing bacteria are diverse (Emerson et al., 2010) and there are nitrate-reducing iron-oxidizing bacteria (Schaedler et al., 2018).

Cadmium was measured at a high concentration, 9 µg/L, at site KB. This is much higher than the U.S. EPA's Aquatic Life Ambient Water Quality Criteria for cadmium (1.8 µg/L acute, 0.72 µg/L chronic) (U.S. EPA, 2016). The reason for this seemingly high presence of cadmium is unclear. Site KB had higher % agricultural land use than most other sites and the highest average concentrations of PP, TDP, and PO_4 (Tables 4.1, 4.2). Cadmium can be elevated in phosphate fertilizers (Williams and David, 1976). Other possible sources at this site are metal stream diversions, other anthropogenic sources, or natural sources due to local geology.

4.3.4 Stream NO_3 and DOM Isotopic Signatures

Compound specific isotope analysis (CSIA) of NO_3 can be used for wastewater tracing, as described in detail in *Chapter 1* (Section 1.2.4). Fractionation processes separate source isotopic signatures and determine the range of observed isotopic values within a NO_3 source, allowing NO_3 isotopic signatures to be related to atmospheric, various fertilizer, soil, or sewage-sourced NO_3 (Kendall et al., 2007). If there is no isotopic signature evidence for significant denitrification fractionation effects, an isotopically "heavier" $\delta^{15}N_{NO3}$ signature can be related to sewage contamination and $\delta^{15}N_{NO3}$ >8.6 ‰ is a more unambiguous marker of sewage-sourced NO_3 (Kendall et al., 2007). Here sewage refers to higher trophic level animal waste and can be human or non-human animal wastewater.

Higher $\delta^{15}N_{NO3}$ was measured at sites with higher STE impact as indicated by numerous wastewater tracers and basin characteristics (Table 4.3, Fig. A3.9). This indicates likely human sewage sourced nitrogen as other animal nitrogen sources are not expected to be significant in these basins and shows that STE is the source of elevated nitrogen in these streams. The 2 highest STE impacted sites were found to have $\delta^{15}N_{NO3}$>8.6 ‰ in all seasonal measurements during the year-long study, while the 3rd highest STE impacted site measured in this more conclusive wastewater $\delta^{15}N_{NO3}$ range in fall (Fig. 4.3).

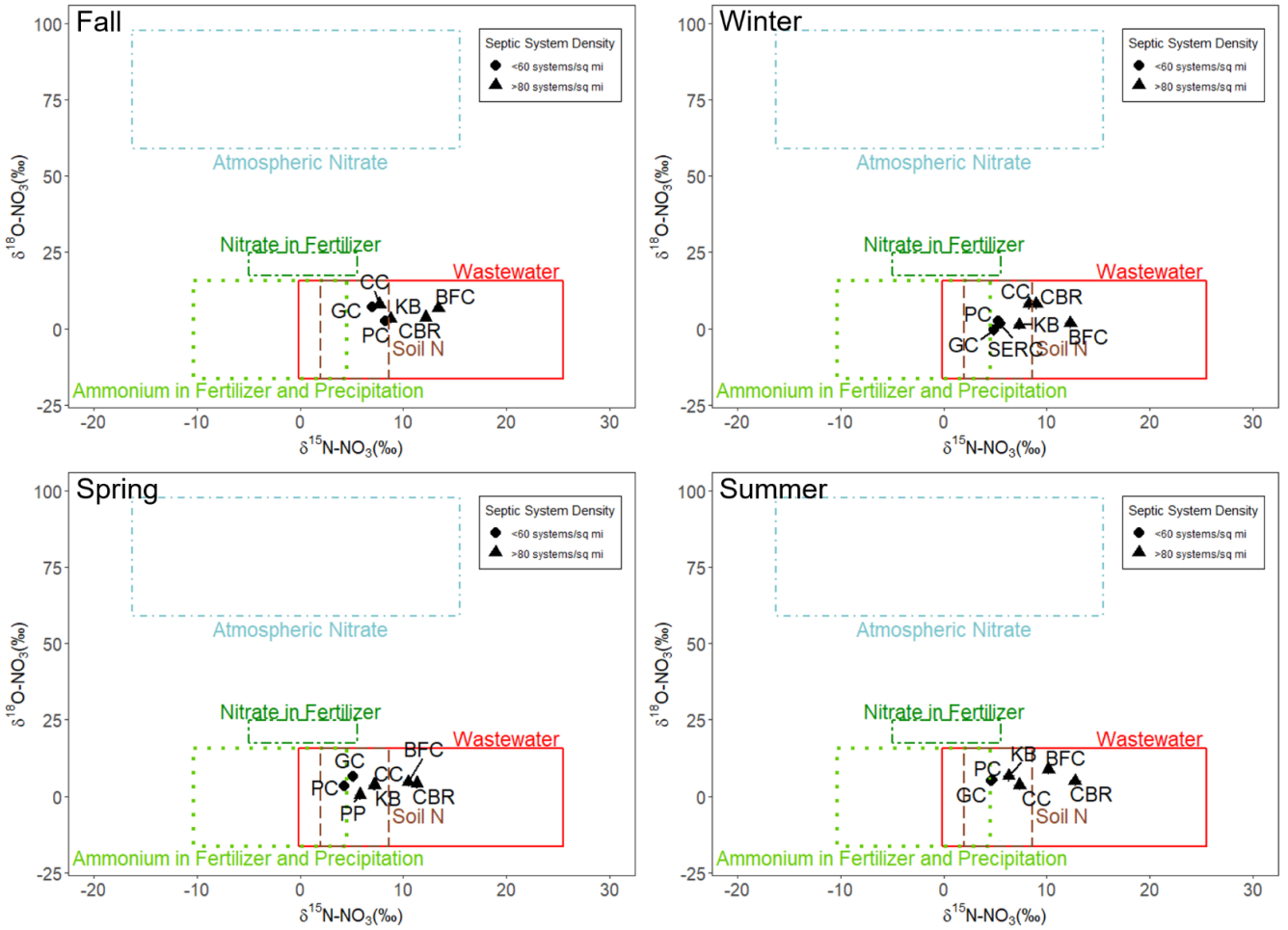

Figure 4.3 Seasonal isotopic signatures of stream $\delta^{15}N_{NO3}$ and $\delta^{18}O_{NO3}$. Source signature regions from Kendall et al. (2007). Error bars show precisions.

Values of $\delta^{18}O_{NO3}$ were low and there were no clear negative correlations between $\delta^{15}N_{NO3}$ and $\delta^{18}O_{NO3}$, indicating atmospheric nitrogen deposition was unimportant. There were also no clear positive correlations between $\delta^{15}N_{NO3}$ and $\delta^{18}O_{NO3}$, indicating that denitrification isotopic fractionation effects were unlikely to have significantly altered measured values (Fig. 4.3). Minimal atmospheric nitrogen contribution was confirmed by $\Delta^{17}O_{NO3}$ which showed average ~2% atmospheric NO_3 contribution across samples with a maximum of ~7%.

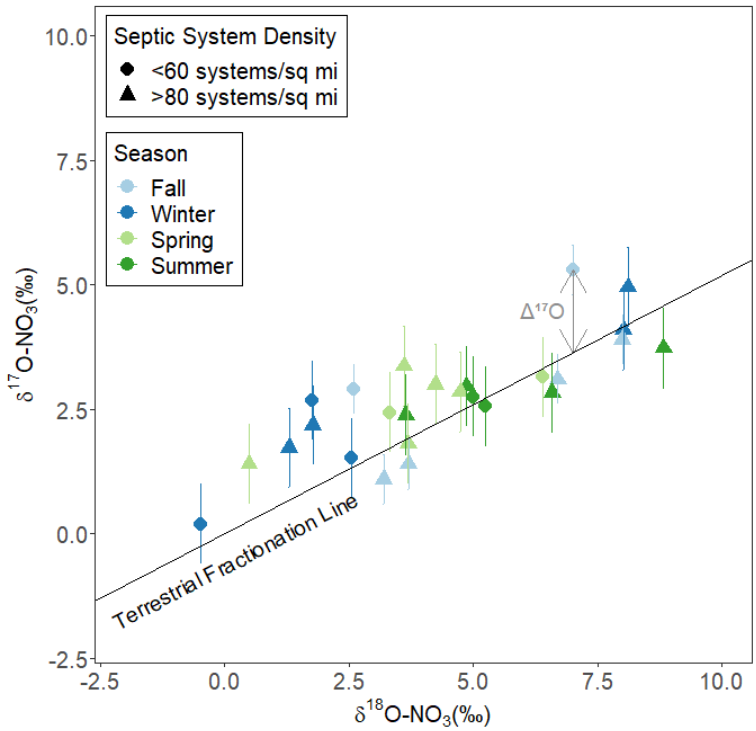

Figure 4.4 Triple oxygen isotope plot of stream NO_3 showing samples plotting near the TFL and minimal to absent atmospheric NO_3 contribution. Only $\delta^{17}O_{NO3}$ precision is shown as error bars for optimized visualization. Slightly negative $\Delta^{17}O_{NO3}$ values are likely from compounded precision error.

While isotopic analysis of nitrate is widely used in source tracking, much less work has used non-specific isotopic analysis of DOM. Isotopic analysis of DOM is complicated by uncertainties in the composition of DOM, differences in recovery efficiencies by various isolation methods, and overlapping and poorly constrained

natural ranges in isotopic values (Raymond and Bauer, 2001). Higher $\delta^{15}N_{DOM}$ values were generally measured at higher STE impact sites, but this may be simply a coincidence (Table 4.3), and there were no clear trends in measured $\delta^{13}C_{DOM}$ and $\delta^{15}N_{DOM}$ in relation to other site parameters (Tables 4.1-4.5).

4.3.5 Multivariate Statistics

The cluster analysis dendrogram and MDS showed similar associated groupings of parameters (Figs. 4.5,4.6). The cluster that appears most representative of STE impact includes SCL, TDN, NO_3-NO_2, % developed and semi-developed land use (combined as LU_Dev), conductivity, and traditional septic system density (Figs. 4.5-4.6). BAT septic system density is proximal in the MDS (Fig. 4.6). Conductivity is likely mainly accounted for by Cl. Another cluster, IBU, DCF, TCS, and NH_4/NH_3, grouped together as parameters associated with STE impact but that were mainly or entirely detected at the highest STE impacted site. CBZ and SMX were associated with STE impact but less strongly than other detected CECs. SMX was only detected at the likely third highest STE impacted site. CAF and PXT were also associated with STE impact but grouped with temperature and sampling month. This is likely because CAF and PXT are generally working as wastewater tracers, with higher averages at sites with higher STE impact (Table 4.5) but were only detected in summer (Fig. A3.2c-d).

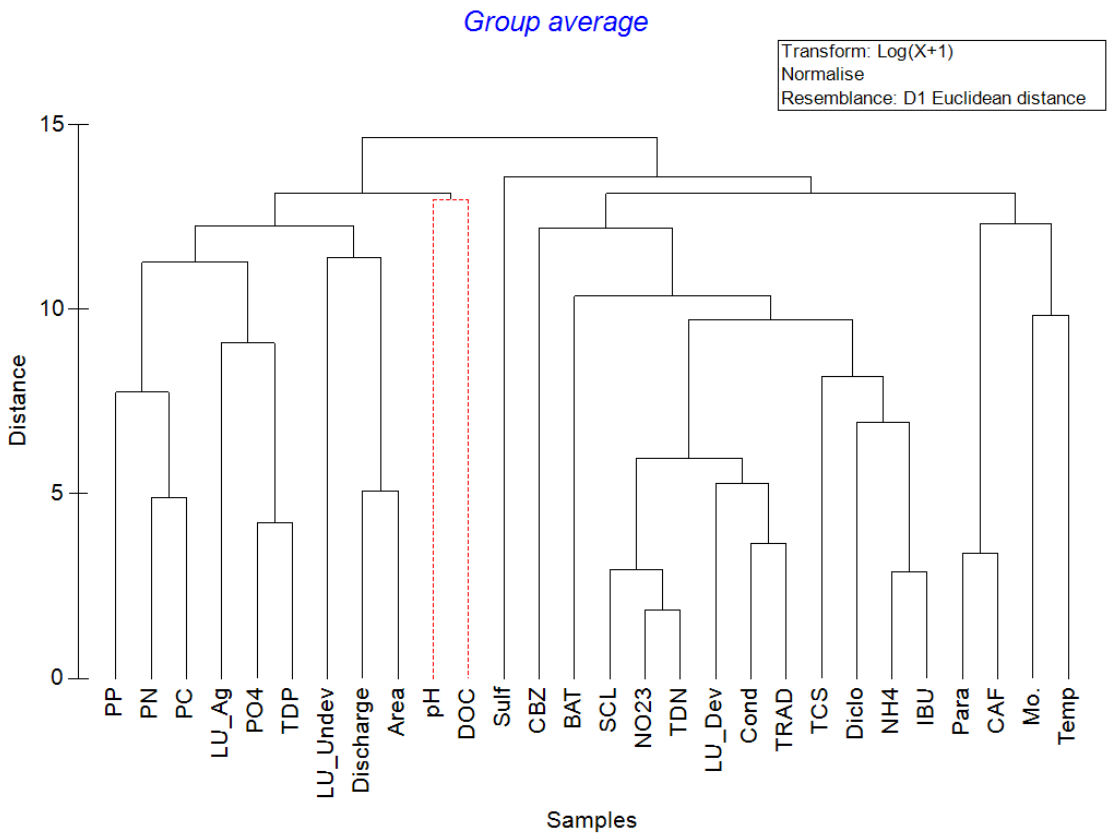

Figure 4.5 Dendrogram of environmental variables and forensic tracers developed from the cluster analysis. Red lines indicate variables (pH and DOC) that were indistinguishable from one another in the resemblance matrix. Abbreviated variable key is provided in *Appendix 3* (Table A3.4).

The parameters most associated with STE impact were not closely related to sampling month or temperature (Fig. 4.6, Fig. A3.3), reflecting low seasonal trends across most measured parameters. Phosphorous parameters, TDP and PO_4, were not associated with STE impact (Figs. 4.5-4.6). This is supported by Robertson (2008) who showed low mobility of septic system phosphorous. Particulate nutrients, PP, PN, PC, were also not associated with STE impact. However, a major grouping showed association between phosphorous parameters, particulates, and % agricultural land use (Figs. 4.5, 4.6) (Figs. A3.4, A3.5). This may reflect agricultural associated

erosion and phosphorous fertilizer use.

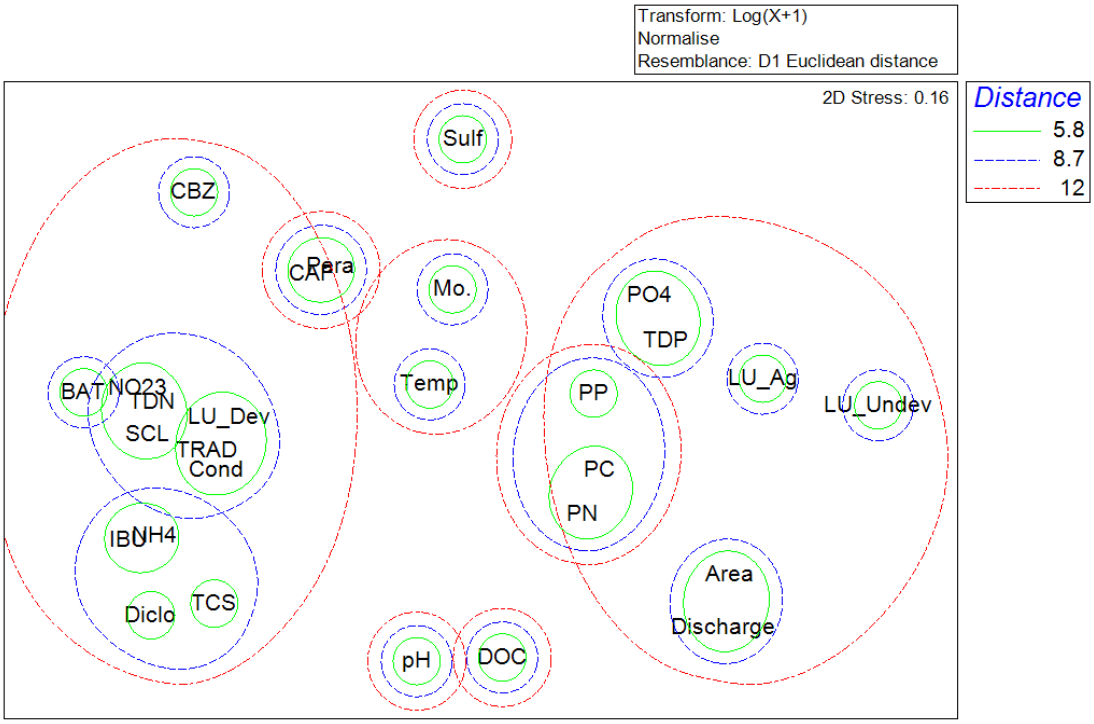

Figure 4.6 MDS plot for environmental variables and forensic tracers. 2D Stress for translating the resemblance matrix into this visualization was < 0.20. Circles are an overlay of the cluster analysis from the dendrogram analysis using resemblance values of 5.8, 8.7, and 12. Abbreviated variable key is provided in *Appendix 3* (Table A3.4).

4.3.6 Trends and Usage of Wastewater Tracers in Streams

The parameters SCL, ace-K, Cl, TDN, NO_3-NO_2, and average $\delta^{15}N_{NO3}$ showed the strongest correlations and relations to septic system density and showed similar site rankings of apparent STE-impact level (Tables 4.1-4.5). These data are also in good agreement with site STE-impact trends observed from nontargeted MS data in *Chapter 3*. Cl is a conservative wastewater tracer that is elevated in domestic wastewater because of human diet and its use in household products and water softening units (Davis et al., 1998; Panno et al., 2006). In this region it is well-performing as an STE tracer (Fig. A3.6) and levels showed minimal effects of winter

road salt usage. Its performance in other regions would depend on geology, road salt usage, and possible wastewater sources as it can also be elevated in animal or industrial wastewater (Panno et al., 2006; Showers et al., 2008), so may be less human specific. Similarly, while $\delta^{15}N_{NO3}$ showed good performance in this region, it may not perform well in other regions. Its values reflect NO_3 source mixing and it can be affected by denitrification. It also can be elevated from biosolid usage or animal waste sources (Kendall et al., 2007).

TDN performed better as an STE impact tracer than NO_3-NO_2 for STE impact ranking because it better accounted for nitrogen transformations. NH_4/NH_3 was generally higher at higher STE impacted sites. The highest values were detected at the most impacted site either due to level of STE loading and/or because this site is likely fed by an anaerobic groundwater seep. The high TDN values at this site were similar to those previously measured in regional basins with high percentage of cropland (Jordan et al., 1997a).

DON also was generally higher at higher STE impacted sites (Tables 4.1-4.5, Figs. 4.5, 4.6, A3.7). While DON was a significant component of TDN at some "cleaner", less STE impacted sites, a lower % DON was seen at more STE impacted sites (Tables 4.1-4.5, Fig. A3.7). Composition of TDN as % NO_3-NO_2, % NH_4/NH_3, and % DON followed expected trends where % NH_4/NH_3 and % DON are inversely related to % NO_3-NO_2 across changed in TDN (Stanley and Maxted, 2008). However, the highest STE impacted site, BFC, did not follow these trends, with higher % NH_4/NH_3 than expected (Fig. A3.7). This further supports that this stream may be fed by highly STE contaminated, anaerobic groundwater. The strong correlations

between anthropogenic artificial sweetener, SCL and ace-K, concentrations and TDN shows that septic systems are the source of elevated nitrogen in these streams.

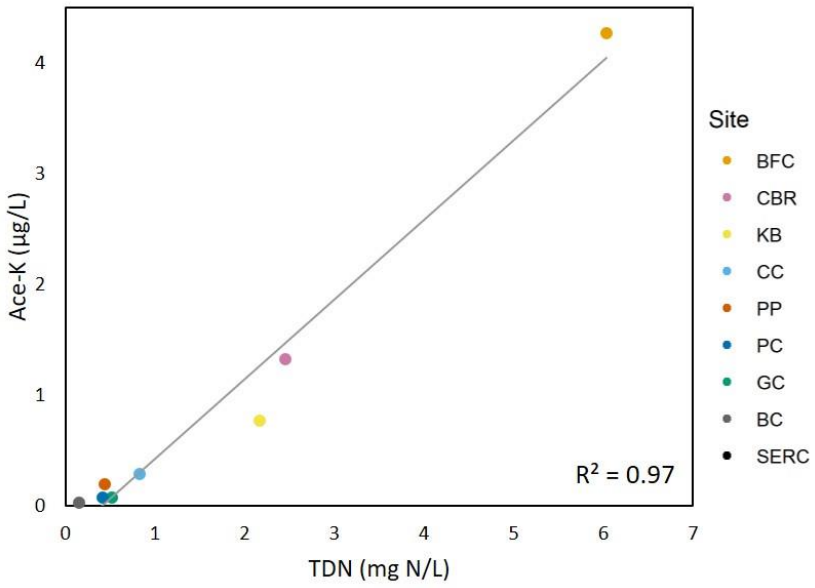

Figure 4.7 Ace-K versus TDN in streams. Legend is in order of highest to lowest STE impact.

While SCL and ace-K are some of the most frequently detected tracers in STE impacted waters, they are also persistent, so may not reflect removal of labile septic contaminants like bacteria and nitrogen. In this study, SCL and ace-K had strong and linear correlations with TDN (Figs. 4.7, 4.8a) and appear to be the best-performing of assessed CECs for identifying level of STE impact. These artificial sweeteners are also of interest because they can provide information about wastewater age and can be used in ratios with more labile tracers to understand treatment level. They also show that some of these streams may receive high volumes of STE-sourced inflow as the highest measured SCL and ace-K concentrations were higher than previous surface water measurements in the United States (Ferrer et al., 2010; Oppenheimer et al., 2011; Ferrer et al., 2013; Batchu et al., 2015; Bernot et al., 2016).

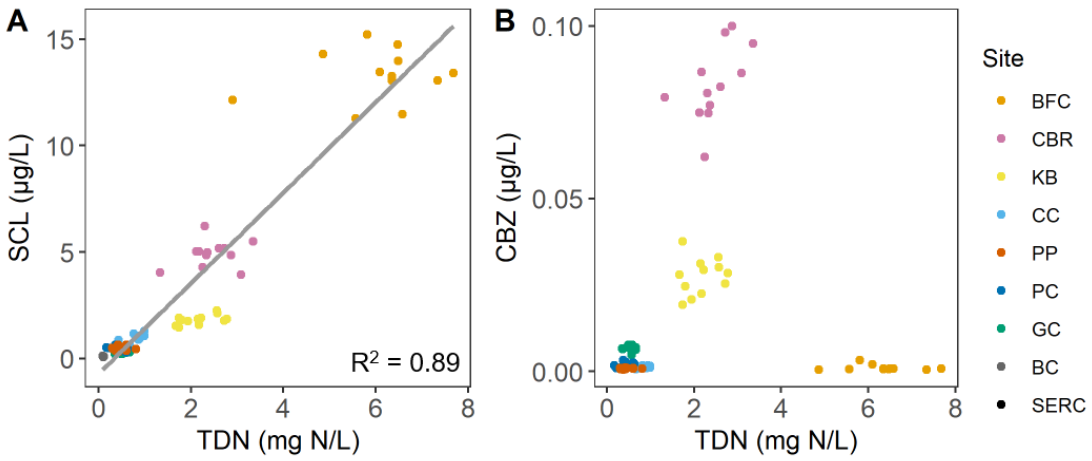

Figure 4.8 SCL versus TDN (A) and CBZ versus TDN (B) in streams. Legend is in order of highest to lowest STE impact.

CBZ concentrations had a weaker correlation to TDN and other markers of STE impact. Values were much lower than expected at the highest STE impacted site, BFC (Fig 4.8b). It appears that CBZ may have failed to identify high STE impact because of the small basin size of this site (0.04 sq mi). This is a prescription pharmaceutical, so its performance as a wastewater tracer depends on widespread societal use, meaning it may not perform well in small basins. However, CBZ was well-ionizing and had low instrument DLs relative to other CEC tracers (Table A3.3).

The prescription antibiotic, SMX, was only detected at the third most STE impacted site, where it was regularly detected and correlated with TDN (Fig. A3.8). This infrequent detection is in contrast to the >60% detection frequency found by other studies on surface waters in the United States (Bernot et al., 2016; James et al., 2016). It is unclear why SMX was only present at this site. Studies have come to inconsistent conclusions on the degradability of SMX in the environment (Barber et al., 2009; Radke et al., 2009), likely because it has a complicated and cyclic

degradation pathway (i.e. degradation products revert back into SMX) (García-Galán et al., 2008; Rodríguez-Escales and Sanchez-Vila, 2016).

CAF and its metabolite PXT were higher at more STE impacted sites but were only detected seasonally between summer-fall 2017 (Fig. A3.2c-d). Values were near MDLs (Table A3.3), but if these parameters do seasonally increase, it could be due to increased STE loading, more storm flushing of soil and groundwater, or lower flow conditions in streams (Fig. A3.5a), though similar trends were not obvious for other tracers. These parameters were higher than expected at the lower STE impacted site, GC (Table. 4.5), which may be because it drains a public recreation area that is popular in summer. CAF and PXT are degradable wastewater tracers which have been suggested to indicate a less treated STE contamination signal and more likely presence of fecal bacteria (James et al., 2016).

The pharmaceutical, DCF, and the antimicrobial, TCS, were only ever detected at low concentrations at the highest STE impacted site, 5/12 and 6/12 months, respectively. Similarly, the NSAID, IBU, was only detected 11/12 months at the highest STE impacted site and a single month at the second highest impacted site. These may indicate higher STE loading or a “fresher” signal, but their use in understanding ranges of STE impact is, therefore, limited. The nicotine metabolite, COT, appears to be working as a wastewater tracer but had significant analytical issues and so was only considered as present/absent. It is also not exclusively related to tobacco nicotine and is also related to other nightshades like tomato, eggplant and other plants, which could complicate interpretation as a human wastewater tracer (Benowitz, 1996).

The CECs ACM, ATS, EST, DCV, MPB, and PPB were never detected. It is not unexpected that these were not detected. DCV is an insecticide with limited household use which should not have significant drain disposal. The others may be more readily removed CECs. While parabens, MPB and PPB are used in large quantities in household and personal care products they are also hydrophobic and are quickly degraded aerobically (Albero et al., 2012; Chen et al., 2017). Despite significant use, the NSAID, ACM, has also been shown to readily undergo mineralization and degradation (Li et al., 2014). The prescription drug ATS has been shown to readily biodegrade (Ottmar et al., 2012) and to photodegrade in aerobic conditions in the presence of DOM (Wang et al., 2018). The hormone, EST, is degradable (Chowdhury et al., 2010) and was rarely detected in a major USGS CEC stream survey (Kolpin et al., 2002).

Site KB appeared to have elevated NO_3-NO_2, and therefore, TDN, considering septic density and Cl, and despite its small basin size. Elevated NO_3-NO_2 was also not clearly accounted for by agricultural land use (Tables 4.1-4.5). While SCL and Ace-K were also elevated at this site, they were measured at lower than expected concentrations based on overall correlations with TDN and NO_3-NO_2 (Figs. 4.7, 4.8a). It is unclear why this is, but this site also had unique features like presence of SMX and extreme concentrations of cadmium. Discrepancies at this site could be a subject of further study.

4.3.7 Septic Tank Wastewater Chemical Data

Chemical data for septic tank wastewater are presented in Table 4.6. Septic tank wastewater had high TDN, which was almost entirely as NH_4/NH_3, as expected

of anaerobic domestic wastewater. An exception to this was tank chamber B2, the second chamber in the sampled system B, which was oxygenated. In this tank TDN was mainly as NO_3-NO_2. In addition to nitrogen transformation, the simple oxygen pump system installed in chamber B2 also appears to show oxygenation leading to decreases in DOC, CAF, PXT, and possibly TDN. This likely reflects biodegradation of CAF and PXT (James et al., 2016). DON estimates may be inaccurate as DON was not directly measured, so values reflect compounded error particularly due to the dilution factors needed for TDN and TIN analyses. TDN values were similar to a previous published range (Richards et al., 2016). TDP was elevated and mainly as PO_4, also similar to previous findings and measured ranges (Richards et al., 2016).

Table 4.6 Septic tank wastewater chemical parameters for 6 septic tanks where 1 and 2 refer to first and second chamber when sampled. B2 was an oxygenated tank chamber. CEC standard deviations are from duplicate SPEs. PXT could not be accurately measured in one tank due to an interfering background signal.

Septic Tank	pH	DOC (mg C/L)	TDN (mg N/L)	NH_4^+/NH_3 (mg N/L)	NO_3^--NO_2^- (mg N/L)	DON (mg N/L)	TDP (mg P/L)	PO_4^{3-} (mg P/L)	SCL (µg/L)	CAF (µg/L)	PXT (µg/L)	TCS (µg/L)
A	7.6	22	63	52	0.01	10.7	7.2	3.3	ND	95.8±1.1	55.3±3.6	0.9±0.10
B1	7.8	33	75	69	0.04	6.2	7.9	6.7	99±33.3	16.9±4.7	24.8±5.3	1.1±0.12
B2	7.1	6	40	4	35.80	0.0	6.8	6.8	109±12.1	1.6±0.0	3.1±0.1	ND
C2	7.8	29	80	75	0.02	4.7	8.3	7.7	3±0.3	3.2±0.3	0.9±0.1	ND
C2	7.4	24	99	99	0.01	0.0	13.9	10.5	9±2.6	0.9±0.3	0.3±0.1	0.2±0.01
D	8.0	27	61	60	0.01	1.4	7.6	7.0	15±2.8	1.4±0.2	3.4±0.5	ND
E	7.1	41	48	47	0.02	0.8	7.7	7.1	15±1.4	1.1±0.1	-	0.7±0.06
F	7.5	25	27	27	0.04	0.0	3.4	3.2	14±0.6	4.4±0.1	10.9±1.0	ND

The dietary CECs, SCL, CAF, and PXT were measured across a wide range of values (Table 4.6). Sucralose concentrations are within the range measured by Snider et al. (2017) for single dwelling septic systems in Canada and are similar to concentrations measured by Oppenheimer et al. (2011) in septic systems the United States. Sucralose can behave as a conservative wastewater tracer (Oppenheimer et al., 2011), so the ~33 µg/L measured average in septic tanks in this study suggests that certain streams in this study (Table 4.5) may be highly STE impacted. We measured a range of CAF/PXT ratios, but values showed similar trends between tank chambers (Table 4.6). Despite the 2017 ban of TCS in household antiseptic wash products (U.S. FDA, 2016), it was measured in septic tank wastewater in this late 2018 sampling. Though there were likely household antiseptic wash products containing triclosan that were still in use and it still has many approved household product uses (U.S. FDA, 2016).

4.3.8 STDOM Optical Properties

STDOM had a diversity in EEM fluorescence signatures, with common peaks at ~240/350-475 nm, 275-300/350, and 340/420 ex/em (Fig. 4.9). The strong 275-300/350 nm ex/em signal is what has sometimes been referred to as “protein-like” fluorescence (Murphy et al., 2014). Of particular interest are samples B1 and B2, where B2 is the second chamber of the septic tank and the one oxygenated chamber sampled. Oxygenated STDOM had a very different fluorescence signature appearing like that which has been related to “humic-like” fluorescence (Murphy et al., 2014).

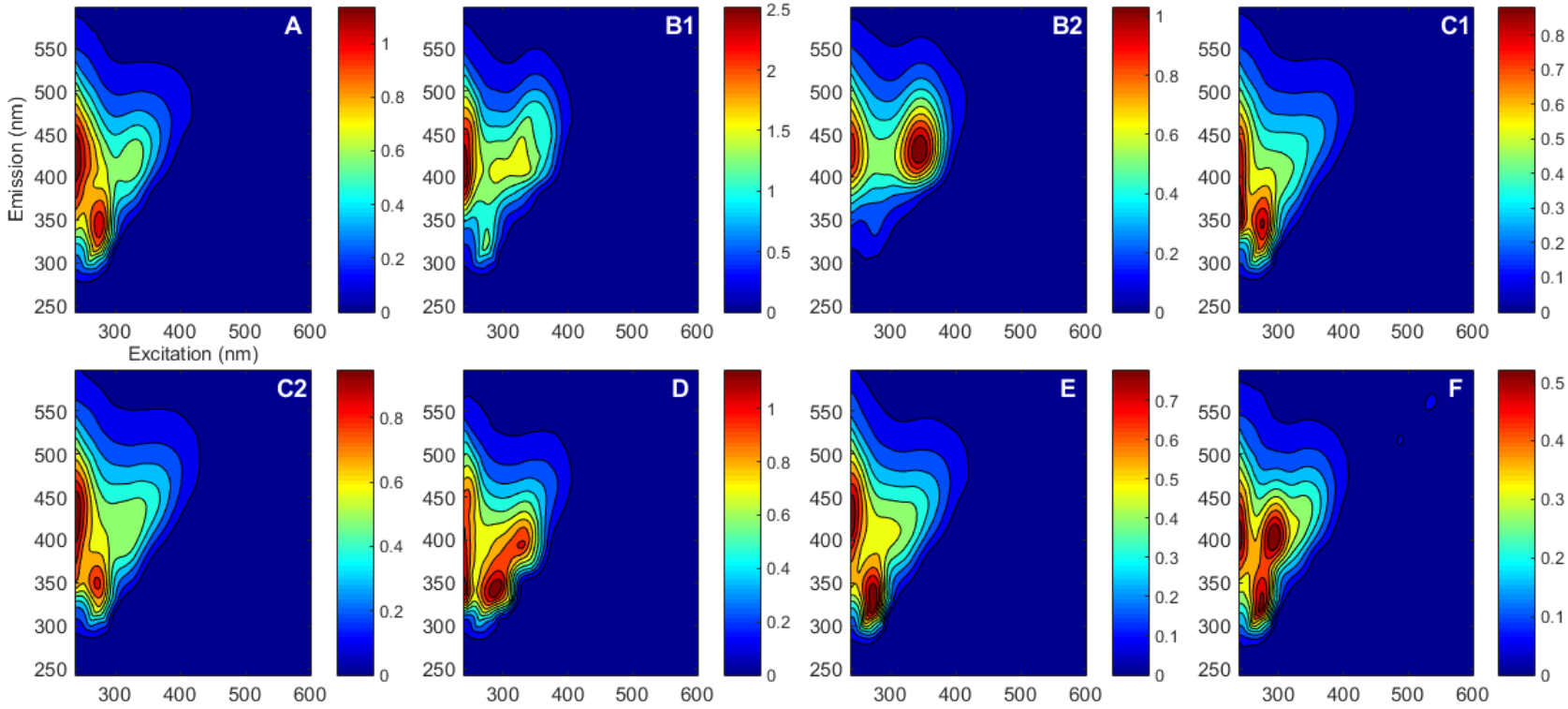

Figure 4.9 Fluorescence EEMs of STDOM from the 6 septic tanks where 1 and 2 refers to first and second chamber when sampled. B2 was the oxygenated chamber. Intensity is in quinine sulfate units (QSU)

4.4 Conclusions

Out of the assessed wastewater tracers, we found that TDN, NO_3-NO_2, NH_4/NH_3, $\delta^{15}N_{NO3}$, Cl, SCL, and ace-K appear to be performing the best as STE tracers in the region. Though all have caveats for use. DOM fluorescence was not found to perform as an STE tracer. A suite of tracers or small selection in combination with nontargeted MS analyses (*Chapter 3*) would likely provide the best tracing information in terms of determining levels of STE impact. A suite of tracers can also provide understanding of treatment level and other possible conflicting contaminant sources.

The artificial sweeteners SCL and ace-K were the best performing of the CECs based on strong linear correlation with TDN and septic system density. These are ubiquitously used, hydrophilic, and persistent wastewater tracers. They were also detected at forested, low septic-system density sites and only never detected at the one site with zero septic systems in its catchment. This suggests that STE presence is essentially ubiquitous in surface waters that have septic systems in their drainage basins. Septic system wastewater was found to have widely varying CEC concentrations, but average measured SCL in septic system wastewater does suggest that certain streams in this study may be highly STE impacted. This is supported by high measured SCL and ace-K concentrations in comparison to previous measurements in surface waters in the United States.

The CECs CBZ, TCS, DCF, IBU, CAF, PXT and SMX were not as well performing across a wide range of sites for determining STE impact level. CBZ performed as a wastewater tracer but was not as consistently present as the artificial

sweetener tracers. CBZ concentrations failed to identify high STE impact at what is likely the most impacted site, BFC, as shown by numerous other tracers. This may be because it is a prescription pharmaceutical tracer that relies on common use so may not perform well in small basins where average use would not be well-represented. This contrasts with artificial sweeteners that are ubiquitously in household diet and personal care products. TCS, DCF, IBU, CAF, and PXT appear to perform as tracers of high and possibly less treated STE impact. CAF and its metabolite, PXT, were essentially only detected across sites in summer for unclear reasons. However, overall, parameters showed minimal seasonal trends, suggesting that in this region a single sampling already provides a good understanding of STE impact levels and a longer-term study may be unnecessary, though this study was conducted during a lower rain year.

Sampling was at baseflow, but future work should look to better understand STE contamination in relation to rain events. Another future goal is to relate data to septic system ages or a rough proxy like structure ages. This was a small study and similar work should be conducted across more streams in the region with different basin characteristics, such as size, septic system densities, geologies, and other wastewater sources such as agricultural or WWTP effluent.

While some septic system nitrogen attenuation occurs before STE reaches surface waters and further attenuation occurs in surface waters, STE does produce elevated nitrogen concentrations. In this study, stream nitrogen concentrations could be clearly related to STE N loading considering land use, the lack of other domestic wastewater sources, concentrations of Cl, NO_3 isotopic signatures, and presence and

concentrations of CECs. The septic systems sampled in this study were not selected to be proximal to streams or within sampled stream basins, so system nitrogen measurements cannot be directly related to stream measurements. While beyond the scope of this study, future goals are to use nutrient data and wastewater tracers to understand nitrogen attenuation from STE and to quantitatively estimate contributed STE volume in streams.

4.5 Acknowledgements

Thank you to the Harris Lab, particularly Mindy Forsyth, Erin Reilly, and Isabel Sanchez-Viruet for assistance with field sampling and sample preparation, and Jessica Flester for GIS assistance. Thank you to Dr. Laura Lapham for use of her IC system. We are deeply grateful to Joel Bostic, Dr. David Nelson, and CASIF, as well as Dr. Cédric Magen, Stable Isotopes Laboratory at CBL, for providing isotopic analytical services. Thank you to Steve Kullen, Dr. David Brownlee, Matthew Cumers, and the Calvert County Department of Planning and Zoning for septic system map data and assistance. We also thank anonymous septic system homeowners. This work was funded by Maryland Sea Grant (NA14OAR4170090 and SA75281450-K).

Chapter 5: Characterization of landfill leachate molecular composition using ultrahigh resolution mass spectrometry

Martin, K. R., N. M. Robey, S. Ma, L. C. Powers, A. Heyes, P. Schmitt-Kopplin, W. J. Cooper, T. G. Townsend, and M. Gonsior, **2021**, Characterization of landfill leachate molecular composition using ultrahigh resolution mass spectrometry. *Environ. Sci. Water Res. Technol*, 7, 1250-1266.
DOI: 10.1039/D1EW00020A

Abstract

Landfill leachate (LL) is a complex wastewater and an important potential source of environmental contamination. LL can contain high concentrations of ammonia, metals, other inorganic species, and dissolved organic carbon; however, bulk composition of dissolved LL organic matter (LLOM) is poorly understood. A better understanding of LLOM composition will inform treatment development and improve LL pollution tracing. In this study, we addressed this need for compositional and treatment information by characterizing LL from an active bioreactor municipal solid waste (MSW) landfill as well as from a closed MSW landfill. Through non-targeted ultrahigh resolution Fourier transform ion cyclotron resonance mass spectrometry (FT-ICR-MS) we were able to assign chemical formulas to thousands of singly charged molecular ions and compare samples to natural dissolved organic matter (DOM). LLOM was differentiated by a higher presence of sulfur-, nitrogen-, and chlorine-, particularly nitrogen-sulfur-, containing formulas. The abundance of chlorine-containing molecular formulas supports the existence of a non-volatile

organochlorine component in MSW LL. We performed tandem MS (MS/MS) analyses to tentatively identify the presence of the flame retardant, chlorendic acid, and likely related compounds. Additionally, we measured contaminants of emerging concern (CECs) and other chemical parameters to further characterize LLs and found evidence suggesting a significant percent of Fe may be bound in Fe-organic complexes.

5.1 Introduction

The wastewater produced by landfills is called leachate, which is generated from disposed liquids, decomposition of waste, precipitation or groundwater that percolates through contained waste, or from water addition as part of engineered treatments. With population growth, municipal solid waste (MSW) production has increased in the U.S. over the past decades; however, the number of operational landfills has decreased over this same period, as more MSW is sent to larger, centralized landfills (U.S. EPA, 2008a). In 1988, there were an estimated 7,924 operational MSW landfills in the U.S. (U.S. EPA, 2008a). The 2020 update of the U.S. Environmental Protection Agency's Landfill and Landfill Gas Energy Project Database, which includes larger MSW landfills operational within the last few decades, lists 2,629 landfills, of which only 1,289 are still in operation (U.S. EPA, 2020b). While it is unknown how many landfills exist in the United States, most are closed, unlined landfills that pre-date engineered treatment to enhance degradation or collect leachate. Long-term waste decomposition in landfills is poorly understood, but waste degradation has been estimated to last thousands of years (Bozkurt et al., 2000; Kjeldsen et al., 2002). Despite this, in the U.S., landfill monitoring is only required

for 30 years, unless extended by a local regulating authority (U.S. EPA, 1991). Landfill leachate (LL) is an important potential source of environmental contamination, and to mitigate leachate pollution risks, it is necessary to understand initial composition, treatment potential, and how to identify contamination. With increasing generated waste, produced leachate, landfill lining failures (U.S. EPA, 1988), and the predicted future importance of landfill mining to recover metal resources (Krook et al., 2012), LL maintenance is likely a growing societal issue.

LL can contain very high concentrations of metals, ammonia, and dissolved organic carbon (DOC) in comparison to domestic wastewaters, limiting treatment options. Ammonia can be a major contributing factor to the persistent toxicity of LL (Berge et al., 2005), as concentrations can be in the g/L range (Kjeldsen et al., 2002). Acute toxicity of LL is generally attributed to ammonia, but MSW LL can also be genotoxic (Kjeldsen et al., 2002) and is known to contain a wide variety of chemicals from household wastes such as plasticizers, pesticides, flame retardants, pharmaceuticals, and chemicals from personal care products (Paxéus, 2000; Slack et al., 2005). Targeted quantification of organic compounds has greatly added to the understanding of MSW landfill leachate organic matter (LLOM) composition (Baun et al., 2004a; Masoner et al., 2014; Masoner et al., 2016); however, beyond general chemical categorization and the identification of functional groups, the bulk composition of LLOM has remained largely unexplored due to analytical limitations. Non-targeted, ultrahigh resolution Fourier transform ion cyclotron resonance mass spectrometry (FT-ICR-MS) has been regularly used to molecularly characterize dissolved organic matter (DOM), wastewaters, and other complex mixtures because it

allows for exact molecular formula assignment of thousands of molecules; however, few studies have analyzed MSW LLOM by FT-ICR-MS. We addressed the need for composition and treatment potential information with an extensive characterization of leachate from two MSW landfills. We molecularly characterized LLOM by FT-ICR-MS and measured a suite of 11 emerging contaminants, dissolved metals, and other chemical properties.

5.2 Materials and Methods

5.2.1 Study Sites and Sample Preparation

Three LL samples were collected in May 2018 from two lined landfills in Florida, USA. All samples were collected from leachate pump stations in amber glass bottles. Two samples were collected from a closed municipal solid waste (MSW) landfill which accepted waste for ten years and stopped accepting waste in the late 1990s. This landfill employs a two stage reverse osmosis (RO) leachate treatment system which removes approximately 30% of the LL volume; the permeate is used at the landfill site for turf irrigation and the remaining leachate brine (70% volume or approximately 1.4 times concentrated) is recirculated through the waste mass to facilitate decomposition and stabilization (Reinhart and Townsend, 1997). The "*Closed*" LL sample is leachate before RO treatment, the "*Closed-Brine*" sample was retentate collected after the first stage of RO treatment. One LL sample, "*Active*", was collected from an active, (i.e., currently accepting waste) MSW landfill that has been in operation for over two decades. Throughout operation, a bioreactor system is treating recirculated LL with air and water addition. The landfills sampled for this

investigation differed in age, however, the waste composition at both facilities is similar and reflective of typical MSW (U.S. EPA, 2020a). Both facilities accepted small quantities of construction and demolition debris (CDD), which typically consists of wood, gypsum drywall, concrete, and other building materials (U.S. EPA, 2020a). Neither facility accepted significant quantities of biosolids, a product derived from municipal wastewater treatment (Reinhart and Townsend, 2007), or yard trash, which may not be disposed of in landfills per Florida regulation (Florida Statute, 2020).

Biological oxygen demand (BOD), chemical oxygen demand (COD), and pH were from whole leachate samples taken at different times from the main sampling, but values are not believed to significantly change over time at these landfills. All other LL sample processing and analyses, besides FT-ICR-MS, were undertaken at the Chesapeake Biological Laboratory (CBL), Maryland, USA. Subsamples were filtered through combusted 0.7 µm glass microfiber filters (Whatman GF/F) into combusted (500 °C) glass bottles. Samples for optical properties analyses, dissolved metals, and chloride concentration measurements were stored at 4 °C, and for non-purgeable DOC/total dissolved nitrogen (TDN) and inorganic nitrogen (IN), at -20 °C, until analysis. Samples were diluted in ultrapure water as needed prior to analyses. Solid-phase extraction (SPE) for DOM characterization and quantification of contaminants of emerging concern (CECs) was performed immediately after filtration, described in detail below. A second SPE on some of the remaining filtered LL was undertaken to quantify acesulfame potassium (ace-K). Samples did not visibly change over storage time. A detailed description of sample processing, purity

and sources of reagents and standards, and analytical methods used in leachate characterization is given in *Appendix 4*.

Initial SPE, for LL dissolved organic matter (LLOM) characterization and quantification of most targeted analytes, was carried out in triplicate using Agilent Bond Elut PPL cartridges (1 g, 3 mL). PPL SPE typically has a high extraction efficiency for DOC (>60%) (Dittmar et al., 2008) and has been shown to be favorable for DOM characterization by FT-ICR-MS (Li et al., 2016; Raeke et al., 2016). SPE-cartridges were activated with 5 mL LC/MS grade methanol (MeOH) then rinsed with 5 mL LC/MS grade 0.1% (v/v) formic acid (FA) water. LL aliquots were acidified to pH 2 using pure grade HCl then gravity-fed onto the cartridges. Extracted sample volumes (*Active* LL: 11.5-16 mL, *Closed* LL: 10 mL; *Closed-Brine* LL: 11.5-12 mL) were chosen to not load >18 mg DOC per g sorbent to avoid breakthrough (Dittmar et al., 2008; Li et al., 2016) but varied slightly among triplicates because of column blockage by precipitates. After sample loading, the outsides of the cartridges were rinsed with ultrapure water, and the sorbent was rinsed with a large volume of 50 mL 0.1% FA water to remove very high concentrations of salts and ammonia. Cartridges were then dried at room temperature with a vacuum pump and eluted with 10 mL MeOH. To quantify the artificial sweetener, ace-K, SPE on the original filtered leachate was also carried out in triplicate using reversed-phase/weak-anion exchange (WAX) mixed mode cartridges. These Waters Oasis WAX (150 mg, 6 mL, 30 µm particle size) cartridges were activated with 5 mL of an approximately 2% NH_3, NH_4OH MeOH solution (reagent grade, NH_4OH water solutions with LC/MS grade MeOH), then rinsed with 5 mL LC/MS grade MeOH, and again rinsed with 5 mL

ultrapure water, 2 mL of the filtered, acidified samples were gravity-fed onto the cartridges, the cartridges were rinsed with 10 mL ultrapure water, dried, and eluted with 3 mL of the NH_4OH MeOH solution. Targeted analytes, described below, were quantitatively recovered in SPEs (A4.12).

5.2.2 Characterization of Landfill Leachates

UV-Vis absorbance spectra and fluorescence excitation-emission matrices (EEMs) were measured simultaneously for diluted raw LL samples over an excitation wavelength range of 240-600 nm by 3 nm increments and emission wavelength range of 250-620 nm by fixed ~3.3 nm increments using a Horiba Aqualog spectrofluorometer. All absorbance and fluorescence spectra were blanked using scans of ultrapure water. Absorbance spectra ($A(\lambda)$) were converted to decadic absorption coefficient spectra ($a(\lambda)$) using the equation $a(\lambda) = A(\lambda)/L$, where L is the pathlength of the spectrofluorometer cell (0.01 m). EEMs were corrected for Rayleigh scattering in MATLAB using methods described previously (Zepp et al., 2004) and inner filter effect corrected using the Aqualog software. To express EEMs in quinine sulfate units (QSU), spectra were normalized to the fluorescence emission area (excitation = 347 nm) of a 1 mg/L Starna quinine sulfate reference standard in 0.1 M $HClO_4$.

Measurements for pH were made by Standard Method (SM) 4500-H^+ B (2017b), while BOD and COD measurements were made by an outside lab, referencing standard methods SM 5210 B (2017d) and EPA Method 410.4 (U.S. EPA, 1993), respectively. Concentrations of DOC and TDN were measured using a Shimadzu total organic carbon analyzer (TOC-VCPH) with a total nitrogen unit

(TNM-1) on samples diluted with ultrapure water and acidified to pH 2 with pure grade HCl. Quantification of Cl^-, NO_3^- and NO_2^- combined (NO_3^--NO_2^-), and NH_3/NH_4^+ was performed by the Nutrient Analytical Services Laboratory, CBL (MD, USA) using standard methods referencing SM 4110 B (2017a), ASTM D7781-14 (ASTM International, 2014), and SM 4500-NH_3 G (2017c), respectively. Dissolved V, Cr, Mn, Fe, Cu, Zn, As, Cd, and Pb were measured on microwave digested, 0.2 µm syringe filtered (Whatman GD/X) LL samples using an Agilent 7500 ICP-MS. Fe was similarly measured in one per sample of the triplicate PPL SPEs. All measured values were blank corrected with a microwave digested ultrapure water blank or a similarly extracted ultrapure water PPL SPE blank. We acknowledge that oxidation, loss of ammonia, and sorption during sampling, transport, and processing could have affected physical and chemical metal speciation and results.

Sucralose, ace-K, triclosan, methylparaben, propylparaben, paraxanthine, cotinine, ibuprofen, acetaminophen, carbamazepine, and sulfamethoxazole were quantified in the LL SPEs by high performance liquid chromatography tandem mass spectrometry (HPLC/MS/MS) using an Agilent 1260 Infinity II LC interfaced with an Agilent 6420 Triple Quadrupole MS. The carrier gas was high purity nitrogen from a nitrogen generator and the collision gas was ultra-high purity nitrogen. Ace-K was measured separately from the other CECs to account for the NH_4OH MeOH matrix. An ACE Excel C18-PFP (3.0 mm i.d. × 100 mm, 2 µm particle size) column was used for both methods. For ace-K, the autosampler injection volume was 3 µL, column temperature was set to 50 °C and flow rate was 250 µL/min. Mobile phase A was LC/MS grade methanol and mobile phase B was 0.1% (w/w) ammonium acetate

water made by adding ≥99.0% purity ammonium acetate to ultrapure water. LC conditions were isocratic, 90% mobile phase A for 4 minutes. The MS was in negative ESI and multiple reaction monitoring (MRM) mode. For all other CECs, the autosampler injection volume was 5 µL, column temperature was set to 50 °C and flow rate was 300 µL/min. Mobile phase A was LC/MS grade methanol and mobile phase B was 0.1% (v/v) LC/MS grade FA water. The separation gradient began at 50% mobile phase A, increased to 97% mobile phase A for 0.2-7 min, and returned to 50% mobile phase A at 8 min. For MS conditions, an ESI polarity switching method was used with dynamic MRM mode. For both methods an internal standard (ISTD) quantification method was used to control for fluctuations in instrument performance and ion suppression. Meaning a primary CEC transition and corresponding stable isotope-labelled (SIL) ISTD transition were monitored for quantification, while a secondary CEC transition was used as a qualifier to further confirm identity. All blanks, calibration standards, quality control standards, and samples were spiked with ISTDs. Significant qualifier transitions were not found for ibuprofen or triclosan, so ibuprofen was run without a qualifier, while a different isotopic transition was used as a qualifier for triclosan because it has 3 chlorine atoms. For full autosampler and LC settings as well as complete MS settings and monitored transitions see *Appendix 4*.

The $\delta^{13}C$ and $\delta^{15}N$ isotopic signatures, weight % C to estimate DOC recovery, and molar C/N ratios of the non-volatile, PPL LLOM were measured by combustion and analysis of the resulting gas by a Costech ECS 4010 elemental analyzer equipped with a Thermal Conduction Detector (TCD) and coupled to a Thermo Scientific Delta V Plus IRMS. Measurements were made separately on the triplicate SPEs according

to optimum measurement ranges for C and N on the IRMS. Aliquots corresponding to approximately 350 µg C for $\delta^{13}C$ and approximately 60 µg N for $\delta^{15}N$ were dried in tin capsules at 45 °C prior to analysis. Values are reported using delta notation and expressed in permil (‰) relative to the standards Pee Dee Belemnite (C) and atmospheric nitrogen (N).

5.2.3 FTICR MS analysis of SPEs

PPL LLOM extracts were diluted with LC/MS grade MeOH at a 1:40 dilution factor and analyzed on a 12 Tesla Bruker solariX FT-ICR-MS with an Apollo II ESI source at the Helmholtz Zentrum München, Munich, Germany. The FT-ICR-MS was calibrated using arginine clusters prior to all analyses. Diluted extracts were injected by an autosampler at a flow rate of 120 µL/h and analyzed in both positive and negative ionization modes. Spectra were acquired with a 500-scan accumulation over a *m/z* range of 100-1,400 *m/z*. Averaged spectra were smoothed and externally calibrated using a mass list of known commonly occurring surfactant and DOM *m/z* ions. Peak lists were exported with a signal-to-noise ratio cutoff ≥10. Mass-aligned matrices with a *m/z* window width of 0.5 ppm of the positive and negative mode peak lists were produced using the proprietary Matrix Generator software (Lucio, 2009). The positive mode matrix was only used in this study to identify the presence of specific masses. The negative mode matrix was filtered for *m/z* ions that appeared in all triplicate extracts and signal intensities were averaged across triplicates. Chemical formulas, with possible elemental assignments including H, C, O, N, S, P, Cl, and Br, were assigned to *m/z* ions individually by sample using an in-house software, NetCalc, that uses a network assignment approach (Tziotis et al., 2011). Chemical

formula assignments were restricted to *m/z* ions less than 600 *m/z* and filtered using common criteria (Kind and Fiehn, 2007; Koch et al., 2007; Herzsprung et al., 2014) along with isotopic pattern matching as applicable. After filtering, 10,270 formula assignments were determined by NetCalc. An additional 16 suspected organohalogens, including polyfluorinated formulas, were assigned using built-in features of the Bruker DataAnalysis 5.0 software and confirming isotopic pattern matching using the Bruker IsotopePattern software and the web interface by Loos et al (2015). Final assignments had a maximum mass error of 0.5 ppm and an average mass error of 0.1 ppm. The formula assignment dataset is available in a data repository (https://figshare.com/s/73e8fed64fb7ea4d54d1, will switch to DOI: 10.6084/m9.figshare.13550573 if the manuscript is accepted). FT-ICR-MS allows for exact molecular formula assignment of singly charged *m/z* ions, but these data are qualitative and non-structural. Assigned ions were assumed to be deprotonated, singly charged, $[M-H]^-$ ions, and protonated corresponding formulas [M] are used in graphics and discussion unless otherwise stated. For discussion, formulas are only considered present in a sample if corresponding masses were found in all extracted triplicates.

For molecular composition comparison, a direct water sample of the Suwannee River, Florida, natural organic matter (SRNOM) was used because SRNOM is a well characterized, high DOC, complex natural reference sample (Green et al., 2015). This direct water sample was filtered and then diluted with LC/MS grade MeOH at a 1:40 dilution factor and injected at the same flow rate in negative mode ESI into the FT-ICR-MS. The spectrum was acquired with a 10,000-scan

accumulation over a range of 147-2,000 *m/z*. Formulae were assigned using the same settings in NetCalc used for the LL samples, similarly filtered, and had the same mass cutoff, maximum mass error, and average mass error.

5.2.4 LC/MS/MS and Orbitrap MS/MS Structural Elucidation

The halogen-containing formulas, $C_9H_4Cl_6O_4$, $C_9H_5Cl_5O_4$, and $C_9H_6Cl_4O_4$, were assessed by MS/MS. One triplicate from both the *Active* and *Closed* PPL LLOM samples was diluted at a 1:40 dilution factor in LC/MS grade MeOH. Using the previously described LC triple quadrupole mass spectrometer, LC/MS/MS analyses were carried out with the same column as the CEC quantification, isocratic 98% LC/MS grade MeOH/2% LC/MS grade FA water (0.1%) conditions, and in negative mode ESI using collision-induced dissociation (CID). Source and MS settings were optimized using built-in instrument software features (Table A4.22). Fragments were generated for the monoisotopic peak of $C_9H_4Cl_6O_4$ (384.8 *m/z*) in the *Active* leachate sample, the monoisotopic peak of $C_9H_5Cl_5O_4$ (350.9 *m/z*) in the *Active* and *Closed* samples, and the most abundant isotopic peak of $C_9H_6Cl_4O_4$ (318.9 *m/z*) in the *Closed* sample. Chosen assignments for fragmentation were based on presence and intensity of signals in the FT-ICR-MS spectra and targeted masses were chosen to minimize background interference. Specific predicted and control transitions were monitored in MRM mode at collision energy steps between 0-40 eV. Full scan mode was also used at 10 eV collision energy for fragment observation.

The three highest abundance chlorine isotopic peaks of $C_9H_5Cl_5O_4$ (350.9, 352.9, and 354.8 *m/z*) were of high enough intensity to also be analyzed by Orbitrap MS/MS using the FT detector. A triplicate PPL SPE of the *Active* sample, diluted

1:40 with LC/MS grade MeOH, and a 100 µg/L chlorendic acid standard were directly injected into the Thermo LTQ Orbitrap XL Hybrid Ion Trap-Orbitrap Mass Spectrometer using a syringe and loop-injection. The mass resolution setting was 15,000 and fragmentation was by collision-induced dissociation (CID) at collision energies of 0 and 10 eV for the *Active* sample and 0, 10, 20, 40, and 60 eV for the standard in full scan mode using the Orbitrap detector recording 0.4 min long scan averages.

5.3 Results and Discussion

Results from the chemical characterization are summarized in Table 5.1. All LL samples had pH >7, with the highest pH observed in the *Active* LL. This is consistent with previous LL characterizations (Kjeldsen et al., 2002; Renou et al., 2008) and observed trends in pH towards basic conditions with landfill decomposition and chemical stabilization (Bozkurt et al., 2000; Berge et al., 2005). The *Active* landfill is a bioreactor system and this technology is used to more rapidly reach stabilization. Chloride concentrations were similar between LL and consistent with previously observed high values (Kjeldsen et al., 2002). Overall, the BOD to COD ratios were consistent with previous studies (Kjeldsen et al., 2002; Renou et al., 2008), though the higher BOD/COD in *Active* LL could reflect its status as a bioreactor landfill or its younger age (Renou et al., 2008). The *Active* LL was much darker in color than the *Closed* or *Closed-Brine* and had the highest DOC and TDN concentrations. The DOC of the *Closed-Brine* LL sample showed a 1.2 times concentration from the corresponding *Closed* LL sample, less than the predicted 1.4 concentration factor. As expected in dominantly anaerobic systems, TDN was almost

entirely composed of NH_3/NH_4^+, hereafter referred to as NH_3. In all LL, NO_3^--NO_2^- was below the method reporting limit (RL) and was essentially absent. Dissolved organic nitrogen (DON) was not measured directly but was estimated by subtracting IN from TDN.

Table 5.1 Chemical characterization of whole LLs and PPL SPEs as indicated. For PPL SPE isotopic measurements and C/N, values are ± standard deviation (SD). NO_3-NO_2 was below the reporting limit (RL) but above the method detection limit, so detected values are listed (Text A4.7). Not detected (ND) indicates the analyte was either below detection limit or absent.

Parameter	Active LL	Closed LL	Closed – R.O. Brine LL
pH	8.4	7.9	7.8
Cl (mg/L)	2336	1899	2124
COD (mg O_2/L)	1600	1900	2200
BOD (mg O_2/L)	240	160	130
BOD/COD	0.15	0.08	0.06
DOC (mg C/L)	1044	538	656
DOC Recovery$_{SPE\text{-}LLOM}$ (%)	63±13	78±4	63±6
TDN (mg N/L)	1528	1048	1182
NH_3 (mg N/L)	1324	900	992
NO_3-NO_2 (mg N/L)	0.5 (<RL)	0.8 (<RL)	0.5 (<RL)
DON (mg N/L)	203	148	189
$\delta^{13}C_{SPE\text{-}LLOM}$ (‰)	-22.5±1.7	-25.7 ± 0.2	-25.1 ± 0.2
$\delta^{15}N_{SPE\text{-}LLOM}$ (‰)	3.4±0.1	4.3 ± 0.1	4.2 ± 0.0
Molar $C/N_{SPE\text{-}LLOM}$	20.4±1.2	14.7±0.7	15.5±0.4
V (µg/L)	153	30	32
Cr (µg/L)	357	72	40
Mn (µg/L)	288	51	74
Fe (µg/L)	7330	3375	4250
$Fe_{SPE\text{-}LLOM}$ (µg/L)	2972	1667	990
Cu (µg/L)	18	38	8
Zn (µg/L)	77	51	33
As (µg/L)	67	20	27
Cd (µg/L)	13	ND	ND
Pb (µg/L)	4	1	1

We found $\delta^{13}C_{SPE\text{-}LLOM}$ values of -22.5‰ and -25.7‰ and $\delta^{15}N_{SPE\text{-}LLOM}$ of 3.4‰ and 4.3‰ for the *Active* and *Closed* LLs, respectively. Measured $\delta^{13}C_{SPE\text{-}LLOM}$ values were within range of observations for non-volatile LLOM (Games and Hayes,

1977) and bulk LLOM (van Breukelen et al., 2003; Mohammadzadeh and Clark, 2008). To the best of our knowledge, there are no previous reports on $\delta^{15}N_{LLOM}$. Bulk DOM isotopic measurements usually require an extraction procedure, potentially biasing representativeness of the total DOM signature and comparison between different extracted DOM pools. Additionally, the complexity and variability of DOM composition can make interpretation of isotopic values ambiguous; however, $\delta^{13}C_{LLOM}$ has been used for source tracing (Mohammadzadeh and Clark, 2011). $\delta^{13}C_{LLOM}$ is known to significantly vary between landfills as well as over time within a landfill (Games and Hayes, 1977; Mohammadzadeh and Clark, 2008), highlighting the need for more data to better interpret the relation of LLOM isotopic signatures to organic matter processing in these systems.

Optical properties of DOM are known to reflect variations in organic matter composition (Stedmon and Bro, 2008). The *Active* LL sample had a different absorbance/fluorescence profile from the *Closed/Closed-Brine* samples and overall had higher fluorescence intensities across all excitation wavelengths (Fig. A4.1). The *Active* LL sample also had higher absorbance values (4 to 9 times higher across all wavelengths) when compared to *Closed/Closed-Brine* LL samples (A4.2). This may be due to differences in Fe concentrations between samples (Table 5.1) because Fe can enhance absorbance values and potentially quench fluorescence (Weishaar et al., 2003; Poulin et al., 2014). Despite the higher DOC concentrations in *Closed-Brine* LL versus *Closed* LL, absorbance and fluorescence spectra did not show any differences between these two samples (Figs. A4.1, A4.2). LLOM optical signatures from both landfills appeared distinct from previous measurements for LLs (Baker and

Curry, 2004; Cui et al., 2016; Oloibiri et al., 2017), demonstrating a diversity of LL optical signatures.

5.3.1 Metals

Measured dissolved metals (V, Cr, Mn, Fe, Cu, Zn, As, Cd, and Pb) were detected in concentrations ranging from 1-7330 µg/L (Table 5.1). All measured metals were within the ranges previously reported (Kjeldsen et al., 2002; Baun and Christensen, 2004b; Masoner et al., 2014). Metals found at concentrations >50 µg/L in the LL samples include Fe, Cr, Mn, V, Zn, and As. Almost all metals detected in this study were highest in the *Active* sample, which corresponds to the observed higher DOC and TDN values. While this study is only on two landfills, this pattern could reflect the expected higher waste degradation rate in the *Active* landfill, the effect of ionic strength on metal leaching, leachate composition controlling physical fractionation of metals, or differences in disposed waste over time. Interestingly, the three measured metals with the greatest ratios between the *Active* and *Closed* LL samples were Mn, V, and Cr, all of which are used as alloying elements in steel (Moskalyk and Alfantazi, 2003; Johnson et al., 2006). V and Cr have been shown to correlate across landfills (Masoner et al., 2014) and co-vary over time in a long-term landfill study (Statom et al., 2004).

As shown in this study and others, Fe concentrations are often found to be in mg/L levels, an order of magnitude higher than most other commonly measured heavy metals in LL samples (Statom et al., 2004; Masoner et al., 2014). For this reason, we also measured Fe in the SPE LLOM samples, detecting values surprisingly also in the mg/L range or 41% and 49% of the whole leachate Fe for the *Active* and

Closed samples, respectively (Table 5.1). While LL samples may have oxidized some during transport and processing, no precipitant was observed during handling beyond on SPE cartridges during extraction. Jensen et al. (1998) showed that in an anaerobic LL groundwater plume, the majority of Fe is in the truly dissolved (<0.001 µm) fraction as free Fe^{2+}, with some Fe in the <0.7 µm fraction as organic complexes. We did not identify Fe chemical speciation in the whole leachates, but if the majority of Fe in these LLs was Fe^{2+}, we are unsure how Fe was significantly extracted, barring an unexpectedly high speciation as Fe-organic complexes in these samples or Fe^{2+} becoming organically bound during extraction. These samples may have oxidized, or chemical speciation may be significantly different than the leachate plume studied by Jensen et al. (1998), as these LLs had approximately 8-15 times greater DOC but approximately 25 times less dissolved Fe. We did not identify the chemical speciation of Fe in these extracts, but this recovery has implications to DOM SPE techniques, instrument methods, and LLOM photochemistry. Extracted Fe is likely stable Fe-organic complexes originally in the leachate samples or that formed during extraction. Furthermore, the low pH used during SPE in this study would allow only very strong Fe-organic complexes to be extracted and the rich dissolved organic nitrogen and sulfur pool might facilitate such complexes (Stookey, 1970; Hider and Kong, 2010; Waska et al., 2015; Bhattacharyya et al., 2019). We searched the FT-ICR-MS dataset generated in this study for *m/z* ions matching Fe-isotope patterns, following Waska et al. (2015) No Fe-organic complexes were identified; however, we used negative ESI and improved Fe-organic complex detection is expected in positive ESI (Waska et al., 2015). Additionally, the second highest abundance stable Fe isotope has a low natural

abundance, so the second isotopic peak is unlikely to be visible for formulas containing one Fe atom. While dissolved Fe is not thought to be predominantly organically bound in anaerobic LL (Jensen et al., 1998), the review of LL metal speciation by Baun and Christensen (2004b) showed Ni, Cu, Zn, Cd, and Pb to have predicted significant presence as dissolved organic complexes, and in light of the perceived SPE recovery of Fe-organic complexes in this study for high DOC LL samples, we suggest that LLOM could be an intriguing mixture to study the SPE extractability of metal organic complexes and to identify specific metal organic complexes or binding ligands present in LLOM by FT-ICR-MS.

5.3.2 Targeted CECs

We measured the artificial sweeteners, sucralose and ace-K; the antimicrobials, triclosan, methylparaben, and propylparaben; the caffeine metabolite, paraxanthine; the nicotine metabolite, cotinine; the nonsteroidal anti-inflammatory drugs (NSAIDs) ibuprofen and acetaminophen, and the prescription drugs carbamazepine and sulfamethoxazole. These CECs have been regularly measured in domestic wastewater studies due to widespread use or resistance to degradation (Oppenheimer et al., 2011; Loos et al., 2013; James et al., 2016; Yang et al., 2016), and these or related compounds have also been measured in studies of MSW LLOM (Masoner et al., 2014; Roy et al., 2014; Clarke et al., 2015; Kapelewska et al., 2016; Masoner et al., 2016). In this study, we only detected sucralose, ace-K, cotinine, and ibuprofen in the LL samples (Table 5.2). Non-detected CECs are presumed to be below method detection limits or absent (Table A4.13). The *Closed-Brine* LL had a 1.1-1.2 concentration factor from the *Closed* LL for measured CECs, reflecting the

DOC concentration factor. In a study of 22 landfills in the U.S., measuring 190 CECs, Masoner et al. (2016) found cotinine to be one of the top six frequently detected CECs, measuring a maximum concentration of approximately 30 µg/L, which is similar to values detected in this study. Ibuprofen measurements in this study are, likewise, similar to past LL studies (Masoner et al., 2014). Ibuprofen was notably one of the few analytes lower in the *Active* LL than the *Closed* LL, though this may just reflect small differences in received waste.

Artificial sweeteners, particularly ace-K and sucralose, and sometimes saccharin, are of particular interest to wastewater studies because they have been used as temporal markers in LL and domestic wastewaters based on dates of usage approval and usage patterns (Roy et al., 2014; Clarke et al., 2015; Robertson et al., 2016; Stefania et al., 2019). Ace-K was approved for use in the U.S. in 1988 (U.S. FDA, 1988), while sucralose was approved in the U.S. in 1998 with widespread commercial use beginning around 2000 (Robertson et al., 2016). Both are persistent in the environment (Buerge et al., 2009; Oppenheimer et al., 2011), though for ace-K, researchers have suggested the recent evolution of a microbial degradation pathway in wastewater treatment plants (Castronovo et al., 2017; Kahl et al., 2018; Kleinsteuber et al., 2019). Sucralose and ace-K appear to be working as time markers in this study. Ace-K is present in both landfills, which corresponds to both accepting municipal waste from after 1988; whereas, sucralose is absent in the *Closed* LL. The *Closed* landfill stopped accepting waste before sucralose received widespread use in the U.S. The sucralose concentration measured in this study for the *Active* LL is within the upper range seen in a previous study (Clarke et al., 2015). The measured

ace-K concentration in the *Active* LL is much higher than previous studies (Roy et al., 2014; Stefania et al., 2019). The markedly higher concentration of ace-K in the *Active* LL compared to the *Closed* LL could be due to degradation processes or trends in artificial sweetener usage, as low-calorie sweetener consumption has significantly increased since the late 1990s (Sylvetsky and Rother, 2016) when the *Closed* LL stopped accepting waste.

Table 5.2 Concentrations of CECs in µg/L. Triplicate instrument measurements per individual SPEs were averaged and SDs calculated. Averages and SDs for triplicate SPEs were further averaged for reported values ± SD. All values were corrected for processing but were not corrected for SPE recoveries. All unlisted measured CECs were not detected in any samples.

CEC	Description	Active LL	Closed LL	Closed – R.O. Brine LL
acesulfame potassium	artificial sweetener	517±36	8±1	9±1
cotinine	nicotine metabolite	24±6	6±1	7±1
ibuprofen	NSAID	242±34	305±13	328±5
sucralose	artificial sweetener	446±37	ND	ND

5.3.3 FTICR MS Molecular Characterization

Spectra of the LLOM samples were remarkedly complex with high peak density (Fig. 5.1A). In the *Active* LL, 7,770 molecular formulas were unambiguously assigned, while 9,039 were assigned for the *Closed* LL, and 9,143 were assigned for the *Closed-Brine* LL. For comparison, 4,862 molecular formulas were assigned for the SRNOM sample, despite the much larger number of averaged scans. Assignments in the *Closed-Brine* LL were like those of the *Closed* LL sample (Table 5.3). Visually, the spectra for LL samples were distinguishable from SRNOM by a higher *m/z* ion distribution and prominent ion peaks at approximately 185.0278 and

417.2283 *m/z* (Figs. 5.1, A4.4), which are assigned as $C_8H_{10}O_3S$ and $C_{24}H_{34}O_6$. This is unexplained, but seems LL characteristic, and could develop from highly ionizing compounds, convergence of structural isomers, and/or high chemical concentrations, and as these prominent signatures have potential use for source tracing this pattern should be further explored in future studies.

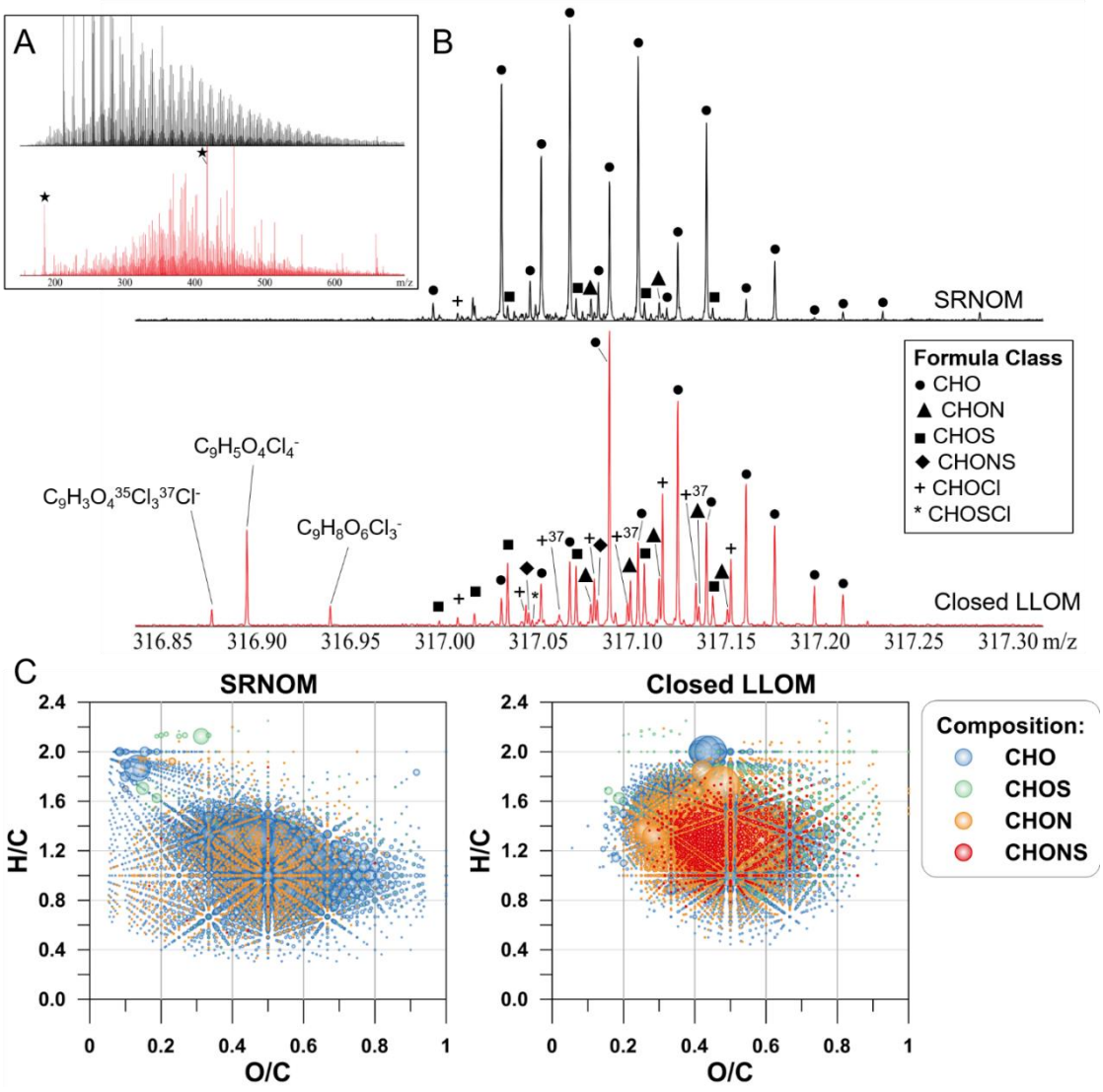

Figure 5.1 Full *m/z* spectra of SRNOM (top) and a *Closed* LL sample (bottom) where stars mark the *m/z* ions at 185.0278 and 417.2283 *m/z* (A). Spectra were scaled to similar relative intensities for comparison purposes. Classes of formulas between the samples at 317 *m/z* (B). Only monoisotopic ions were assigned formulas in the dataset, but isotopic masses corresponding to dataset assignments are included in this diagram to better depict complexity. Assigned ions with >1 Cl atom are labelled as

$[M-H]^-$ formulas. Van Krevelen diagrams of CHO, CHOS, CHON, and CHONS formula classes in the SRNOM and *Closed* LL samples (C). Point size scale is independent by sample, but within sample scaling corresponds to signal intensity. Known high intensity CHO fatty acids, sulfur-containing background surfactant contaminants, and the 417.2283 *m/z* ion assignment were not plotted for optimized visualization reasons.

Table 5.3 Summary of top six formula classes in molecular characterization of LL and comparison to SRNOM. Number of formulas and percent of total assigned formulas are presented.

	Active LL	**Closed LL**	**Closed – R.O. Brine LL**	**SRNOM**
CHO	2547 (32.8%)	2362 (26.1%)	2392 (26.2%)	2925 (60.2%)
CHON	2688 (34.6%)	3307 (36.6%)	3295 (36.0%)	1439 (29.6%)
CHOS	1161 (14.9%)	1213 (13.4%)	1253 (13.7%)	255 (5.2%)
CHONS	592 (7.6%)	1072 (11.9%)	1072 (11.7%)	14 (0.3%)
CHOCl	674 (8.7%)	830 (9.2%)	863 (9.4%)	136 (2.8%)
CHONCl	90 (1.2%)	206 (2.3%)	215 (2.4%)	7 (0.1%)
Other	16 (0.2%)	49 (0.5%)	53 (0.6%)	86 (1.8%)
Total	7768	9039	9143	4862

Beyond these obvious spectral difference, molecular characterization shows LLOM to have a higher diversity in formula class distribution than SRNOM with a predominance of formula classes containing heteroatoms (Figs. 5.1B and C, Table 5.3). Here, the formula class CHO is formulas that contain only carbon, hydrogen, and oxygen, CHON also contain nitrogen but no other heteroatoms, and so on for the heteroatoms N, S, P, F, Cl, and Br included in assignment. In the SRNOM sample, 60.2% of formula assignments were CHO, while only 32.8% of the *Active* LL and 26.1% of the *Closed* LL assignments were CHO. This difference is primarily derived from the higher percentage of CHON, CHOS, CHONS, CHOCl, and CHONCl assignments for LLOM (Table 5.3). The greater number of CHON formula assignments seen in the LL samples had higher H/C and O/C ratios than SRNOM, while the higher number of CHOS assignments for LLOM showed a similar pattern.

For the fewer total CHO formula assignments this same pattern was also observed (Figs. 5.1C, 5.2). The LL samples were both particularly distinguishable by a very high percent CHONS compared to SRNOM (Figs. 5.1C, 5.2, Table 5.3). Differences within the 'Other' formula class category included the minor presence of CHONSCl, CHOF, CHOFS, and CHOBr classes not seen in SRNOM (Table A4.17).

A distinguishing feature of LLOM signatures was prominent 58.0419 *m/z* and 22.0131 *m/z* spacing patterns. The 58.0419 *m/z* pattern, seen in Van Krevelen diagrams at H/C=2, is C_3H_6O and likely propylene oxide [$CH_2CH(CH_3)O$] units (Fig. 5.2). The homologous series continues past the 600 *m/z* cutoff used in producing the final dataset. The 22.0131 *m/z* patterns are visible in the raw, unassigned data among *m/z* ions with decimal values between 0.55 and 0.75 *m/z* (Table A4.16). Based on decimal values, these are likely doubly charged ions (McMillan et al., 2016), and the corresponding singly charged *m/z* spacing would be 44.0262 *m/z*, or C_2H_4O, likely ethylene oxide (CH_2CH_2O) units. Corresponding singly charged ions are present in the dataset and supercharging of polyethylene glycols in ESI is a known phenomenon (Iavarone and Williams, 2003). Molecular characterization is non-structural, so further analyses are needed for any true structural identification, but these homologous series patterns suggest LL could be a good medium for further study of alkoxylated surfactants and their degradation.

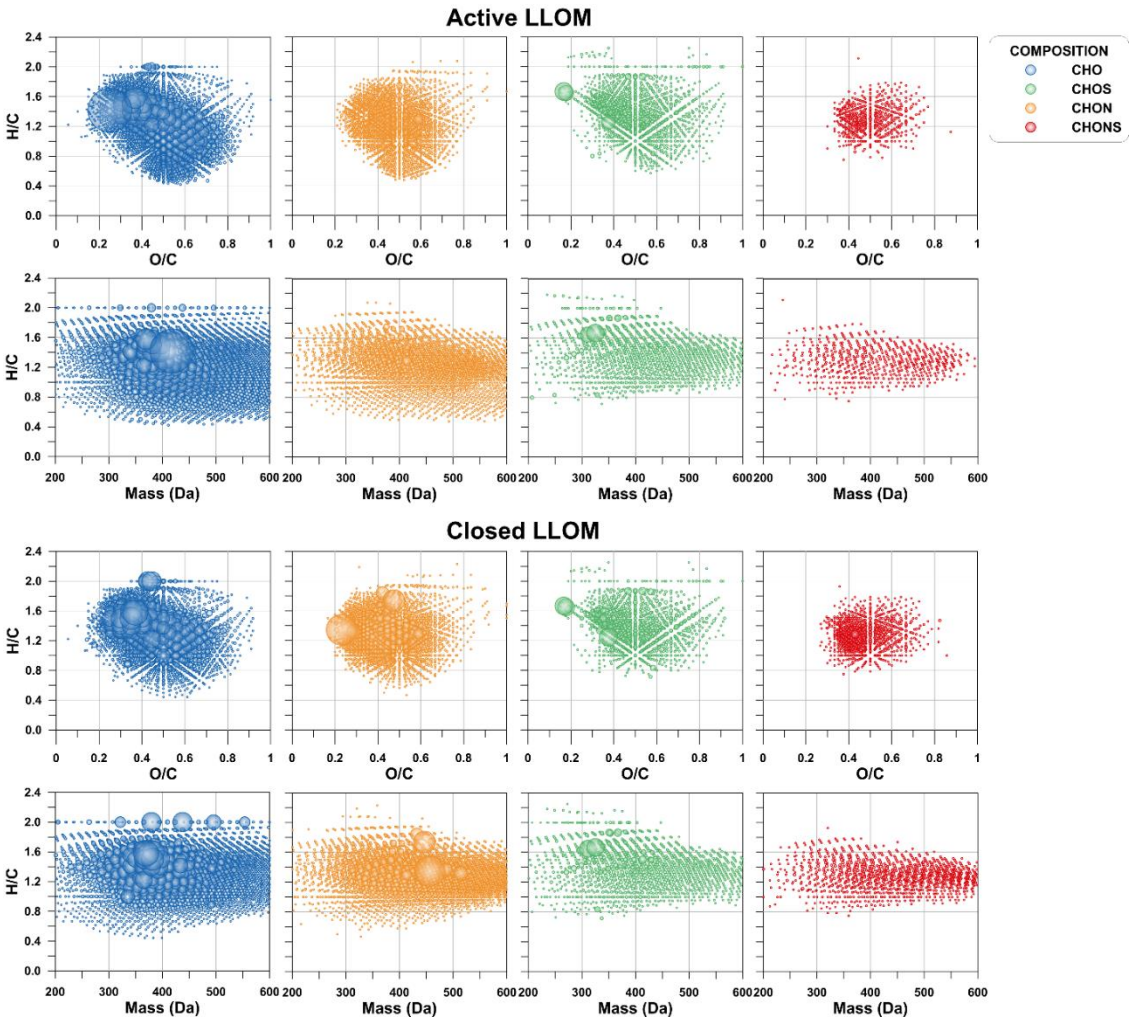

Figure 5.2 Van Krevelen diagrams and H/C *vs.* Mass plots of CHO, CHOS, CHON, and CHONS formula classes in the *Active* and *Closed* LL samples. The mass spacing pattern in CHO plots at H/C=2, most prominent in the *Closed LL* sample, is a 58.0419 *m/z* spacing, most likely propylene oxide units [$CH_2CH(CH_3)O$]. Point size scale is independent by sample, but within sample scaling corresponds to signal intensity. Known high intensity CHOS background surfactant contaminants and the 417.2283 *m/z* ion assignment in the *Closed LL* sample were not plotted for visualization. The 417.2283 *m/z* ion assignment remains plotted in the *Active* LL sample.

Another major difference from SRNOM was the high number of CHOCl formula assignments (Table 5.3, Fig. 5.3). This is particularly noteworthy because a high presence of non-volatile organic halogens in LLs has been previously suggested based on high adsorbable organic halogen (AOX) measurements or differences in purgeable organic halogen (POX) measurements from AOX, but this fraction has

remained essentially unidentified due to instrument limitations (Yasuhara et al., 1999; Grøn et al., 2000; Kjeldsen et al., 2002). While some of these determinations were made in mixed-use landfills, through FT-ICR-MS molecular characterization in this study we found evidence supporting the existence of an extensive non-volatile organochlorine fraction in MSW LLs and were able to identify over a thousand LL non-volatile or semi-volatile organochlorine formulas. This fraction could contain synthetic organochlorine related chemicals, as LL is known to contain chlorinated flame retardants, pesticides, plasticizers, and household chemicals (Slack et al., 2005). CHOCl formulas were very different from those in SRNOM (Fig. A4.6) and unlike SRNOM, included 98 formulas with 2-6 chlorine atoms (Fig. 5.3), which is evidence for covalently bound chlorine and not feasible by adduct formation alone. The CHOCl assignments with 4-6 chlorine atoms had similar formulas and are discussed in detail in the following section.

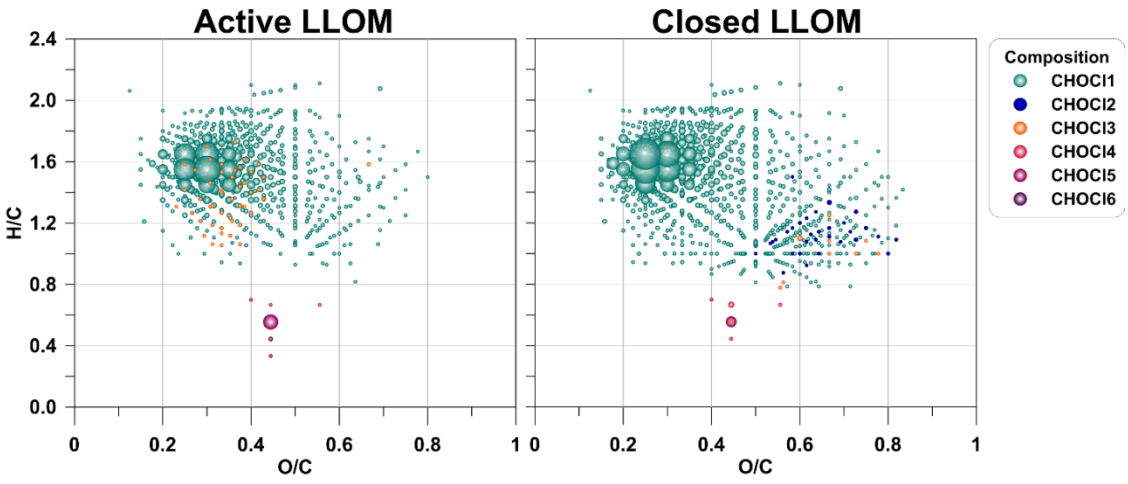

Figure 5.3 Van Krevelen diagrams of CHOCl formula assignments in the *Active* and *Closed* LL samples. The highest O/C, 3 chlorine atom formula in the *Active* LL is $C_{12}H_{19}Cl_3O_8$ and corresponds to sucralose. Point size scaling corresponds to signal intensity.

While FT-ICR-MS is non-structural and a single formula cannot be presumed to correspond to a single chemical, 564/674 of the *Active* LL CHOCl formulas were identical to those in the *Closed* or *Closed-Brine* LLs. This may suggest common disposal sources or transformation processes that should be further explored; however, a striking difference between the different LL samples was seen among the CHOCl assignments with 2 and 3 chlorine atoms. All 2 chlorine CHOCl formulas were found across all triplicates exclusively in the *Closed* and the corresponding *Closed-Brine* LLs (Fig. 5.3). This class of 2 chlorine chemicals had similar formulas with 9-16 carbon atoms, even 10-18 hydrogen atoms, and 6-10 oxygen atoms. The highest signal intensity peak in this group was assigned as $C_{12}H_{16}Cl_2O_8$. Within the 3 chlorine CHOCl formulas a smaller group exclusive to the *Closed* and *Closed-Brine* LLs occupying the same Van Krevelen space as the 2 chlorine group was found (Fig. 5.3). Another 3 chlorine group exclusive to the *Closed* and *Closed-Brine* LLs all had 9 carbon atoms and is discussed in the following section. In contrast to the 2 chlorine formulas, the majority of 3 chlorine were exclusive to the *Active* LL sample (Fig. 5.3). This group all had similar formulas with 10-18 carbon atoms, odd 17-25 hydrogen atoms, and 3-6 oxygen atoms. The highest signal intensity peak in this group was assigned as $C_{16}H_{19}Cl_3O_6$. The one 3 chlorine formula exclusive to the *Active* sample outside this group matches the artificial sweetener, sucralose, which was confirmed and quantified as part of this study (Fig. 5.3). These 2 and 3 chlorine patterns do not appear to be due to assignment bias. This was checked for by comparable formula assignment using a different in-house software which does not use a network approach, FormCalc, which showed the same patterns. This is

unexplained, and while we can't rule out fundamental transformation differences in the two landfills, this seems to point to specific disposal origins, possibly of technical mixtures, or subsequent degradation of specific disposals in the individual landfills.

Though not included in the CHOCl grouping, in CHONSCl there was one 2 chlorine formula, $C_6H_5Cl_2NO_3S$, found in all LL samples. This was similar to the only 2 chlorine CHOSCl formula, $C_6H_4Cl_2O_3S$, found in the *Closed* and *Closed-Brine* LL. These formulas are structurally limited and appear to be benzenesulfonate based. These are the only formulas in the other formula classes with >1 chlorine. Other LL sample specific features include the presence of one brominated formula, $C_9H_{10}Br_2O_4$, and likely presence of $C_9H_8Br_2O_2$ and $C_6H_3Br_3O_2$ in the *Closed* and *Closed-Brine* samples (Table A4.19, A4.21). These latter two formulas were not included in the main dataset because only the higher abundance isotopic peaks, and not the monoisotopic peaks, were visible across triplicates in the data matrix.

The LL samples also included the CHOF and CHOFS formula classes. These *m/z* ions were initially identified in the raw dataset by decimal values characteristic of highly substituted organohalogens and the absence of chlorine or bromine isotopic peaks, suggesting monoisotopic fluorine. Within CHOF are the formulas $C_6HF_{11}O_2$ and $C_8HF_{15}O_2$ in all LL samples and $C_7HF_{13}O_2$ in the *Closed* and *Closed-Brine* samples. These structurally limited formulas appear to correspond to the common perfluoroalkyl carboxylates, perfluorohexanoic acid (PFHxA), perfluorooctanoic acid (PFOA), and perfluoroheptanoic acid (PFHpA), respectively. Within CHOFS are the formulas $C_4HF_9O_3S$ and $C_6HF_{13}O_3S$ in all LL samples and $C_8HF_{17}O_3S$ in the *Closed* and *Closed-Brine* samples. These appear to correspond to the common perfluoroalkyl

sulfonates, perfluorobutanesulfonic acid (PFBuS), perfluorohexanesulfonic acid (PFHxS), and perfluorooctanesulfonic acid (PFOS), respectively. The widespread presence of these persistent chemicals in MSW LLs is well known (Wei et al., 2019; Masoner et al., 2020).

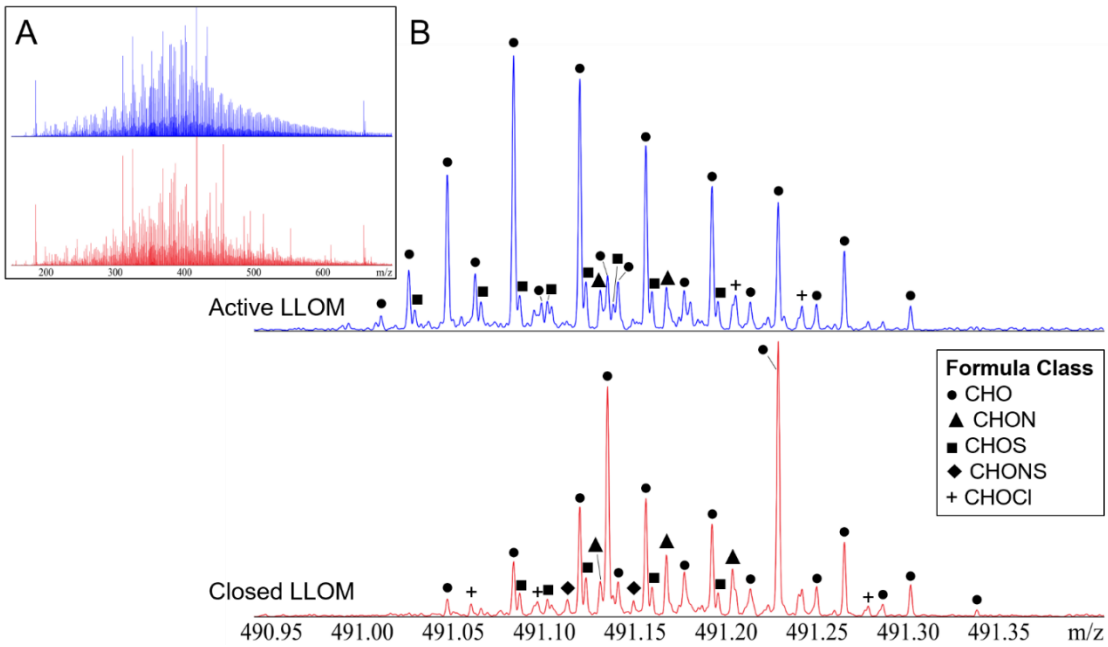

Figure 5.4 Full *m/z* spectra of an *Active* LL sample (top) and a *Closed* LL sample (bottom) (A). Spectra were scaled to similar relative intensities for comparison purposes. Classes of formulas between the samples at 491 *m/z* (B).

This limited sample dataset revealed both similarities that may be MSW LL characteristic but also diversity in LL composition (Fig. 5.4). A major difference seen across CHO, CHON, and CHOS formula classes was more low H/C formulas with approximately 0.4-0.8 O/C in the *Active* LL (Fig. 5.5). Signal intensity across these classes was also weighted to lower H/C formulas than in the *Closed* LL (Fig. 5.2). While in the *Closed* LL, within CHO, formula signal intensity was weighted to higher H/C and lower O/C formulas and most unique CHO formulas were within this region. In the *Closed* LL, there were more CHON and CHONS formulas in the higher H/C and lower O/C region, between 0.8-1.8 H/C and 0.2-0.5 O/C, than in the *Active* LL

(Fig. 5.5). The *Closed* LL also had a much greater number of CHON and CHONS formulas with 2 and 3 nitrogen atoms, most of which fell in this Van Krevelen space (Figs. A4.7, A4.8). Most between landfill formula differences were higher (>400 Da) molecular weight signatures (Fig. 5.5).

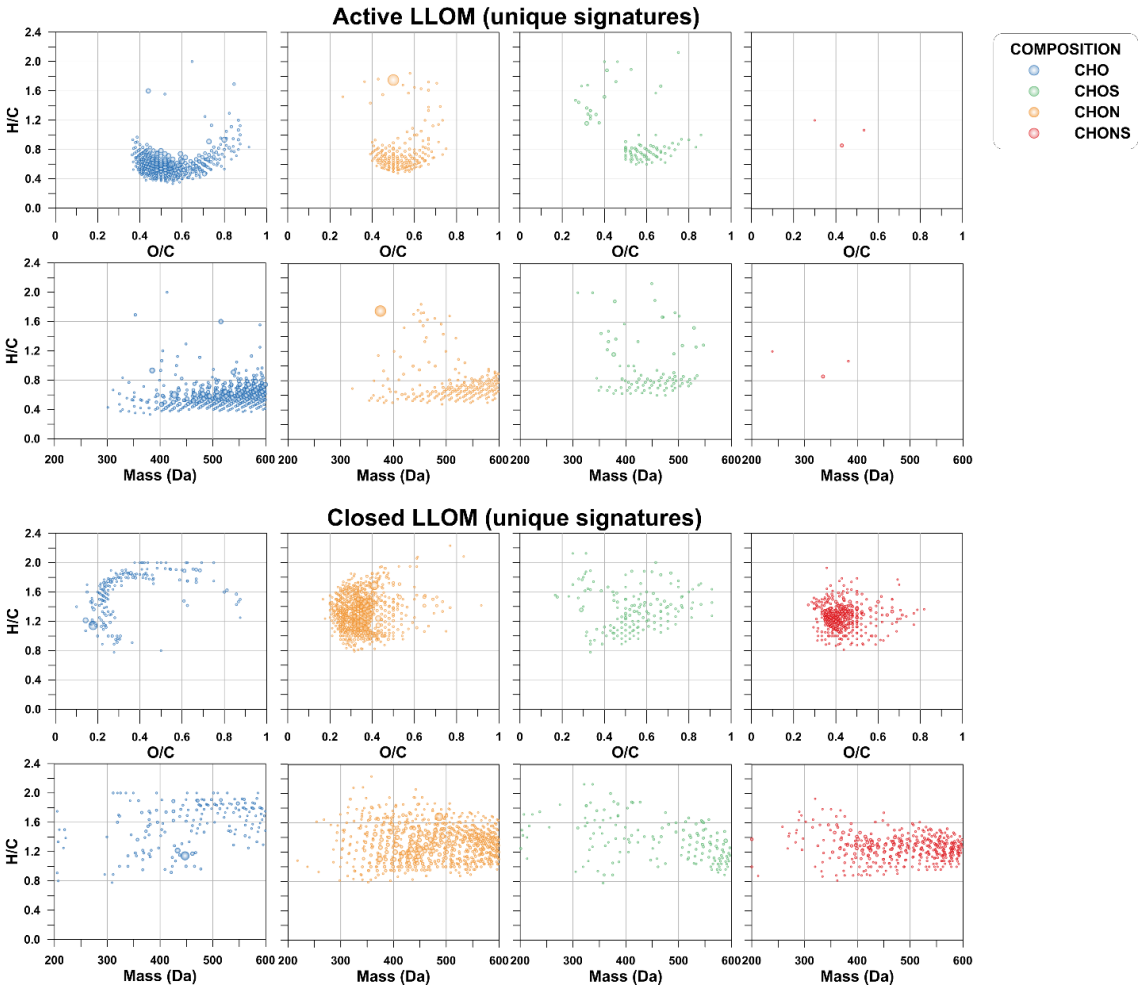

Figure 5.5 Van Krevelen diagrams and H/C *vs.* Mass plots of unique formula assignments with a >4,000,000 arbitrary units signal intensity cutoff between the *Active* and *Closed LL* samples for CHO, CHOS, CHON, and CHONS formula classes. Point size scale is independent by sample, but within sample scaling corresponds to signal intensity.

The results from these samples highlights the benefits of non-targeted ultrahigh resolution MS for understanding the molecular composition of LLOM. Molecular trends and similarities between samples are difficult to interpret because of

the lack of similar data and the poor scientific understanding of long term abiotic and biotic transformations in landfills, but high intensity *m/z* ion peaks at 185.0278 and 417.2283 *m/z* and higher presence of sulfur-, nitrogen-, and chlorine-, particularly nitrogen-sulfur-, containing molecular formulas may be LL characteristic. Yuan et al. (2017) found a similar high presence of CHONS molecular formulas and found this group resistant to removal during leachate treatment. High presence of CHONS formulas may be more LL specific, as high presence of CHOS, CHON, and CHOCl formulas can also be features of domestic wastewaters (Gonsior et al., 2011; Maizel and Remucal, 2017). These incredibly complex mixtures represent the diverse array of natural and synthetic chemicals that make up societal disposal and subsequent in-landfill degradation and transformation. More non-targeted molecular characterizations of LLs will increase compositional understanding for treatment and source tracing, and with more data from MSW landfills with different ages and engineered treatments, composition could possibly be linked to specific transformation processes. Additional analyses using other sample extraction processes, positive ESI, different ion sources, and MS/MS for structural elucidation of prominent ions would also aid in the understanding of these mixtures in future studies.

5.3.4 LC/MS/MS and Orbitrap MS/MS on $C_9H_4Cl_6O_4$ and similar formula organohalogens

In FT-ICR-MS molecular characterization, the formula $C_9H_4Cl_6O_4$ was notable for having the highest number of chlorine atoms in the dataset. It was further observed that the only three assignments with five chlorine atoms and the only three

assignments with four chlorine atoms had formulas that appeared to be analogues (Fig. 5.3). Following this, a suite of 12 total similar formulas, 11 with 3-6 chlorines and 1 with 2 bromines, was identified. These 12 formulas in order of increasing *m/z* of the corresponding highest abundance $[M-H]^-$ ion were: $C_9H_5Cl_3O_4$, $C_9H_7Cl_3O_5$, $C_9H_4Cl_4O_4$, $C_9H_9Cl_3O_6$, $C_9H_6Cl_4O_4$, $C_9H_9Cl_3O_7$, $C_9H_6Cl_4O_5$, $C_9H_{10}Br_2O_4$, $C_9H_3Cl_5O_4$, $C_9H_5Cl_5O_4$, $C_{10}H_7Cl_5O_4$, and $C_9H_4Cl_6O_4$. The original 12 formulas have masses from 280.918-384.817 *m/z*, KMDs 0.389-0.607, double bond equivalents 4-6, H/C ratios 0.3-1.1, and O/C ratios 0.4-0.8. All corresponding ions were confirmed with isotope pattern matching in the Bruker DataAnalysis software. There was no obvious assignment bias for these types of formulas by the employed network formula assignment approach. To investigate this, *m/z* decimal vs. *m/z* plots were produced for original *m/z* ion lists and checked for high chlorine isotope patterns (Fig. A4.3), following McMillan et al. (2016), who showed the power of these "generalized mass defect" plots to exploit halogen mass properties while avoiding formula assignment. While $C_9H_6Cl_4O_4$, $C_9H_5Cl_5O_4$, and $C_9H_4Cl_6O_4$ could be misidentified $[M+Cl]^-$ adducts of $C_9H_5Cl_3O_4$, $C_9H_4Cl_4O_4$, and $C_9H_3Cl_5O_4$, respectively, the existence of masses corresponding to $[M+Na]^+$ sodium adducts of $C_9H_6Cl_4O_4$ and $C_9H_5Cl_5O_4$ in the corresponding positive mode ESI dataset shows this is unlikely. Instead, for reasons discussed later, we expect an opposite relationship, and that $C_9H_5Cl_3O_4$, $C_9H_4Cl_4O_4$, and $C_9H_3Cl_5O_4$ may not be present in the samples and are instead misidentified $[M-HCl-H]^-$ in-source fragmentation products of $C_9H_6Cl_4O_4$, $C_9H_5Cl_5O_4$, and $C_9H_4Cl_6O_4$.

Non-targeted ultrahigh resolution MS is non-structural, but the highest chlorine formula, $C_9H_4Cl_6O_4$, is interestingly the same formula as chlorendic acid. Chlorendic acid is a reactive flame retardant, meaning it is chemically bonded to a material to impart flame resistance. It is used to produce flame resistant polyurethane foams and flame and corrosion resistant polymer resins, among other uses (NTP (National Toxicology Program), 2016). In 1996, worldwide production levels were estimated at 4 million kgs (NTP (National Toxicology Program), 2016). Chlorendic acid has a hexachloronorbornene structure and is structurally related to the chlorinated cyclodiene insecticides (NTP (National Toxicology Program), 2016), all of which are persistent organic pollutants (Stockholm Convention, 2017). It is also a degradation product of some of these insecticides (NTP (National Toxicology Program), 2016).

To explore this possible connection, we performed the aforementioned LC/MS/MS and Orbitrap MS/MS analyses on the *m/z* ions corresponding to $C_9H_4Cl_6O_4$, $C_9H_5Cl_5O_4$, and $C_9H_6Cl_4O_4$. These three formulas were the only ones of the suite with high enough expected signal intensity to be analyzed by LC/MS/MS (Table A4.19). Chlorendic acid fragmentation data are available in the mzCloud Database (Thermo Fisher Scientific) for negative mode ESI with higher-energy C-trap dissociation (HCD) on a Q Exactive Orbitrap (mzCloud: Advanced Mass Spectral Database, 2018). The LTQ Orbitrap XL Hybrid used in this study is an older model than the Q Exactive Orbitrap, so it is unable to reflect the HCD improvements available in the Q Exactive instrument line (Hecht et al., 2006). For this reason, LC/MS/MS experiments were performed using negative ESI with CID on a triple

quadrupole MS. CID in a triple quadrupole MS is similar to Orbitrap HCD, as both are beam, also known as non-resonant, CID processes (de Graaf et al., 2011; Ichou et al., 2014), meaning multiple disassociation steps are likely, so more and smaller fragments can be produced. Of the suite, $C_9H_5Cl_5O_4$, had the overall highest signal intensity, so it was selected for higher mass resolution Orbitrap CID MS/MS on individual isotopic peaks. In contrast to CID in a triple quadrupole MS, Orbitrap CID is an ion-trap, or resonant, CID process, so multiple fragmentation steps in MS/MS are unlikely, without additional dissociation (de Graaf et al., 2011).

For LC/MS/MS, transitions corresponding to loss of 36 *m/z* (-HCl), 44 *m/z* (-CO_2), 116 *m/z* (-$CH_2Cl_2O_2$), 108 *m/z* (-H_3Cl_3), and 136 *m/z* (-CH_3Cl_3O) were monitored for the three parent ions in MRM mode. These are all previously observed fragmentation patterns for chlorendic acid by Orbitrap HCD in the mzCloud library (mzCloud: Advanced Mass Spectral Database, 2018) and appear to correspond to the neutral losses of HCl, CO_2, 2HCl+CO_2, 3HCl, and 3HCl+CO, respectively. Additionally, the loss of 18 *m/z* (-H_2O) and 62 *m/z* (-CH_2O_3), corresponding to neutral loss of H_2O and CO_2+H_2O, were monitored by MRM as controls because these are common loss patterns that are not expected for chlorendic acid, but could help identify background noise. All chlorendic acid characteristic transitions were clearly observed for the parent ions in selected samples at 10 eV CID, beyond -CO_2 for $C_9H_4Cl_6O_4$ and $C_9H_6Cl_4O_4$, which could not be resolved from the background (Figs. A4.9-11). These transitions were observed together at the approximate retention times 2.05, 1.98, and 2.02 min for $C_9H_4Cl_6O_4$, $C_9H_5Cl_5O_4$, and $C_9H_6Cl_4O_4$, respectively. As expected, control transitions did not have distinct peaks at the apparent retention

times and are not believed to be losses from the parent ions. Beyond the comparable retention times, all parent ions were similarly sensitive to beam CID with transitions following the same intensity shifts with higher energy CID. Unexpectedly, all showed loss of -HCl, $-CH_2Cl_2O_2$, and $-H_3Cl_3$ at 0 eV collision energy. Possible loss of $-CO_2$ was also visible in the $C_9H_5Cl_5O_4$ chromatograms for both samples at 0 eV CID. This appears to be unintended dissociation after the first mass filter (Q1). A similar fragile behavior can be seen in the mzCloud database, where with negative ESI and under no dissociation, the chlorendic acid standard forms a deprotonated ion $[M-H]^-$, a minor sodium adduct $[M-2H+Na]^-$, and minor ions $[M-H-HCl]^-$ and $[M-H-CO_2]^-$ that appear to represent in-source fragmentation (Gabelica and Pauw, 2005; Song, 2011; Xu et al., 2015; mzCloud: Advanced Mass Spectral Database, 2018). In this study, unintended CO_2 loss could be occurring for all parent ions and in all samples but cannot be clearly distinguished from the background. The *m/z* scan range used in the mzCloud data does not include the region where $-CH_2O_2Cl_2$ or $-H_3Cl_3$ loss would be observed (mzCloud: Advanced Mass Spectral Database, 2018).

Following this, LC/MS/MS experiments were undertaken in the less sensitive full scan mode, averaging spectra over the identified retention times, to eliminate potential bias of monitoring only specific transitions. For $C_9H_4Cl_6O_4$, fragments were observed to represent loss of -HCl, $-CO_2$, $-CHClO_2$, and $-H_3Cl_3$. While for $C_9H_5Cl_5O_4$, fragments were identified as loss of -HCl, $-CO_2$, $-CHClO_2$, $-C_2O_4$, $-H_3Cl_3$, $-CH_2Cl_2O_2$, and $-C_2HClO_4$. For $C_9H_6Cl_4O_4$, the chosen parent ion was not the monoisotopic ion (all ^{35}Cl) but the highest abundance ion, $C_9H_5{}^{35}Cl_3{}^{37}ClO_4^-$. This was to avoid background interference from other members of the 12 formula suite with

isotopic ions at similar masses, but had the added bonus of confirming the identity and source of the higher chlorine number losses, showing product ions corresponding to loss of -$H^{35}Cl$, -CO_2, -C_2O_4, -$H_3{}^{35}Cl_3$, -$H_3{}^{35}Cl_2{}^{37}Cl$, -$CH_2{}^{35}Cl_2O_2$, and -$CH_2{}^{35}Cl^{37}ClO_2$. The losses seen in full scan mode among the parent ions that were not monitored for in MRM, -$CHClO_2$, -C_2O_4, and -C_2HClO_4, could correspond to neutral losses of HCl+CO_2, 2CO_2, and HCl+2CO_2, respectively. All of these are also shown for chlorendic acid in the mzCloud Database (mzCloud: Advanced Mass Spectral Database, 2018). These results show different but remarkably similar fragmentation patterns for the three parent ions, and while this is a less sensitive method, results were consistent with the MRM experiments. Spectra do not include lower intensity fragments identified in the MRM experiments but include higher intensity fragments that were not initially monitored for. These other fragments still correspond to loss pathways observed for dissociation of chlorendic acid by Orbitrap HCD (mzCloud: Advanced Mass Spectral Database, 2018).

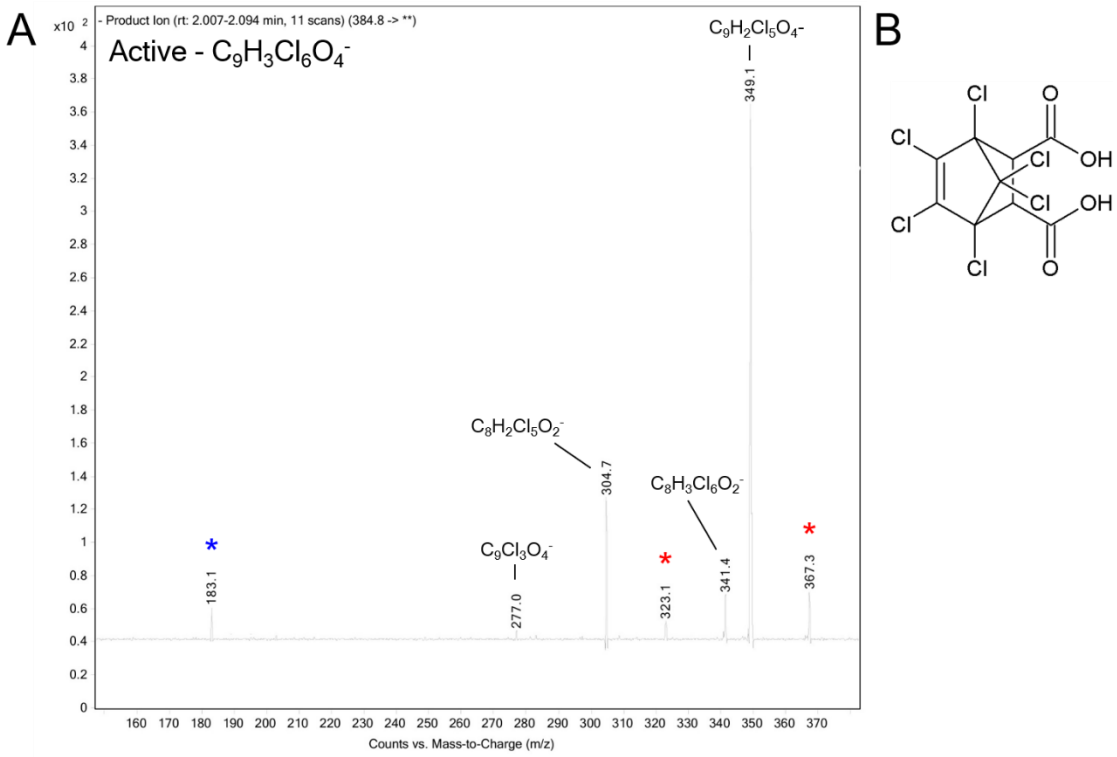

Figure 5.6 LC/MS/MS, full scan mode CID spectrum at 10 eV collision energy of 384.8 *m/z* ion, assigned $C_9H_4Cl_6O_4$, in the *Active* LL sample by triple quadrupole MS (A). Spectrum is average of 11 scans at approximate 2.05 min retention time. Red asterisks mark common background fragments that were present throughout the run, and likely correspond to loss of H_2O and H_2O+CO_2. The blue asterisk marks an unidentified fragment at the retention time that may be unrelated. Low mass resolution and error is typical of a triple quadrupole MS operating in full scan mode. Results are believed to be most consistent with a chlorendic acid identity. The chemical structure of chlorendic acid (B).

Direct injection Orbitrap CID on the three major isotopic ions of $C_9H_5Cl_5O_4$: $C_9H_4{}^{35}Cl_5O_4^-$, $C_9H_4{}^{35}Cl_4{}^{37}ClO_4^-$, and $C_9H_4{}^{35}Cl_3{}^{37}Cl_2O_4^-$, showed loss of -HCl, -$CO_2$, and -$CH_2Cl_2O_2$, following expected isotopic abundance patterns (Tables. A4.23, A4.24). These fewer fragments that do not appear to represent multiple dissociation steps are consistent with expected differences between beam and ion trap CID and these fragments could reasonably come from the expected structure of singly dechlorinated chlorendic acid. The $C_9H_6Cl_4O_4$ ion was of too low signal intensity for Orbitrap CID, but analysis of a chlorendic acid standard showed the loss of -HCl, -

H_3Cl_3, and -$CH_2Cl_2O_2$. We were unable to reliably analyze the standard by LC/MS/MS on a triple quadrupole MS beyond establishing the same retention time because of coeluting issues in the system of known phthalate plasticizer contaminants with the same parent ion mass.

We believe the combination of characteristic fragmentation patterns and similar retention times and fragmentation behavior, including distinctive molecular fragility during analysis, identifies $C_9H_4Cl_6O_4$ as likely chlorendic acid and $C_9H_5Cl_5O_4$ and $C_9H_6Cl_4O_4$ as related compounds, possibly from the use of technical mixtures (Shen et al., 2011), manufacturing by-products, or abiotic or biotic dechlorination. While other possible structures cannot be wholly discounted, fragmentation patterns and known manufacturing processes seem most consistent with a chlorendic acid identification. Observed fragment ions may provide information on the dechlorination positions on the norbornene structure. With MS/MS evidence and the signal correlations in the ESI FTICR MS data, we suggest that the ions appearing to correspond to $C_9H_5Cl_3O_4$, $C_9H_4Cl_4O_4$, and $C_9H_3Cl_5O_4$ could be misidentified $[M-HCl-H]^-$ in-source fragmentation products. The other formulas in the suite with lower signal intensity, including $C_9H_7Cl_3O_5$, $C_9H_9Cl_3O_6$, $C_9H_6Cl_4O_4$, $C_9H_9Cl_3O_7$, $C_9H_{10}Br_2O_4$, and $C_{10}H_7Cl_5O_4$, may be unrelated, but their similar formulas suggest potential relation should be explored. As previously mentioned, $C_9H_8Br_2O_2$ was tentatively also identified in FT-ICR-MS spectra but was not included in the final dataset. These could be the result of degradation, the use of technical mixtures, or other produced flame retardants entirely. Lower chlorine number formulas in this dataset could also be related and should be further explored.

In this study chlorendic acid and likely related compounds were tentatively identified in two unrelated MSW landfills. To our best knowledge, chlorendic acid has only once been previously described in MSW leachate (Öman and Hynning, 1993). The likely related compound $C_9H_5Cl_5O_4$ had particularly high signal intensity in our FT-ICR-MS dataset. The average signal intensity of the monoisotopic peak was >99% of the assigned peaks in the *Active* LL and >98% in the *Closed* LL. This is the highest intensity multichlorine signal in the dataset. FT-ICR-MS characterization data cannot be used quantitatively, but this does suggest that this compound may be highly ionizing or in high abundance and could be prominent in future LL molecular characterizations. A future goal should be quantification of this chemical and chlorendic acid in other MSW LLs. Interestingly, the formula believed to be chlorendic acid, $C_9H_4Cl_6O_4$, was only found in the *Active* LL, while lower molecular weight formulas within the suite, not including in-source fragmentation products, generally had higher signal intensity or were only identified in the *Closed* LL (Tables. A4.19, A4.20).

Chlorendic acid is classified as "reasonably anticipated to be a human carcinogen" by the National Toxicology Program (NTP (National Toxicology Program), 2016). The apparent appearance of it and related compounds in MSW landfills warrants future study to determine how ubiquitous this signal is and where it is coming from. Chlorendic acid could leach from disposed materials or could be from degradation of or technical mixtures of cyclodiene pesticides. Certain emerging dechlorane-related flame retardants are also structurally related to chlorendic acid (Shen et al., 2011). The facts that these are MSW landfills, the *Active* LL only

contains waste from the last two decades, and the absence of masses corresponding to higher molecular weight similar formulas does suggest chlorendic acid leaching could be the source. A caveat being that many related chemicals are poorly ionizing and are not expected to be detectable by FT-ICR-MS. Environmental leaching of chlorendic acid is essentially unstudied, though it could be released by polymer degradation in landfills (Hamilton et al., 1995; NTP (National Toxicology Program), 2016; Gaytán et al., 2020). Chlorendic acid is known to be resistant to degradation, but environmental degradation is also largely unknown. Jambon et al. (2019) isolated bacteria and fungi from a chlorendic acid containing industrial waste site, identifying the first unmodified microbes capable of chlorendic acid degradation. Recent work has also revealed that reductive stepwise dechlorination by zero-valent metals is possible for chlorendic acid (Kim et al., 2020) and the structurally similar endosulfan (Singh and Bose, 2017), and metal waste in landfills is capable of abiotic dehalogenation (Vogel et al., 1987; Reynolds et al., 1990).

5.4 Environmental Relevance

LL is a significant pollution risk to groundwater and surface waters. The extensive quantitative and non-quantitative chemical characterizations developed in this study can inform policy, landfill management, and LL treatment technology. Results from this study indicate the need for more data on the presence of less studied metals in LL, such as vanadium. Increased understanding of metal chemical speciation and identification of specific metal-organic complexes in LL would better inform risk assessment and mobility modelling. Measured targeted CECs in this study show how common household chemicals can be found in LL at high concentrations

(1s-100s of µg/L) and could be used for LL pollution tracing. Results also support the use of the artificial sweeteners, sucralose and ace-K, as LL age markers.

While the results of this study contribute to the understanding of LLOM composition, bulk composition is still minimally characterized, particularly organochlorines in LLOM. We assigned over ten thousand unique molecular formulas in LLOM, more than a thousand of which contained nitrogen and sulfur together and more than a thousand of which contained chlorine. About one hundred of assigned formulas had 2-6 chlorine atoms. All 4-6 chlorine atom formulas are tentatively related to chlorendic acid, and the presence of this flame retardant in MSW LLs should be further explored. Most 2 and 3 chlorine atom formulas appear to be linked to specific product disposals or transformation processes.

Nontargeted results appear to show both surprising similarity in LLOM between the closed, older landfill and active, bioreactor landfill samples, but also considerable molecular diversity between these unrelated MSW LLs. Non-targeted molecular characterization can inform LL pollution tracing and our understanding of long-term waste degradation in landfills. Future analyses can investigate the relation of molecular fingerprinting to specific chemical transformation pathways, particularly the contribution of original disposals and subsequent alteration to identified molecular diversity.

5.5 Acknowledgements

We would like to thank Dr. Cédric Magen, Stable Isotopes Laboratory at CBL, for providing isotopic analytical services, and Dr. Mourad Harir for assistance in FTICR MS analyses. This work was supported by the Maryland Sea Grant REU

Program to S.M. and the Maryland Sea Grant Research Fellowship and University System of Maryland MEES graduate program Reid Evans Menzer Research Fellowship to K.R.M. We also thank anonymous reviewers for their constructive comments.

Chapter 6: Conclusions and Future Work

Septic systems do not meet the treatment level of municipal wastewater treatment plants (WWTPs) and release contaminants to the environment. However, they are still a widely used and necessary sewage treatment option in the United States and globally, particularly when connection to municipal wastewater treatment is unavailable. Septic system-contributed nitrogen is of particular concern in the Chesapeake Bay Region as the public and lawmakers seek solutions to address eutrophication and a decline in ecological health. Understanding and reducing septic system pollution is necessary to address U.S. Environmental Protection Agency Clean Water Act total maximum daily load (TMDL) regulations, as well as to protect groundwater resources in the present and for the future.

In the process of the septic system study, I had the opportunity to further explore side questions and directions that developed, namely landfill leachate composition and sucralose (SCL) adduct formation. SCL adduct formation was prominent in Fourier-transform ion cyclotron resonance (FTICR) mass spectrometry (MS) data from samples in the septic system study and other wastewater samples. While not discussed in this dissertation, SCL adduct formation was also prominent in Active landfill leachate spectra. The landfill leachate samples in this work were originally part of a different study in the Gonsior Lab when molecular composition became a topic of interest to better understand the extreme dissolved organic carbon (DOC) concentrations in leachates. While landfill leachate is very molecularly

distinct from septic system wastewater, they are both anaerobic, anthropogenic wastewaters, with many of the same household product chemical contributions.

In *Chapter 2*, I presented evidence that SCL has extensive adduct ion formation potential in commonly used mass spectrometric analytical techniques. In FTICR MS spectra of Agilent Bond Elut PPL solid-phase extracted (SPE) dissolved organic matter (DOM), SCL was shown to readily form molecular ions, as well as adduct ions with chloride, formate, nitrate, bromide, and iodide, along with apparent in-source fragmentation product ions. SCL also tentatively can form adduct ions with trifluoroacetate, bisulfate, certain benzenesulfonates, and other molecules. SCL has three chlorine atoms, so has many isotopologues with high natural abundances. This means that in certain samples more than 50 *m/z* ions can be attributed to SCL. This in-instrument behavior complicates nontargeted data interpretation but could also be exploited to improve future SCL quantification, which is a goal that should be further explored. Future work should also explore the factors controlling this adduct formation and identify other possible adducting ions of SCL in positive and negative ion mode.

In *Chapter 3*, I used FTICR MS to molecularly characterize septic tank effluent (STE) impacted and reference stream DOM and septic tank DOM (STDOM), to identify new chemical wastewater tracers for STE impact. I related molecular features to higher impact and identified 137 molecular tracer ions that were only present in higher STE impacted streams. Tracers were mainly sulfur (CHOS) and sulfur and nitrogen (CHONS) containing molecules. CHOS tracers are believed to relate to sulfonated surfactants and their degradation products, while CHONS tracers

are thought to be related to microbial activity. I identified which of these may be the best performing and also identified other chemical features which can be used to distinguish STE impacted water bodies and approximate level of impact. Septic tank dissolved organic matter (STDOM) was found to have a more aliphatic molecular signature with high hydrogen-to-carbon (H/C) ratios, as well as a high presence of CHOS and CHONS formulas. STDOM samples had diverse molecular signatures. In assessing the presence of identified tracer formulas, 108/137 were also identified in STDOM, supporting that these are STE impact tracers.

While there are many organic chemical tracers used to identify domestic wastewater input, currently used tracers are mainly contaminants of emerging concern (CECs) known to be present in household products or human diet. New tracers identified using a nontargeted approach can include unknown chemicals from complex product formulations or food composition, metabolites, or transformation products. These chemical tracers which have not been previously considered may be better performing or address shortcomings of currently used tracers.

This work is only preliminary but provides new tools for identifying STE impact and lays the groundwork for future investigations. Similar studies should be conducted in more regions and in different types of natural waters. STDOM molecular composition in relation to tank treatment technologies could also be explored. A future goal is to identify the molecular structures of these tracers and to develop quantification methods for them. Another future goal is to identify molecular differences that could help better distinguish different types of wastewater impact, such as STE, combined sewer overflow (CSO), and treated WWTP effluent. FTICR

MS data should be further explored, in particular the apparent ethylene oxide and propylene oxide homologous series in STDOM and STE impacted waters and corresponding singly-, doubly-, and triply- charged ions, as these molecules may also function as wastewater tracers. STDOM molecular composition could be studied more in-depth and stream data molecular composition could be considered in relation to sampling time. Positive mode ESI FTICR MS data for STDOM and streams should also be analyzed for characterization and additional tracer development, and improved ionization of nitrogen-containing molecules is expected in positive ion mode. Different SPE and ionization techniques could also be used to analyze additional fractions of chemical composition.

Chapter 4 explored traditionally used tracer methods to give context to nontargeted tracer development and to aid in the regional understanding of septic system wastewater presence in surface waters. A suite of chemical species, CECs, and other water quality parameters were measured in small streams in Calvert County and Anne Arundel County, MD. These streams drained areas with varying septic system densities and land uses. Many of the same parameters were also measured in septic tank wastewater. The statistical techniques, cluster analysis and multi-dimensional scaling (MDS), were used to assess data.

Commonly used wastewater tracers like Cl, $\delta^{15}N_{NO3}$, SCL, acesulfame-K (ace-K), carbamazepine, total dissolve nitrogen (TDN) and the specific species NO_2-NO_3 and NH_4/NH_3 are performing well in this region. Many tracers showed the same site ranking of perceived level of STE impact. Ibuprofen, diclofenac, and triclosan also

could be used as tracers for higher levels of STE impact. In contrast, DOM fluorescence was not found to perform well as a wastewater tracer in streams.

Chemical tracers showed few seasonal trends, suggesting that, at least in this region, a longer-term study is not needed to identify relative level of STE impact. The artificial sweeteners, SCL and Ace-K, appear to be the best performing of the measured CECs based on strong linear correlations with septic system density and TDN. These are both ubiquitously used and persistent tracers. Septic tank wastewater had widely varying concentrations of measured parameters which is expected based on varying household diet and product use. The averages of these measurements can aid in interpreting measured concentrations in streams.

While DON was found to be elevated in more STE impacted streams, it also accounted for a lower % of TDN at these same sites, with "cleaner" and less STE impacted streams having higher values of DON/TDN. However, DON still provides critical access to wastewater tracers needed to understand presence of STE. Some of the CEC tracers used in this study are organic nitrogen compounds. Additionally, as shown in *Chapter* 3, even when only assessing negative mode ESI FTICR MS data, many of the identified potential tracer ions were nitrogen- and nitrogen with sulfur-containing organics (Table A2.3).

There is a common public misconception that for properly performing septic systems, STE does not impact surface waters and only impacts shallow groundwater aquifers. STE impact was found to be essentially ubiquitous in surface waters with septic systems in their catchments. Even at forested, reference sites with low septic

system densities, SCL and Ace-K could be detected, with both only being never detected at the site with no septic systems in its catchment.

A future goal of this work is to integrate measured data with septic system age data or an approximate proxy for this like structure age. Measurements could also be compared to results modeled using the Chesapeake Bay Program's Chesapeake Assessment Scenario Tool (CAST). Other statistical techniques like generalized additive models (GAMs) could also be valuable for interpreting data. A final goal is to be able to quantitatively estimate contributed STE volume in streams.

In *Chapter 5,* I molecularly characterized landfill leachate organic matter (LLOM) from two Florida municipal solid waste (MSW) landfills using FTICR MS, also measuring many targeted chemical parameters. Analyzed landfill leachates (LLs) were from a bioreactor landfill that is actively receiving waste and a landfill that closed in the late 1990s and its reverse osmosis (RO) treatment system. LLOM was found to be extremely complex with a high presence of sulfur-, nitrogen-, and chlorine-, particularly nitrogen-sulfur-, containing formulas. There were 2 specific *m/z* ions in LLOM, assigned as $C_8H_{10}O_3S$ and $C_{24}H_{34}O_6$, that were at very high signal intensity relative to natural DOM or other wastewaters and that may perform as tracers for LL. The organochlorine formula assignments included formulas with 2-6 chlorine atoms. Testing showed that the 6-chlorine formula, $C_9H_4Cl_6O_4$, may be the flame retardant, chlorendic acid, and that other 3-5 chlorine molecules may be related compounds.

Concentrations of DOC and ammonia were hundreds of, to more than a thousand, mg C/L and N/L. LLOM also had high concentrations of CECs, with

ibuprofen, SCL, and ace-K measured in the hundreds of μg/L. Sucralose and ace-K were demonstrated to work as time markers for landfill age. Dissolved iron was also measured at mg/L levels and there was evidence to suggest a significant percent of this may be organically complexed.

A future research direction is to explore the identities of the 2 high signal intensity potential "LL tracer" *m/z* ions. While not described in this chapter, these high intensity signals were also seen in a likely LL plume-impacted groundwater sample in MD. The structural identity of the molecules in the ethylene oxide and propylene oxide homologous series in LLOM could also be explored. Apparent organic complexation of iron could be confirmed by keeping samples anoxic at sampling and performing size separation and metal chemical speciation experiments. Differences in the LLOM composition of the Closed LL and its RO Brine could be further considered. Calibration of FTICR MS spectra optimized for the high *m/z* region would allow for additional analysis of the high mass region of LLOM. This is of significant interest as the signatures between the two landfills have greater differences in this region, and it would aid in understanding the identities of the multiply charged ions which were only apparent in the Active LL spectra. The presence of chlorendic acid should be analytically confirmed and measured. In the samples in this study, gas chromatography/MS (GC/MS) could be used to measure concentrations of structurally related cyclodiene pesticides to better understand the apparent chlorendic acid signal.

There is still minimal data available on bulk composition of LLOM and LL in general. This study only included 2 landfills, so a future goal is to molecularly

characterize LLOM from additional landfills, as well as to better relate composition to received waste, treatment technologies, or landfill age. Though it would be complicated by adduct formation, formulas could also be assigned in positive mode ESI data to better understand LLOM composition. Using different SPE methods or ionization techniques would also allow for the identification of different molecules in LLOM. Long-term waste processing in landfills and the microbial community and chemical transformations involved in long term waste degradation are still poorly understood. A major question to explore is the roles of initial disposal and subsequent alteration in molecular composition and complexity.

Landfills and septic systems are currently necessary treatment technologies that meet societal needs and help decrease environmental contamination when alternative technologies are unavailable. However, both can also be contamination sources to surface and groundwaters. There is a need for improved engineered waste treatments and better ways to track landfill and septic system pollution. I hope this work can assist in these goals and aid future research into these topics.

Appendix 1

Supplemental Materials to Chapter 2

Text A1.1 Description of Data

FTICR MS data for related signals, SCL, Cl, and NO_3 is available (https://figshare.com/s/3352e8215764b8c102d3). Sample data are from data matrices processed for other studies and show some increase in mass error due to necessary light smoothing and matrix generation, as well as instrument error that affected the calibration of septic system sample B2_2 at >580 m/z.

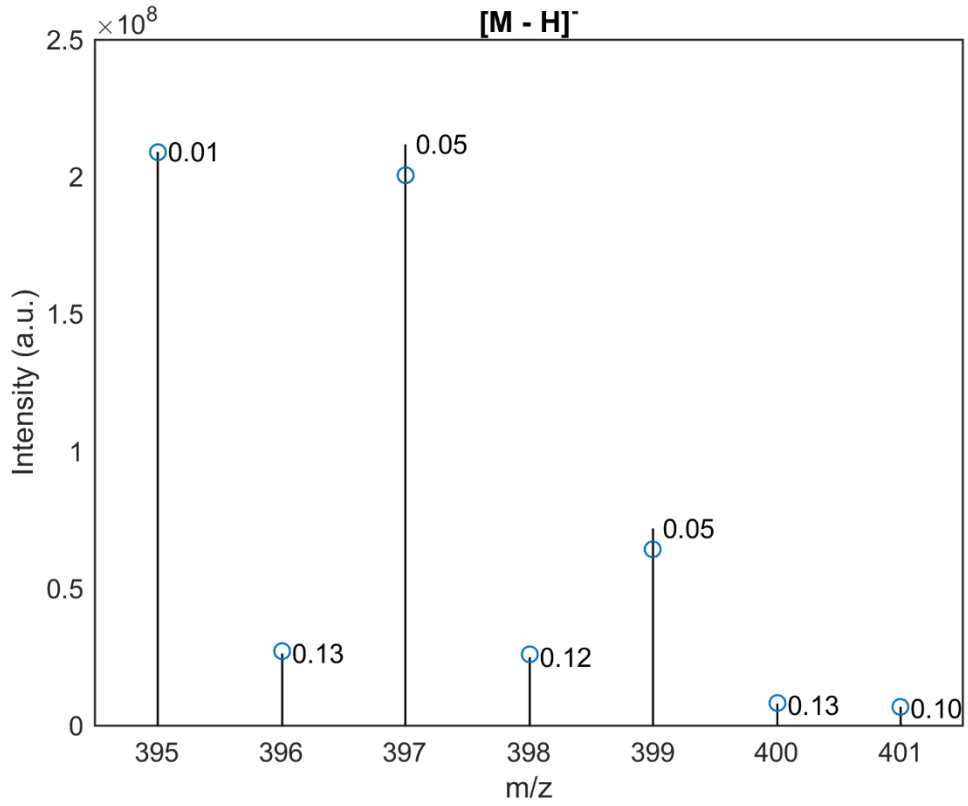

Figure A1.1 SCL, $[M - H]^-$, *m/z* ions (black bars), as observed in the Influent-B2 SPE by FTICR MS, compared to scaled corresponding theoretical isotopic patterns (blue circles) at 650,000 resolution at 400 *m/z*. Labels on experimental data are mass accuracy (ppm). Note, background ions are not shown for optimized visualization.

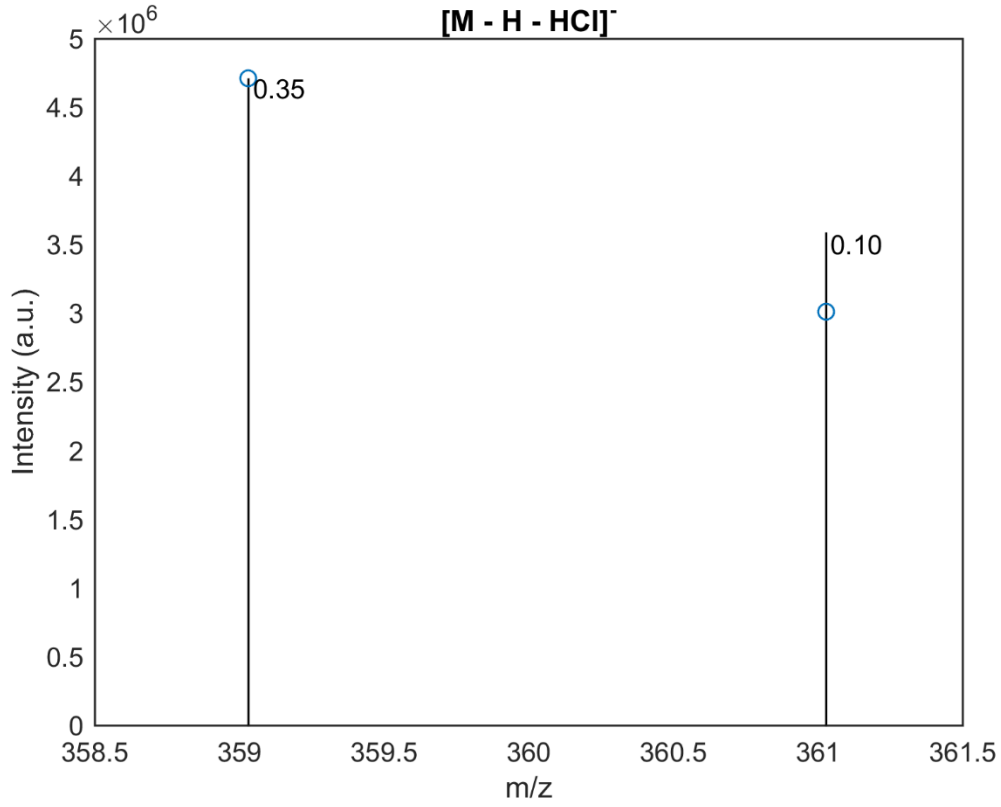

Figure A1.2 SCL in-source fragmentation product, $[M - H - HCl]^-$, *m/z* ions (black bars), as observed in the Influent-B2 SPE by FTICR MS, compared to scaled corresponding theoretical isotopic patterns (blue circles) at 650,000 resolution at 400 *m/z*. Labels on experimental data are mass accuracy (ppm). Note, background ions are not shown for optimized visualization.

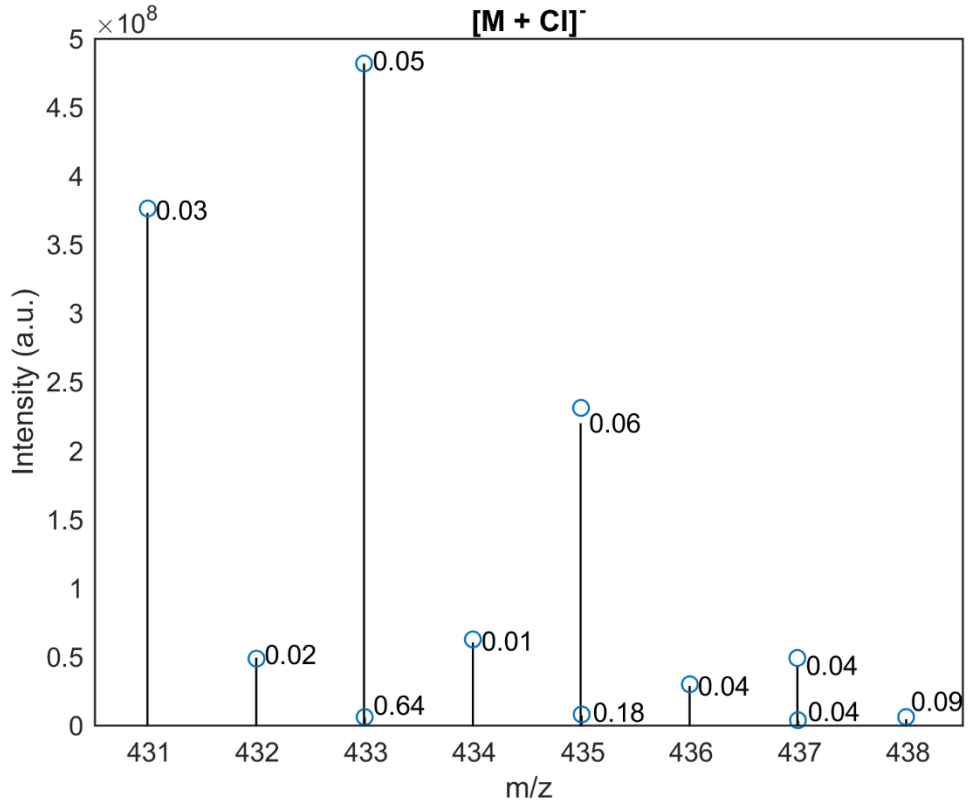

Figure A1.3 SCL chloride adduct, $[M + Cl]^-$, *m/z* ions (black bars), as observed in the Influent-B2 SPE by FTICR MS, compared to scaled corresponding theoretical isotopic patterns (blue circles) at 650,000 resolution at 400 *m/z*. Labels on experimental data are mass accuracy (ppm). Note, background ions are not shown for optimized visualization.

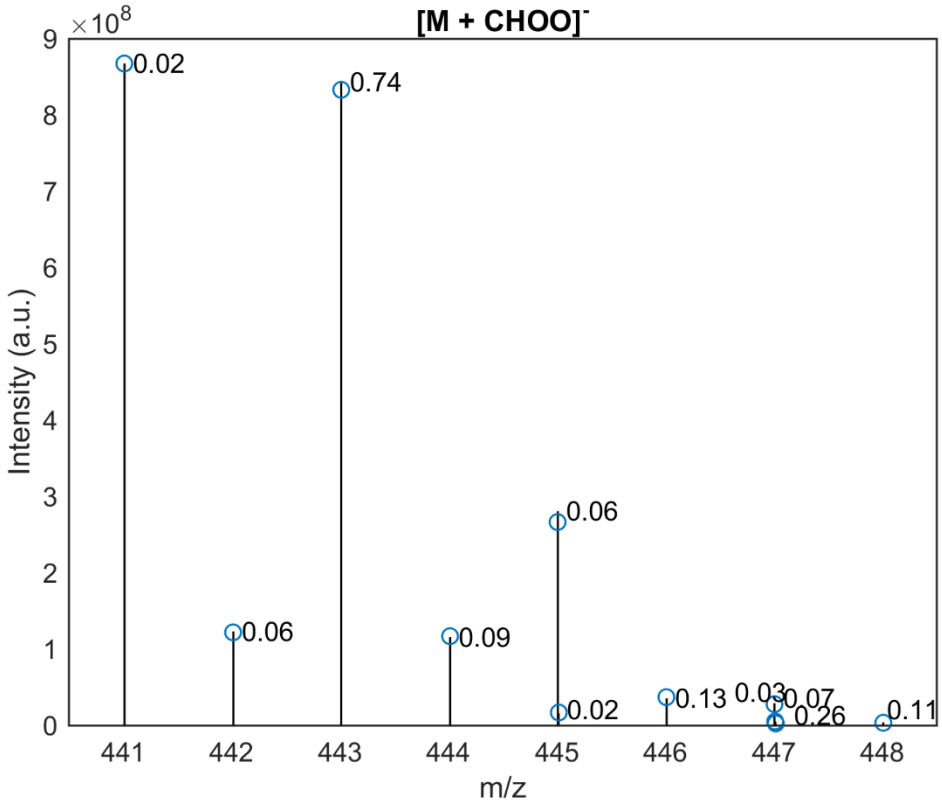

Figure A1.4 SCL formate adduct, $[M + CHOO]^-$, *m/z* ions (black bars), as observed in the Influent-B2 SPE by FTICR MS, compared to scaled corresponding theoretical isotopic patterns (blue circles) at 650,000 resolution at 400 *m/z*. Labels on experimental data are mass accuracy (ppm). Note, background ions are not shown for optimized visualization.

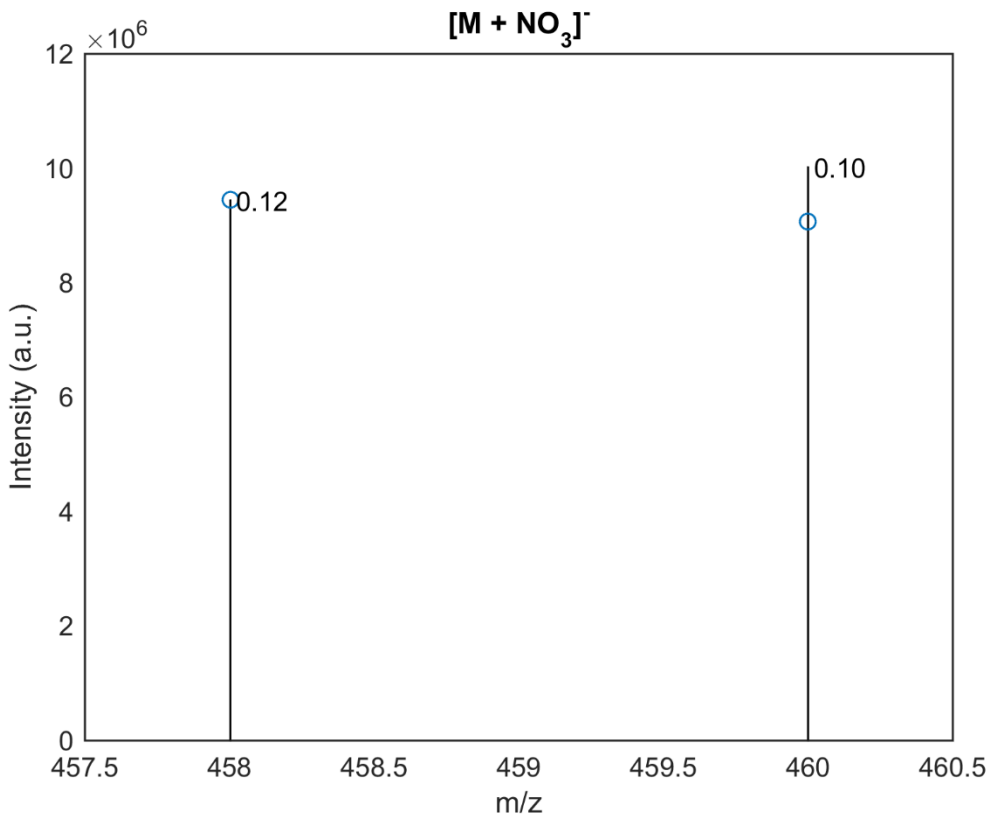

Figure A1.5 SCL nitrate adduct, $[M + NO_3]^-$, *m/z* ions (black bars), as observed in the Influent-B2 SPE by FTICR MS, compared to scaled corresponding theoretical isotopic patterns (blue circles) at 650,000 resolution at 400 *m/z*. Labels on experimental data are mass accuracy (ppm). Note, background ions are not shown for optimized visualization.

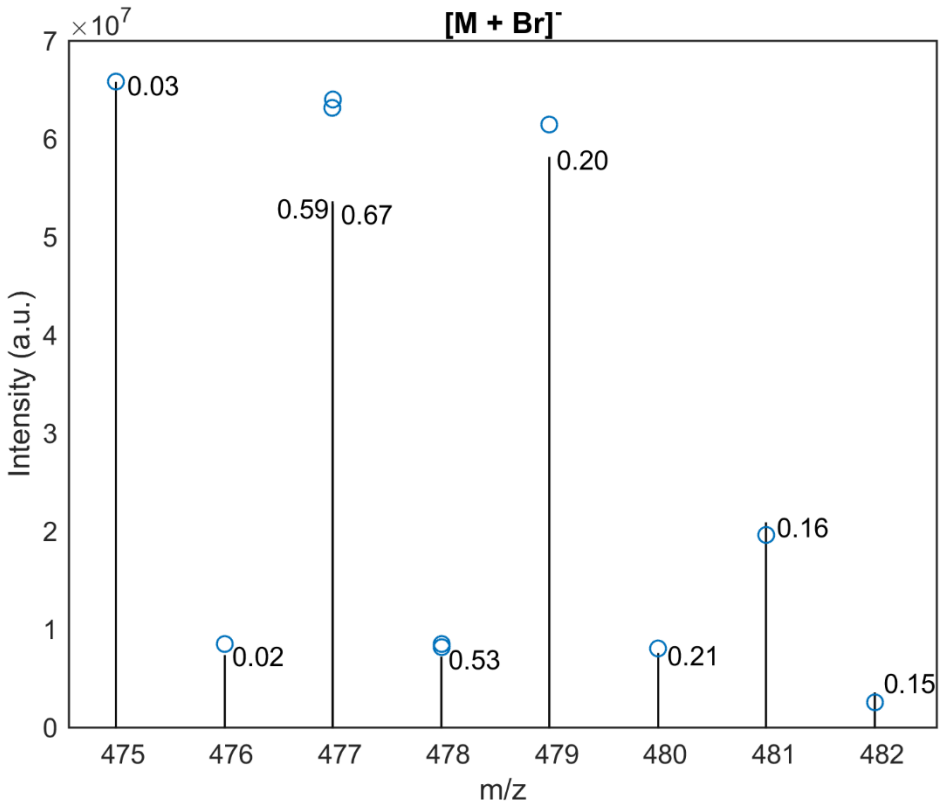

Figure A1.6 SCL bromide adduct, $[M + Br]^-$, *m/z* ions (black bars), as observed in the Influent-B2 SPE by FTICR MS, compared to scaled corresponding theoretical isotopic patterns (blue circles) at 650,000 resolution at 400 *m/z*. Labels on experimental data are mass accuracy (ppm). Note, background ions are not shown for optimized visualization.

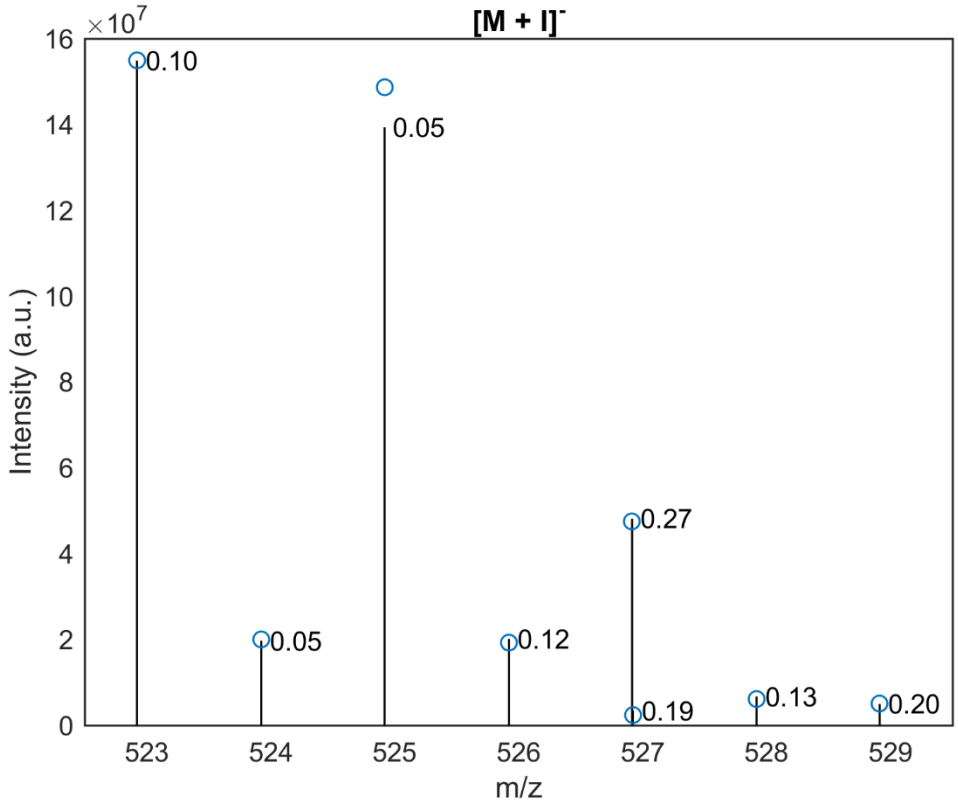

Figure A1.7 SCL iodide adduct, $[M + I]^-$, *m/z* ions (black bars), as observed in the Influent-B2 SPE by FTICR MS, compared to scaled corresponding theoretical isotopic patterns (blue circles) at 650,000 resolution at 400 *m/z*. Labels on experimental data are mass accuracy (ppm). Note, background ions are not shown for optimized visualization.

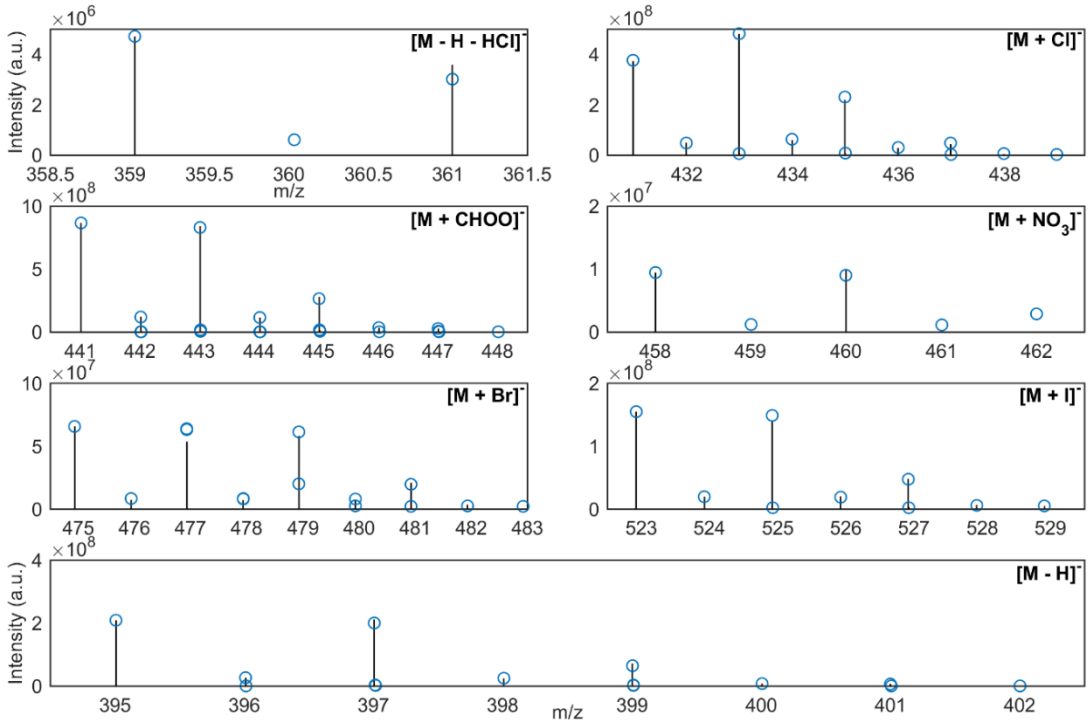

Figure A1.8 SCL related *m/z* ions (black bars), as observed in the Influent-B2 SPE by FTICR MS, compared to scaled theoretical isotopic patterns (blue circles) at 650,000 resolution at 400 *m/z* with isotopic pattern abundance thresholds selected from results of all collected data. Note, background ions are not shown for optimized visualization.

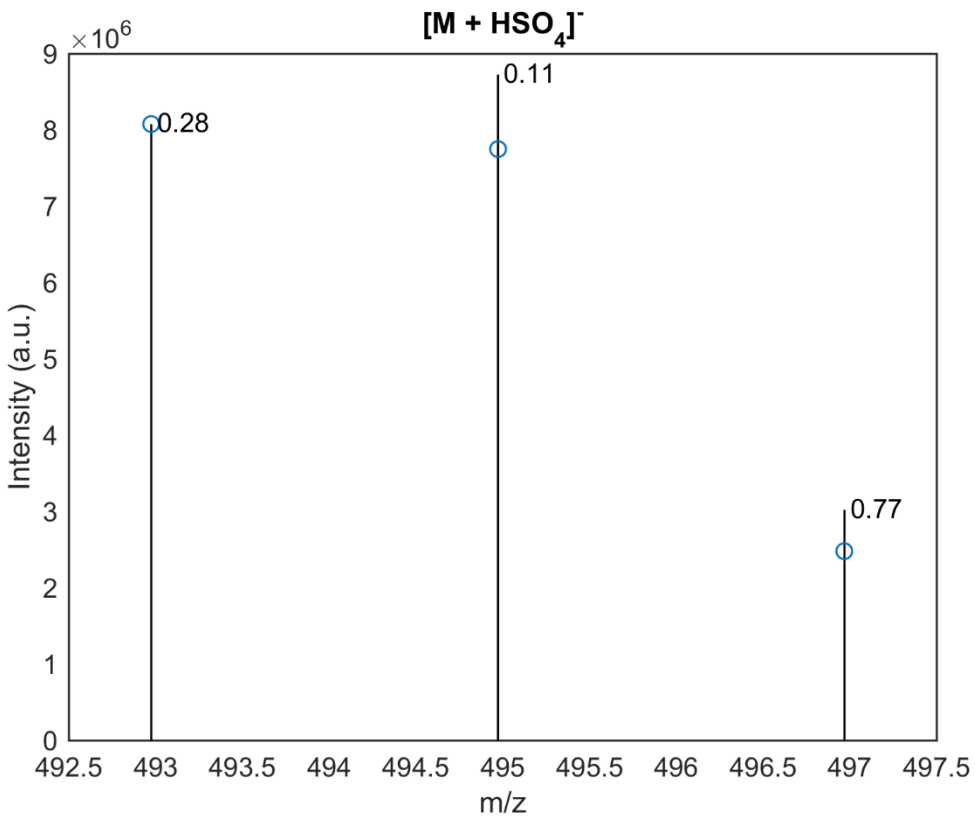

Figure A1.9 Potential bisulfate adduct, $[M + HSO_4]^-$, *m/z* ions (black bars), as observed in a lake sample SPE by FTICR MS, compared to scaled corresponding theoretical isotopic patterns (blue circles) at 650,000 resolution at 400 *m/z*. Labels on experimental data are mass accuracy (ppm). Note, background ions are not shown for optimized visualization.

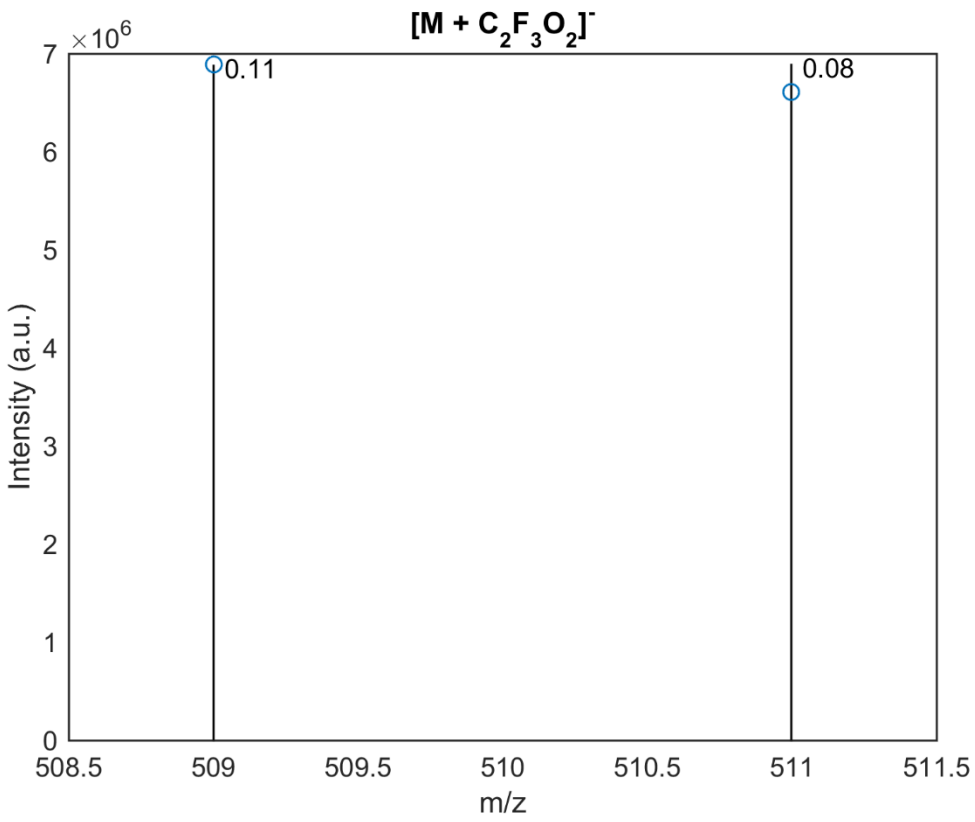

Figure A1.10 Potential trifluoroacetate adduct, $[M + C_2F_3O_2]^-$, *m/z* ions (black bars), as observed in the Effluent-B SPE by FTICR MS, compared to scaled corresponding theoretical isotopic patterns (blue circles) at 650,000 resolution at 400 *m/z*. Labels on experimental data are mass accuracy (ppm). Note, background ions are not shown for optimized visualization.

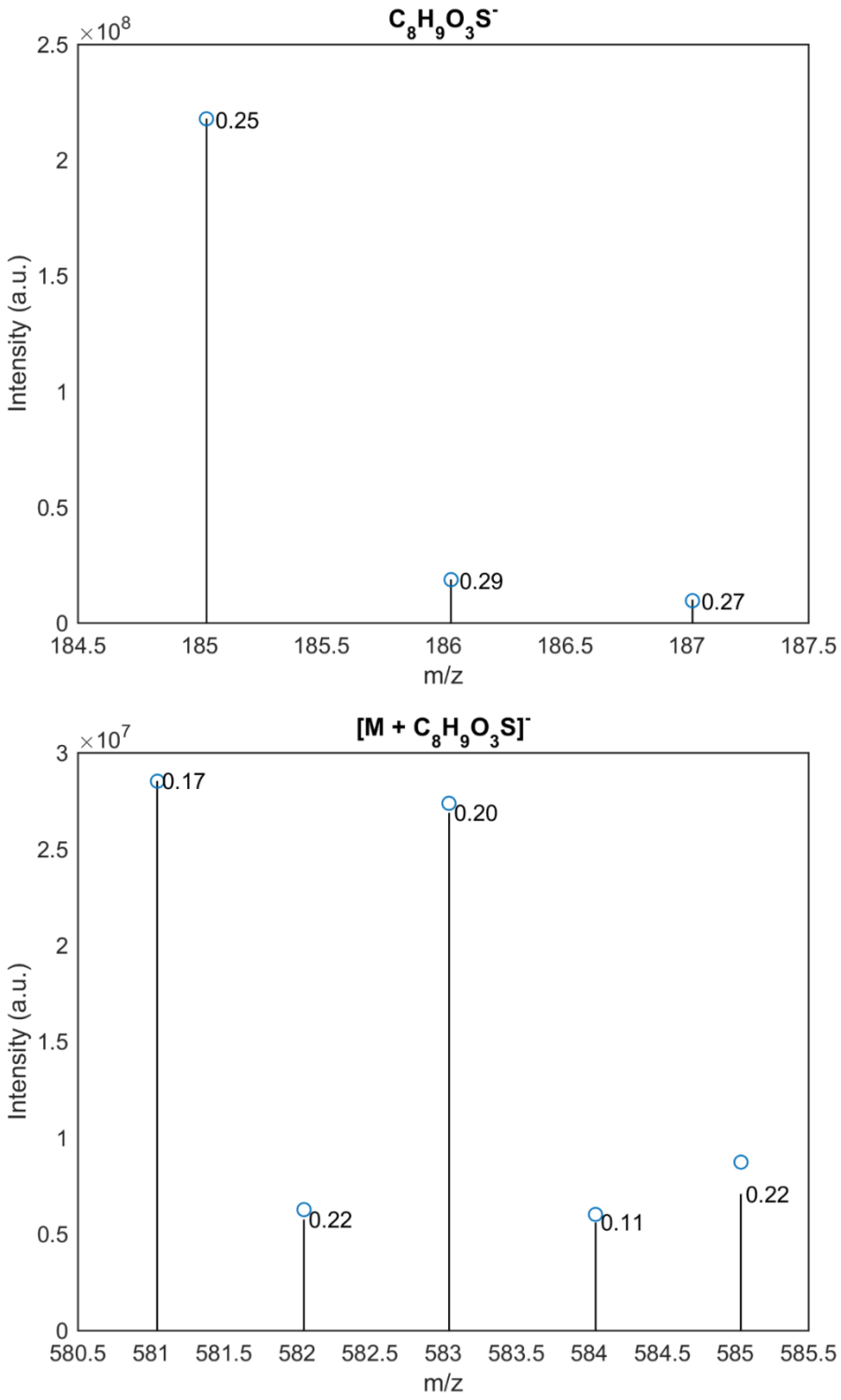

Figure A1.11 $C_8H_9O_3S^-$ (top) and potential $[M + C_8H_9O_3S]^-$ adduct (bottom) *m/z* ions (black bars), as observed in the Influent-B1 SPE by FTICR MS, compared to scaled corresponding theoretical isotopic patterns (blue circles) at 650,000 resolution at 400 *m/z*. Labels on experimental data are mass accuracy (ppm). Note, background ions are not shown for optimized visualization.

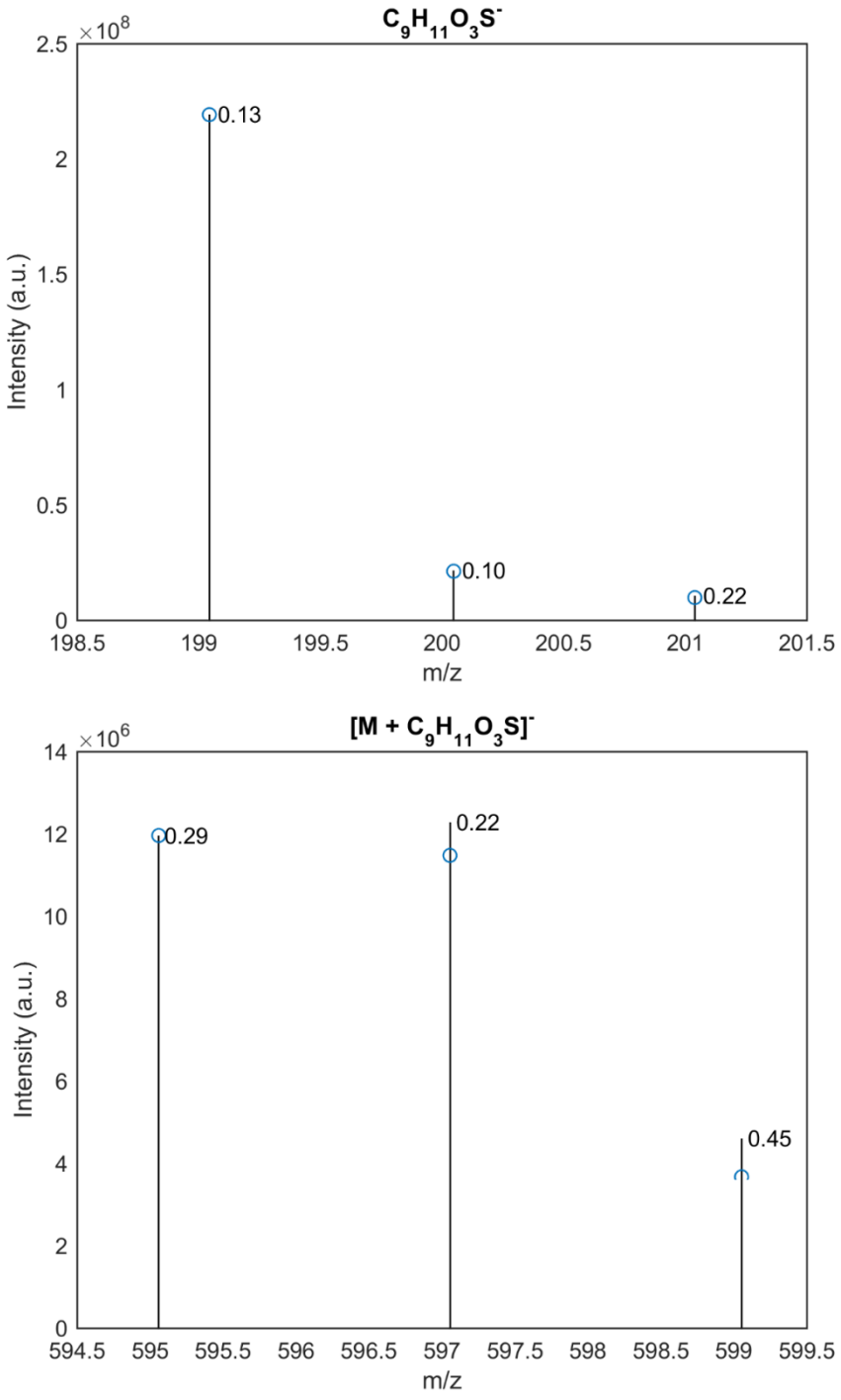

Figure A1.12 $C_9H_{11}O_3S^-$ (top) and potential $[M + C_9H_{11}O_3S]^-$ adduct (bottom) *m/z* ions (black bars), as observed in the Influent-B1 SPE by FTICR MS, compared to scaled corresponding theoretical isotopic patterns (blue circles) at 650,000 resolution at 400 *m/z*. Labels on experimental data are mass accuracy (ppm). Note, background ions are not shown for optimized visualization.

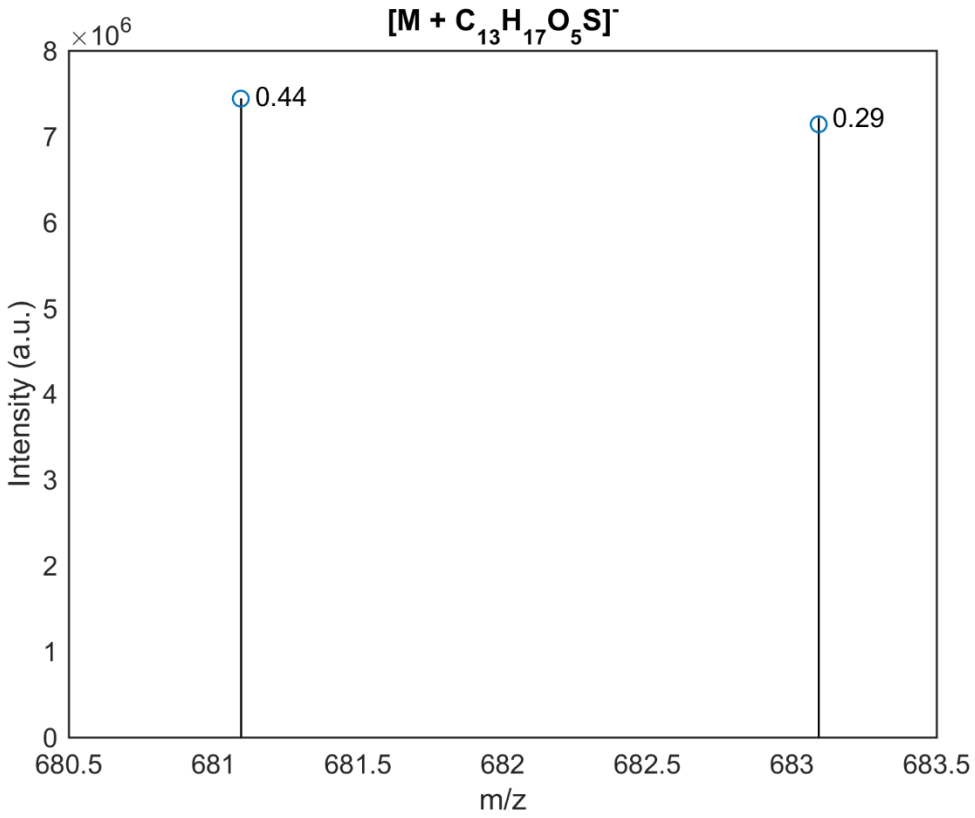

Figure A1.13. $C_{13}H_{17}O_5S^-$ (top) and potential $[M + C_{13}H_{17}O_5S]^-$ adduct (bottom) *m/z* ions (black bars), as observed in the Influent-B2 SPE by FTICR MS, compared to scaled corresponding theoretical isotopic patterns (blue circles) at 650,000 resolution at 400 *m/z*. Labels on experimental data are mass accuracy (ppm). Note, background ions are not shown for optimized visualization.

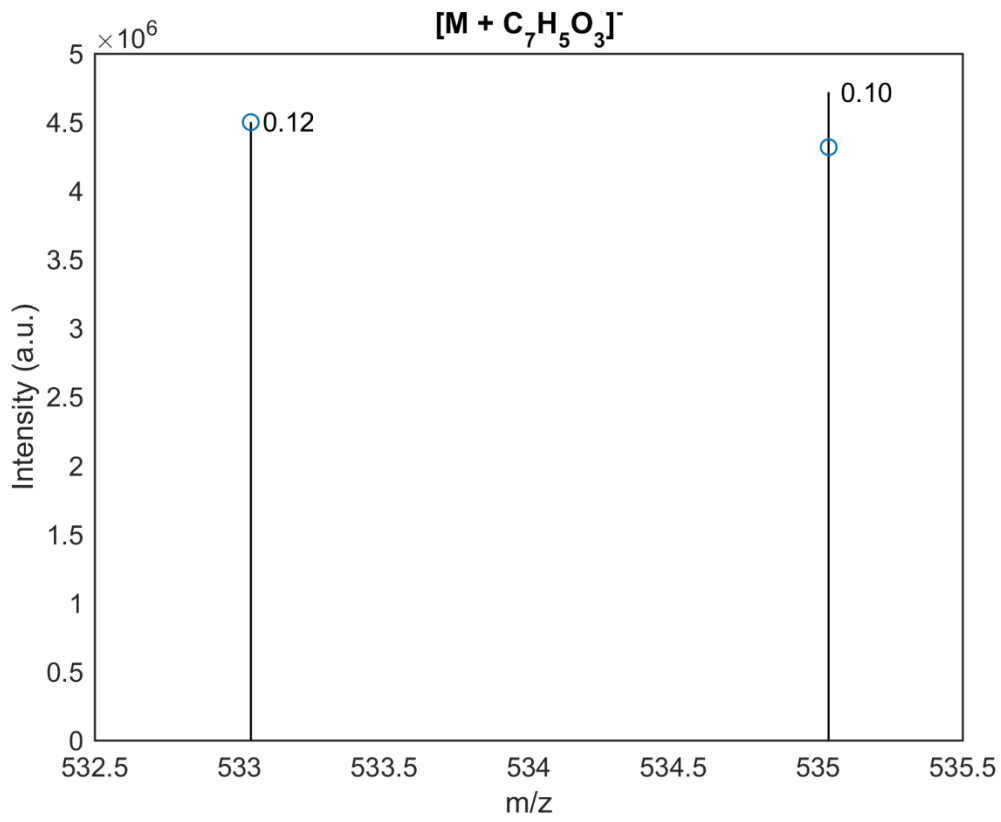

Figure A1.14. Potential $[M + C_7H_5O_3]^-$ *m/z* ions (black bars), as observed in the Influent-B1 SPE by FTICR MS, compared to scaled corresponding theoretical isotopic patterns (blue circles) at 650,000 resolution at 400 *m/z*. Labels on experimental data are mass accuracy (ppm). Note, background ions are not shown for optimized visualization.

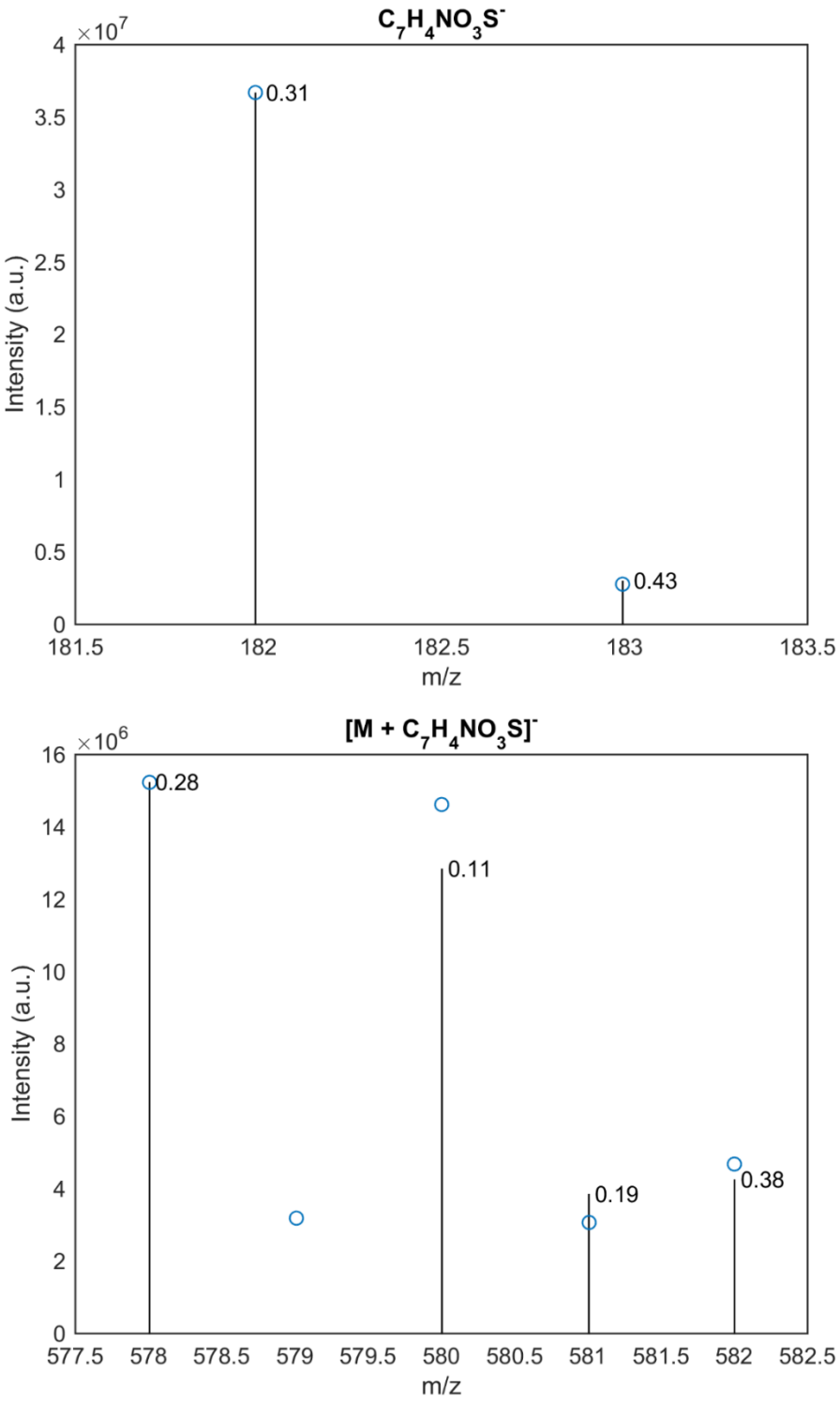

Figure A1.15 $C_7H_4NO_3S^-$ (top) and potential $[M + C_7H_4NO_3S]^-$ adduct (bottom) *m/z* ions (black bars), as observed in the Influent-B2 SPE by FTICR MS, compared to scaled corresponding theoretical isotopic patterns (blue circles) at 650,000 resolution at 400 *m/z*. Labels on experimental data are mass accuracy (ppm). Note, background ions are not shown for optimized visualization.

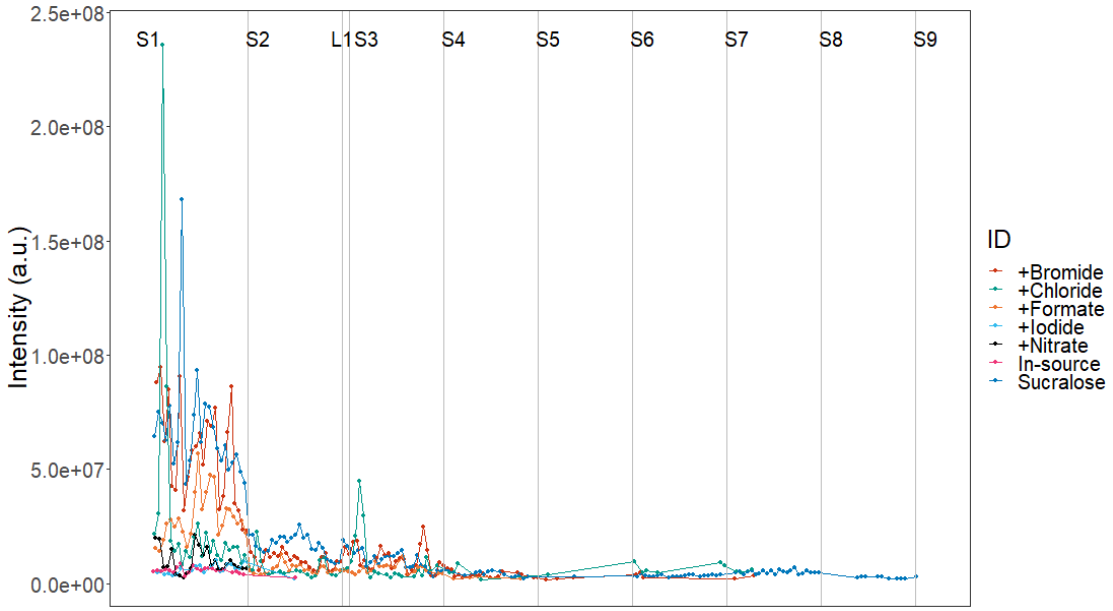

Figure A1.16 SCL related ion signal intensities from freshwater FTICR MS data by site in order of decreasing average SCL concentration. S1-9 refer to the nine stream sites and L1 is the one sampled lake. Within sites, data are in order of sampling throughout the year-long survey and all duplicate SPEs are represented as individual points.

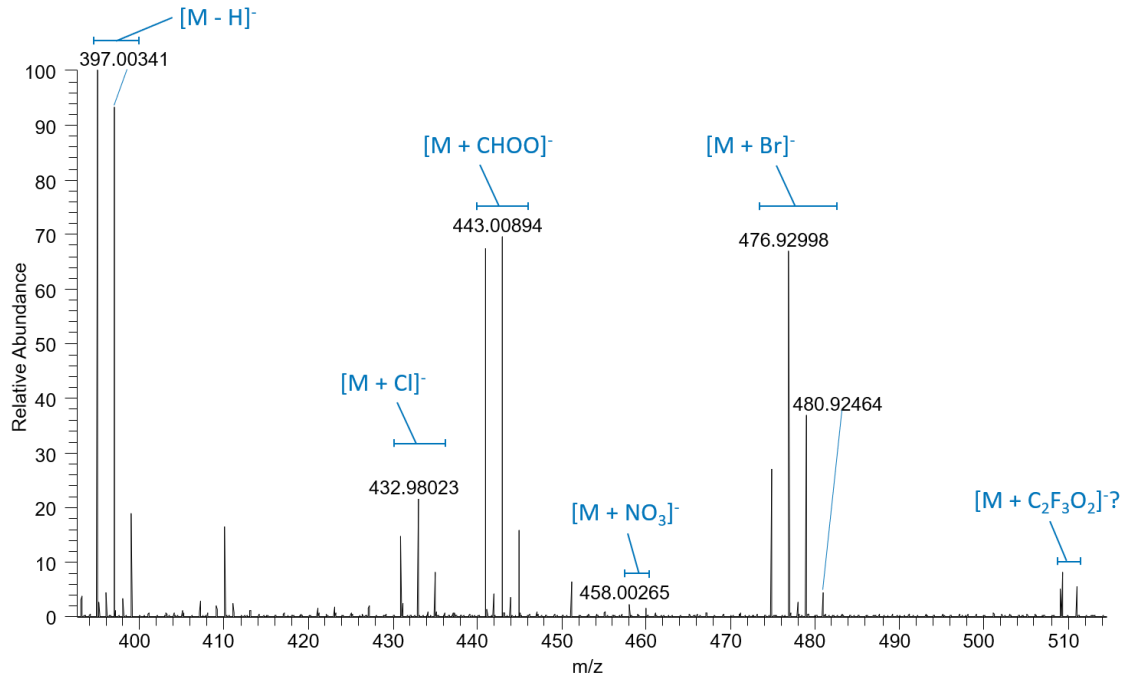

Figure A1.17 Magnification of the mass spectrum of the Effluent-B wastewater SPE by Orbitrap MS (full scan, 80-700 *m/z*) showing SCL molecular ions and chloride, formate, nitrate, bromide, and, tentatively, trifluoroacetate SCL adduct ions.

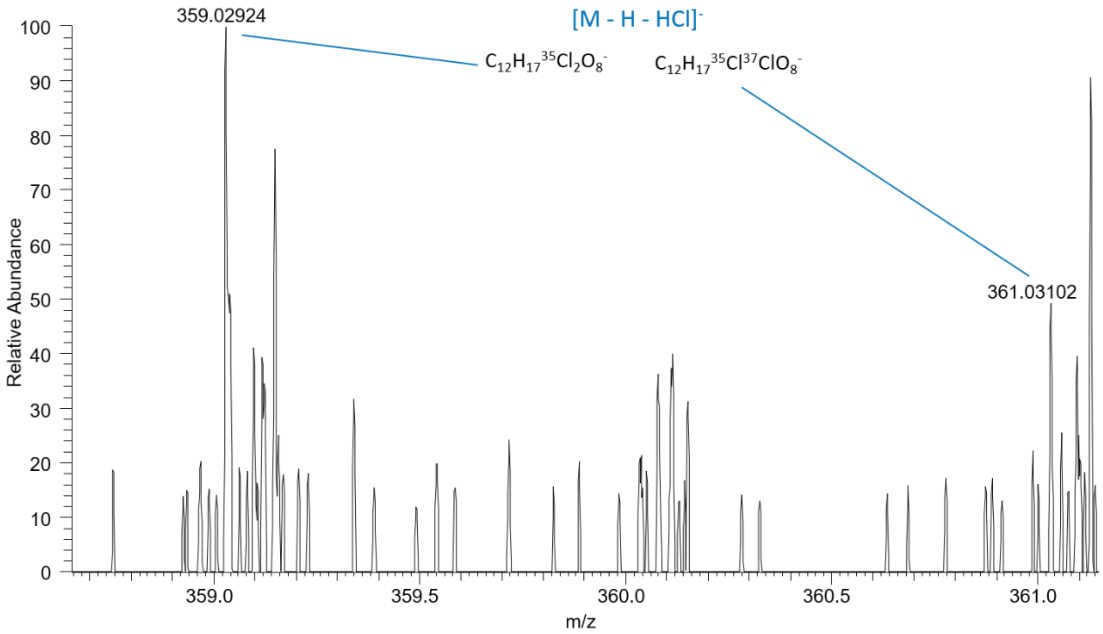

Figure A1.18 Magnification of the mass spectrum of the Effluent-B wastewater SPE by Orbitrap MS (full scan, 80-700 *m/z*) showing SCL in-source fragmentation product ions.

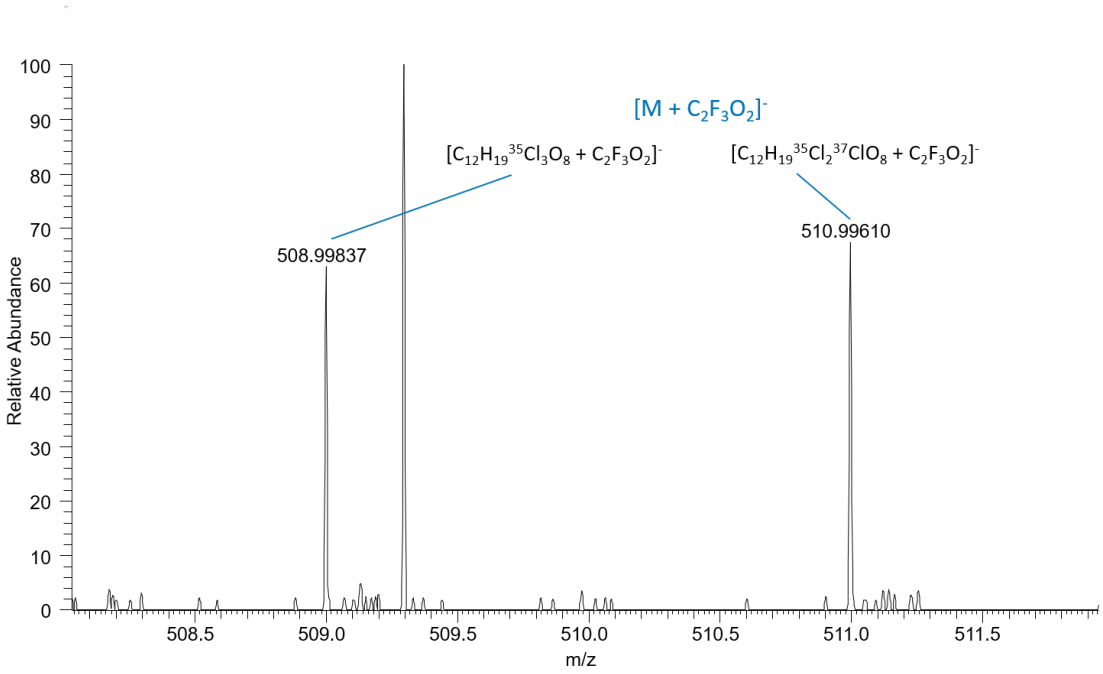

Figure A1.19 Magnification of the mass spectrum of the Effluent-B wastewater SPE by Orbitrap MS (full scan, 80-700 *m/z*) showing potential trifluoroacetate SCL adduct ions.

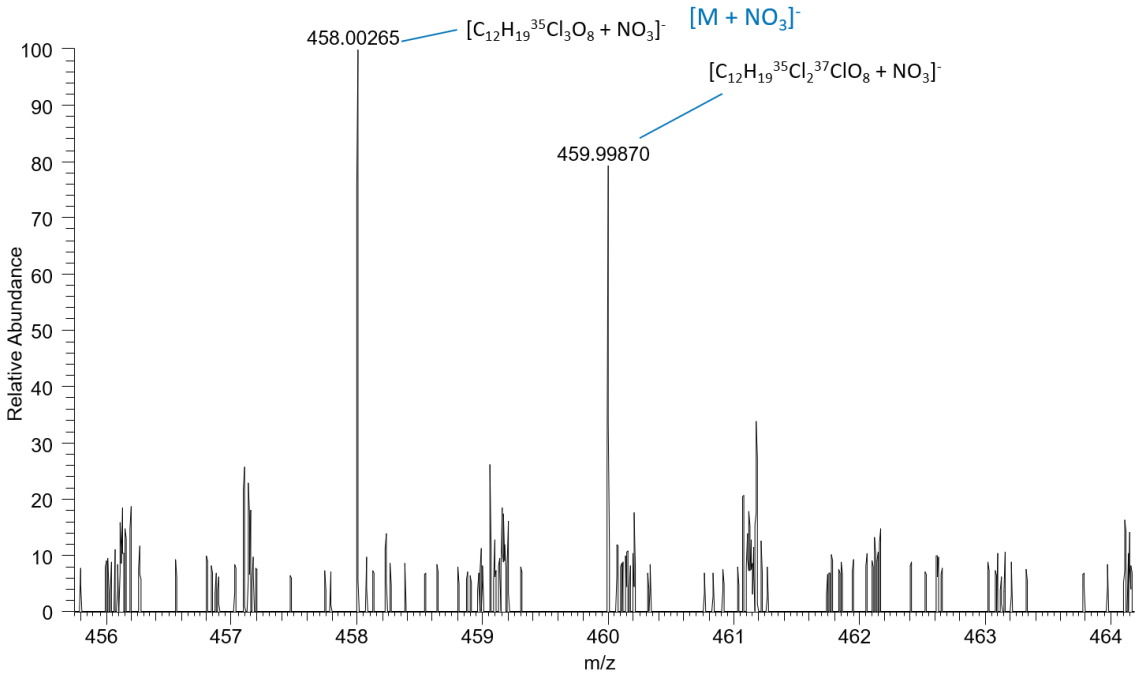

Figure A1.20 Magnification of the mass spectrum of the Effluent-B wastewater SPE by Orbitrap MS (full scan, 80-700 *m/z*) showing nitrate SCL adduct ions.

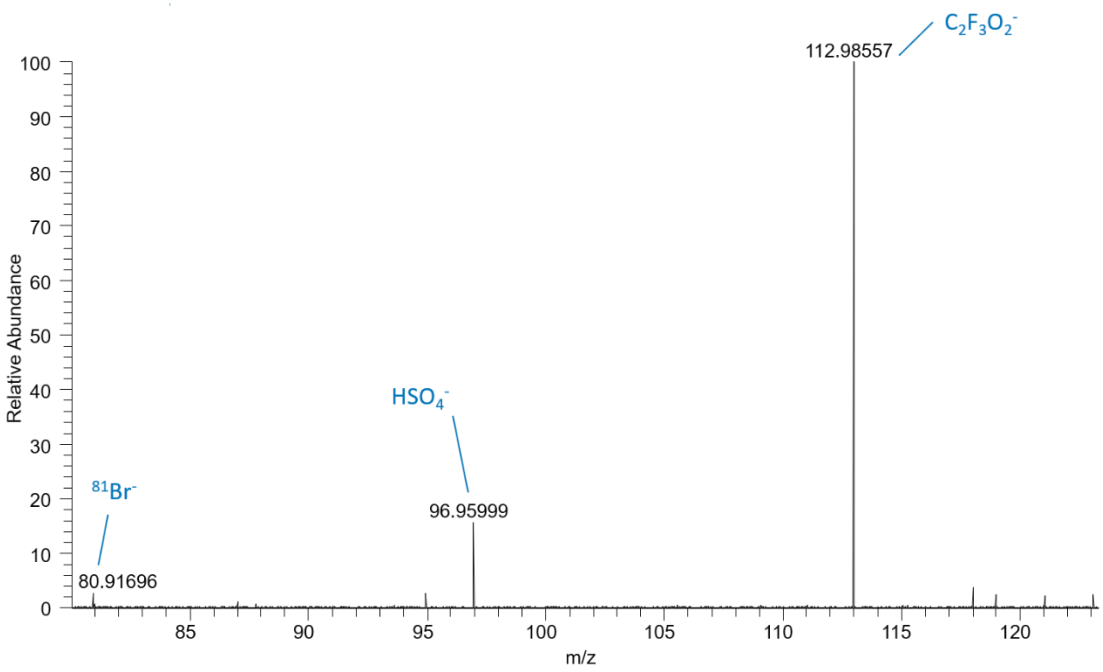

Figure A1.21 Magnification of the mass spectrum of the Effluent-B wastewater SPE by Orbitrap MS (full scan, 80-700 *m/z*) showing *m/z* ions identified as bromide-81, bisulfate, and trifluoroacetate.

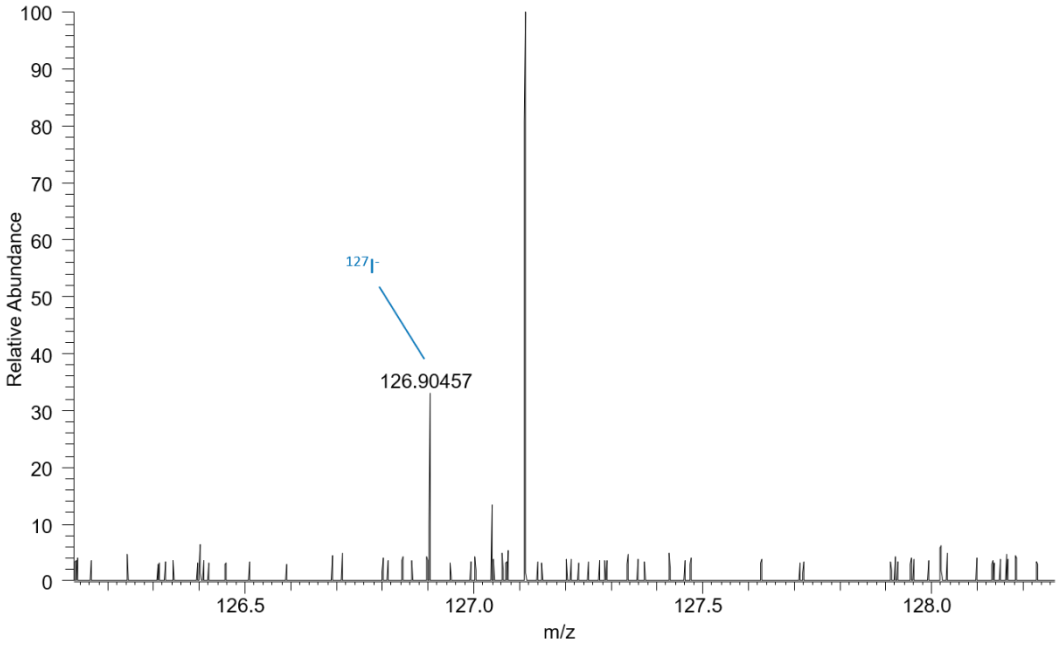

Figure A1.22 Magnification of the mass spectrum of the Effluent-B wastewater SPE by Orbitrap MS (full scan, 80-700 *m/z*) showing an *m/z* ion identified as iodine-127.

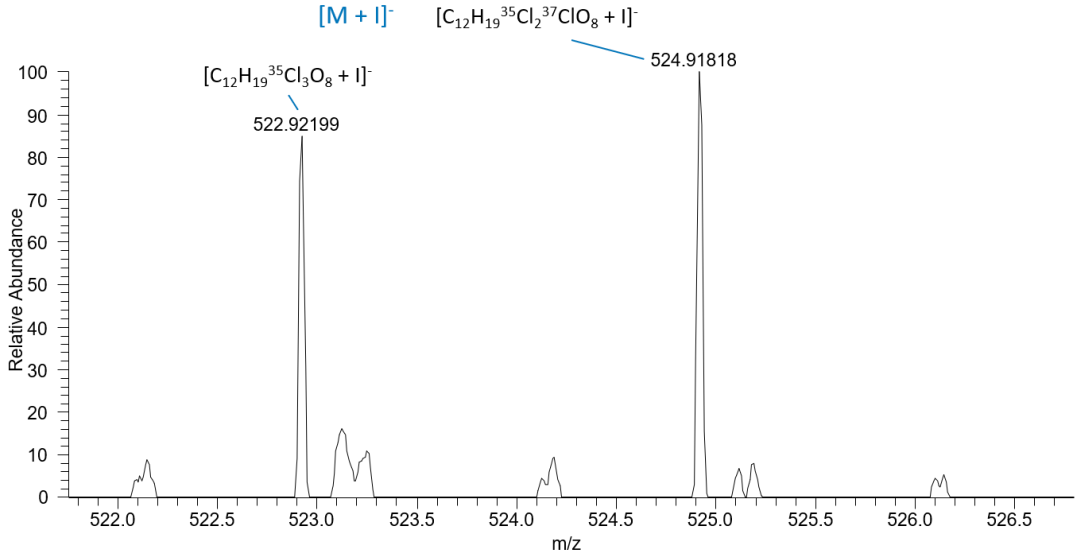

Figure A1.23 Magnification of the mass spectrum of the Effluent-B wastewater SPE by Orbitrap MS (full scan, 500-600 *m/z*) showing iodide SCL adduct ions.

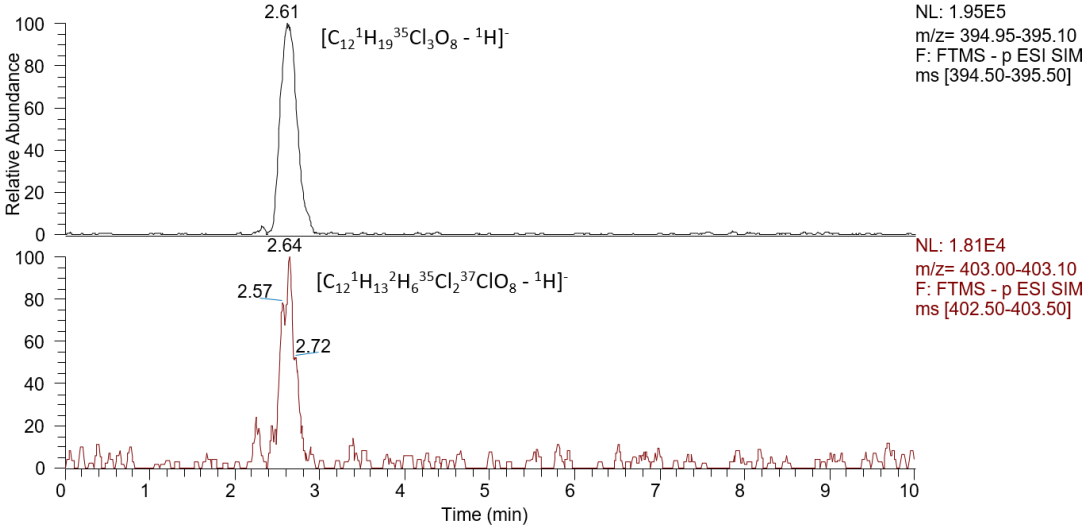

Figure A1.24 HPLC/Orbitrap MS chromatograms of molecular SCL (top) and SIL-ISTD SCL-d6 (bottom). Chromatograms have been smoothed and post-acquisition mass-filtered to 0.15 and 0.10 *m/z* windows around exact masses 395.007 *m/z* and 403.042 *m/z*, respectively, for SCL and SCL-d6.

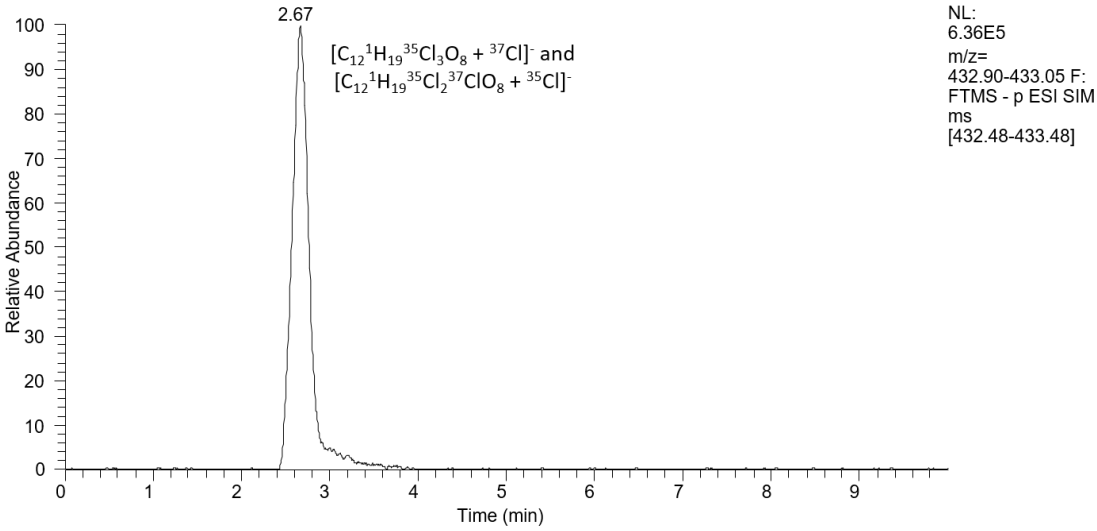

Figure A1.25 HPLC/Orbitrap MS chromatogram of the SCL chloride adduct. Chromatogram has been smoothed and post-acquisition mass-filtered to a 0.15 *m/z* windows around the exact mass 432.981 *m/z*.

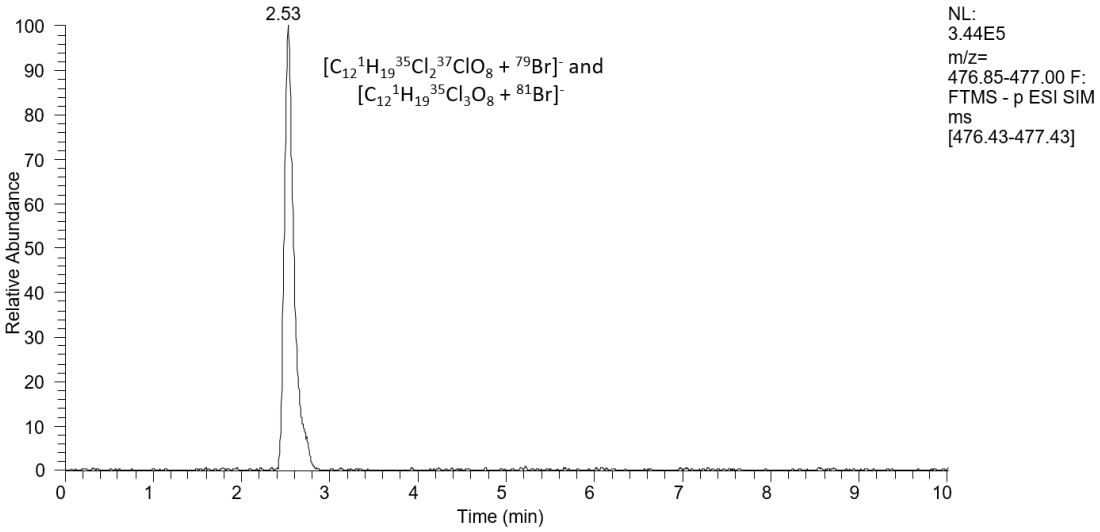

Figure A1.26 HPLC/Orbitrap MS chromatogram of the SCL bromide adduct. Chromatogram has been smoothed and post-acquisition mass-filtered to a 0.15 *m/z* windows around the exact masses 476.930 *m/z* and 476.931 *m/z*.

Appendix 2

Supplemental Materials to Chapter 3

Table A2.1 Neutral CHOBr formulas assigned in stream DOM.

$C_{15}H_{21}BrO_7$	$C_{17}H_{21}BrO_7$	$C_{16}H_{19}BrO_8$	$C_{16}H_{21}BrO_8$	$C_{17}H_{17}BrO_8$	$C_{17}H_{19}BrO_8$
$C_{17}H_{21}BrO_8$	$C_{17}H_{23}BrO_8$	$C_{18}H_{21}BrO_8$	$C_{18}H_{23}BrO_8$	$C_{17}H_{21}BrO_9$	$C_{19}H_{23}BrO_8$
$C_{18}H_{21}BrO_9$	$C_{19}H_{25}BrO_8$	$C_{18}H_{23}BrO_9$	$C_{19}H_{21}BrO_9$	$C_{19}H_{23}BrO_9$	

Table A2.2 Neutral CHOSCl formulas assigned in stream DOM.

$C_{16}H_9ClO_6S$	$C_{17}H_9ClO_8S$	$C_{18}H_9ClO_8S$

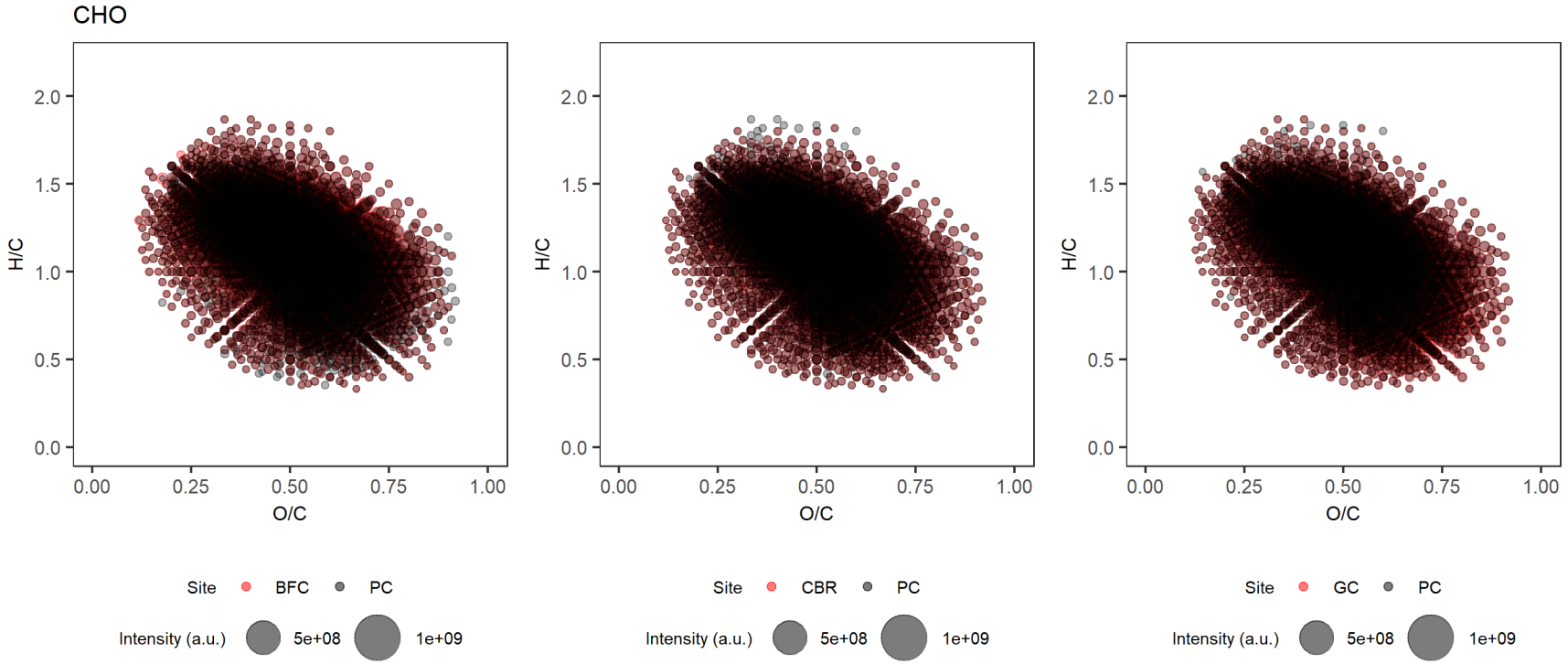

Figure A2.1 Van Krevelen diagrams showing intensity averaged CHO formula assignments for sites BFC (2134 septic systems/sq mi) (left), CBR (864 septic systems/sq mi) (middle), and GC (14 septic systems/sq mi) (right) versus PC (55 septic systems/sq mi).

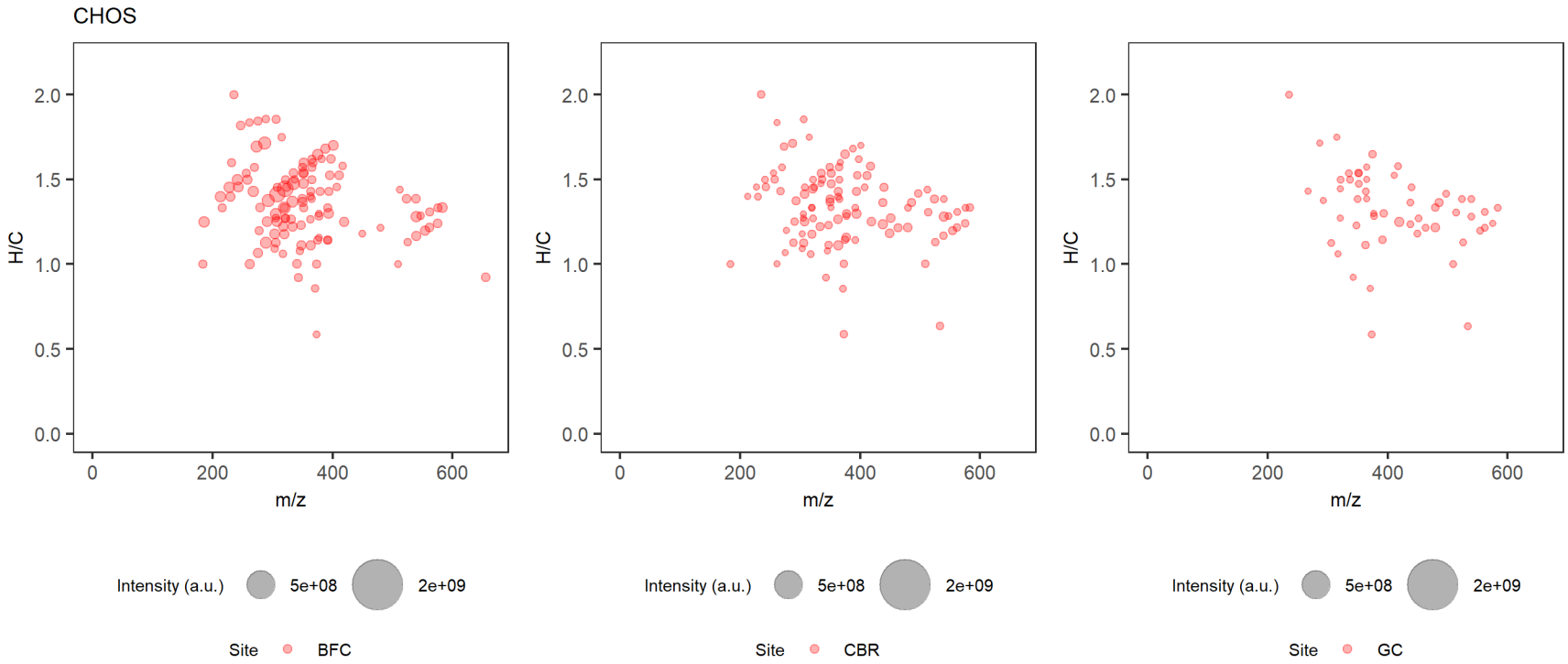

Figure A2.2 H/C vs *m/z* plots showing intensity averaged unique CHOS formula assignments versus PC for sites BFC (left), CBR (middle), and GC (right).

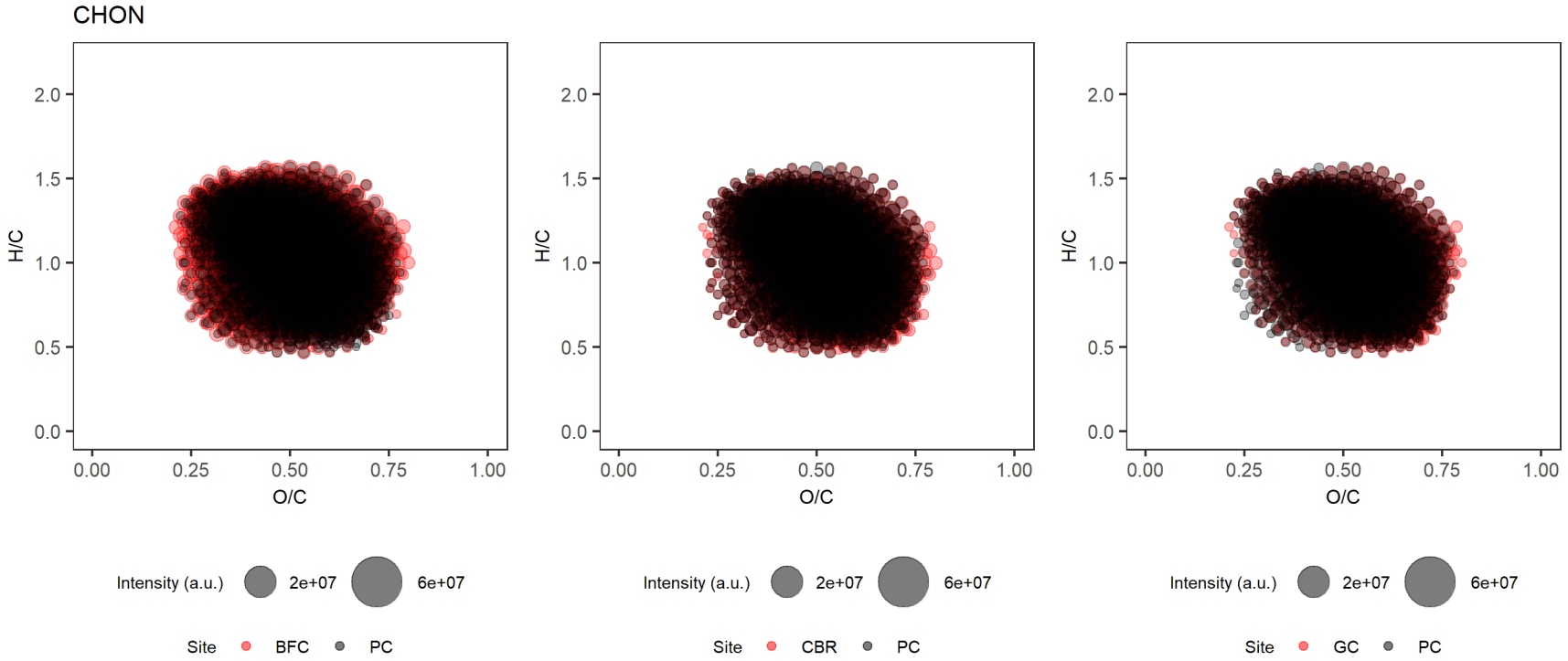

Figure A2.3 Van Krevelen diagrams showing intensity averaged CHON formula assignments for sites BFC (left), CBR (middle), and GC (right) versus PC.

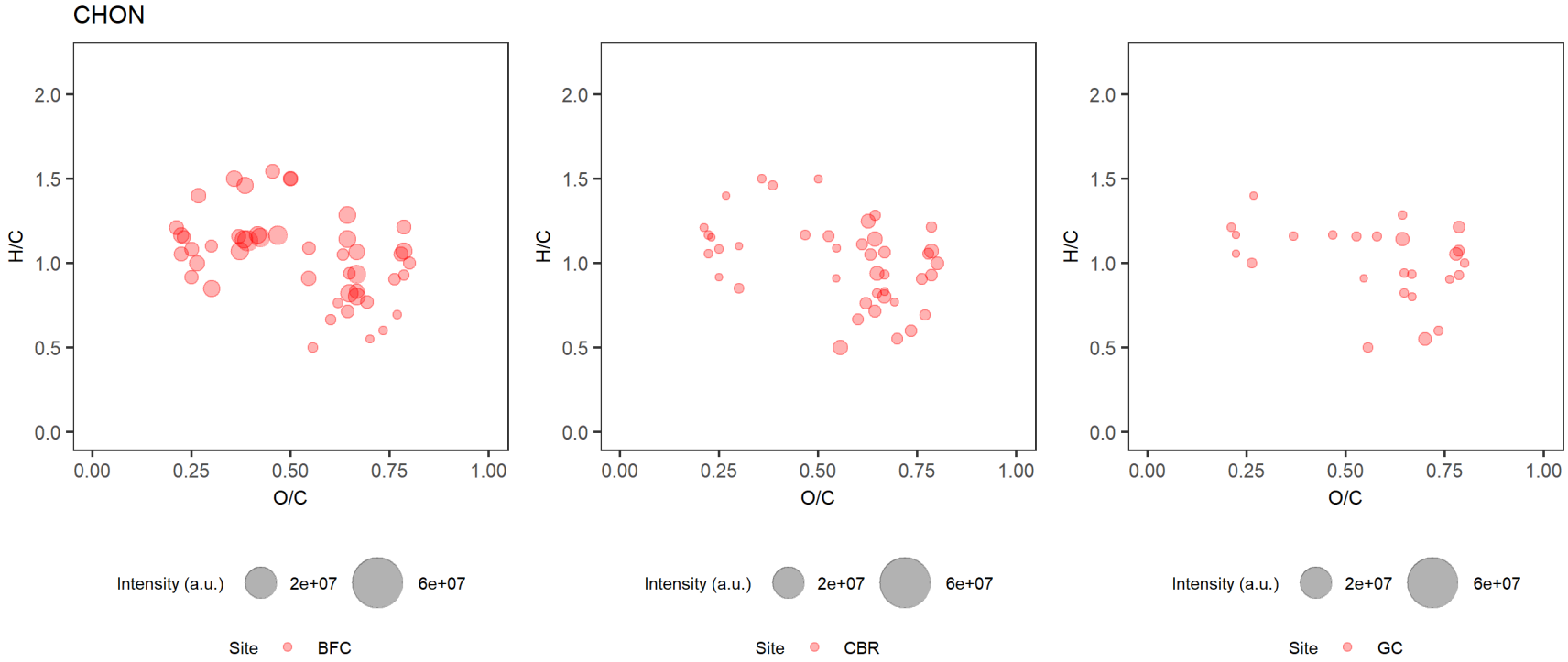

Figure A2.4 Van Krevelen diagrams showing intensity averaged unique CHON formula assignments versus PC for sites BFC (left), CBR (middle), and GC (right).

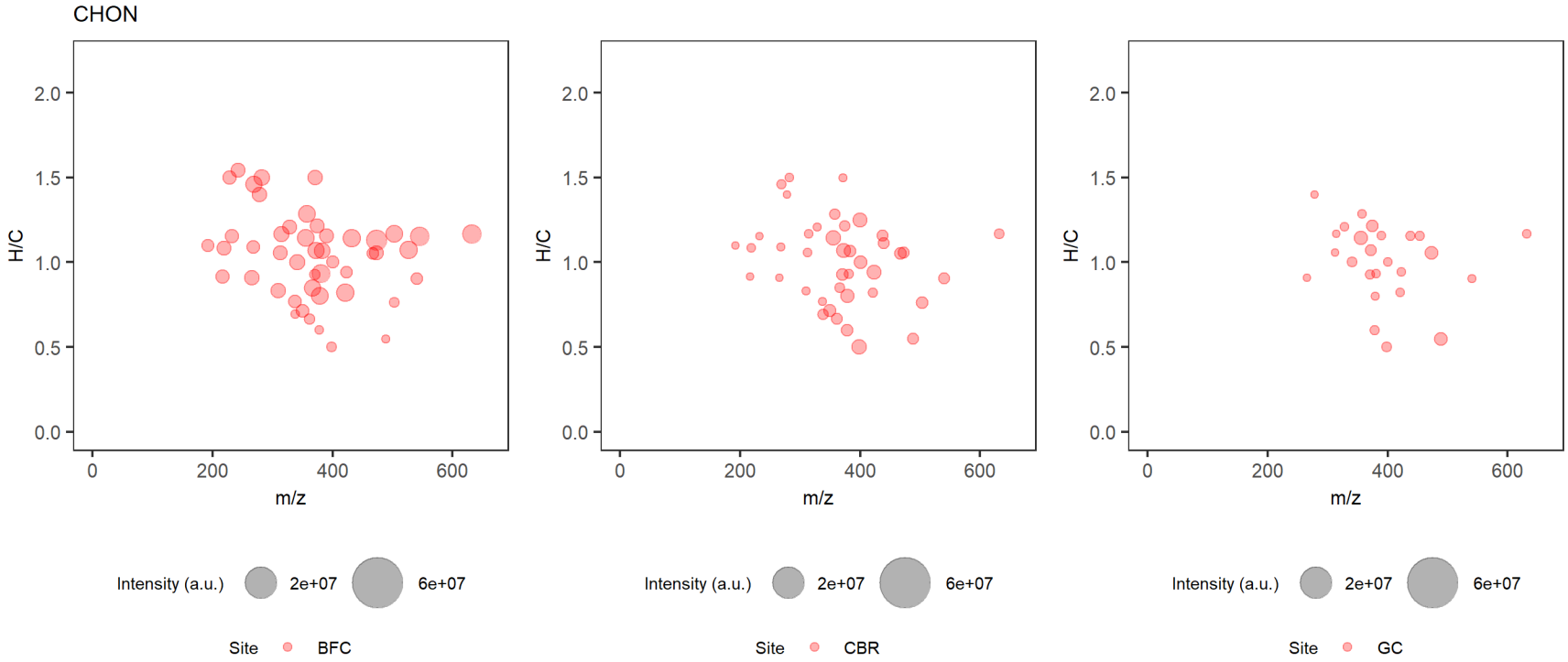

Figure A2.5 H/C vs *m/z* plots showing intensity averaged unique CHON formula assignments versus PC for sites BFC (left), CBR (middle), and GC (right).

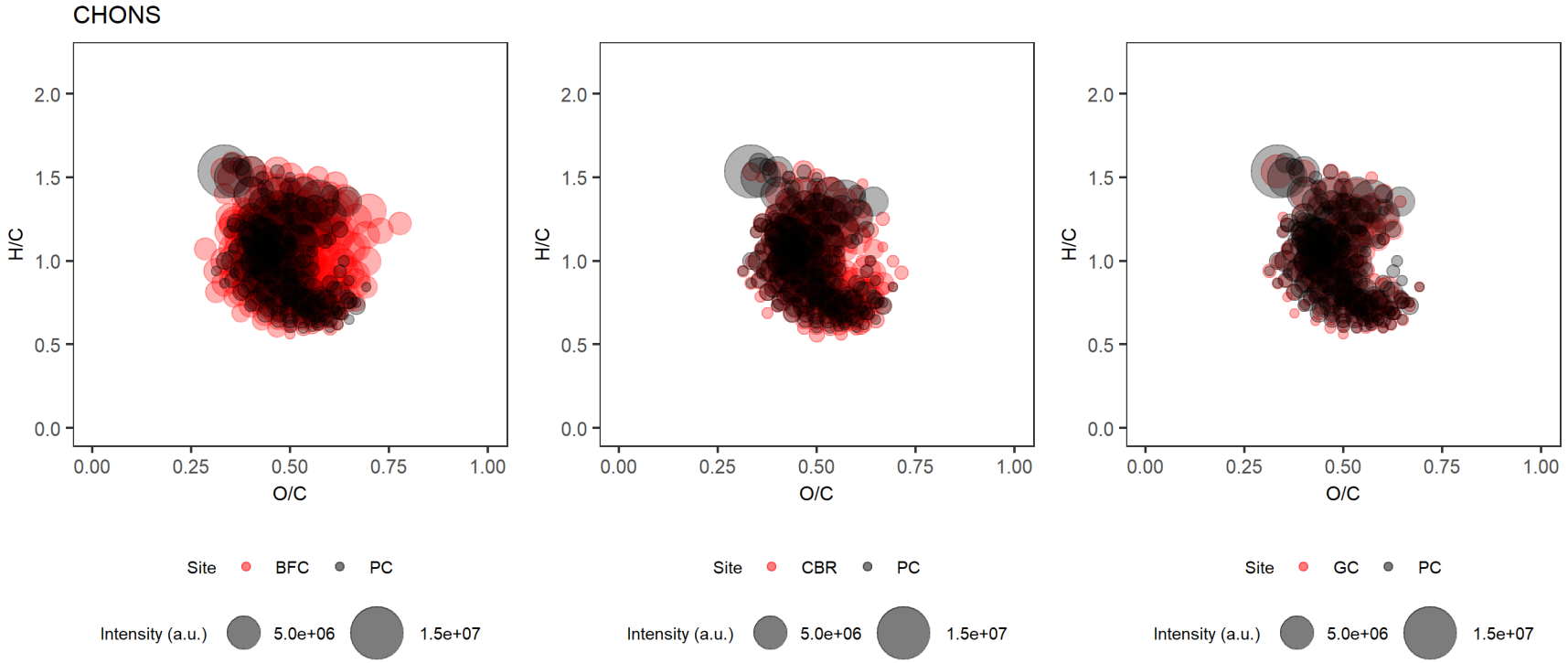

Figure A2.6 Van Krevelen diagrams showing intensity averaged CHONS formula assignments for sites BFC (left), CBR (middle), and GC (right) versus PC.

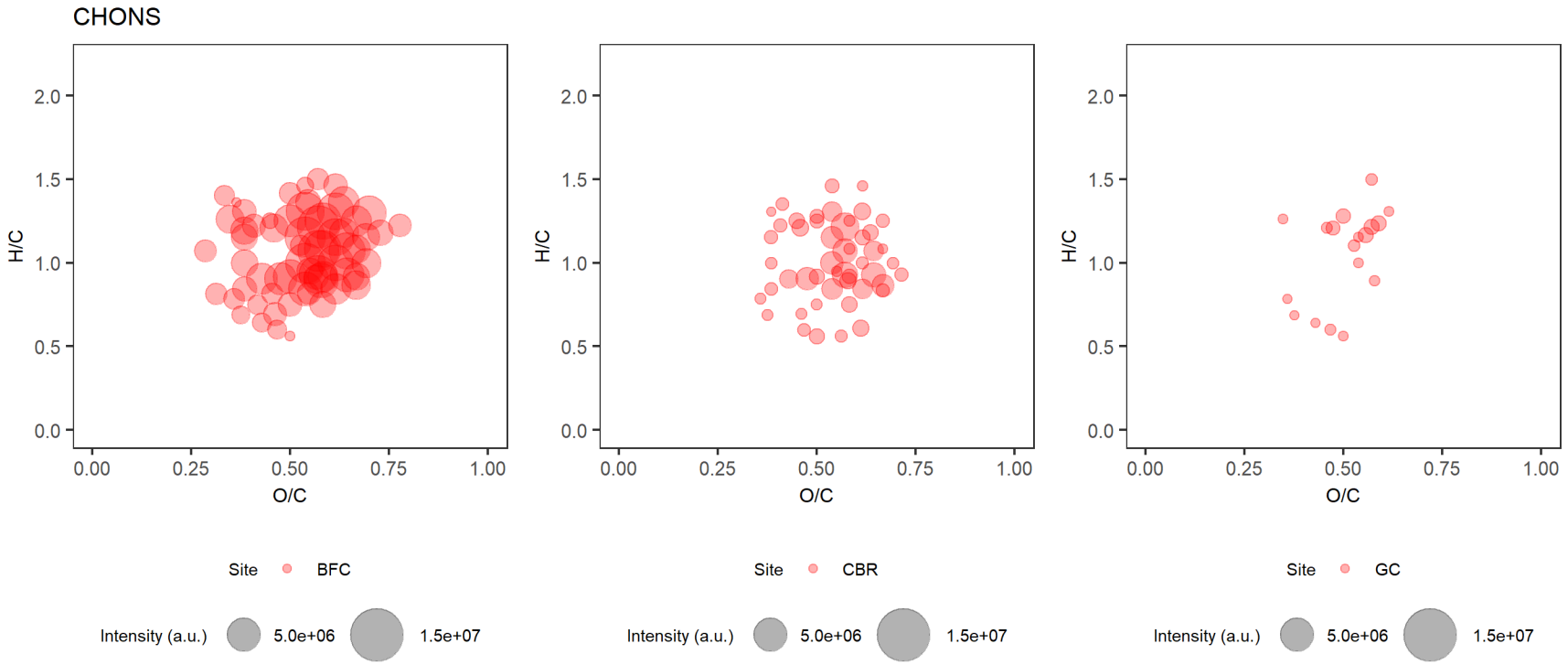

Figure A2.7 Van Krevelen diagrams showing intensity averaged unique CHONS formula assignments versus PC for sites BFC (left), CBR (middle), and GC (right).

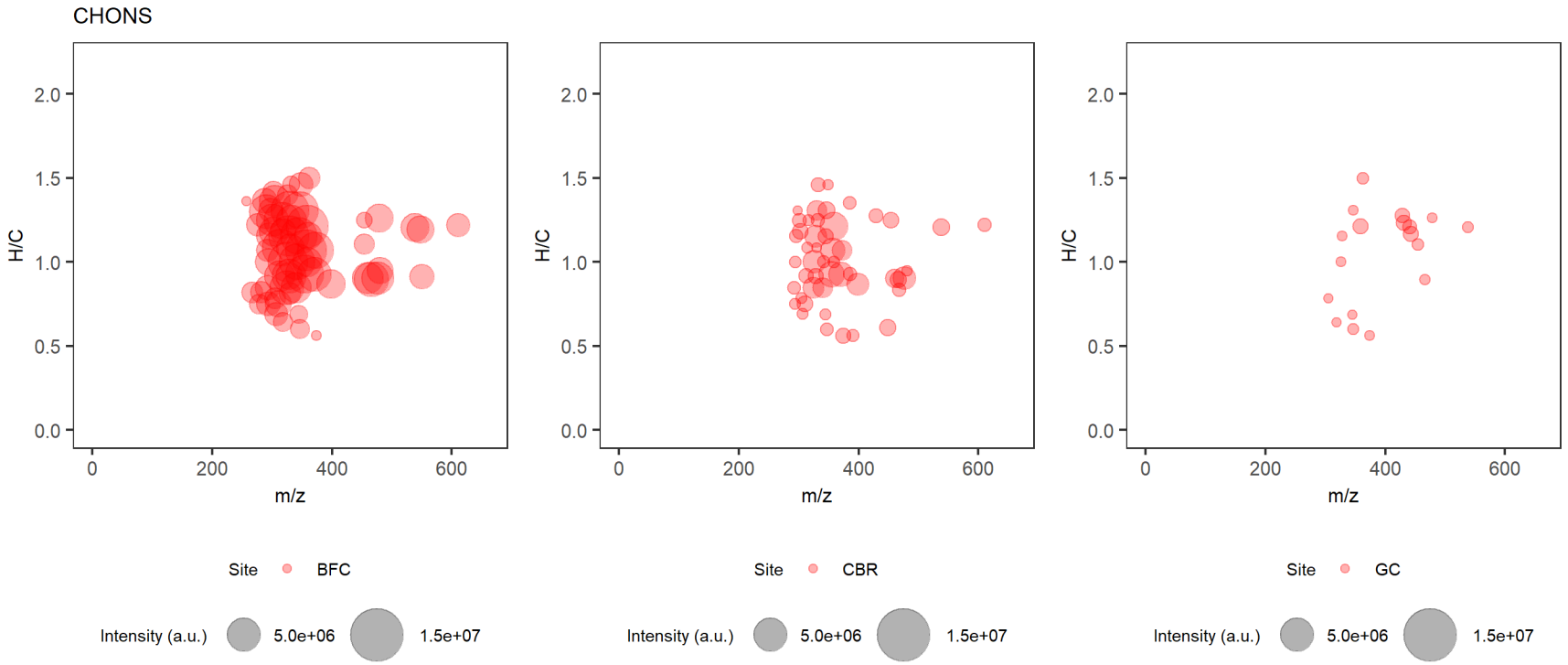

Figure A2.8 H/C vs *m/z* plots showing intensity averaged unique CHONS formula assignments versus PC for sites BFC (left), CBR (middle), and GC (right).

Table A2.3 List of 137 potential tracers that were unique to higher septic tank effluent (STE) impact sites (n=120), in order of *m/z*. Average signal intensity is averaged across all higher impact samples, including 0 values for nondetects. Potential tracers not also detected in septic tank dissolved organic matter (STDOM) have been marked with the * symbol.

Theoretical Exact *m/z*	Error of Assignment (ppm)	Neutral Formula	DBE	H/C	O/C	Number of Detections	Avg. Signal Intensity (a.u.)	ND in STDOM
183.01214	0.60	C8H8O3S	5	1.00	0.38	32	758454	
185.02779	0.49	C8H10O3S	4	1.25	0.38	23	3909199	
192.06662	0.50	C10H11NO3	6	1.10	0.30	26	394920	
213.05909	0.15	C10H14O3S	4	1.40	0.30	25	3493446	
215.03835	0.17	C9H12O4S	4	1.33	0.44	29	901069	
216.06662	0.27	C12H11NO3	8	0.92	0.25	28	446849	
218.08227	0.12	C12H13NO3	7	1.08	0.25	35	554497	
227.07474	0.06	C11H16O3S	4	1.45	0.27	25	3194691	
228.08775	0.11	C10H15NO5	4	1.50	0.50	22	353966	
229.05400	0.21	C10H14O4S	4	1.40	0.40	46	2406707	
231.06965	0.07	C10H16O4S	3	1.60	0.40	31	729920	
232.09792	0.07	C13H15NO3	7	1.15	0.23	24	396728	
241.09039	0.03	C12H18O3S	4	1.50	0.25	32	3693981	
242.10340	0.00	C11H17NO5	4	1.55	0.45	31	503752	
243.06965	0.13	C11H16O4S	4	1.45	0.36	53	3017268	
247.10095	-0.05	C11H20O4S	2	1.82	0.36	25	1535323	
255.10604	-0.01	C13H20O3S	4	1.54	0.23	31	882368	
256.06490	0.07	C11H15NO4S	5	1.36	0.36	25	1922719	
261.05909	0.01	C14H14O3S	8	1.00	0.21	25	1830527	
261.11660	-0.20	C12H22O4S	2	1.83	0.33	20	370012	
266.01287	-0.10	C11H9NO5S	8	0.82	0.45	23	377065	
267.06226	0.01	C11H12N2O6	7	1.09	0.55	22	411201	
268.11905	-0.04	C13H19NO5	5	1.46	0.38	44	934763	
269.12169	-0.14	C14H22O3S	4	1.57	0.21	27	837504	
275.07474	-0.04	C15H16O3S	8	1.07	0.20	25	2024918	
275.13225	-0.14	C13H24O4S	2	1.85	0.31	25	807769	
276.01835	-0.19	C9H11NO7S	5	1.22	0.78	20	366320	
277.09039	0.04	C15H18O3S	7	1.20	0.20	24	783424	*
278.01287	-0.12	C12H9NO5S	9	0.75	0.42	21	341845	
279.10604	-0.01	C15H20O3S	6	1.33	0.20	25	1227624	
282.00778	-0.16	C11H9NO6S	8	0.82	0.55	32	534395	
282.13470	-0.10	C14H21NO5	5	1.50	0.36	38	776278	
288.05473	-0.07	C11H15NO6S	5	1.36	0.55	24	521876	
289.09039	-0.12	C16H18O3S	8	1.13	0.19	38	4884676	
289.14790	-0.03	C14H26O4S	2	1.86	0.29	20	381619	
290.03400	-0.10	C10H13NO7S	5	1.30	0.70	24	1073086	
291.10604	-0.11	C16H20O3S	7	1.25	0.19	37	3407583	
292.02852	-0.10	C13H11NO5S	9	0.85	0.38	36	687178	
292.06490	0.04	C14H15NO4S	8	1.07	0.29	22	404513	
294.00778	-0.07	C12H9NO6S	9	0.75	0.50	41	734685	
294.04417	0.01	C13H13NO5S	8	1.00	0.38	35	745831	
296.05982	0.08	C13H15NO5S	7	1.15	0.38	49	948488	
298.07547	-0.20	C13H17NO5S	6	1.31	0.38	26	549782	*
300.05473	-0.05	C12H15NO6S	6	1.25	0.50	54	1508005	
302.03400	-0.07	C11H13NO7S	6	1.18	0.64	42	1086369	
302.07038	0.00	C12H17NO6S	5	1.42	0.50	20	452434	
303.00025	-0.07	C11H12O6S2	6	1.09	0.55	20	352907	
303.10604	-0.10	C17H20O3S	8	1.18	0.18	26	2382945	
304.04965	-0.13	C11H15NO7S	5	1.36	0.64	25	892533	
305.01590	-0.11	C11H14O6S2	5	1.27	0.55	25	517397	
305.12169	-0.11	C17H22O3S	7	1.29	0.18	25	4178115	
305.14282	-0.24	C14H26O5S	2	1.86	0.36	32	1172695	*
306.00778	0.01	C13H9NO6S	10	0.69	0.46	33	592722	

307.03155	-0.19	C11H16O6S2	4	1.45	0.55	28	640785	
307.13734	-0.17	C17H24O3S	6	1.41	0.18	53	16737978	
309.03644	0.04	C12H10N2O8	9	0.83	0.67	36	706970	
310.00270	-0.19	C12H9NO7S	9	0.75	0.58	46	954610	
312.01835	-0.05	C12H11NO7S	8	0.92	0.58	62	1536899	
314.03400	-0.17	C12H13NO7S	7	1.08	0.58	56	2003438	
316.04965	-0.19	C12H15NO7S	6	1.25	0.58	43	1701106	
317.12169	-0.12	C18H22O3S	8	1.22	0.17	23	1902521	
318.02891	-0.13	C11H13NO8S	6	1.18	0.73	21	543675	
319.03155	-0.18	C12H16O6S2	5	1.33	0.50	39	1047894	
319.10095	-0.24	C17H20O4S	8	1.18	0.24	50	2589798	*
319.13734	-0.08	C18H24O3S	7	1.33	0.17	25	5405075	
321.02858	-0.39	C11H14O9S	5	1.27	0.82	44	991657	
323.02647	-0.24	C11H16O7S2	4	1.45	0.64	27	660725	
324.01835	-0.20	C13H11NO7S	9	0.85	0.54	89	2452797	
326.10677	0.19	C15H21NO5S	6	1.40	0.33	26	530282	
327.99550	-0.05	C12H11NO6S2	8	0.92	0.50	32	1159909	
328.01326	-0.08	C12H11NO8S	8	0.92	0.67	42	911348	
330.02891	0.02	C12H13NO8S	7	1.08	0.67	29	799497	
330.04417	-0.21	C16H13NO5S	11	0.81	0.31	20	355329	*
330.06530	-0.30	C13H17NO7S	6	1.31	0.54	81	2790581	
331.13734	-0.22	C19H24O3S	8	1.26	0.16	23	1202559	
332.04456	-0.18	C12H15NO8S	6	1.25	0.67	31	985660	
332.08095	-0.04	C13H19NO7S	5	1.46	0.54	36	935323	
333.11660	-0.27	C18H22O4S	8	1.22	0.22	42	2329460	*
333.15299	-0.22	C19H26O3S	7	1.37	0.16	24	4187417	
335.16864	-0.01	C19H28O3S	6	1.47	0.16	26	7133527	
337.03136	-0.12	C13H10N2O9	10	0.77	0.69	29	543840	*
338.01537	-0.21	C13H9NO10	10	0.69	0.77	19	362074	*
340.01326	0.03	C13H11NO8S	9	0.85	0.62	79	2051478	
341.01590	-0.17	C14H14O6S2	8	1.00	0.43	22	1515077	
342.02891	-0.04	C13H13NO8S	8	1.00	0.62	65	2185663	
344.04456	-0.03	C13H15NO8S	7	1.15	0.62	62	2284339	
345.01082	-0.09	C13H14O7S2	7	1.08	0.54	25	808396	
347.09587	-0.53	C18H20O5S	9	1.11	0.28	39	2141516	*
348.07586	-0.06	C13H19NO8S	5	1.46	0.62	32	877136	
349.03136	0.19	C14H10N2O9	11	0.71	0.64	56	1226815	*
349.07850	-0.23	C14H22O6S2	4	1.57	0.43	25	919404	
349.14790	-0.34	C19H26O4S	7	1.37	0.21	32	2680569	
351.02138	-0.22	C12H16O8S2	5	1.33	0.67	38	843546	
351.19994	-0.10	C20H32O3S	5	1.60	0.15	24	2059938	
354.02891	0.13	C14H13NO8S	9	0.93	0.57	111	4056143	
356.04456	0.01	C14H15NO8S	8	1.07	0.57	100	4352721	
358.02383	0.00	C13H13NO9S	8	1.00	0.69	55	1365736	
360.03948	0.10	C13H15NO9S	7	1.15	0.69	41	1021916	
361.03136	0.20	C15H10N2O9	12	0.67	0.60	24	735131	*
362.97356	-0.35	C16H9ClO6S	12	0.56	0.38	22	684254	*
363.12717	-0.27	C19H24O5S	8	1.26	0.26	21	1614187	*
363.16355	-0.43	C20H28O4S	7	1.40	0.20	21	605697	
365.21559	-0.17	C21H34O3S	5	1.62	0.14	21	707189	
366.09831	-0.12	C20H17NO6	13	0.85	0.30	31	969949	
367.19485	-0.15	C20H32O4S	5	1.60	0.20	25	820777	
372.03948	0.19	C14H15NO9S	8	1.07	0.64	83	3118074	
373.00573	-0.19	C14H14O8S2	8	1.00	0.57	62	1707421	
375.02138	0.02	C14H16O8S2	7	1.14	0.57	73	2285225	
377.10643	-0.39	C19H22O6S	9	1.16	0.32	33	1963563	
379.05268	-0.09	C14H20O8S2	5	1.43	0.57	22	1062990	
381.21050	-0.23	C21H34O4S	5	1.62	0.19	20	373176	
384.11225	-0.44	C17H23NO7S	7	1.35	0.41	27	754949	
386.01874	0.30	C14H13NO10S	9	0.93	0.71	24	520244	*
387.18468	-0.24	C19H32O6S	4	1.68	0.32	36	2552131	
389.99253	0.20	C16H9NO9S	13	0.56	0.56	22	386074	*
391.01630	-0.12	C14H16O9S2	7	1.14	0.64	49	1445171	
391.15847	-0.15	C21H28O5S	8	1.33	0.24	22	867712	*
397.20542	-0.21	C21H34O5S	5	1.62	0.24	27	1185647	*
398.01874	0.27	C15H13NO10S	10	0.87	0.67	75	2197712	

401.20033	-0.21	C20H34O6S	4	1.70	0.30	33	3150669	
406.96339	-0.07	C17H9ClO8S	13	0.53	0.47	23	631523	*
407.18977	-0.21	C22H32O5S	7	1.45	0.23	30	545122	*
418.96339	-0.16	C18H9ClO8S	14	0.50	0.44	22	675993	*
431.14599	0.06	C21H24N2O8	11	1.14	0.38	42	1931425	
439.09944	0.25	C18H20N2O11	10	1.11	0.61	48	3152142	*
447.99801	0.59	C18H11NO11S	14	0.61	0.61	23	424443	*
468.02422	-0.13	C18H15NO12S	12	0.83	0.67	25	498732	*
473.15656	0.00	C23H26N2O9	12	1.13	0.39	39	1724348	
503.05797	0.29	C21H16N2O13	15	0.76	0.62	26	928094	
503.16712	-0.07	C24H28N2O10	12	1.17	0.42	20	905233	*
526.17187	-0.21	C27H29NO10	14	1.07	0.37	23	1003376	
545.17769	0.04	C26H30N2O11	13	1.15	0.42	23	1126529	
547.20073	-0.24	C28H36O9S	11	1.29	0.32	34	961593	*
548.15959	0.55	C26H31NO10S	12	1.19	0.38	24	731866	*
575.23203	0.08	C30H40O9S	11	1.33	0.30	26	765642	*
610.14223	0.05	C27H33NO11S2	12	1.22	0.41	23	941263	*
655.06106	0.14	C26H24O18S	15	0.92	0.69	20	984017	*

Table A2.4 List of top 10 potential tracers that were not unique to higher STE impact sites, in order of decreasing average signal intensity. Average signal intensity is averaged across all higher impact samples (n=120), including 0 values for nondetects.

Theoretical Exact *m/z*	**Error of Assignment (ppm)**	**Neutral Formula**	**DBE**	**H/C**	**O/C**	**Number of Detections**	**Avg. Signal Intensity (a.u.)**
269.04892	-0.11	C12H14O5S	6	1.17	0.42	120	32298286
243.03327	0.08	C10H12O5S	5	1.20	0.50	115	23627063
321.15299	-0.15	C18H26O3S	6	1.44	0.17	46	18746052
255.03327	-0.17	C11H12O5S	6	1.09	0.45	120	16992881
307.13734	-0.17	C17H24O3S	6	1.41	0.18	53	16737978
199.04344	0.24	C9H12O3S	4	1.33	0.33	44	13722420
295.06457	-0.12	C14H16O5S	7	1.14	0.36	120	11707614
273.04383	-0.01	C11H14O6S	5	1.27	0.55	120	10742884
255.06965	-0.52	C12H16O4S	5	1.33	0.33	85	10672895
323.13225	-0.22	C17H24O4S	6	1.41	0.24	94	9855486

Table A2.5 Perfluoroalkyl sulfonate (PFAS) and perfluoroalkyl carboxylate (PFAC) classes of per- and poly- fluorinated compounds (PFCs) in stream data.

Theoretical Exact *m/z*	**Error of Assignment (ppm)**	**Neutral Formula**
PFASs		
298.94299	-0.12	C4HF9O3S
348.93980	0.26	C5HF11O3S
398.93660	0.16	C6HF13O3S
448.93341	-0.43	C7HF15O3S
498.93022	0.23	C8HF17O3S
PFACs		
262.97601	0.05	C5HF9O2
312.97281	-0.07	C6HF11O2
362.96962	-0.20	C7HF13O2
412.96643	0.08	C8HF15O2
Possible In-Source Fragmentation Products of PFACs		
218.98618	-0.01	C4HF9
268.98298	-0.12	C5HF11
318.97979	-0.16	C6HF13
368.97660	-0.01	C7HF15

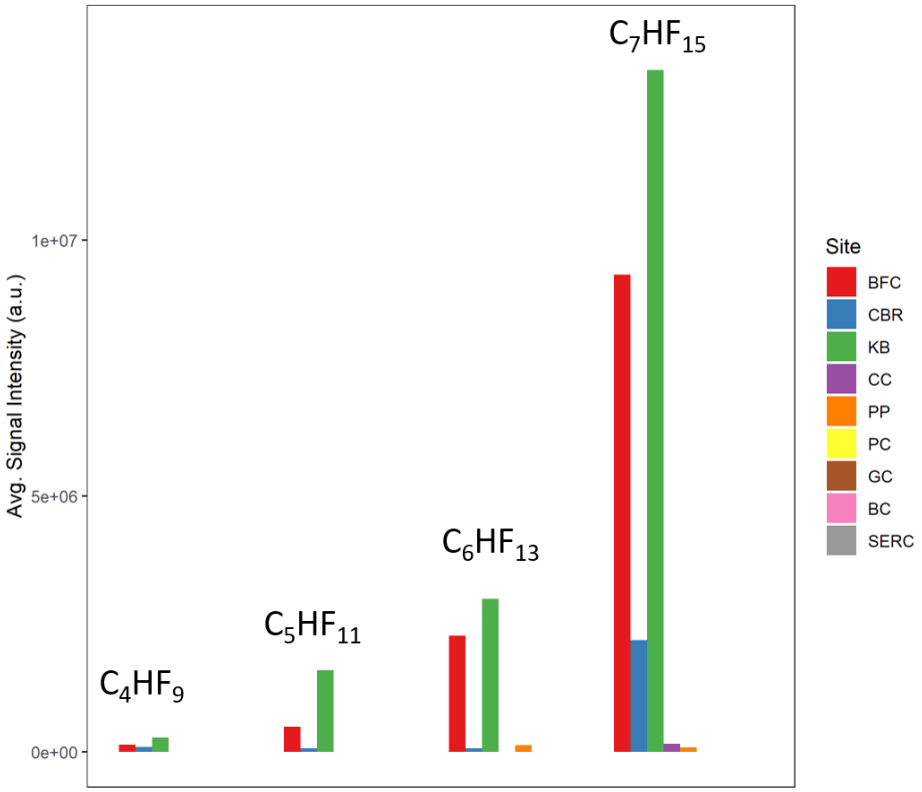

Figure A2.9 Grouped bar plot of likely in-source fragmentation products of PFACs, in order of decreasing STE impact. Groups show $+CF_2$ homologous series. Neutral formulas are shown, but measured ions are $[M - H]^-$.

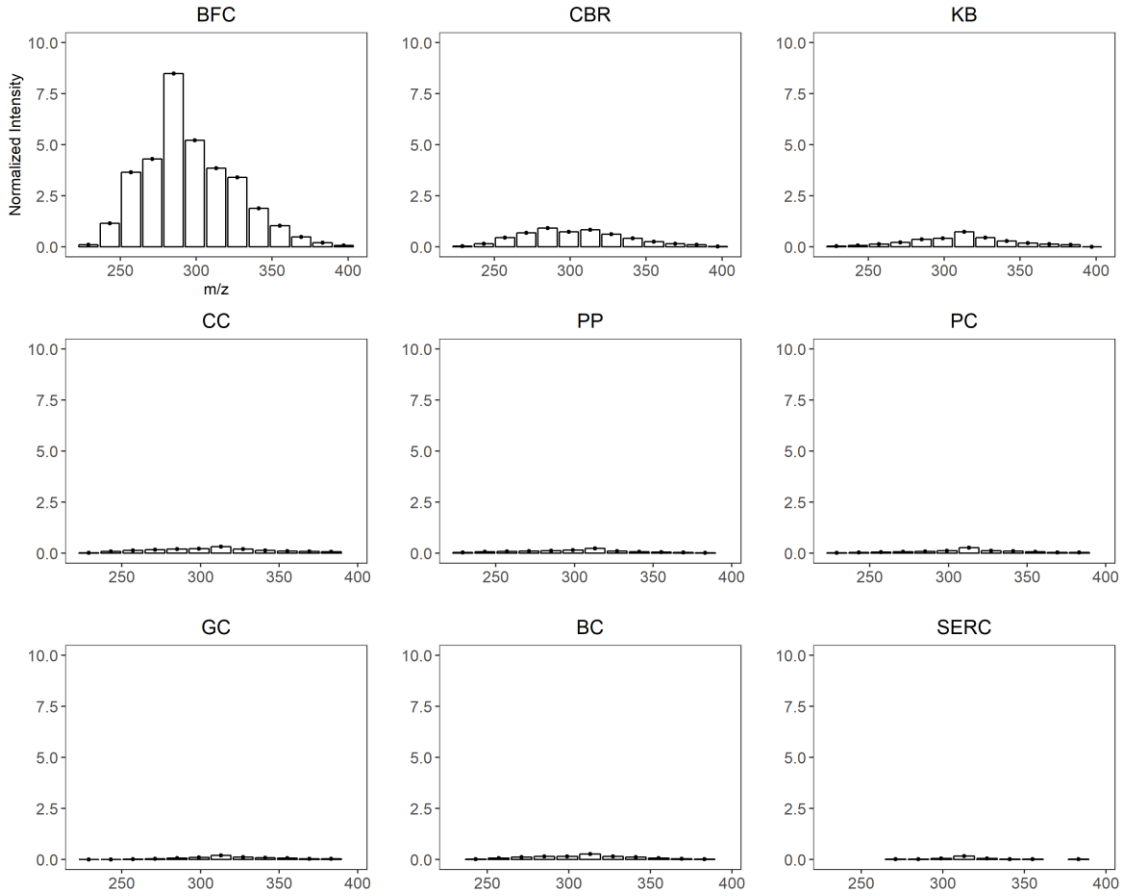

Figure A2.10 Sulfophenyl carboxylic acids (SPC) signal intensities for stream sites in STE impact order. Points are at exact measured *m/z* values and show $+CH_2$ homologous series related to chain length. Signal intensity (a.u.) was normalized to the average intensity (a.u.) of all CHO signals in each sample, and then averaged by site.

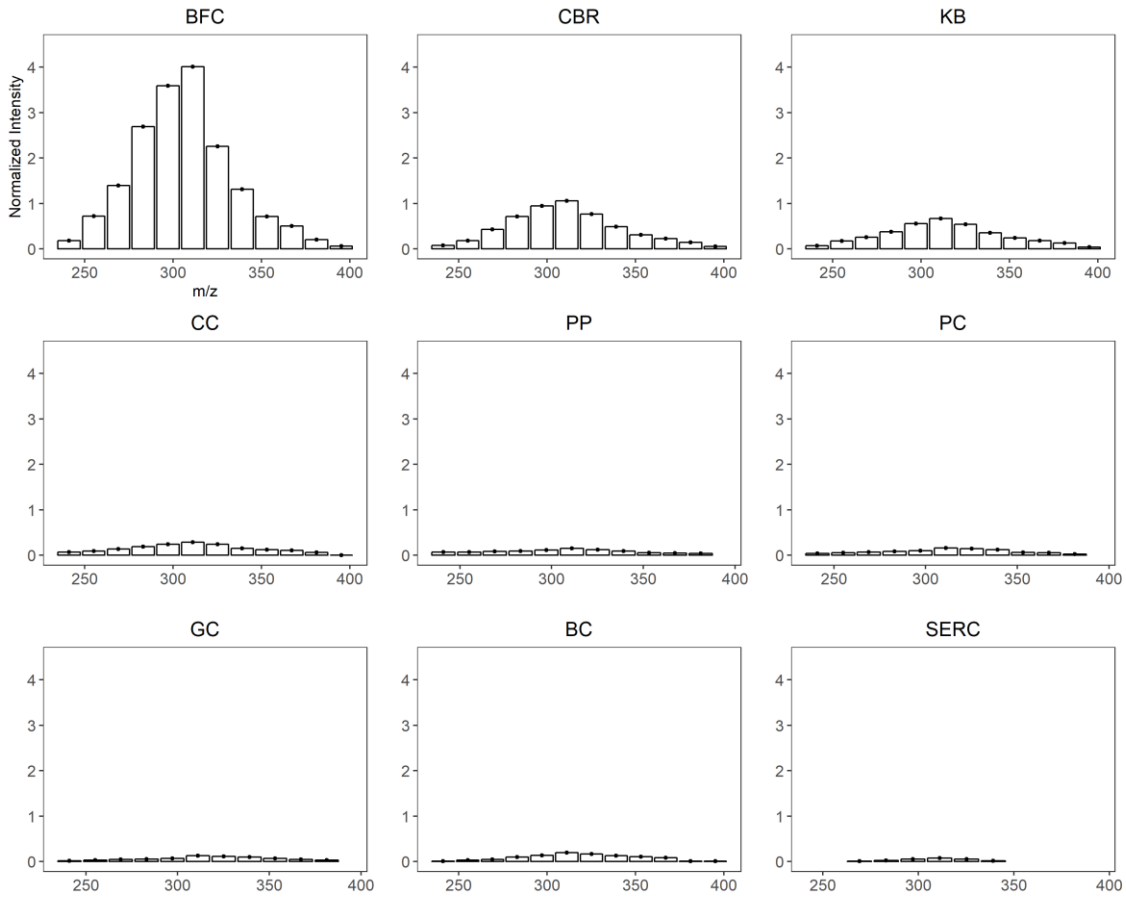

Figure A2.11 Dialkyl tetralin sulfonate intermediates (DATSI) signal intensities for stream sites in STE impact order. Points are at exact measured *m/z* values and show $+CH_2$ homologous series related to chain length. Signal intensity (a.u.) was normalized to the average intensity (a.u.) of all CHO signals in each sample, and then averaged by site.

Table A2.6 SPC and DATSI classes of surfactants in stream data.

SPC		
Theoretical Exact *m/z*	**Error of Assignment (ppm)**	**Neutral Formula**
229.01762	0.11	C9H10O5S
243.03327	0.08	C10H12O5S
257.04892	0.00	C11H14O5S
271.06457	0.08	C12H16O5S
285.08022	-0.07	C13H18O5S
299.09587	-0.11	C14H20O5S
313.11152	-0.06	C15H22O5S
327.12717	-0.35	C16H24O5S
341.14282	-0.33	C17H26O5S
355.15847	-0.26	C18H28O5S
369.17412	-0.13	C19H30O5S
383.18977	-0.12	C20H32O5S
397.20542	-0.21	C21H34O5S
DATSI		
Theoretical Exact *m/z*	**Error of Assignment (ppm)**	**Neutral Formula**
241.01762	-0.02	C10H10O5S
255.03327	-0.17	C11H12O5S
269.04892	-0.11	C12H14O5S
283.06457	-0.09	C13H16O5S
297.08022	0.02	C14H18O5S
311.09587	-0.07	C15H20O5S
325.11152	-0.05	C16H22O5S
339.12717	-0.25	C17H24O5S
353.14282	-0.30	C18H26O5S
367.15847	-0.21	C19H28O5S
381.17412	-0.18	C20H30O5S
395.18977	-0.20	C21H32O5S

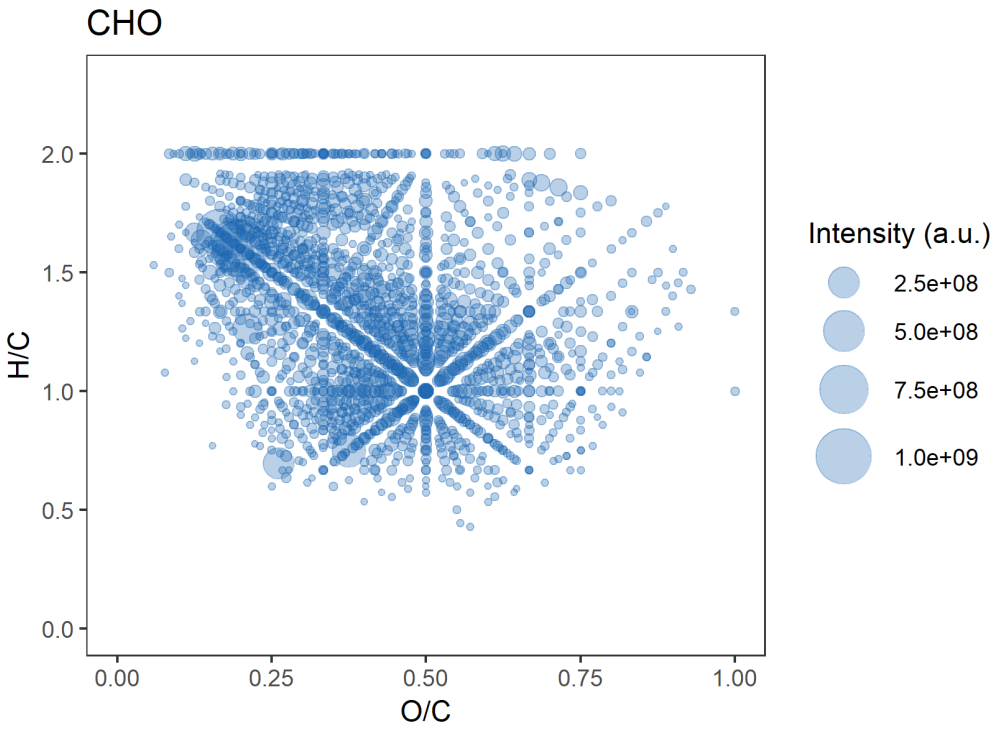

Figure A2.12 Van Krevelen diagram showing intensity averaged CHO formula assignments in STDOM.

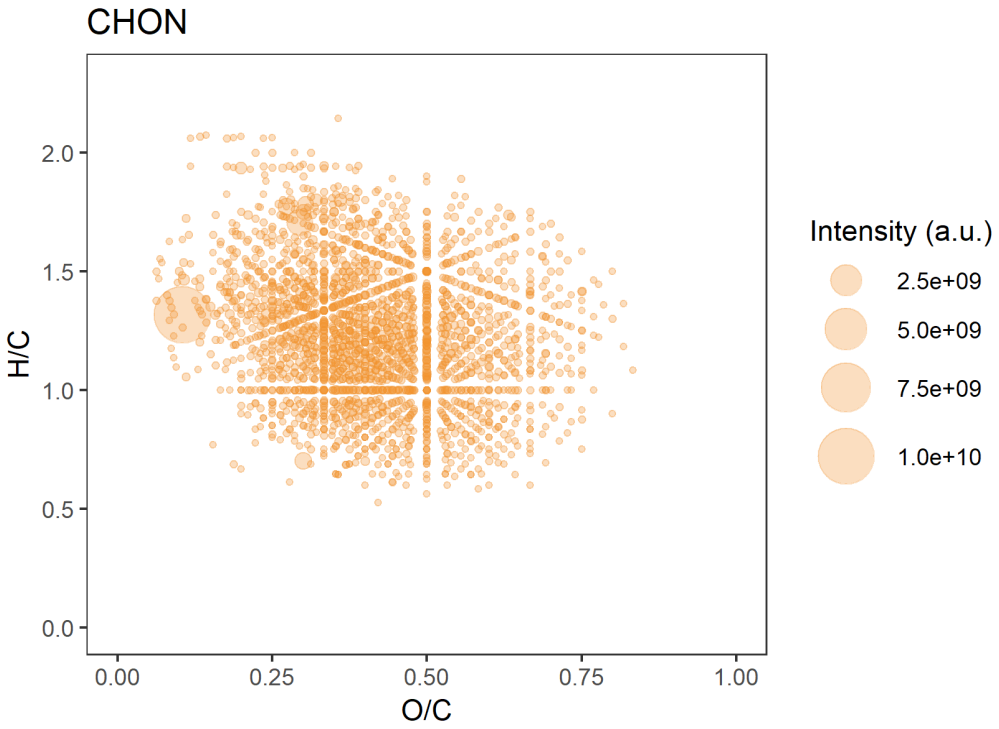

Figure A2.13 Van Krevelen diagram showing intensity averaged CHON formula assignments in STDOM.

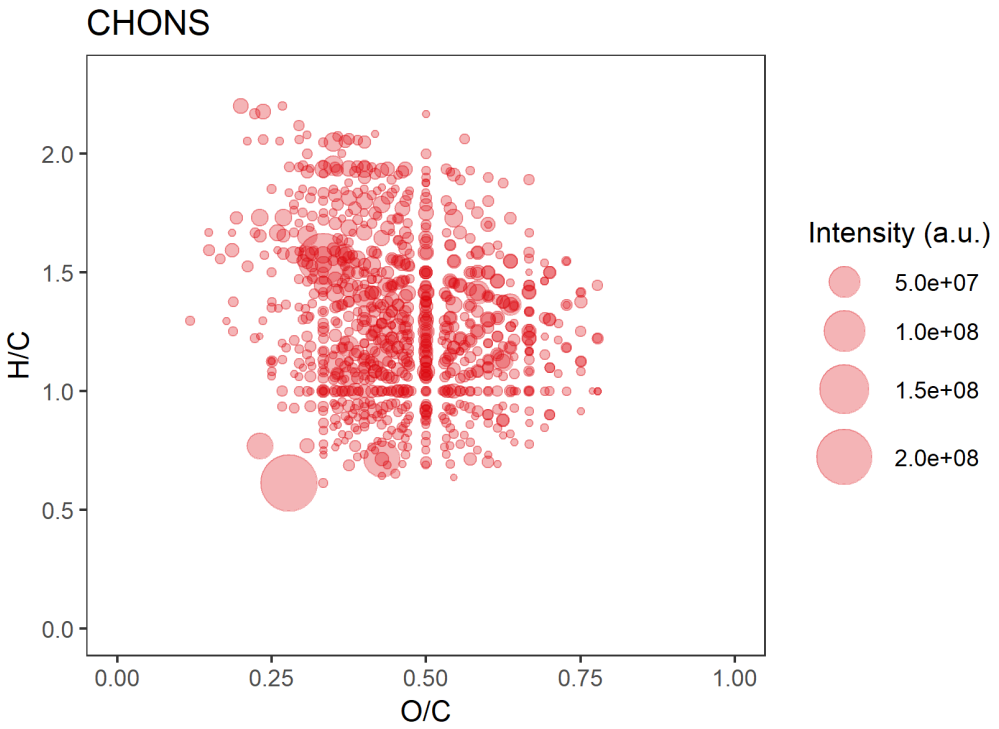

Figure A2.14 Van Krevelen diagram showing intensity averaged CHON formula assignments in STDOM.

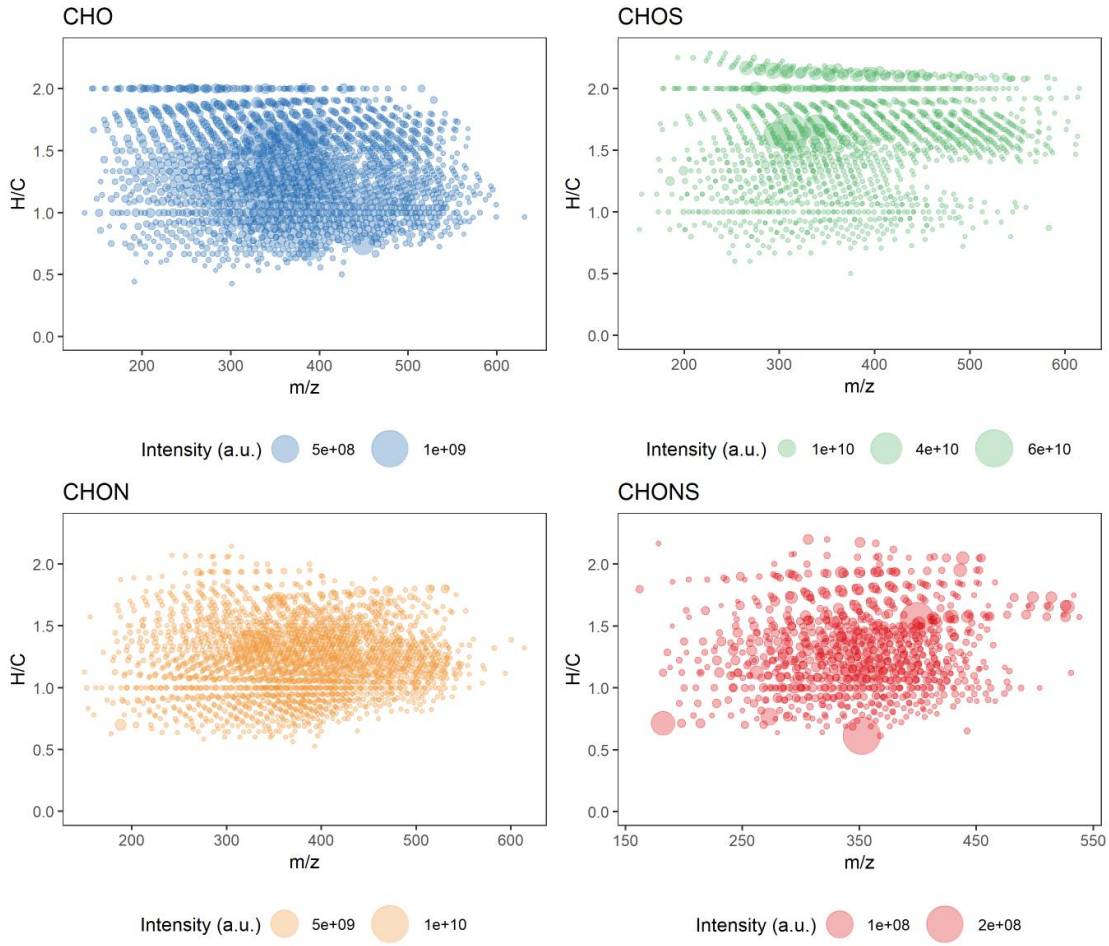

Figure A2.15 H/C vs *m/z* plots showing intensity averaged formula assignments for STDOM.

Appendix 3

Supplemental Materials to Chapter 4

Table A3.1 Sources and purities of additional CEC standards and SIL-ISTDs. Purities are guaranteed from the manufacturer or from lot assays as available. Original compound purity is not available for most SIL-standards. For other standards used see *Appendix 4* (Table A4.2).
[a] Sigma-Aldrich
[b] Toronto Research Chemicals

CEC	Standard	Source/Purity	Description	SIL-ISTD	Source/ Isotopic Purity
atorvastatin	atorvastatin calcium	95.3%[a]	prescription drug	atorvastatin-d5 sodium	99.1%[b]
caffeine	caffeine	99.1%[a]	stimulant	caffeine-d9	99.7%[b]
dichlorvos	dichlorvos	95%[b]	insecticide	dichlorvos-d6	99.5%[b]
diclofenac	diclofenac sodium	99.7%[a]	prescription and OTC NSAID	diclofenac-d4	99.0%[b]
estrone	estrone	99.5%[a]	steroid hormone	estrone-d2	99.9%[b]

Table A3.2 MRM settings in the Main CEC Method.

Compound	Transition Type	Ion Mode	Transition	RT (min)	FV (V)	CE (V)	CAV (V)
acetaminophen	target	positive	152.0 → 110.2	2.78	110	16	2
acetaminophen	qualifier	positive	152.0 → 65.0	2.78	110	35	2
acetaminophen-d3	ISTD	positive	155.2 → 111.0	2.78	110	16	2
atorvastatin	target	positive	559.2 → 440.2	7.23	130	22	1
atorvastatin	qualifier	positive	559.2 → 250.1	7.23	130	49	1
atorvastatin-d5	ISTD	positive	564.3 → 445.2	7.22	130	22	1
caffeine	target	positive	195.1 → 138.0	3.57	108	19	3
caffeine	qualifier	positive	195.1 → 110.1	3.57	108	25	3
caffeine-d9	ISTD	positive	204.2 → 144.0	3.53	108	19	3
carbamazepine	target	positive	237.0 → 194.0	6.33	120	18	4
carbamazepine	qualifier	positive	237.0 → 179.0	6.33	120	39	4
carbamazepine-d10	ISTD	positive	247.2 → 204.2	6.28	120	18	4
cotinine	target	positive	177.2 → 80.2	2.46	90	22	3
cotinine	qualifier	positive	177.2 → 98.1	2.46	90	22	3
cotinine-d3	ISTD	positive	180.2 → 101.0	2.45	90	22	3
dichlorvos	target	positive	221.0 → 109.0	6.22	100	15	4
dichlorvos	qualifier	positive	221.0 → 145.0	6.22	100	10	4
dichlorvos-d6	ISTD	positive	227.1 → 115.0	6.21	100	15	4
diclofenac	target	positive	296.0 → 215.0	8.13	85	19	1
diclofenac	qualifier	positive	296.0 → 250.0	8.13	85	10	1
diclofenac-d4	ISTD	positive	300.0 → 254.0	8.12	85	10	1
estrone	target	positive	271.0 → 159.0	7.42	100	20	3
estrone	qualifier	positive	271.0 → 157.0	7.42	100	20	3

estrone-d2	ISTD	positive	273.0 → 159.0	7.42	100	20	3
ibuprofen	target	positive	207.2 → 161.1	7.69	100	3	3
ibuprofen	qualifier	NA	NA	NA	NA	NA	NA
ibuprofen-13C,d3	ISTD	positive	211.3 → 165.3	7.68	100	7	3
methylparaben	target	positive	153.0 → 65.0	5.86	110	30	3
methylparaben	qualifier	positive	153.0 → 121.0	5.86	110	18	3
ethylparaben-d4	ISTD	positive	171.0 → 99.2	6.41	80	18	3
propylparaben	target	positive	181.0 → 95.0	6.87	80	18	3
propylparaben	qualifier	positive	181.0 → 121.0	6.87	80	18	3
propylparaben-d4	ISTD	positive	185.0 → 99.2	6.85	80	18	3
paraxanthine	target	positive	181.1 → 124.1	2.95	90	23	3
paraxanthine	qualifier	positive	181.1 → 96	2.95	90	29	3
paraxanthine-d3	ISTD	positive	184.1 → 127.1	2.99	90	23	3
sucralose	target	positive	419.0 → 239.0	3.52	120	19	7
sucralose	qualifier	positive	419.0 → 221.0	3.52	120	15	7
sucralose-d6	ISTD	positive	425.0 → 243.0	3.43	120	19	7
sulfamethoxazole	target	positive	254.0 → 92.0	3.87	110	25	4
sulfamethoxazole	qualifier	positive	254.0 → 156.0	3.87	110	15	4
Sulfamethoxazole-d4	ISTD	positive	258.1 → 160.1	3.84	110	15	4
triclosan	target	negative	287.0 → 35.1	8.80	80	8	4
triclosan	qualifier	negative	289.0 → 37.1	8.79	80	8	4
triclosan-d3 1	ISTD	negative	292.0 → 37.1	8.79	80	8	4

Text A3.1 SPE Recovery

SPE recovery experiments for most compounds are described in *Appendix 4* (Text A4.3, Tables A4.11, A4.12). Recoveries for atorvastatin, caffeine, diclofenac, dichlorvos, and estrone were not measured. Caffeine is structurally similar to its metabolite, paraxanthine, and is expected to have similar recovery. While we expect quantitative recoveries for the remaining compounds, recoveries should be confirmed. To be conservative and because most CECs were quantitatively recovered, measurements were not corrected for SPE recovery.

Text A3.2 Stream CEC MDLs

All HPLC/QqQMS/MS measurements were corrected for exact SPE concentration factors and dilutions before analyses. Sample acidification was not accounted for as a dilution, as it is negligible. MDLs were approximated to be representative of the most common stream SPE and dilution conditions. This was by (lowest measured calibration standard value × lowest DF)/SPE CF. For ace-K this was ~ CF=96.7, DF=2, and for other CECs this was ~ CF=210, DF=10. True sample specific MDLs varied, and all reproducibly measured data, based on instrument replicability and extraction replicates, was retained for averages and plotting. STDOM SPEs were analyzed at a minimum dilution factor of 10.

Table A3.3 Approximate stream CEC MDLs.

Compound	**~MDL (ng/L)**
acesulfame-K	3
acetaminophen	2
atorvastatin	1
caffeine	24
carbamazepine	1
cotinine	1
dichlorvos	7
diclofenac	2
estrone	23
ibuprofen	50
methylparaben	138
propylparaben	27
paraxanthine	11
sucralose	42
sulfamethoxazole	3
triclosan	21

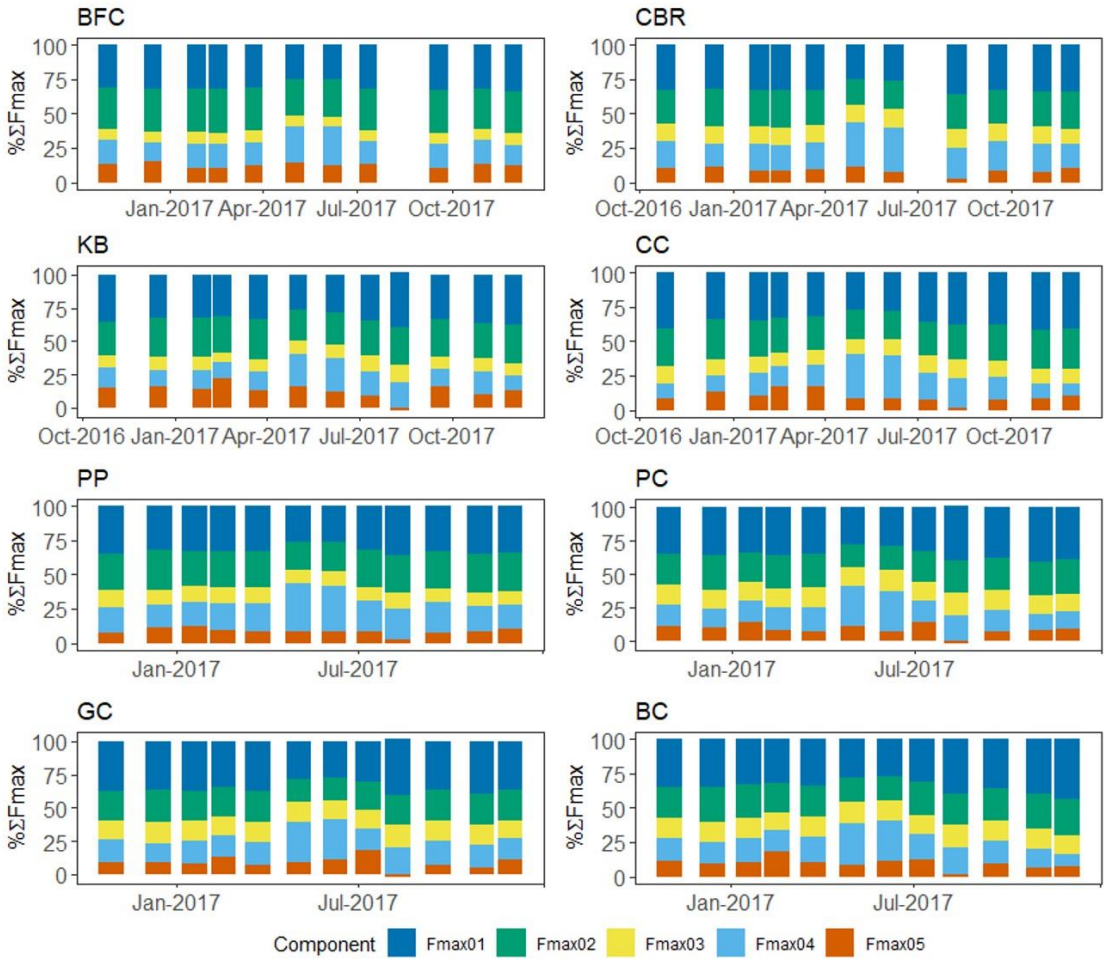

Figure A3.1 Stream DOM %Fmax01-05 for PARAFAC components by site showing increased %Fmax04 in May-June. There were no clear differences or trends related to STE impact.

Table A3.4 Abbreviations used in dendrogram and MDS diagrams.

Abbreviation	Parameter
BAT	Best Available Technology septic system density
Cond	conductivity
Diclo	diclofenace (DCF)
LU_Dev	% developed and semi-developed land use
Mo.	sampling month
Para	paraxanthine (PXT)
Sulf	sulfamethoxazole (SMX)
TRAD	traditional septic system density

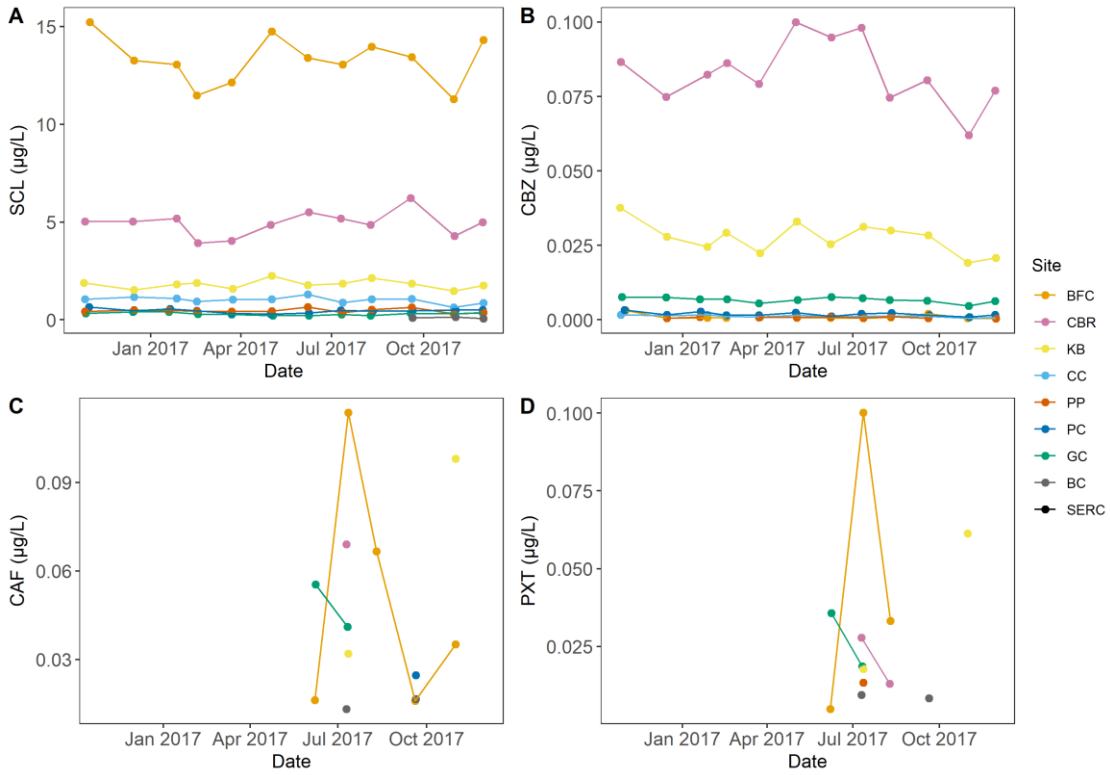

Figure A3.2 Timeseries of SCL (A), CBZ (B), CAF (C), and PXT (D) in streams. Legend is in order of highest to lowest STE impact.

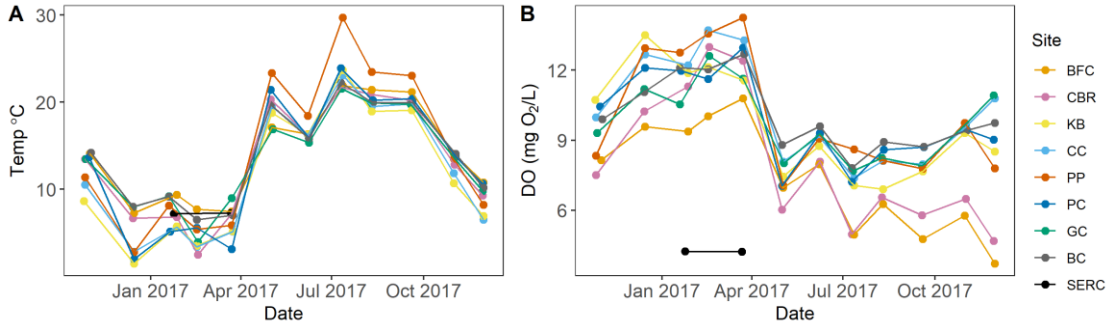

Figure A3.3 Timeseries of temperature (A) and DO (B) in streams.

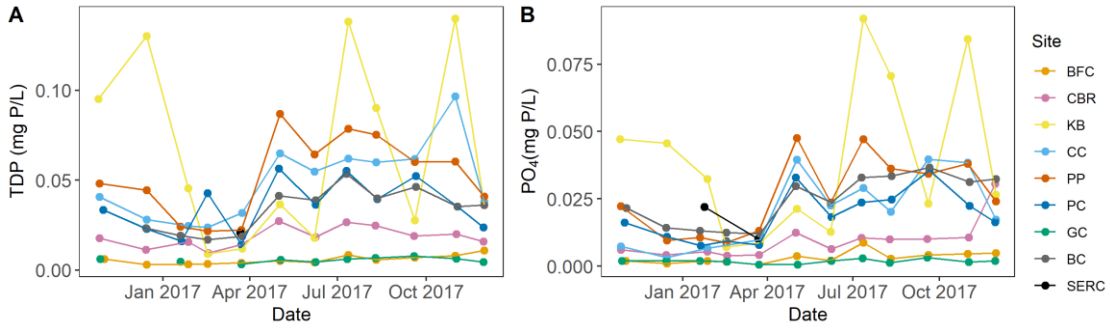

Figure A3.4 Timeseries of TDP (A) and PO_4 (B) in streams.

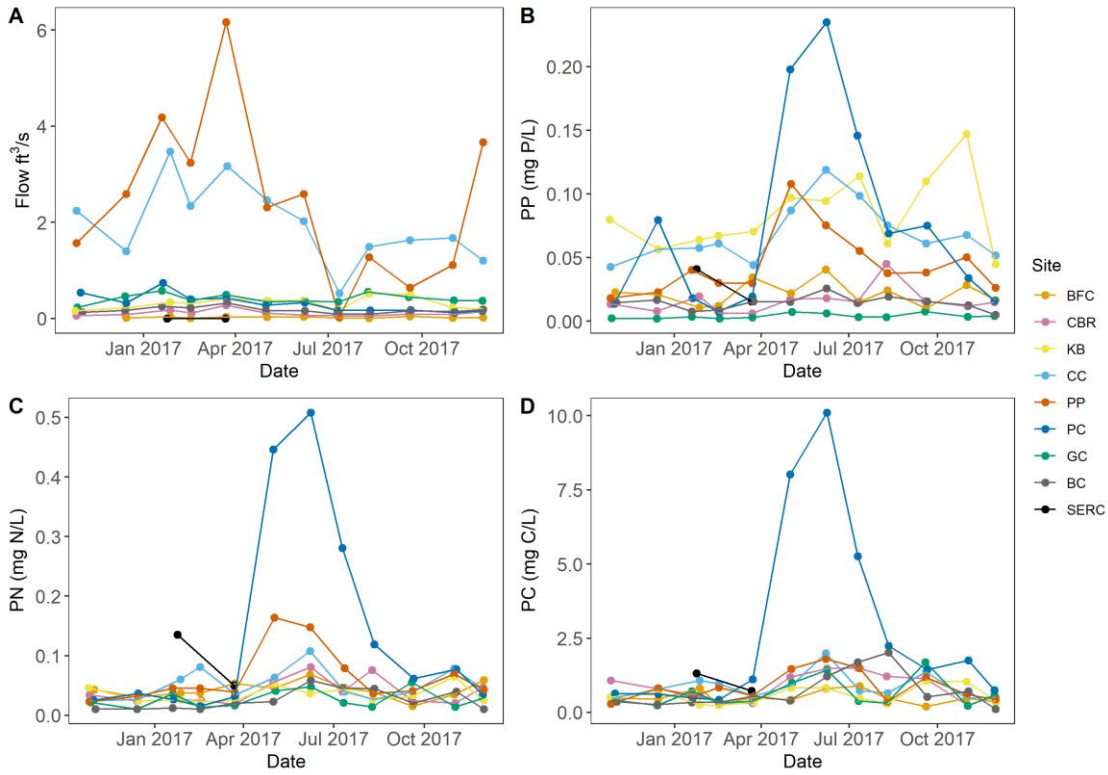

Figure A3.5 Timeseries of flow (A) and particulate nutrients: PP (B), PN (C), and PC (D) in streams.

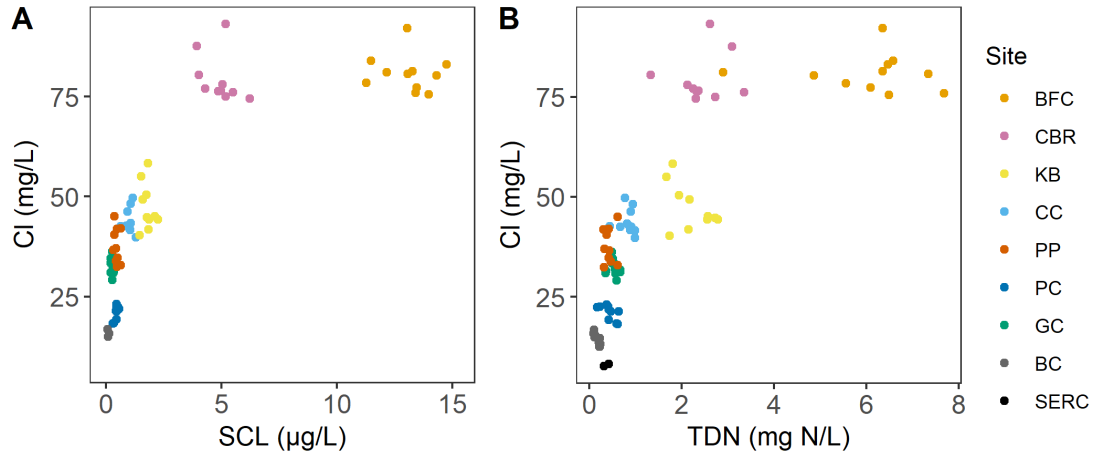

Figure A3.6 Cl versus SCL (A) and CL versus TDN (B) in streams. Legend is in order of highest to lowest STE impact.

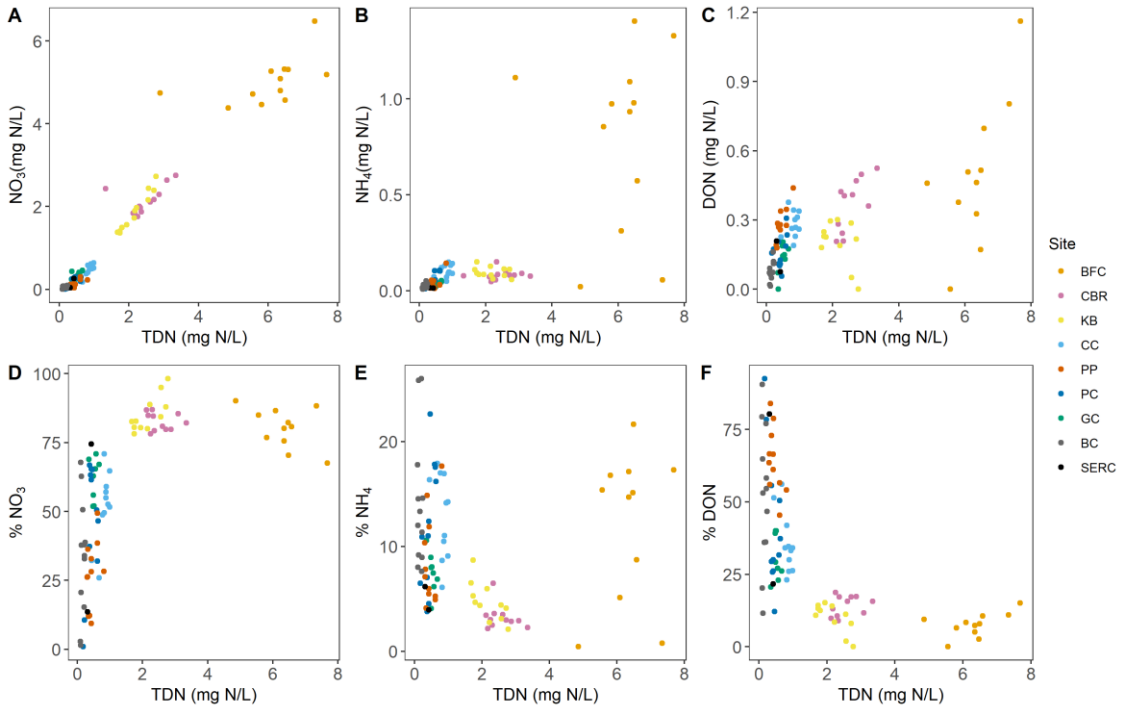

Figure A3.7 NO_3-NO_2 versus TDN (A), NH_4/NH_3 versus TDN (B), and DON versus TDN (C) in streams. Composition of TDN as % NO_3-NO_2 (D), % NH_4/NH_3 (E), and % DON (F) in streams, NH_4/NH_3 at the site BFC does not follow expected % NH_4/NH_3 trends (Stanley and Maxted, 2008). Legend is in order of highest to lowest STE impact.

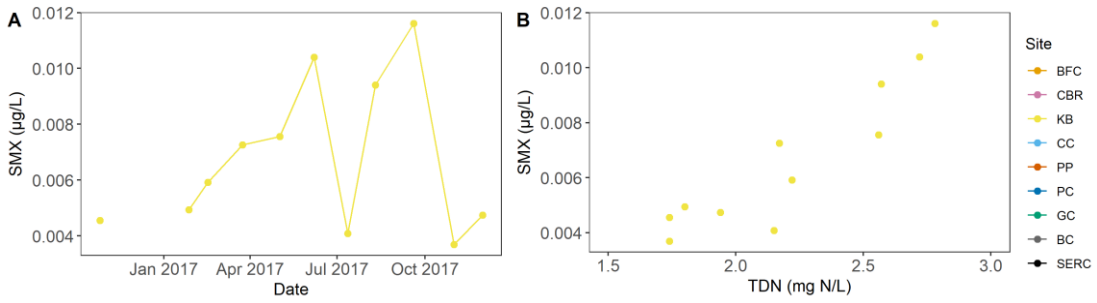

Figure A3.8 Timeseries of SMX at stream site KB (A) and SMX versus TDN (B).

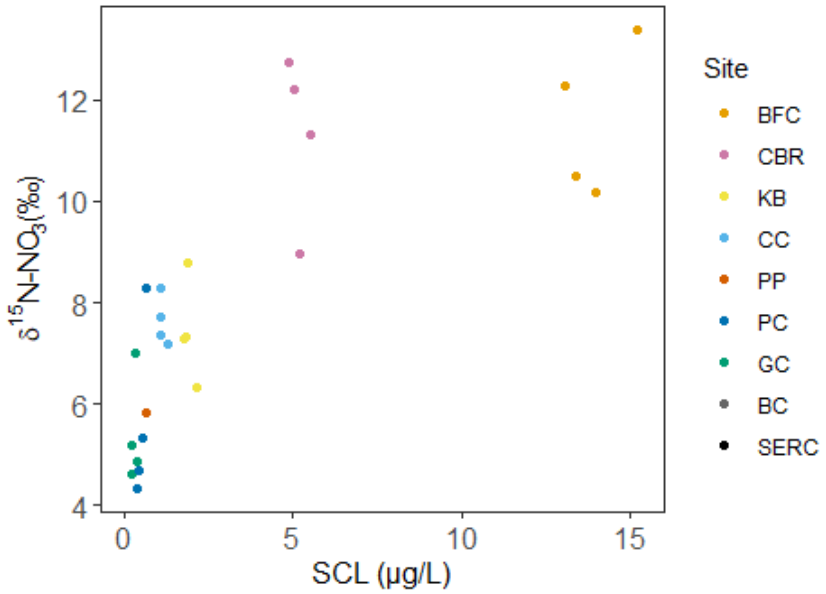

Figure A3.9 Seasonal $\delta^{15}N_{NO3}$ versus SCL from same sample times in streams. Legend is in order of highest to lowest STE impact.

Appendix 4

Supplemental Materials to Chapter 5

Text A4.1 Filtering and SPEs

Whole leachate was filtered by vacuum filtration using base-washed filter holders. HCl for sample acidification was a pure grade, 32% solution. A mixed-mode reversed-phase, weak anion exchange extraction was used for acesulfame potassium because acesulfame is an acidic anion and because of previous unpublished recovery estimates which showed poor recovery by Agilent Bond Elut PPL. Methanol and 0.1% (v/v) formic acid water used in SPEs were LC-MS grade. Water was ultrapure water generated from an in-lab system. The NH_4OH MeOH was approximately 92% methanol, 8% water and was made by diluting reagent grade, NH_4OH water solutions with methanol. SPEs were done on a vacuum manifold. For the PPL extractions, the larger volume wash step after sample loading was done by putting the formic acid water wash in a combusted glass vial (500 °C) and sending it by peristaltic pump through acid-washed tubing connected with base-washed tube adaptors to the cartridges. Samples were eluted into either new, trace contaminant certified or acid-washed and combusted amber vials with new or base washed caps. SPEs were stored at -20 °C between analyses.

Table A4.1 Volume of leachate loaded onto cartridges for triplicate SPEs. Cartridges were not loaded with >18 mg DOC/ 1 g sorbent. Concentration factors of extracts are (loaded volume (mL) / elution volume (mL)).

Extraction	**Loaded Sample Volume (mL)**		
	1	**2**	**3**
PPL			
Active	12	16	11.5
Closed	10	10	10
Closed-Brine	11.5	11.5	12
WAX			
Active	2	2	2
Closed	2	2	2
Closed-Brine	2	2	2

Text A4.2 HPLC-MS/MS Methods for Quantification of CECs

The carrier gas was high purity nitrogen from a nitrogen generator and the collision gas was ultra-high purity nitrogen. An ISTD quantification method was used to control for fluctuations in instrument performance. All blanks, calibration standards, quality control standards, and samples were spiked with ISTDs. A separate method was used to account for the different SPE matrix of the WAX extracts. Here, the two HPLC-MS/MS methods are referred to as Acesulfame Potassium Method and Other

CECs Method. Qualifier transitions were used to further confirm identities of measured compounds. Significant qualifier transitions using different fragment ions were not found for ibuprofen or triclosan. Ibuprofen was run without a qualifier, while a different isotopic transition was used as a qualifier for triclosan because it has three chlorine atoms.

Table A4.2 Sources and purities of CEC standards and SIL-ISTDs. Purities are guaranteed from the manufacturer or from lot assays as available. Original compound purity is not available for most SIL-standards.
[a] Sigma-Aldrich
[b] Toronto Research Chemicals
[c] CDN Isotopes
[d] Cerilliant

CEC	Standard	Source/Purity	Description	SIL-ISTD	Source/ Isotopic Purity
acesulfame potassium	acesulfame potassium	99.9%[a]	artificial sweetener	acesulfame potassium-d4	≥98.0%[b]
acetaminophen	acetaminophen	≥98.0%[a]	NSAID	acetaminophen-d3	99.2%[c]
carbamazepine	carbamazepine	99.7%[d]	prescription drug	carbamazepine-d10	98.0%[b]
cotinine	(-)-cotinine	99.5%[a]	nicotine metabolite	(±)-cotinine-d3	99.8%[c]
ibuprofen	ibuprofen	99.7%[a]	NSAID	ibuprofen-13C,d3	98.6%[b]
methylparaben	methylparaben	98.5%[a]	antimicrobial	ethylparaben-d4	98.7%[c]
propylparaben	n-propylparaben	99.9%[a]	antimicrobial	n-propylparaben-d4	98.8%[c]
paraxanthine	paraxanthine	>99.9%[d]	caffeine metabolite	paraxanthine-d3	99.8%[b]
sucralose	sucralose	99.2%[a]	artificial sweetener	sucralose-d6	95.2%[b]
sulfamethoxazole	sulfamethoxazole	≥98.0%[a]	prescription drug	sulfamethoxazole-d4	98.9%[c]
triclosan	triclosan	99.9%[a]	antimicrobial	triclosan-d3	97.5%[b]

Quantification of Acesulfame Potassium

Table A4.3 Separation gradient used in Acesulfame Potassium Method, where mobile phase A is LC-MS grade methanol and mobile phase B is 0.1% (w/w) ammonium acetate water made by adding ≥99.0% purity ammonium acetate to ultrapure water. Flow after 4 minutes was sent to waste using the divert valve.

Time (min)	A (%)	B (%)
0.00	90.0	10.0
4.00	90.0	10.0
5.00	60.0	40.0
6.00	60.0	40.0
7.00	90.0	10.0
10.00	90.0	10.0

Table A4.4 Autosampler and LC settings for Acesulfame Potassium Method.

Parameter	Setting
Flow	0.250 mL/min
Column Temperature	50 °C
Injection Volume	3 uL
Needle Wash	Flush Port = 10 s
Draw Speed	200 uL/min
Eject Speed	400 uL/min
Wash time after draw	1.2 s
Needle height offset	0.0 mm
Sample Flush-out factor	5 times injection volume

Table A4.5 MS settings for Acesulfame Potassium Method.

Parameter	Setting
Ion source	ESI
Capillary voltage	Positive = 4000 V, Negative = 2500 V
Gas temperature	350 °C
Gas flow	10 L/min
Nebulizer gas pressure	40 psi
MS1/MS2 resolution	Unit
Time filtering	peak width = 0.03 min
Scan type	MRM
Delta EMV (-)	400 V

Table A4.6 MRM settings in Acesulfame Potassium Method.

Compound	Transition Type	Ion Mode	Transition	RT (min)	FV (V)	CE (V)	CAV (V)
acesulfame potassium	target	negative	162.0 → 82.0	1.50	80	10	7
acesulfame potassium	qualifier	negative	162.0 → 78.0	1.50	80	34	7
acesulfame potassium-d4	ISTD	negative	166.0 → 86.0	1.50	80	10	7

Quantification of Other CECs

Table A4.7 Separation gradient used in the Other CECs Method, where mobile phase A is LC-MS grade methanol and mobile phase B is 0.1% (v/v) LC-MS grade formic acid water. Flow after 8 minutes was sent to waste using the divert valve.

Time (min)	A (%)	B (%)
0.00	50.0	50.0
0.10	50.0	50.0
0.20	97.0	3.0
7.00	97.0	3.0
8.00	50.0	50.0

Table A4.8 Autosampler and LC settings for the Other CECs Method.

Parameter	**Setting**
Flow	0.3 mL/min
Column Temperature	50 °C
Injection Volume	5 uL
Needle Wash	Flush Port = 10 s
Draw Speed	200 uL/min
Eject Speed	400 uL/min
Wash time after draw	1.2 s
Needle height offset	0.0 mm
Sample Flush-out factor	5 times injection volume

Table A4.9 MS settings for Other CECs Method.

Parameter	**Setting**
Ion source	ESI
Capillary voltage	Positive = 5000 V, Negative = 2600 V
Gas temperature	350 °C
Gas flow	10 L/min
Nebulizer gas pressure	35 psi
MS1/MS2 resolution	Unit
Time filtering	peak width = 0.03 min
Scan type	dynamic MRM
Delta EMV (+/-)	400 V

Table A4.10 MRM settings in Other CECs Method.

Compound	Transition Type	Ion Mode	Transition	RT (min)	FV (V)	CE (V)	CAV (V)
acetaminophen	target	positive	152.0 → 110.2	1.90	110	16	2
acetaminophen	qualifier	positive	152.0 → 65.0	1.90	110	35	2
acetaminophen-d3	ISTD	positive	155.2 → 111.0	1.88	110	16	2
carbamazepine	target	positive	237.0 → 194.0	4.73	160	18	4
carbamazepine	qualifier	positive	237.0 → 179.0	4.73	160	18	4
carbamazepine-d10	ISTD	positive	247.2 → 204.2	4.7	160	18	4
cotinine	target	positive	177.2 → 80.2	1.74	90	22	3
cotinine	qualifier	positive	177.2 → 98.1	1.74	90	22	3
cotinine-d3	ISTD	positive	180.2 → 101.0	1.74	90	22	3
ibuprofen	target	positive	207.2 → 161.1	5.56	100	3	3
ibuprofen	qualifier	NA	NA	NA	NA	NA	NA
ibuprofen-13C,d3	ISTD	positive	211.3 → 165.3	5.58	100	7	3
methylparaben	target	positive	153.0 → 121.0	4.40	110	18	3
methylparaben	qualifier	positive	153.0 → 65.0	4.40	110	30	3
ethylparaben-d4	ISTD	positive	171.0 → 99.2	4.8	80	18	3
propylparaben	target	positive	181.0 → 95.0	5.12	80	18	3
propylparaben	qualifier	positive	181.0 → 121.0	5.12	80	18	3
propylparaben-d4	ISTD	positive	185.0 → 99.2	5.11	80	18	3
paraxanthine	target	positive	181.1 → 124.1	2.00	90	23	3
paraxanthine	qualifier	positive	181.1 → 96	2.00	90	23	3
paraxanthine-d3	ISTD	positive	184.1 → 127.1	1.99	90	23	3
sucralose	target	positive	419.0 → 221.0	2.36	160	15	7
sucralose	qualifier	positive	419.0 → 239.0	2.36	160	15	7
sucralose-d6	ISTD	positive	425.0 → 223.0	2.34	160	15	7
sulfamethoxazole	target	positive	254.0 → 92.0	2.69	110	25	4
sulfamethoxazole	qualifier	positive	254.0 → 156.0	2.69	110	15	4
sulfamethoxazole-d4	ISTD	positive	258.1 → 160.1	2.67	110	15	4
triclosan	target	negative	289.0 → 37.0	6.35	80	8	4
triclosan	qualifier	negative	287.0 → 35.0	6.35	80	8	4
triclosan-d3 1	ISTD	negative	292.0 → 37.0	6.34	80	8	4

Text A4.3 Recovery Experiments for CECs

Recovery experiments were conducted after initial quantification of CECs by spiking *Active* and *Closed* whole leachate samples with analytical standards and measuring spike recovery by triplicate SPEs comparable to original extraction procedures. Whole leachates were re-extracted in triplicate as a base level to account for any degradation/sorption between original extractions (PPL: 05/2018; WAX: 06/2019) and recovery experiments (11/2019-12/2019). Whole leachates were filtered again, spiked as applicable, and acidified as described in the article methods. WAX spikes (acesulfame potassium) were approximately 1500 µg/L for the *Active* sample and 50 µg/L for the *Closed* sample. PPL spikes (other CECs) were chosen to be approximately 100 µg/L for non-detect measurements or measurements at <50 µg/L, or 1000 µg/L for all other measurements. All spikes were within calibration curves at the same dilution levels as the original quantification. The same cartridge types were

used for the equivalent recovery experiments and all extraction steps remained the same.

Table A4.11 Loaded sample volumes for CEC recovery experiments. All PPL cartridges were eluted with 10 mL MeOH. All WAX cartridges were eluted with 3 mL of the NH_4OH MeOH solution.

Extraction	**Loaded Sample Volume (mL)**		
	1	**2**	**3**
PPL			
Active	10	10	10
Closed	10	10	10
Active-spike	10	10	10
Closed-spike	10	10	10
WAX			
Active	2	2	2
Closed	3	3	3
Active-spike	2	2	2
Closed-spike	3	3	3

Table A4.12 Measured CEC recoveries calculated as % of spike addition detected over base level.

CEC	**SPE Recovery (%)**					
	Active			**Closed**		
	1	2	3	1	2	3
PPL						
acetaminophen	104	119	120	118	130	121
carbamazepine	102	113	113	115	127	117
cotinine	102	114	111	108	126	112
ibuprofen	99	113	112	107	118	108
methylparaben	91	127	104	111	141	122
propylparaben	92	110	108	121	141	117
paraxanthine	101	116	112	110	122	115
sucralose	109	122	107	159	150	139
sulfamethoxazole	67	76	74	25	30	26
triclosan	42	50	38	44	46	45
WAX						
acesulfame potassium	76	91	84	80	105	78

Detection Limits for CECs

Table A4.13 Approximate LOD is the lowest standard included in the quantification standard curve. Approximate matrix detection limits were calculated as [concentration of lowest standard curve level (µg/L) × maximum LLOM dilution factor] ÷ [minimum measured recovery (%)/100]. Measured recoveries >100% were considered as 100%.

CEC	~Limit of Detection (µg/L)	~Matrix Detection Limit (µg/L)
acesulfame potassium	0.125	5.7
acetaminophen	0.25	8.7
carbamazepine	0.05	1.7
cotinine	0.05	1.7
ibuprofen	0.075	2.6
methylparaben	2	76.4
propylparaben	0.45	17.0
paraxanthine	0.55	19.1
sucralose	3	104.3
sulfamethoxazole	0.06	8.3
triclosan	0.125	11.4

Text A4.4 ICP-MS Method

The acidification of samples resulted in precipitation of organic matter that would interfere with analysis. As a result, the samples required stronger digestion before analysis. This was done using a Milestone EOTHO-EZ microwave. 20 mL quartz reaction vessels were placed inside Teflon cups, which pressure seal during digestion. For this digestion the 2 mL of sample was placed in the quartz vessel with 2 mL of concentrated ultrapure nitric acid and 6 mL of ultrapure water. 5 mL of 30% hydrogen peroxide was added to the Teflon cup along with 5 mL of ultrapure water, and the cup was sealed. The samples were heated to 180 °C and allowed to reflux for 15 minutes then diluted to 10 mL with ultrapure water. These were diluted and analyzed for trace elements. For analysis of the SPEs, 1 mL of extract was placed in a glass vial and evaporated to dryness. 2 mL of nitric acid was added to the vial and swirled, capped, and left for 24 hrs. 8 mL of ultrapure water was added to the vial, and the sample was further diluted prior to analysis.

The standards used for ICP-MS analysis were made from Multi-Element Solution 2A (Spex CertiPrep) and the internal standard used was ICP-MS Alternate Internal Standard 1 (Spex CertiPrep), containing ^{6}Li, Sc, Ge, Y, In, Tb, and Bi. The ICP-MS used was an Agilent 7500C. All elements except Cd and Pb were measured using helium in the collision cell in order to reduce interferences. Detection limits for each element are listed in parentheses: Mn (0.1), Fe (0.5), Cd (0.01), Pb (0.01), V (0.04),

Cr (0.03), Cu (0.02), Zn (3.9), As (0.04) in ug/L. All samples were spiked with standard to test recoveries by standard addition. Recoveries ranged from 92 to 100%.

Text A4.5 EA-IRMS Method

Standards were acetanilide and bass protein lab standards calibrated against USGS40 and USGS41a (Reston Stable Isotope Laboratory). Molar C/N is from the higher volume, $\delta^{15}N$ analysis.

Text A4.6 Excitation-Emission Matrices

Dilution factors of 1:420, 1:110, and 1:130 were used for the *Active*, *Closed*, and *Closed-Brine* LL samples respectively. Raman, first-order Rayleigh, and second-order Rayleigh scatter was corrected and EEMs were smoothed. Values have been corrected for dilution and fluorescence was converted to QSU using a 1 mg/L quinine sulfate reference standard (Starna).

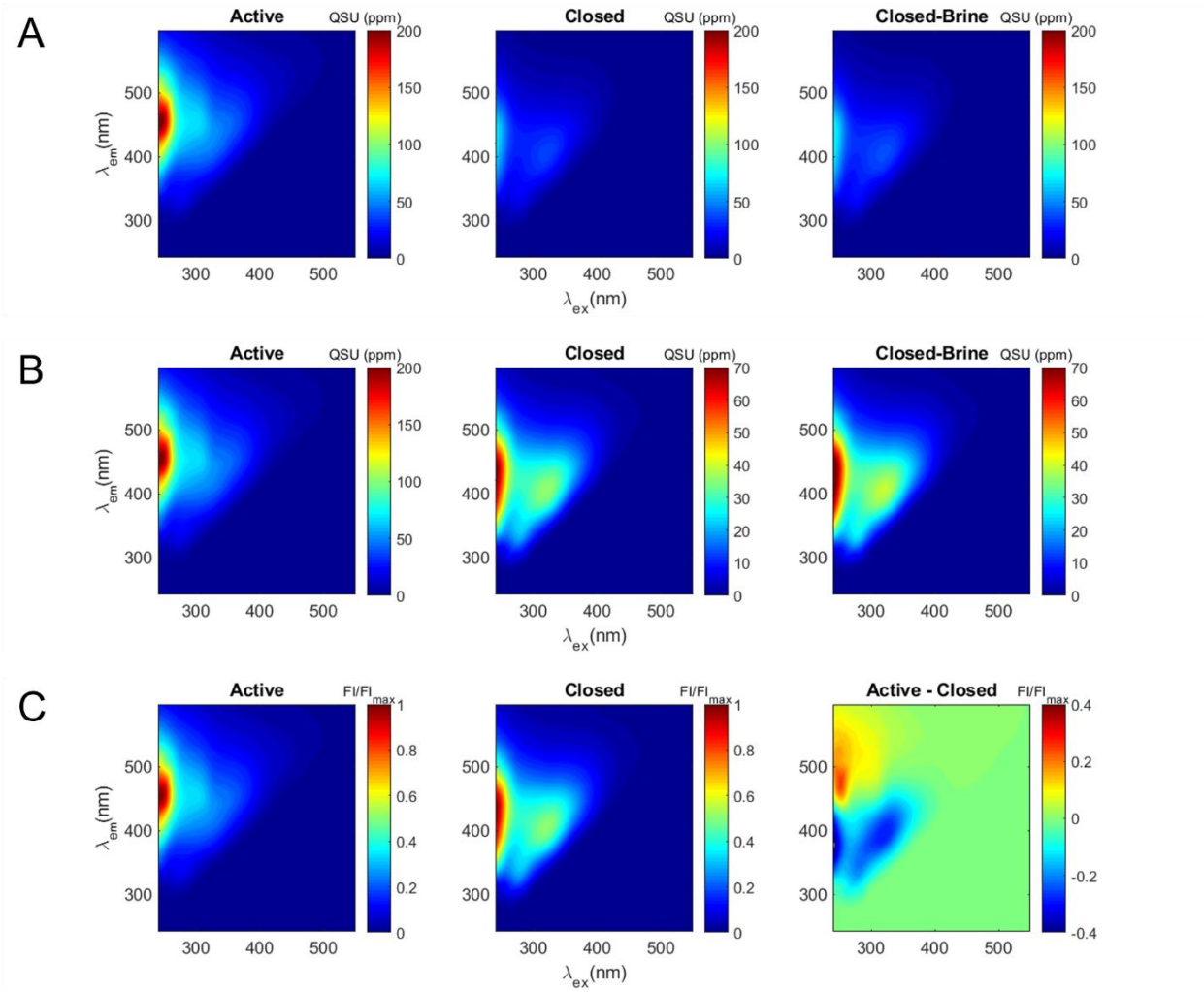

Figure A4.1 Fluorescence EEMs of *Active*, *Closed*, and *Closed-Brine* LL samples on the same fluorescence scale (A). Fluorescence EEMs of *Active*, *Closed*, and *Closed-Brine* LL samples on separate fluorescence scales (B). Fluorescence normalized to max fluorescence for the Active and Closed LL samples and normalized Active LL subtracting normalized Closed LL (C).

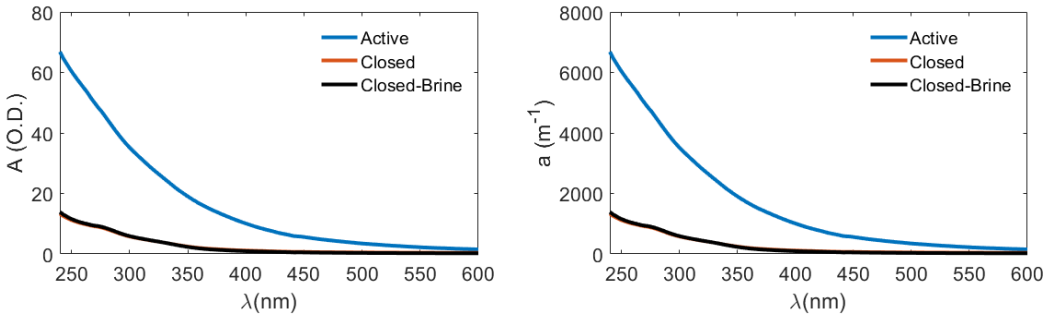

Figure A4.2 Raw absorbance as optical density (left) and absorbance as decadic absorption coefficient (right).

Table A4.14 Optical parameters where S is spectral slope(Twardowski et al., 2004) between the stated wavelengths, S_R is spectral slope ratio as ($S_{275-295}/S_{350-400}$), A_{254} is raw absorbance at 254 nm, Dec. a_{254} is decadic absorption coefficient at 254 nm, and $SUVA_{254}$ is the specific UV absorbance at 254 nm (Weishaar et al., 2003).

Parameter	Active	Closed	Closed-Brine
$S_{300-600}$ (nm^{-1})	0.011	0.009	0.011
$S_{275-295}$ (nm^{-1})	0.012	0.017	0.017
$S_{350-400}$ (nm^{-1})	0.013	0.015	0.018
S_R	0.971	1.138	0.978
A_{254} (O.D.)	58.219	10.639	10.953
Dec. a_{254} (m^{-1})	5821.918	1063.878	1095.266
$SUVA_{254}$ ($L\ mg^{-1}\ m^{-1}$)	5.577	1.976	1.671

Text A4.7 Quantification of DOC, TDN, Cl^-, NO_3^--NO_2^-, and NH_4^+/NH_3

All LL samples were diluted at a 1:40 dilution factor before analyses and reported values were corrected for this. Carbon standard for DOC was potassium hydrogen phthalate (Sigma-Aldrich, ≥99.5% purity). Nitrogen standard for TDN was potassium nitrate (Acros Organics, ≥99% purity). Blanks, standards, and samples were all acidified to pH 2 with pure grade HCl before DOC and TDN analyses. Other analytes run by Nutrient Analytical Services Laboratory, Chesapeake Biological Laboratory (MD, USA). For NO_3^--NO_2^- the given method reporting limit/method detection limit was 0.028/0.0057 mg N/L or approximately 1.12/0.228 mg N/L when considering the 1:40 dilution factors.

Text A4.8 Multiple Formula Assignments for FT-ICR-MS Data

NetCalc uses a network assignment approach that does not allow for multiple formula assignments for the same *m/z* ion, but because network assignments were done individually by sample there was some possibility of multiply assigned ions. Thirty-four ions were doubly assigned across samples, twenty-one of which fell under the final 600 *m/z* cutoff. No ions were triply assigned. For most of these the clear, more likely, formula assignments based on mass error, isotopic patterns, and fewer heteroatoms were chosen, but a common mass overlap was found between the $CHON_2Cl_1$ and $CHOS_1$ formulas. This is caused by the similarity of H_3O_4S (98.9757529) vs C_3N_2Cl (98.9755493). For this reason, the final dataset has N_1Cl_1 and N_3Cl_1 formula assignments in the CHONCl class, but N_2Cl_1 assignments were removed. Evidence against the N_2Cl_1 assignments was that higher signal intensity ions assigned as this type did not have ^{37}Cl isotopic peaks when expected with no obvious overlap to obscure the isotopic peaks. This evidence favors the CHOS assignments in cases of multiple formula assignments. Logically, some $CHON_2Cl_1$ formulas must be present for the existence of $CHON_3Cl_1$, but the lower intensity N_2Cl_1 assignments that did not belong to multiply assigned ions, though plausible, were removed because they could not be verified from their corresponding possible CHOS assignments. This overlap did not seem to continue to the N_3Cl_1 assignments,

where a mass overlap of $CHON_1S_1$ with $CHON_3Cl_1$ might be expected. The high intensity N_3Cl_1 peaks had corresponding ^{37}Cl isotopic peaks at expected ratios.

Text A4.9 Formula Protocols

Final formula assignments have only positive, integer DBEs and do not violate the nitrogen rule. All 2- and 4-N assignments correspond to even integer neutral masses, and all 1- and 3-N assignments correspond to odd integer neutral masses. All assignments containing only C, H, O, S, P, or halogens correspond to even integer neutral masses. Final formula assignments all have O/C≤1 and ≥0.05, H/C>0.3, N/C ≤ 1, H≤(2C+2+N), and O≤(C+2), following commonly used filtering protocols (Koch et al., 2007; Herzsprung et al., 2014). Final formula assignment N/C is between 0-0.3.

m/z Decimal vs. m/z Plots

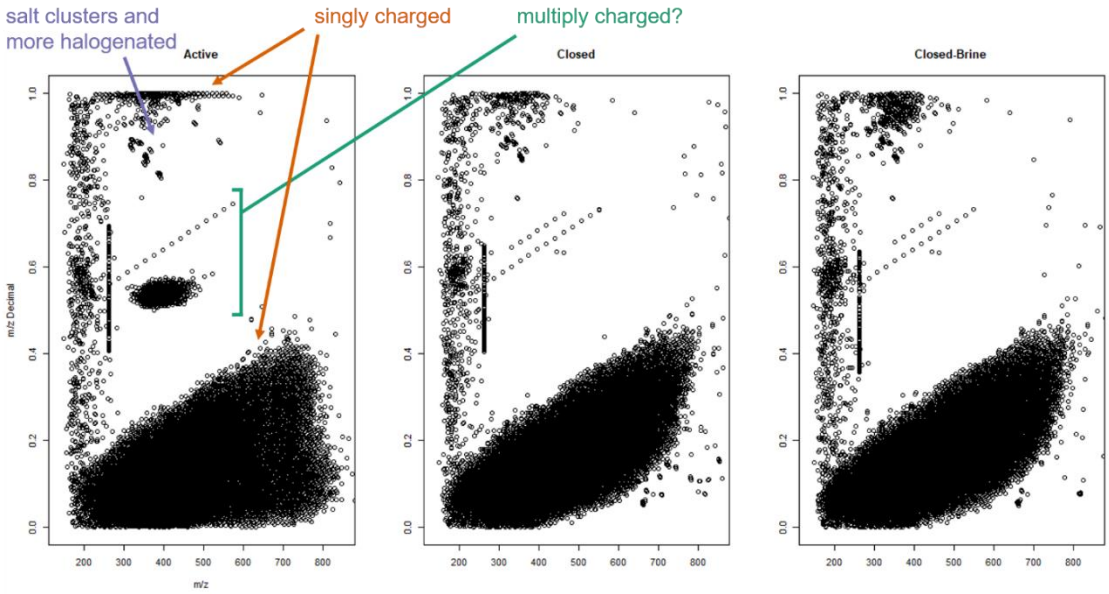

Figure A4.3 *Active*, *Closed*, and *Closed-Brine m/z* decimal vs. *m/z* plots, following McMillan et al. (2016), made using unassigned, signal intensity averaged data matrix, including ions not measured in all triplicates. The multiply charged cluster distinct to the *Active* LL sample appears to be doubly charged ions corresponding to the one ^{13}C isotopic peak of a group of >600 *m/z*, singly charged, CHO ions. Doubly charged ions of the singly charged, monoisotopic peaks are also present but have mass decimals within the singly charged window, so are not distinguishable in the figure. The singly charged formulas believed to correspond are approximately 0.75 H/C, 0.5 O/C, and have low *m/z* decimals. This group, and the high mass, low *m/z* decimal region of ions in the Active LL sample in general, should be a subject of further study. The linear homologous series in the "multiply charged" decimal region, one in the *Active* LL and two in the *Closed* and *Closed-Brine* LL samples, have 22.0131 *m/z* spacing patterns, and we believe these are doubly charged ethylene oxide (44.0262 *m/z*, CH_2CH_2O) series. The small *m/z* spaced linear series in the "singly charged"/"salt clusters and more halogenated" region are 1.9970 *m/z*, Cl and 1.9980 *m/z*, Br isotopic patterns and

are highly substituted organohalogens. Highly fluorinated, singly charged ions also plot in this region. The vertical, linear feature at approximately 262.5 *m/z* is a known instrument artifact.

185.0278 and 417.2283 m/z Ion Peaks

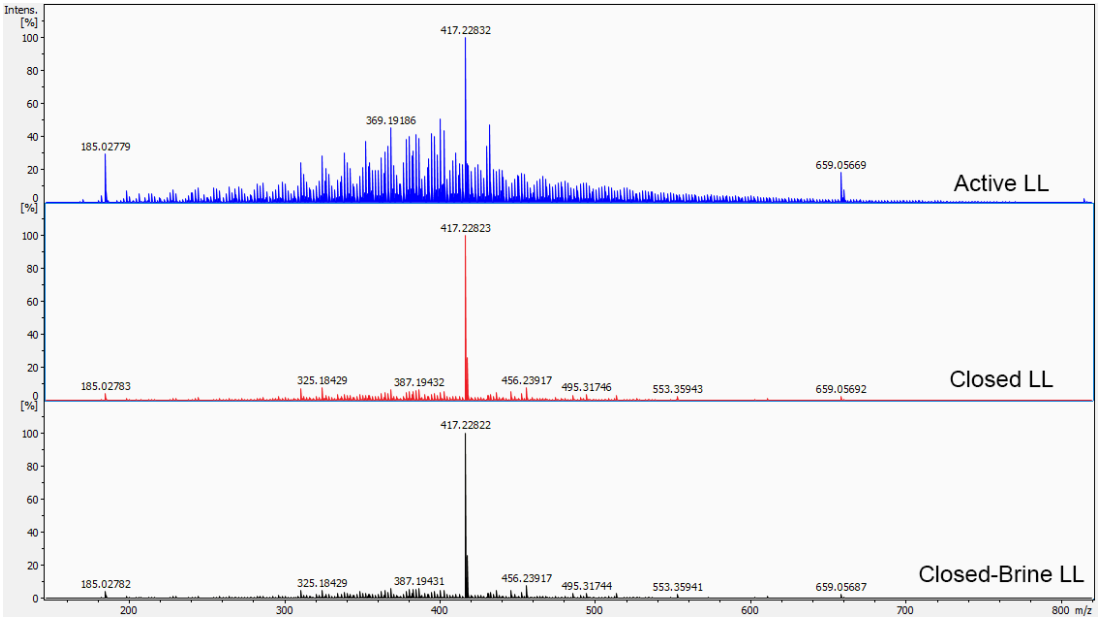

Figure A4.4 Full spectra of representative LL samples showing 185.0278 and 417.2283 *m/z* ion peaks. Relative intensity is as % of the base peak.

58.0419 m/z and 22.0131 m/z Spacing Patterns

Table A4.15 Signal intensity data in arbitrary units from the unprocessed data matrix showing the 58.0419 *m/z* spacing pattern seen in LLOM Van Krevelen diagrams at H/C = 2. We believe this spacing represents propylene oxide [$CH_2CH(CH_3)O$] units. Formula assignments and mass error are given, but not every ion in the series was included in the final dataset due to mass cutoffs. Molecular characterization is non-structural, but the formulas in the series, interestingly, are the same as known monocarboxylated polypropylene glycols that Rogers et al. (2019) identified as polypropylene glycol degradation products. Further analyses are needed for any actual structural identification, but future studies could explore this.

m/z (avg.)	Neutral Mass (Da)	Closed 3	Closed 2	Closed 1	Closed-Brine 3	Closed-Brine 2	Closed-Brine 1	Active 3	Active 2	Active 1	Formula	Error (ppm)
205.10814	206.11541	67852216	65962500	68244320	69225376	68378296	67495024	23479682	23104544	25695702	$C_9H_{18}O_5$	0.07
263.15001	264.15729	78334232	75619512	93037392	95281320	88424872	92152440	49800188	46577104	58985840	$C_{12}H_{24}O_6$	0.01
321.19189	322.19916	217510032	211008576	231359136	233065872	223496000	232897472	106577056	99940696	111281664	$C_{15}H_{30}O_7$	0.03
379.23367	380.24095	420118784	396005152	448960256	445561536	420853760	451843168	161805904	148984256	178470960	$C_{18}H_{36}O_8$	0.19
437.27568	438.28296	418919328	396441472	456347008	458718336	444891424	467750496	132004032	116536720	147835056	$C_{21}H_{42}O_9$	0.16
495.31744	496.32472	310886080	297842592	328262144	323221728	319677920	334547712	88002848	72415800	97085112	$C_{24}H_{48}O_{10}$	0.06
553.35942	554.36669	212087952	202552688	240801792	236346240	229916672	236014592	46482152	43017660	50360172	$C_{27}H_{54}O_{11}$	0.14
611.40138	612.40866	116858752	111321088	130495520	127251968	123022832	130500272	22242016	18790498	25594906	$C_{30}H_{60}O_{12}$	0.29
669.44314	670.45041	51338496	46461144	54713220	52598912	53124616	58302560	8270220	7349626	9907421	$C_{33}H_{66}O_{13}$	0.10
727.48504	728.49231	17387626	14427860	17451072	16323350	16705752	17150874	3967939	3404953	5245720	$C_{36}H_{72}O_{14}$	0.14
785.52718	786.53445	3048311	3257178	4668662	3727650	3785597	4303722	0	0	0	$C_{39}H_{78}O_{15}$	0.48

Table A4.16 Signal intensity data in arbitrary units from the unprocessed data matrix showing the 22.0131 *m/z* spacing pattern seen in *m/z* decimal vs. *m/z* plots. We believe these are doubly charged ions and the corresponding singly charged *m/z* spacing would be 44.0262 *m/z*, likely ethylene oxide (CH_2CH_2O) units. We believe "Series 1" could be doubly charged CHON ions, where the 242.548 *m/z* ion would be doubly deprotonated $C_{23}H_{21}NO_{11}$, with the other series formulas following the $+C_2H_4O$ pattern. "Series 2" could be doubly charged, one ^{13}C ions, where the 330.644 *m/z* ion would be doubly deprotonated $^{12}C_{26}{}^{13}CH_{50}O_{18}$, with the other series formulas following the $+{}^{12}C_2H_4O$ pattern. These assignments have reasonable mass error, as the average mass error is 0.5 ppm for the "Series 1" assignments and 0.1 ppm for the "Series 2" assignments. This is our current best, but preliminary, understanding based on corresponding singly charged formula assignments and *m/z* ions for "Series 1" and corresponding singly charged *m/z* ions; doubly charged, monoisotopic *m/z* ions; and singly charged, monoisotopic *m/z* ions for "Series 2".

m/z (avg.)	Closed 3	Closed 2	Closed 1	Closed-Brine 3	Closed-Brine 2	Closed-Brine 1	Active 3	Active 2	Active 1
Series 1									
242.54816	0	0	0	0	0	2137647	0	1694626	0
264.56135	0	0	0	0	0	2110252	0	2033392	0
286.57448	2358242	2650029	0	2663982	2908474	2534715	2956017	2806082	2625640
308.58757	4507414	5163214	4841418	4062526	5317520	4873693	4672188	4565506	5560497
330.60064	7209036	7536954	7852868	8073698	8189627	9290743	7651678	8288083	7827040
352.61374	10068126	9614192	9587009	11400531	10775060	11161236	10922593	12142078	11343610
374.62690	12667240	10007515	10942243	11731192	11023662	11531185	13134411	16126356	13704150
396.64000	14766681	12881492	12955909	13931315	13184135	14342559	17770594	19670432	17849336
418.65312	14046840	11419255	12768891	14112148	11387536	13590834	14567060	16772714	16280733
440.66623	13028552	11515873	13829915	15740329	14258615	14393151	16895696	20370492	17567490
462.67933	9698504	10117837	9706141	11164203	10637038	12126784	14497692	16537918	15346020
484.69242	9113498	6687133	9171263	9268702	8757239	9950836	11911092	13250079	12991395
506.70562	7574209	5871404	6445912	7678060	7550081	6824286	10408285	11422973	10398072
528.71871	5395387	4756049	5284161	6012281	6783027	5951607	8298198	9072633	8691347
550.73188	0	0	3919683	3900163	4446978	3886463	6333157	7289357	5852649
572.74491	0	0	0	0	0	0	4271517	4767705	4157758
Series 2									
330.64426	0	2626405	0	0	0	0	0	0	0
352.65736	5009094	4861336	4851562	3398529	3892802	4753086	0	0	0
374.67043	8469902	7820289	6251338	6892836	4739420	5609434	0	0	0
396.68361	8068733	8753782	8491305	6395739	6042802	6216133	0	0	0
418.69675	7052953	7635606	7637662	5971383	4476084	6839636	0	0	0
440.70982	6272230	6885373	7344954	5172679	4746706	6132572	0	0	0
462.72297	4393187	4553446	4341946	0	0	3995736	0	0	0

Formula Distributions

Table A4.17 Numbers of formulas in formula classes in molecular characterization of LL and comparison to SRNOM. A conservative approach was used for SRNOM formula assignment filtering for comparison purposes.

	Active LL	**Closed LL**	**Closed-Brine LL**	**SRNOM**
CHO	2547	2362	2392	2925
CHON	2688	3307	3295	1439
CHOS	1161	1213	1253	255
CHONS	592	1072	1072	14
CHOCl	674	830	863	136
CHONCl	90	206	215	7
CHOSCl	10	30	33	14
CHONSCl	1	12	13	0
CHOF	3	3	3	0
CHOFS	2	3	3	0
CHOBr	0	1	1	0
CHOP	0	0	0	50
CHONP	0	0	0	21
CHOSP	0	0	0	1
Total	**7768**	**9039**	**9143**	**4862**

Table A4.18 Number and percent of unique formulas for the *Active* LL, *Closed* LL, *Closed-Brine* LL, and *Closed* and *Closed-Brine* LLs combined.

	Active LL	**Closed LL**	**Closed-Brine LL**	**Closed and Closed-Brine LLs**
Unique	857 (11.0%)	220 (2.4%)	297 (3.2%)	2516 (26.7%)
Total	**7768**	**9039**	**9143**	**9427**

Other Halogenated Formula Classes

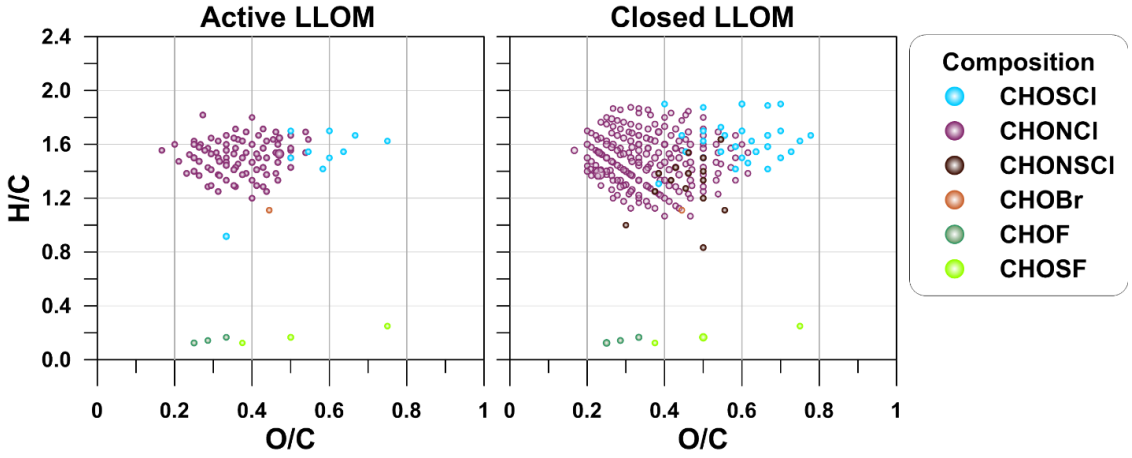

Figure A4.5 Van Krevelen diagrams of other halogenated formula assignments in the *Active* and *Closed* LL samples. Point size corresponds to signal intensity.

Additional Van Krevelen Diagrams

Van Krevelen plotting in this section was done with the R package ggplot2 (Wickham, 2016).

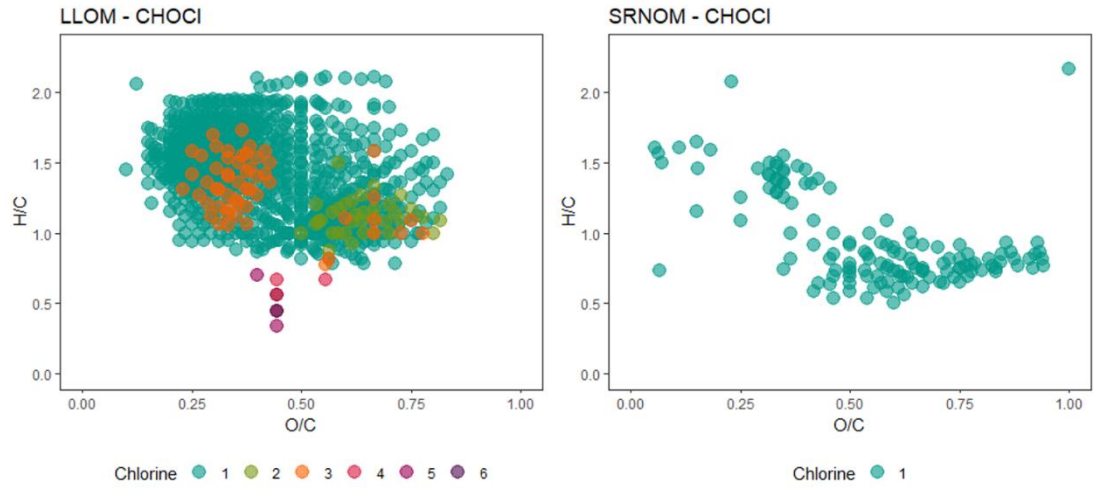

Figure A4.6 Van Krevelen diagrams of CHOCl formula assignments for LLOM (across all samples) and SRNOM.

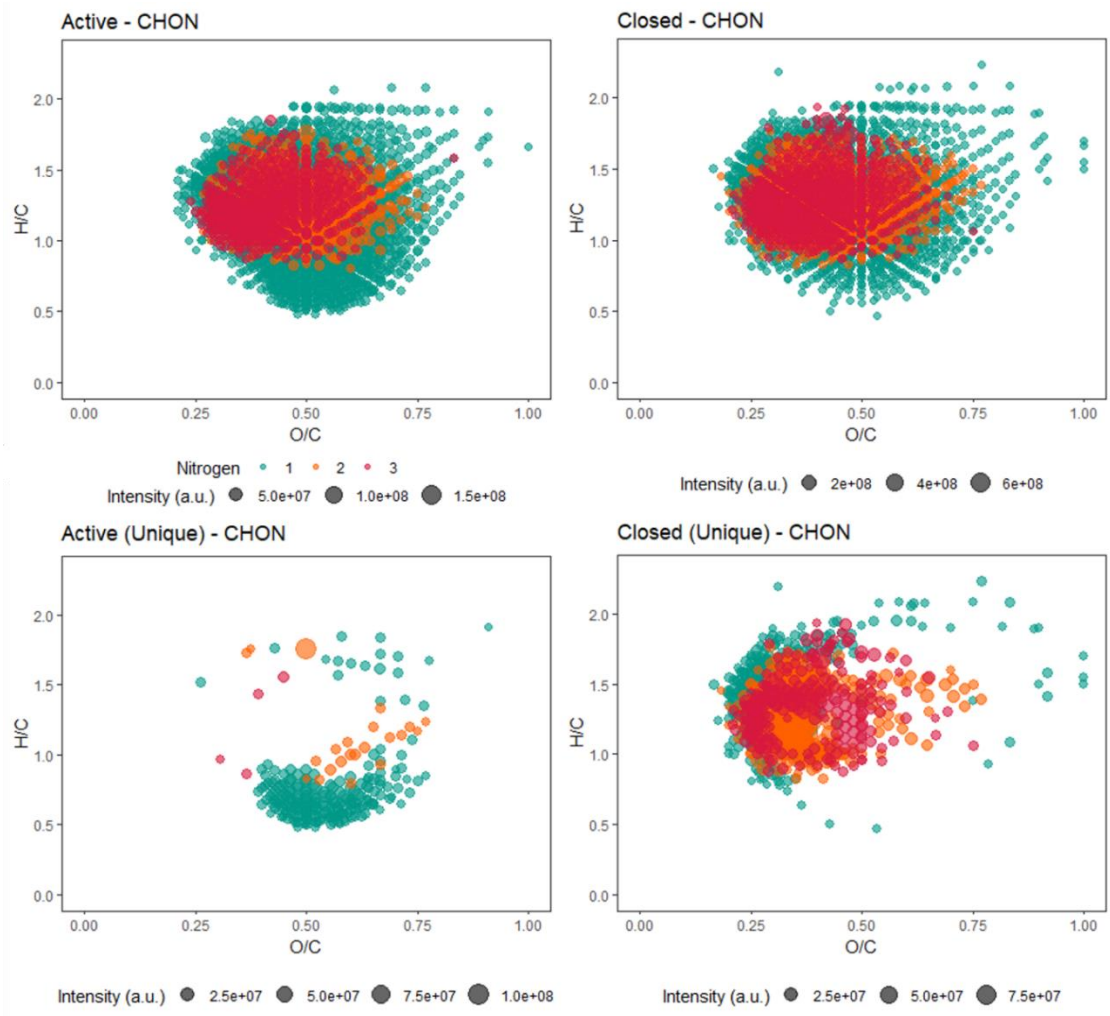

Figure A4.7 Van Krevelen diagrams of CHON and unique CHON formula assignments for *Active* and *Closed* LL by nitrogen number.

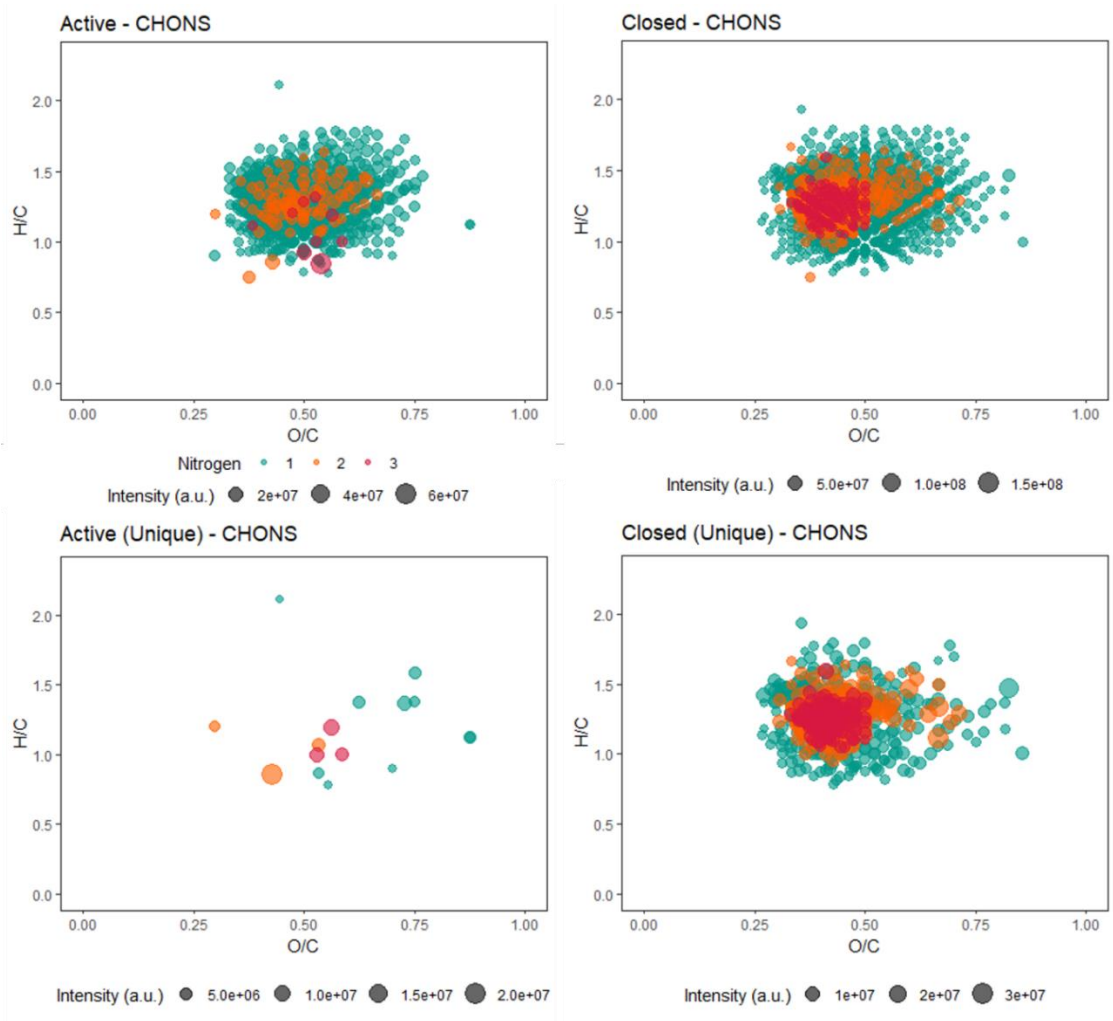

Figure A4.8 Van Krevelen diagrams of CHONS and unique CHONS formula assignments for *Active* and *Closed* LL by nitrogen number.

$C_9H_4Cl_6O_4$ and Similar Formula Organohalogens

Table A4.19 Signal intensity data in arbitrary units from the unprocessed data matrix to show isotopic patterns which were checked for assignment accuracy with the web interface by Loos et al. (2015). Formulas are protonated, as assigned in the dataset, assuming deprotonated, singly charged, $[M-H]^-$ ions. Isotopic composition is as assigned for ions.

$C_9H_9Cl_3O_4$

m/z (avg.)	Closed 3	Closed 2	Closed 1	Closed-Brine 3	Closed-Brine 2	Closed-Brine 1	Active 3	Active 2	Active 1	C12	C13	H	O	Cl35	Cl37	Br79	Br81	Mass Diff (Da)	Error (ppm)
280.91807	3985300	3851287	3891356	4120565	3842625	4375238	0	0	0	9	0	4	4	3	0	0	0	0.00001	0.03
282.91514	3262054	4355118	4016057	3876463	4212346	4063399	0	0	0	9	0	4	4	2	1	0	0	0.00003	0.10

$C_9H_7Cl_3O_5$

m/z (avg.)	Closed 3	Closed 2	Closed 1	Closed-Brine 3	Closed-Brine 2	Closed-Brine 1	Active 3	Active 2	Active 1	C12	C13	H	O	Cl35	Cl37	Br79	Br81	Mass Diff (Da)	Error (ppm)
298.92865	10481598	8125932	10231619	9990851	9543553	9437780	0	2568901	2213272	9	0	6	5	3	0	0	0	0.00002	0.06
300.92569	10517500	9679995	8984515	10262485	9240647	10791580	0	0	2330363	9	0	6	5	2	1	0	0	0.00001	0.05
302.92270	3715628	3172860	3006770	3580124	3799554	2809813	0	0	0	9	0	6	5	1	2	0	0	-0.00003	0.10

$C_9H_4Cl_4O_4$

m/z (avg.)	Closed 3	Closed 2	Closed 1	Closed-Brine 3	Closed-Brine 2	Closed-Brine 1	Active 3	Active 2	Active 1	C12	C13	H	O	Cl35	Cl37	Br79	Br81	Mass Diff (Da)	Error (ppm)
314.87910	6538760	6555325	5887345	5892620	6122628	7023354	13149028	14955918	13081876	9	0	3	4	4	0	0	0	0.00001	0.03
316.87611	10256344	9367260	9269624	9900747	8449282	9255643	19642516	20452948	18035244	9	0	3	4	3	1	0	0	-0.00003	0.10
317.87960	0	0	0	0	0	0	0	2584766	0	8	1	3	4	3	1	0	0	0.00010	0.32
318.87316	4326812	5260013	3947890	4714880	4128121	5648049	9888208	10915614	9386835	9	0	3	4	2	2	0	0	-0.00004	0.11
320.87017	0	0	0	0	0	0	0	0	2399367	9	0	3	4	1	3	0	0	-0.00007	0.23

$C_9H_9Cl_3O_6$

m/z (avg.)	Closed 3	Closed 2	Closed 1	Closed-Brine 3	Closed-Brine 2	Closed-Brine 1	Active 3	Active 2	Active 1	C12	C13	H	O	Cl35	Cl37	Br79	Br81	Mass Diff (Da)	Error (ppm)
316.93918	11838487	10074909	11366841	11792145	11863366	10632986	0	0	0	9	0	8	6	3	0	0	0	-0.00001	0.05
318.93623	11829211	10418989	10848690	11509702	11600317	11419376	0	0	0	9	0	8	6	2	1	0	0	-0.00001	0.05
320.93324	4611474	3385904	4231070	4112497	3961902	4329660	0	0	0	9	0	8	6	1	2	0	0	-0.00005	0.17

$C_9H_6Cl_4O_4$

m/z (avg.)	Closed 3	Closed 2	Closed 1	Closed-Brine 3	Closed-Brine 2	Closed-Brine 1	Active 3	Active 2	Active 1	C12	C13	H	O	Cl35	Cl37	Br79	Br81	Mass Diff (Da)	Error (ppm)
316.89477	56926188	48524016	52789644	56023776	52638996	56642284	3473066	3859049	2731331	9	0	5	4	4	0	0	0	0.00003	0.10
317.89812	5349331	5113598	5254031	5772097	5601624	6618847	0	0	0	8	1	5	4	4	0	0	0	0.00002	0.07
318.89180	80717744	69546752	76306824	78332824	76635536	78467776	4499431	4705587	4613993	9	0	5	4	3	1	0	0	0.00001	0.02
319.89510	8127377	6631688	8243586	8113137	7772619	7899823	0	0	0	8	1	5	4	3	1	0	0	-0.00005	0.16
320.88884	38444904	32160514	39170416	38825024	36759036	39758480	2367282	2847492	2762141	9	0	5	4	2	2	0	0	0.00000	0.01
321.89215	3491650	3096836	3643239	4313751	4437561	4313206	0	0	0	8	1	5	4	2	2	0	0	-0.00005	0.16
322.88586	8847122	6451960	8833360	8836321	8754792	8391249	0	0	0	9	0	5	4	1	3	0	0	-0.00004	0.11

$C_9H_9Cl_3O_7$

m/z (avg.)	Closed 3	Closed 2	Closed 1	Closed-Brine 3	Closed-Brine 2	Closed-Brine 1	Active 3	Active 2	Active 1	C12	C13	H	O	Cl35	Cl37	Br79	Br81	Mass Diff (Da)	Error (ppm)
332.93405	5216003	4694586	4375088	5806020	4147830	4799704	0	0	0	9	0	8	7	3	0	0	0	-0.00006	0.18
334.93111	5246575	4190687	4371911	4680239	5135046	4319850	0	0	0	9	0	8	7	2	1	0	0	-0.00005	0.14

$C_9H_6Cl_4O_5$

m/z (avg.)	Closed 3	Closed 2	Closed 1	Closed-Brine 3	Closed-Brine 2	Closed-Brine 1	Active 3	Active 2	Active 1	C12	C13	H	O	Cl35	Cl37	Br79	Br81	Mass Diff (Da)	Error (ppm)
332.88963	11805913	10458638	11357189	12601235	10684486	13691052	7118982	7376299	8094067	9	0	5	5	4	0	0	0	-0.00003	0.09
334.88674	15092804	12705204	14290844	15947775	15454358	15259710	8186459	10689214	9148213	9	0	5	5	3	1	0	0	0.00003	0.08
336.88370	9974694	7912781	7239464	9080929	9112803	8759242	4537928	5748703	5271315	9	0	5	5	2	2	0	0	-0.00006	0.18
338.88075	0	0	2683818	0	0	0	0	0	0	9	0	5	5	1	3	0	0	-0.00006	0.17

$C_9H_{10}Br_2O_4$

m/z (avg.)	Closed 3	Closed 2	Closed 1	Closed-Brine 3	Closed-Brine 2	Closed-Brine 1	Active 3	Active 2	Active 1	C12	C13	H	O	Cl35	Cl37	Br79	Br81	Mass Diff (Da)	Error (ppm)
338.88729	3887877	4702944	5537456	3975363	3346997	3294038	3701335	0	3384852	9	0	9	4	0	0	2	0	-0.00001	0.04
340.88521	10695253	11153504	10827304	7484694	7052670	8645335	6999162	4932181	7143723	9	0	9	4	0	0	1	1	-0.00005	0.15
342.88317	5425053	4961237	4333975	3499105	3771846	4789332	3960506	2737572	2967264	9	0	9	4	0	0	0	2	-0.00004	0.12

$C_9H_3Cl_5O_4$

m/z (avg.)	Closed 3	Closed 2	Closed 1	Closed-Brine 3	Closed-Brine 2	Closed-Brine 1	Active 3	Active 2	Active 1	C12	C13	H	O	Cl35	Cl37	Br79	Br81	Mass Diff (Da)	Error (ppm)
348.84014	0	0	0	0	0	0	4845053	5195726	4588691	9	0	2	4	5	0	0	0	0.00002	0.07
350.83718	0	0	0	0	0	0	7434424	8618341	7570767	9	0	2	4	4	1	0	0	0.00001	0.03
352.83425	0	0	0	0	0	0	4698006	5946128	5804080	9	0	2	4	3	2	0	0	0.00003	0.08

$C_9H_5Cl_5O_4$

m/z (avg.)	Closed 3	Closed 2	Closed 1	Closed-Brine 3	Closed-Brine 2	Closed-Brine 1	Active 3	Active 2	Active 1	C12	C13	H	O	Cl35	Cl37	Br79	Br81	Mass Diff (Da)	Error (ppm)
350.85571	150281824	128199960	147944160	159746608	149979856	155413520	207147216	246137216	228317552	9	0	4	4	5	0	0	0	-0.00006	0.16
351.85913	12636653	12499127	14061188	14104128	14094068	14645191	18671172	23060052	20952794	8	1	4	4	5	0	0	0	0.00000	0.01
352.85277	249308528	211629136	249379360	266392144	245418768	260387696	364338080	423447328	404317248	9	0	4	4	4	1	0	0	-0.00005	0.14
353.85618	22106378	18876392	21843392	23940704	21688122	22656816	31154484	35414028	32168400	8	1	4	4	4	1	0	0	0.00001	0.02
354.84990	150006928	128826232	150503760	159898208	146346848	150371040	207939248	244897008	225603408	9	0	4	4	3	2	0	0	0.00003	0.07
355.85324	15706143	11966219	15109364	15554168	13758338	14714520	20343880	24922584	23598316	8	1	4	4	3	2	0	0	0.00002	0.05
356.84696	49853348	40370836	47585416	52527740	48831396	51823176	70734296	80707264	75881088	9	0	4	4	2	3	0	0	0.00004	0.12
357.85029	5063982	3995683	5292576	5753481	5059533	5263871	6960002	8023994	7440434	8	1	4	4	2	3	0	0	0.00002	0.05
358.84396	9794223	7189926	8392622	9565834	8208365	8398253	12299557	14311598	13217244	9	0	4	4	1	4	0	0	-0.00001	0.04

$C_{10}H_7Cl_5O_4$

m/z (avg.)	Closed 3	Closed 2	Closed 1	Closed-Brine 3	Closed-Brine 2	Closed-Brine 1	Active 3	Active 2	Active 1	C12	C13	H	O	Cl35	Cl37	Br79	Br81	Mass Diff (Da)	Error (ppm)
364.87143	4084683	3920564	5210904	4254887	3939569	4197364	4370947	5249824	5811446	10	0	6	4	5	0	0	0	0.00001	0.03
366.86853	6222523	6903189	7603232	6744723	7333176	6851407	7794633	8107353	8753366	10	0	6	4	4	1	0	0	0.00006	0.16
368.86558	4563876	4435051	5322016	4977781	4635514	4544677	4509094	6303650	6233296	10	0	6	4	3	2	0	0	0.00006	0.16

$C_9H_4Cl_6O_4$

m/z (avg.)	Closed 3	Closed 2	Closed 1	Closed-Brine 3	Closed-Brine 2	Closed-Brine 1	Active 3	Active 2	Active 1	C12	C13	H	O	Cl35	Cl37	Br79	Br81	Mass Diff (Da)	Error (ppm)
384.81688	0	0	0	0	0	0	20744306	23863094	21859032	9	0	3	4	6	0	0	0	0.00008	0.20
386.81388	0	0	0	0	0	0	38241448	46660036	45428544	9	0	3	4	5	1	0	0	0.00003	0.07
387.81722	0	0	0	0	0	0	3354828	4476178	3676026	8	1	3	4	5	1	0	0	0.00002	0.04
388.81085	0	0	0	0	0	0	30613726	38577236	35806116	9	0	3	4	4	2	0	0	-0.00005	0.12
389.81422	0	0	0	0	0	0	3244797	3317665	4751326	8	1	3	4	4	2	0	0	-0.00004	0.09
390.80797	0	0	0	0	0	0	13559051	17024736	16363526	9	0	3	4	3	3	0	0	0.00002	0.06
392.80509	0	0	0	0	0	0	3765553	4660589	4188256	9	0	3	4	2	4	0	0	0.00010	0.24

Table A4.20 Averaged signal intensity data in arbitrary units for the most abundant isotopic peak corresponding to the formula. Formulas are ordered from lowest (left) to highest (right) *m/z*. We believe that $C_9H_5Cl_3O_4$, $C_9H_4Cl_4O_4$, and $C_9H_3Cl_5O_4$ may not be present in the samples and are instead misidentified $[M-HCl-H]^-$ in-source fragmentation products of $C_9H_6Cl_4O_4$, $C_9H_5Cl_5O_4$, and $C_9H_4Cl_6O_4$. These signals theorized to correspond based on signal correlation and in MS behavior are highlighted by color, with the darker shaded title believed to be the false assignment. Removing likely misidentified, in-source fragmentation products, lower *m/z* formulas within the suite generally had higher signal intensity or were only identified in the *Closed* and *Closed-Brine* LL samples.

Sample	C9H5Cl3O4	C9H7Cl3O5	C9H4Cl4O4	C9H9Cl3O6	C9H6Cl4O4	C9H9Cl3O7	C9H6Cl4O5	C9H10Br2O4	C9H3Cl5O4	C9H5Cl5O4	C10H7Cl5O4	C9H4Cl6O4
Active	0	1594058	19376903	0	4606337	0	9341295	2362062	7874511	397367552	8218451	43443343
Closed	3909314	9613050	9631076	11093412	75523773	4761892	14029617	4709426	0	236772341	6909648	0
Closed-Brine	4112809	9657395	9201891	11429499	77812045	4917851	15553948	3538799	0	257399536	6976435	0

Likely Brominated Ions Not Included in Final Dataset

Table A4.21 Signal intensity data in arbitrary units from the unprocessed data matrix showing brominated formulas likely present in LLOM that were not included in the final dataset because low signal intensity meant only the higher abundance isotopic peaks, and not the monoisotopic peaks, were visible across triplicates in the data matrix. Signal intensities match expected isotopic patterns.

$C_9H_6Br_2O_2$																			
m/z (avg.)	Closed 3	Closed 2	Closed 1	Closed-Brine 3	Closed-Brine 2	Closed-Brine 1	Active 3	Active 2	Active 1	C12	C13	H	O	Cl35	Cl37	Br79	Br81	Mass Diff (Da)	Error (ppm)
304.88181	2788389	0	0	0	0	0	0	0	0	9	0	7	2	0	0	2	0	-0.00002	0.06
306.87977	4603449	5346732	4501178	3819168	4848689	3748343	0	0	0	9	0	7	2	0	0	1	1	-0.00001	0.05
308.87771	2743103	2655747	2825467	0	0	0	0	0	0	9	0	7	2	0	0	0	2	-0.00002	0.08
$C_6H_3Br_3O_2$																			
m/z (avg.)	Closed 3	Closed 2	Closed 1	Closed-Brine 3	Closed-Brine 2	Closed-Brine 1	Active 3	Active 2	Active 1	C12	C13	H	O	Cl35	Cl37	Br79	Br81	Mass Diff (Da)	Error (ppm)
344.75897	3676267	3478216	4453000	3435554	3619724	2738775	2699892	2956657	0	6	0	2	2	0	0	2	1	-0.00003	0.07
346.75696	3807650	4761636	3823075	3489118	4171218	3631820	0	0	0	6	0	2	2	0	0	1	2	0.00001	0.03

MS settings for QqQ HPLC-MS-MS Experiments

Table A4.22 MS settings for QqQ HPLC-MS-MS Experiments.

Parameter	**Setting**
Ion source	ESI
Capillary voltage	-3600 V
Gas temperature	350 °C
Gas flow	8 L/min
Nebulizer gas pressure	25 psi
MS1/MS2 resolution	Unit
Time filtering	peak width = 0.03 min
FV	110 V
CAV	2 V

Targeted QqQ HPLC-MS-MS Experiments

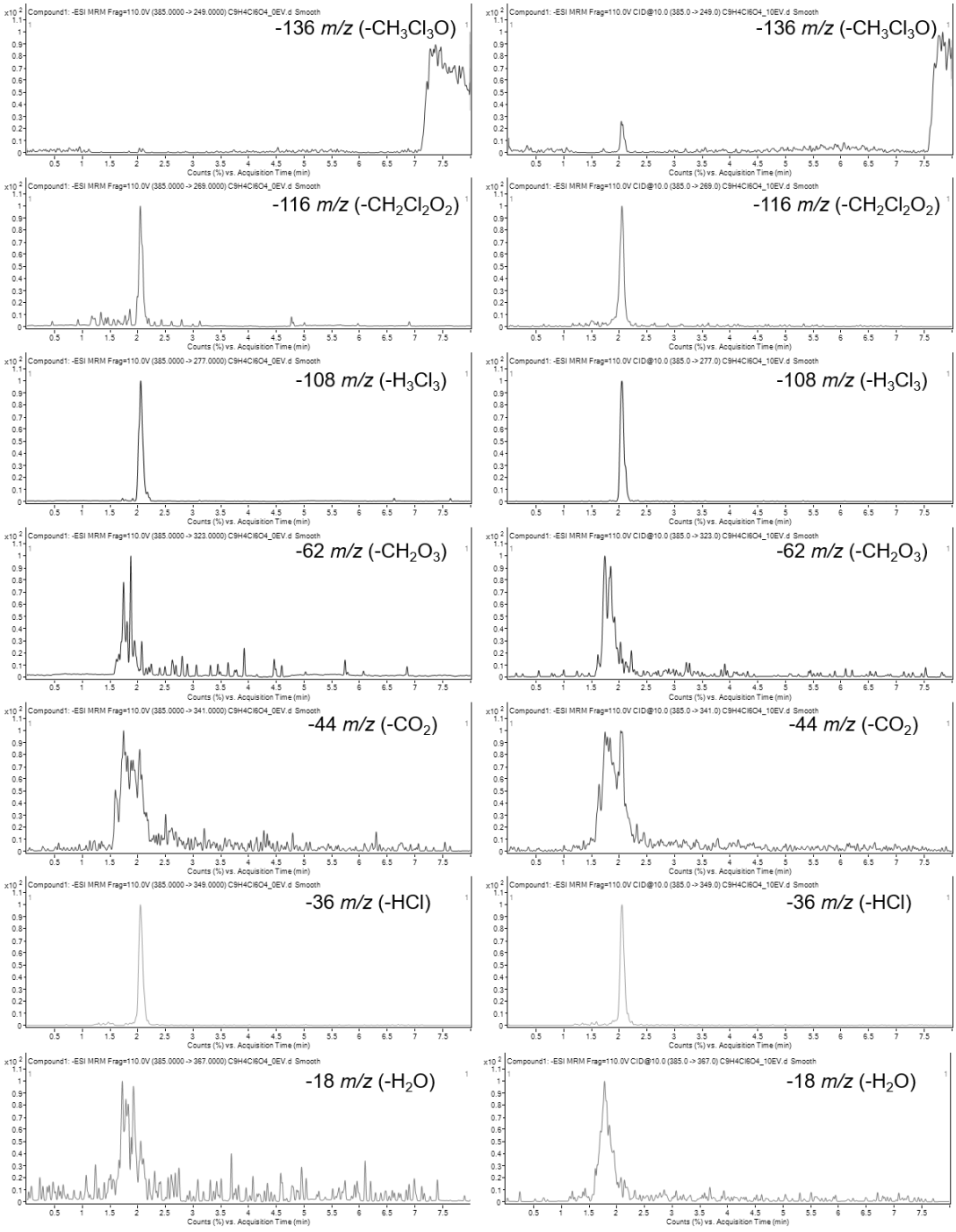

Figure A4.9 Smoothed chromatograms of QqQ CID HPLC-MS-MS experiments in MRM mode showing monitored transitions at 0 eV (left) and 10 eV (right) CEs for the 384.8 *m/z* ion, assigned $C_9H_4Cl_6O_4$, in the *Active* LL sample. Fragments corresponding to loss of $-CH_2Cl_2O_2$, $-H_3Cl_3$, and -HCl were found at 0 eV at the 2.05 min RT. Fragments corresponding to loss of $-CH_3Cl_3O$, $-CH_2Cl_2O_2$, $-H_3Cl_3$, and -HCl were found at 10 eV at the RT. The loss of $-CO_2$ may also occur at both 0 and 10 eV, but this could not be fully resolved from the background. The y-axis represents counts as % base peak, so displayed peak size is not reflective of size as raw counts.

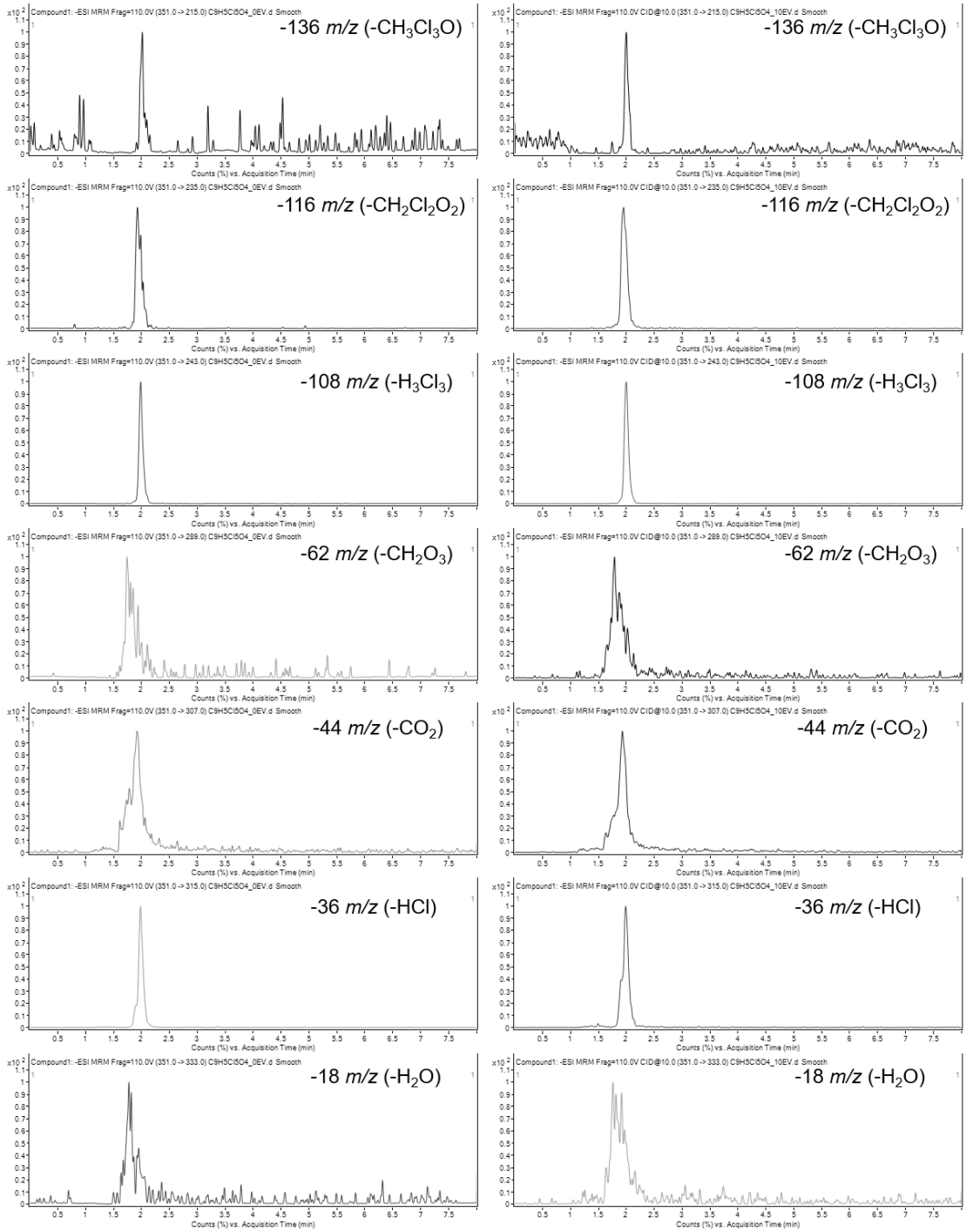

Figure A4.10 Smoothed chromatograms of QqQ CID HPLC-MS-MS experiments in MRM mode showing monitored transitions at 0 eV (left) and 10 eV (right) CEs for the 350.9 *m/z* ion, assigned $C_9H_5Cl_5O_4$, in the *Active* LL sample. Fragments corresponding to loss of -CH_3Cl_3O, -$CH_2Cl_2O_2$, -H_3Cl_3, -CO_2, and -HCl were found at 0 and 10 eV at the 1.98 min RT. Analyses of the 350.9 *m/z* ion in the *Closed* LL sample showed the same results. The y-axis represents counts as % base peak, so displayed peak size is not reflective of size as raw counts.

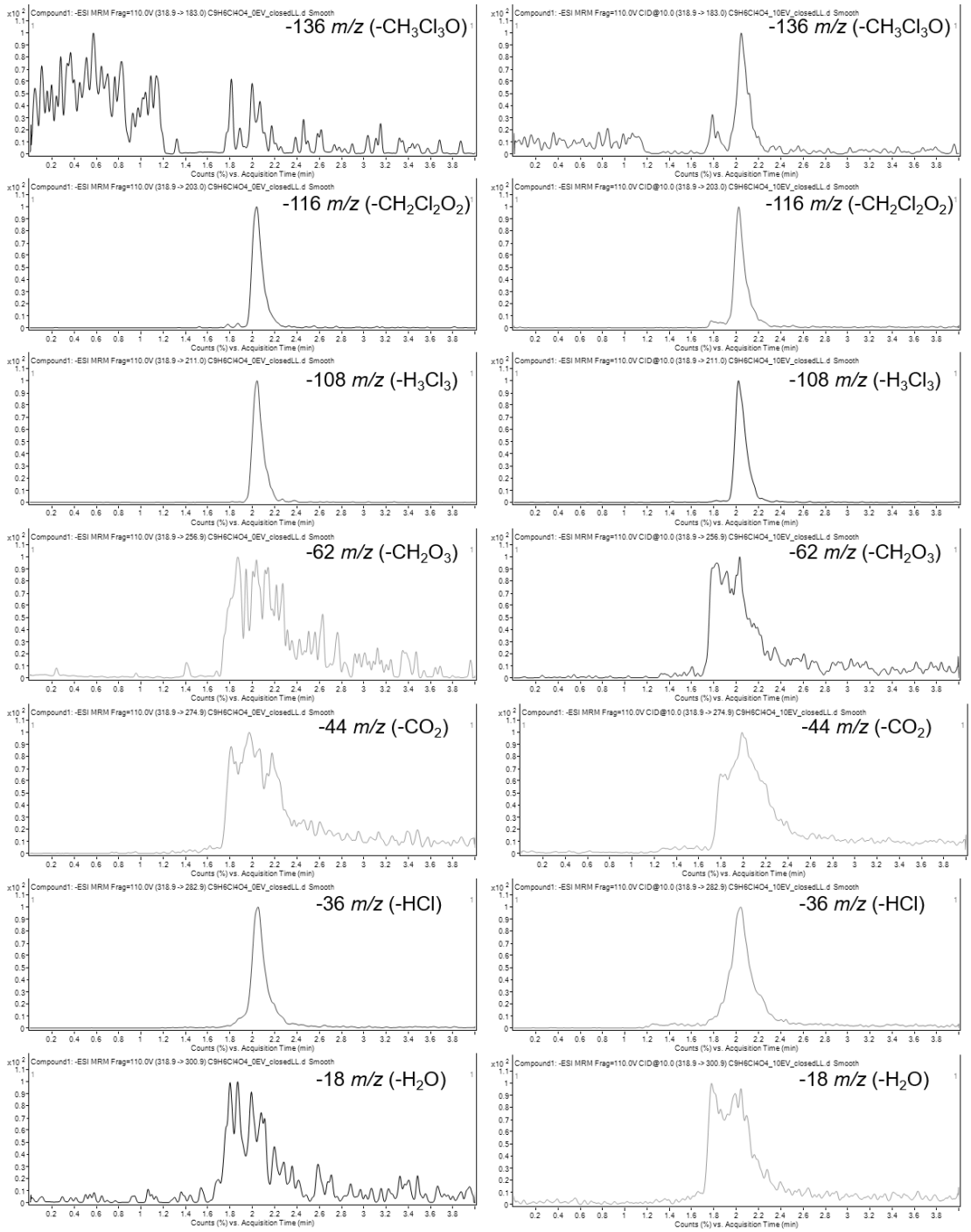

Figure A4.11 Smoothed chromatograms of QqQ CID HPLC-MS-MS experiments in MRM mode showing monitored transitions at 0 eV (left) and 10 eV (right) CEs for the 318.9 *m/z* ion, assigned $C_9H_6Cl_4O_4$, in the *Closed* LL sample. Fragments corresponding to loss of $-CH_2Cl_2O_2$, $-H_3Cl_3$, and -HCl were found at 0 eV at the 2.02 min RT. Fragments corresponding to loss of $-CH_3Cl_3O$, $-CH_2Cl_2O_2$, $-H_3Cl_3$, and -HCl were found at 10 eV at the RT. The y-axis represents counts as % base peak, so displayed peak size is not reflective of size as raw counts.

Full Scan Mode QqQ HPLC-MS-MS Experiments

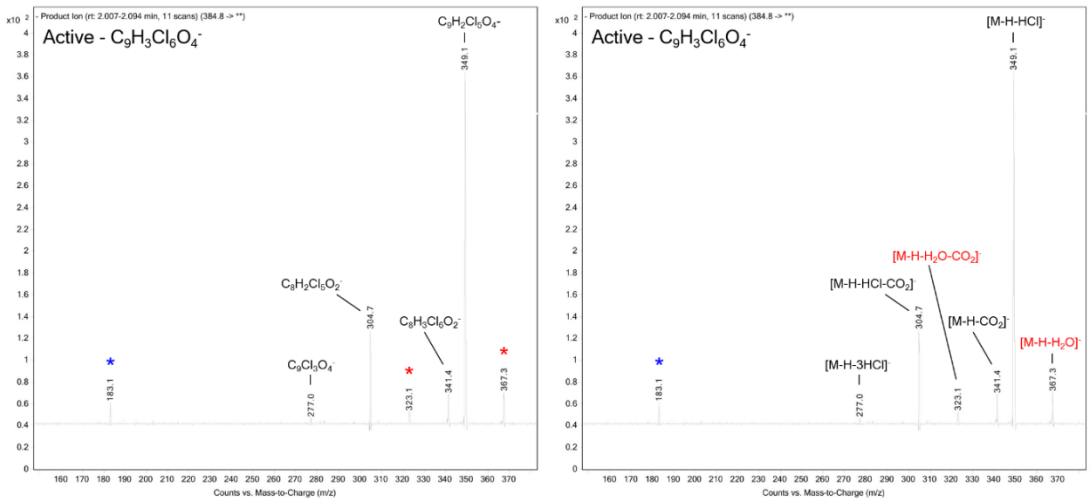

Figure A4.12 HPLC-MS-MS, full scan mode CID spectrum at 10 eV CE of 384.8 *m/z* ion, assigned $C_9H_4Cl_6O_4$, in the *Active* LL sample by QqQ MS. Spectrum is average of 11 scans at approximate 2.05 min RT. Fragment identification (left) and possible corresponding neutral losses (right) are shown. Red asterisks and text mark common background fragments that were present throughout the run. The blue asterisk marks an unidentified fragment at the RT that may be unrelated. Low mass resolution and error is typical of a QqQ MS operating in full scan mode.

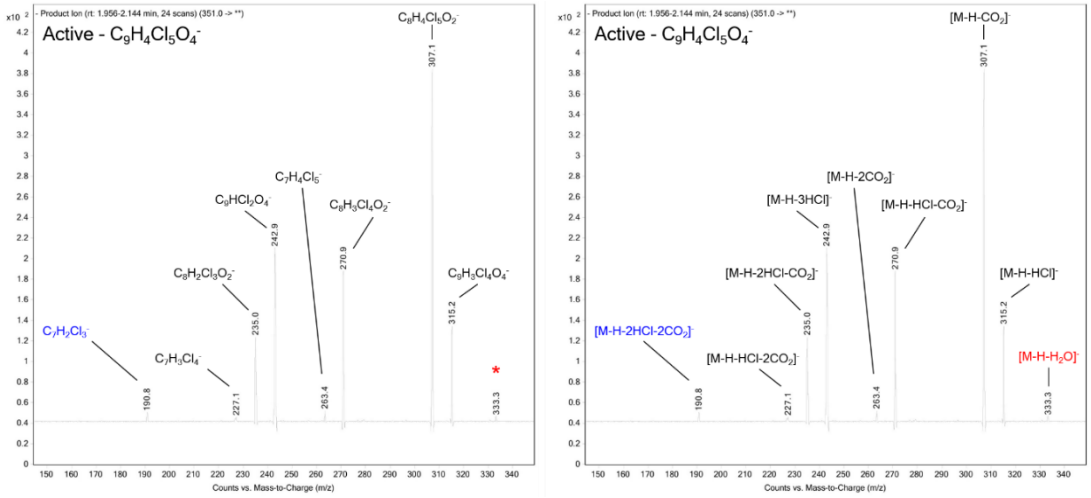

Figure A4.13 HPLC-MS-MS, full scan mode CID spectrum at 10 eV CE of 350.9 *m/z* ion, assigned $C_9H_5Cl_5O_4$, in the *Active* LL sample by QqQ MS. Spectrum is average of 24 scans at approximate 1.98 min RT. Fragment identification (left) and possible corresponding neutral losses (right) are shown. The red asterisk and text marks a common background fragment that was present throughout the run. The blue text marks a fragment at the RT that may be unrelated.

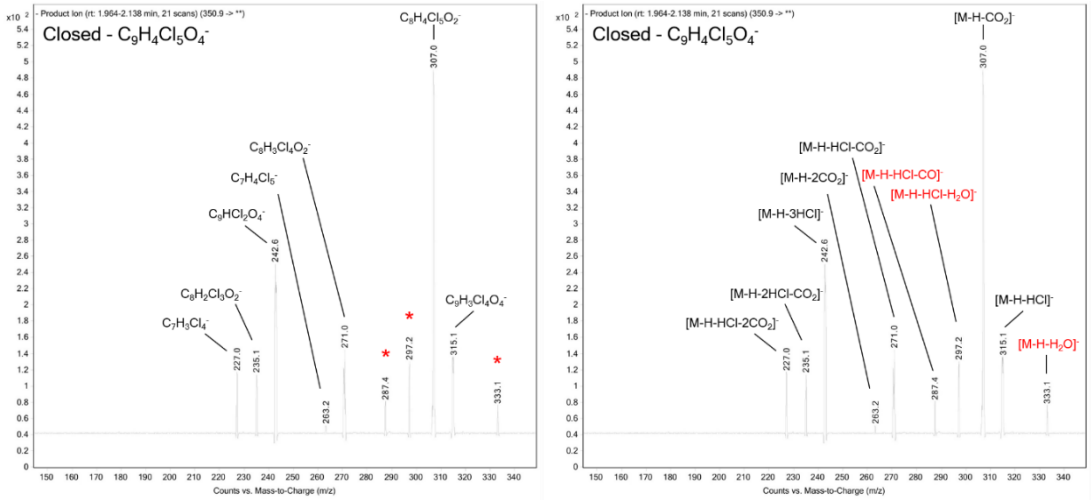

Figure A4.14 HPLC-MS-MS, full scan mode CID spectrum at 10 eV CE of 350.9 *m/z* ion, assigned $C_9H_5Cl_5O_4$, in the *Closed* LL sample by QqQ MS. Spectrum is average of 21 scans at approximate 1.98 min RT. Fragment identification (left) and possible corresponding neutral losses (right) are shown. The red asterisks and text mark background fragments that were present throughout the run.

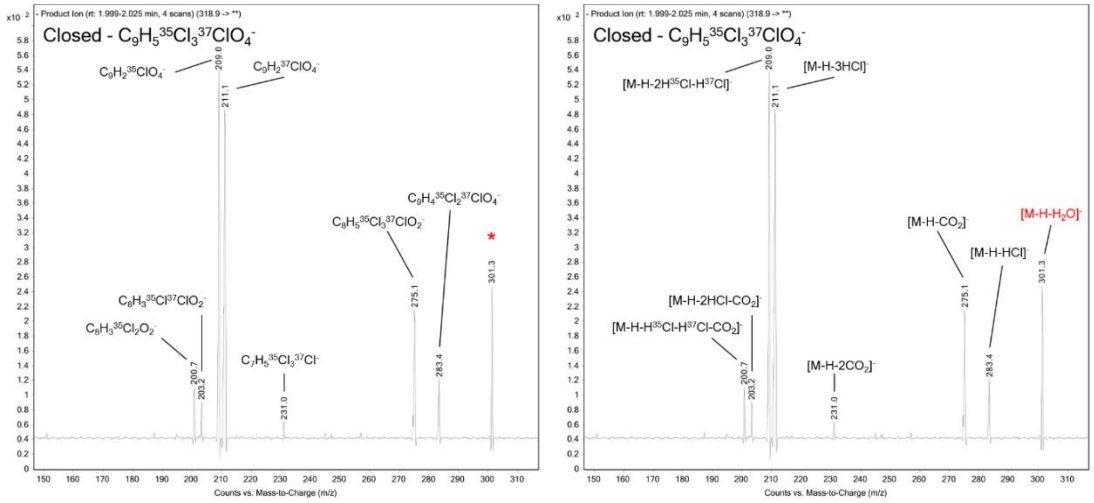

Figure A4.15. HPLC-MS-MS, full scan mode CID spectrum at 10 eV CE of 318.9 *m/z* ion in the *Closed* LL sample by QqQ MS. The corresponding monoisotopic ion (316.9 *m/z*) was assigned $C_9H_6Cl_4O_4$. Spectrum is average of 4 scans at approximate 2.02 min RT. Fragment identification (left) and possible corresponding neutral losses (right) are shown. The red asterisk and text marks a common background fragment that was present throughout the run.

Orbitrap MS-MS Experiments

Table A4.23 Ion lists of 20 highest intensity peaks from direct injection Orbitrap MS-MS on the highest abundance chlorine isotopic peak of $C_9H_5Cl_5O_4$ (352.85 *m/z*) in the *Active* sample. Mass resolution was 15,000, fragmentation was by CID at CEs of 0 (left) and 10 eV (right) in full scan mode using the FTMS (Orbitrap) detector, recording 0.4 min long scan averages. Fragments identified as related to the parent compound are highlighted. Fragmentation of other isotopic peaks (350.86 and 354.85 *m/z*) showed the same fragment formation following expected isotopic patterns.

FTMS - p ESI Full ms2 352.85@cid0.00 [95.00-353.00]					FTMS - p ESI Full ms2 352.85@cid10.00 [95.00-353.00]					
Scan #: 1-37					Scan #: 1-36					
RT: 0.01-0.41					RT: 0.01-0.40					
AV: 37					AV: 36					
m/z	Intensity	Relative	Formula	Loss	m/z	Intensity	Relative	Formula	Loss	Possible Neutral Loss
108.5925	223.1	0.22			101.6826	201.6	0.77			
173.91633	204.4	0.2			103.52215	199.8	0.76			
175.83216	229.1	0.22			109.22732	189.7	0.72			
185.81465	196.8	0.19			124.21209	191.7	0.73			
197.2459	544.4	0.53			168.59209	289.1	1.1			
203.70446	724.4	0.7			186.02932	196.1	0.75			
254.26967	2268.9	2.19			203.7062	562.7	2.15			
273.65148	2723	2.63			215.3538	188.4	0.72			
277.43503	196.3	0.19			228.48514	203.5	0.78			
283.90569	324.2	0.31			234.91095	1008.1	3.84	$C_8H_2{}^{35}Cl_3O_2^-$	$CH_3{}^{35}Cl^{37}ClO_2$	$H + H^{35}Cl + H^{37}Cl + CO_2$
340.56887	209.5	0.2			236.90795	1511	5.76	$C_8H_2{}^{35}Cl_2{}^{37}ClO_2^-$	$CH_3{}^{35}Cl_2O_2$	$H + 2H^{35}Cl + CO_2$
352.51528	278.6	0.27			254.26993	1796.3	6.85			
352.53105	1292.7	1.25			272.88436	587.8	2.24			
352.53751	1388.9	1.34			273.65167	2672.8	10.19			
352.55891	694.3	0.67			274.32805	200.5	0.76			
352.57894	631	0.61			308.86059	4263	16.26	$C_8H_4{}^{35}Cl_4{}^{37}ClO_2^-$	CHO_2	$H + CO_2$
352.61113	3170.1	3.06			309.03692	240.5	0.92			
352.68417	248.9	0.24			316.87382	3869.9	14.76	$C_9H_3{}^{35}Cl_3{}^{37}ClO_4^-$	$H_2{}^{35}Cl$	$H + H^{35}Cl$
352.85068	103591	100	$C_9H_4{}^{35}Cl_4{}^{37}ClO_4^-$	H	352.61152	3912.6	14.92			
352.993	315.5	0.3			352.85062	26220.5	100	$C_9H_4{}^{35}Cl_4{}^{37}ClO_4^-$	H	H

Table A4.24 Ion lists of 20 highest intensity peaks from direct injection Orbitrap MS-MS on the highest abundance chlorine isotopic peak ($C_9H_4Cl_6O_4$, 386.81 *m/z*) of the 100 µg/L chlorendic acid standard solution, made with a chlorendic acid standard (Sigma-Aldrich, 99%) and ultrapure water. Mass resolution was 15,000, fragmentation was by CID at CEs of 0 eV (top left), 10 eV (top right), 20 eV (bottom left), and 60 eV (bottom right) in full scan mode using the FTMS (Orbitrap) detector, recording 0.4 min long scan averages. Fragmentation of other isotopic peaks (384.82, 388.81, and 390.81 *m/z*) showed the same fragment formation following expected isotopic patterns.

FTMS - p ESI Full ms2 386.81@cid0.00 [105.00-387.00]					
Scan #: 1-19					
RT: 0.01-0.39					
AV: 19					
m/z	Intensity	Relative	Formula	Loss	Possible Neutral Loss
109.9198	188.4	1.65			
120.4691	247.2	2.16			
129.7376	207.2	1.81			
134.1164	190.3	1.66			
156.2447	198.8	1.74			
163.0515	221	1.93			
184.6679	177.4	1.55			
188.6685	237.6	2.08			
200.3261	197.2	1.72			
228.8981	221.5	1.94			
273.665	4325.8	37.84			
313.8162	250	2.19			
379.6384	283.6	2.48			
379.6678	1727.5	15.11			
379.6825	2439.6	21.34			
379.6928	2734.4	23.92			
379.7012	2579.1	22.56			
379.7179	1464.5	12.81			
386.7147	508.5	4.45			
386.8127	11431.4	100	$C_9H_3{}^{35}Cl_5{}^{37}ClO_4^-$	H	

FTMS - p ESI Full ms2 386.81@cid10.00 [105.00-387.00]					
Scan #: 1-19					
RT: 0.00-0.39					
AV: 19					
m/z	Intensity	Relative	Formula	Loss	Possible Neutral Loss
119.556	224.5	2.88			
119.7411	233.1	2.98			
128.048	244	3.12			
173.9636	280.9	3.6			
190.8639	237.5	3.04			
195.8224	246.3	3.15			
198.3531	247.6	3.17			
207.5571	244.2	3.13			
253.4998	299.6	3.84			
273.665	4442.1	56.89			
278.8823	421.3	5.4	$C_9{}^{35}Cl_2{}^{37}ClO_4^-$	$H_4{}^{35}Cl_3$	$H+3H^{35}Cl$
317.2019	228.6	2.93			
348.8389	750.2	9.61	$C_9H_2{}^{35}Cl_5O_4^-$	$H_2{}^{37}Cl$	$H+H^{37}Cl$
350.8356	7808.2	100	$C_9H_2{}^{35}Cl_4{}^{37}ClO_4^-$	$H_2{}^{35}Cl$	$H+H^{35}Cl$
379.6528	367.2	4.7			
379.6815	2863.6	36.68			
379.6928	3312.3	42.42			
379.703	2467.6	31.6			
379.7114	2250.6	28.82			
386.8127	2160.8	27.67	$C_9H_3{}^{35}Cl_5{}^{37}ClO_4^-$	H	H

FTMS - p ESI Full ms2 386.81@cid20.00 [105.00-387.00]					
Scan #: 1-19					
RT: 0.01-0.39					
AV: 19					
m/z	Intensity	Relative	Formula	Loss	Possible Neutral Loss
119.5662	245.5	1.85			
167.9652	180.8	1.36			
204.4308	175.7	1.33			
214.0743	259.6	1.96			
253.5	1079.3	8.14			
270.8693	226.4	1.71	$C_8H^{35}Cl_3{}^{37}ClO_2^-$	$CH_3{}^{35}Cl_2O_2$	$H+2H^{35}Cl+CO_2$
273.6649	3646.1	27.51			
276.0752	178	1.34			
278.8817	297.1	2.24	$C_9{}^{35}Cl_2{}^{37}ClO_4^-$	$H_4{}^{35}Cl_3$	$H+3H^{35}Cl$
282.3669	244.5	1.84			
283.9194	339	2.56			
306.7672	178.1	1.34			
348.8385	1339.1	10.1	$C_9H_2{}^{35}Cl_5O_4^-$	$H_2{}^{37}Cl$	$H+H^{37}Cl$
350.8359	13252.3	100	$C_9H_2{}^{35}Cl_4{}^{37}ClO_4^-$	$H_2{}^{35}Cl$	$H+H^{35}Cl$
351.2254	176.2	1.33			
379.622	181.8	1.37			
379.6432	329.5	2.49			
379.6698	1895.2	14.3			
379.6899	4483.2	33.83			
379.7202	974.6	7.35			

FTMS - p ESI Full ms2 386.81@cid60.00 [105.00-387.00]					
Scan #: 1-19					
RT: 0.01-0.39					
AV: 19					
m/z	Intensity	Relative	Formula	Loss	Possible Neutral Loss
111.838	177.1	3.24			
117.6897	187.9	3.44			
119.9337	175.4	3.21			
126.1023	226	4.13			
136.6582	233.2	4.26			
253.4995	349.2	6.39			
266.25	260.2	4.76			
273.665	3528.3	64.53			
276.8848	538.3	9.84	$C_9{}^{35}Cl_3O_4^-$	$H_4{}^{35}Cl_2{}^{37}Cl$	$H+2H^{35}Cl+H^{37}Cl$
277.427	177.9	3.25			
278.8826	301.3	5.51	$C_9{}^{35}Cl_2{}^{37}ClO_4^-$	$H_4{}^{35}Cl_3$	$H+3H^{35}Cl$
305.127	176.6	3.23			
348.8383	846.5	15.48	$C_9H_2{}^{35}Cl_5O_4^-$	$H_2{}^{37}Cl$	$H+H^{37}Cl$
350.8357	5468	100	$C_9H_2{}^{35}Cl_4{}^{37}ClO_4^-$	$H_2{}^{35}Cl$	$H+H^{35}Cl$
351.4641	235.7	4.31			
357.4682	257.2	4.7			
379.6369	267.4	4.89			
379.6422	296.7	5.43			
379.6856	5204.8	95.18			
379.7313	281.7	5.15			

References

4110 Determination of Anions by Ion Chromatography. **2017a**, In *Standard Methods For the Examination of Water and Wastewater*.

4500-H^+ pH Value. **2017b**, In *Standard Methods For the Examination of Water and Wastewater*.

4500-NH_3 Nitrogen (Ammonia). **2017c**, In *Standard Methods For the Examination of Water and Wastewater*.

5210 Biochemical Oxygen Demand (BOD). **2017d**, In *Standard Methods For the Examination of Water and Wastewater*.

Albero, B., R. A. Pérez, C. Sánchez-Brunete, and J. L. Tadeo, **2012**, Occurrence and analysis of parabens in municipal sewage sludge from wastewater treatment plants in Madrid (Spain). *J. Hazard. Mater.*, *239*, 48-55.

Alexander, B., M. Hastings, D. Allman, J. Dachs, J. Thornton, and S. Kunasek, **2009**, Quantifying atmospheric nitrate formation pathways based on a global model of the oxygen isotopic composition ($\Delta^{17}O$) of atmospheric nitrate. *Atmos. Chem. Phys.*, *9* (14), 5043-5056.

Anderson, K. A., and J. A. Downing, **2006**, Dry and wet atmospheric deposition of nitrogen, phosphorus and silicon in an agricultural region. *Water, Air, Soil Pollut.*, *176* (1), 351-374.

Arnold, W. A., K. Longnecker, K. D. Kroeger, and E. B. Kujawinski, **2014**, Molecular signature of organic nitrogen in septic-impacted groundwater. *Environ. Sci. Process. Impacts*, *16* (10), 2400-2407.

Aspila, K., H. Agemian, and A. Chau, **1976**, A semi-automated method for the determination of inorganic, organic and total phosphate in sediments. *Analyst*, *101* (1200), 187-197.

Assaad, A., S. Pontvianne, and M.-N. Pons, **2014**, Photodegradation-based detection of fluorescent whitening agents in a mountain river. *Chemosphere*, *100*, 27-33.

ASTM International, **2014**, ASTM D7781-14, Standard Test Method for Nitrite-Nitrate in Water by Nitrate Reductase. West Conshohocken, PA.

Baker, A., **2001**, Fluorescence excitation− emission matrix characterization of some sewage-impacted rivers. *Environ. Sci. Technol.*, *35* (5), 948-953.

Baker, A., **2002**, Fluorescence excitation− emission matrix characterization of river waters impacted by a tissue mill effluent. *Environ. Sci. Technol., 36* (7), 1377-1382.

Baker, A., and M. Curry, **2004**, Fluorescence of leachates from three contrasting landfills. *Water Res., 38* (10), 2605-2613.

Baltimore Sun, **2016**, Rollback of septic system requirements raises questions about bay impact, August 23, 2016. Available from: https://www.baltimoresun.com/politics/bs-bz-hogan-septic-system-regulation-20160823-story.html.

Barber, L. B., S. H. Keefe, D. R. LeBlanc, P. M. Bradley, F. H. Chapelle, M. T. Meyer, K. A. Loftin, D. W. Kolpin, and F. Rubio, **2009**, Fate of sulfamethoxazole, 4-nonylphenol, and 17β-estradiol in groundwater contaminated by wastewater treatment plant effluent. *Environ. Sci. Technol., 43* (13), 4843-4850.

Batchu, S. R., N. Quinete, V. R. Panditi, and P. R. Gardinali, **2013**, Online solid phase extraction liquid chromatography tandem mass spectrometry (SPE-LC-MS/MS) method for the determination of sucralose in reclaimed and drinking waters and its photo degradation in natural waters from South Florida. *Chem. Cent. J., 7* (1), 1-16.

Batchu, S. R., C. E. Ramirez, and P. R. Gardinali, **2015**, Rapid ultra-trace analysis of sucralose in multiple-origin aqueous samples by online solid-phase extraction coupled to high-resolution mass spectrometry. *Anal. Bioanal. Chem., 407* (13), 3717-3725.

Baun, A., A. Ledin, L. Reitzel, P. L. Bjerg, and T. H. Christensen, **2004a**, Xenobiotic organic compounds in leachates from ten Danish MSW landfills—chemical analysis and toxicity tests. *Water Res., 38* (18), 3845-3858.

Baun, D. L., and T. H. Christensen, **2004b**, Speciation of heavy metals in landfill leachate: a review. *Waste Manage. Res., 22* (1), 3-23.

Bayer, E., P. Gfrörer, and C. Rentel, **1999**, Coordination-ionspray-MS (CIS-MS), a universal detection and characterization method for direct coupling with separation techniques. *Angew. Chem. Int. Ed., 38* (7), 992-995.

Benitez-Nelson, C. R., **2000**, The biogeochemical cycling of phosphorus in marine systems. *Earth-Sci. Rev., 51* (1-4), 109-135.

Benowitz, N. L., **1996**, Cotinine as a biomarker of environmental tobacco smoke exposure. *Epidemiol. Rev., 18* (2), 188-204.

Berge, N., D. Reinhart, and T. Townsend, **2005**, The fate of nitrogen in bioreactor landfills. *Crit. Rev. Environ. Sci. Technol., 35* (4), 365-399.

Bernot, M. J., J. C. Becker, J. Doll, and T. E. Lauer, **2016**, A national reconnaissance of trace organic compounds (TOCs) in United States lotic ecosystems. *Sci. Total Environ.*, *572*, 422-433.

Berset, J.-D., and N. Ochsenbein, **2012**, Stability considerations of aspartame in the direct analysis of artificial sweeteners in water samples using high-performance liquid chromatography–tandem mass spectrometry (HPLC–MS/MS). *Chemosphere*, *88* (5), 563-569.

Bhattacharyya, A., M. P. Schmidt, E. Stavitski, B. Azimzadeh, and C. E. Martínez, **2019**, Ligands representing important functional groups of natural organic matter facilitate Fe redox transformations and resulting binding environments. *Geochim. Cosmochim. Acta*, *251*, 157-175.

Bjerregaard-Olesen, C., C. C. Bach, M. Long, M. Ghisari, R. Bossi, B. H. Bech, E. A. Nohr, T. B. Henriksen, J. Olsen, and E. C. Bonefeld-Jørgensen, **2016**, Time trends of perfluorinated alkyl acids in serum from Danish pregnant women 2008–2013. *Environ. Int.*, *91*, 14-21.

Boutegrabet, L., B. Kanawati, I. Gebefügi, D. Peyron, P. Cayot, R. D. Gougeon, and P. Schmitt-Kopplin, **2012**, Attachment of chloride anion to sugars: mechanistic investigation and discovery of a new dopant for efficient sugar ionization/detection in mass spectrometers. *Chem.-Eur. J.*, *18* (41), 13059-13067.

Boyer, E. W., C. L. Goodale, N. A. Jaworski, and R. W. Howarth, **2002**, Anthropogenic nitrogen sources and relationships to riverine nitrogen export in the northeastern USA. *Biogeochemistry*, *57* (1), 137-169.

Bozkurt, S., L. Moreno, and I. Neretnieks, **2000**, Long-term processes in waste deposits. *Sci. Total Environ.*, *250* (1-3), 101-121.

Buerge, I. J., H.-R. Buser, M. Kahle, M. D. Muller, and T. Poiger, **2009**, Ubiquitous occurrence of the artificial sweetener acesulfame in the aquatic environment: an ideal chemical marker of domestic wastewater in groundwater. *Environ. Sci. Technol.*, *43* (12), 4381-4385.

Cai, Y., M. C. Concha, J. S. Murray, and R. B. Cole, **2002**, Evaluation of the role of multiple hydrogen bonding in offering stability to negative ion adducts in electrospray mass spectrometry. *J. Am. Soc. Mass. Spectrom.*, *13* (12), 1360-1369.

Canter, L., and R. C. Knox, **1984**, Evaluation of septic tank system effects on ground water quality. EPA-600/S2-84-107.

Cantwell, M. G., D. R. Katz, J. C. Sullivan, D. Shapley, J. Lipscomb, J. Epstein, A. R. Juhl, C. Knudson, and G. D. O'Mullan, **2018**, Spatial patterns of pharmaceuticals and wastewater tracers in the Hudson River Estuary. *Water Res., 137*, 335-343.

Carrara, C., C. J. Ptacek, W. D. Robertson, D. W. Blowes, M. C. Moncur, E. Sverko, and S. Backus, **2008**, Fate of pharmaceutical and trace organic compounds in three septic system plumes, Ontario, Canada. *Environ. Sci. Technol., 42* (8), 2805-2811.

Carstea, E. M., J. Bridgeman, A. Baker, and D. M. Reynolds, **2016**, Fluorescence spectroscopy for wastewater monitoring: a review. *Water Res., 95*, 205-219.

Caschetto, M., W. Robertson, M. Petitta, and R. Aravena, **2018**, Partial nitrification enhances natural attenuation of nitrogen in a septic system plume. *Sci. Total Environ., 625*, 801-808.

Castronovo, S., A. Wick, M. Scheurer, K. Nödler, M. Schulz, and T. A. Ternes, **2017**, Biodegradation of the artificial sweetener acesulfame in biological wastewater treatment and sandfilters. *Water Res., 110*, 342-353.

Chen, H.-C., S.-P. Wang, and W.-H. Ding, **2006**, Determination of fluorescent whitening agents in environmental waters by solid-phase extraction and ion pair liquid chromatography–tandem mass spectrometry. *J. Chromatogr. A, 1102* (1-2), 135-142.

Chen, J., B. F. Pycke, B. J. Brownawell, C. A. Kinney, E. T. Furlong, D. W. Kolpin, and R. U. Halden, **2017**, Occurrence, temporal variation, and estrogenic burden of five parabens in sewage sludge collected across the United States. *Sci. Total Environ., 593*, 368-374.

Chowdhury, R. R., P. Charpentier, and M. B. Ray, **2010**, Photodegradation of estrone in solar irradiation. *Ind. Eng. Chem. Res., 49* (15), 6923-6930.

Clarke, B. O., T. Anumol, M. Barlaz, and S. A. Snyder, **2015**, Investigating landfill leachate as a source of trace organic pollutants. *Chemosphere, 127*, 269-275.

Colorado Department of Public Health and Environment, **2019**, Closed Municipal Solid Waste Landfills Initiative, Available from: https://www.colorado.gov/pacific/cdphe/closed-mun-sw-landfills-initiative.

COMAR 26.04.02.07, **2004**, Best Available Technology for Removal of Nitrogen (BAT). Available from: http://mlis.state.md.us/2004rs/billfile/sb0320.htm.

Correll, D. L., T. E. Jordan, and D. E. Weller, **1999**, Effects of precipitation and air temperature on nitrogen discharges from Rhode River watersheds. *Water, Air, Soil Pollut., 115* (1), 547-575.

Cui, Y., Q. Wu, M. Yang, and F. Cui, **2016**, Three-dimensional excitation-emission matrix fluorescence spectroscopy and fractions of dissolved organic matter change in landfill leachate by biological treatment. *Environ. Sci. Pollut. Res., 23* (1), 793-799.

Davis, S. N., D. O. Whittemore, and J. Fabryka-Martin, **1998**, Uses of chloride/bromide ratios in studies of potable water. *Groundwater, 36* (2), 338-350.

de-Bashan, L. E., and Y. Bashan, **2004**, Recent advances in removing phosphorus from wastewater and its future use as fertilizer (1997–2003). *Water Res., 38* (19), 4222-4246.

de Graaf, E. L., A. M. Altelaar, B. van Breukelen, S. Mohammed, and A. J. Heck, **2011**, Improving SRM assay development: a global comparison between triple quadrupole, ion trap, and higher energy CID peptide fragmentation spectra. *J. Proteome Res., 10* (9), 4334-4341.

de Oliveira, D. N., M. de Menezes, and R. R. Catharino, **2015**, Thermal degradation of sucralose: a combination of analytical methods to determine stability and chlorinated byproducts. *Sci. Rep., 5* (1), 1-5.

Dickerson Jr., J., C. Hagedorn, and A. Hassall, **2007**, Detection and remediation of human-origin pollution at two public beaches in Virginia using multiple source tracking methods. *Water Res., 41* (16), 3758-3770.

Dittmar, T., B. Koch, N. Hertkorn, and G. Kattner, **2008**, A simple and efficient method for the solid-phase extraction of dissolved organic matter (SPE-DOM) from seawater. *Limnol. Oceanogr. Methods, 6* (6), 230-235.

Duan, S., S. S. Kaushal, E. J. Rosenfeldt, J. Huang, and S. Murthy, **2021**, Changes in concentrations and source of nitrogen along the Potomac River with watershed land use. *Appl. Geochem.*, 105006.

Dubber, D., and L. W. Gill, **2017**, Suitability of fluorescent whitening compounds (FWCs) as indicators of human faecal contamination from septic tanks in rural catchments. *Water Res., 127*, 104-117.

Eisenreich, A., R. Gürtler, and B. Schäfer, **2020**, Heating of food containing sucralose might result in the generation of potentially toxic chlorinated compounds. *Food Chem., 321*, 126700.

El-Hage, R., A. El-Hellani, C. Haddad, R. Salman, S. Talih, A. Shihadeh, T. Eissenberg, and N. Aoun Saliba, **2019**, Toxic emissions resulting from sucralose added to electronic cigarette liquids. *Aerosol Sci. Technol., 53* (10), 1197-1203.

Ellis, D. A., J. W. Martin, A. O. De Silva, S. A. Mabury, M. D. Hurley, M. P. Sulbaek Andersen, and T. J. Wallington, **2004**, Degradation of fluorotelomer alcohols: a likely

atmospheric source of perfluorinated carboxylic acids. *Environ. Sci. Technol.*, *38* (12), 3316-3321.

Elmund, G. K., M. J. Allen, and E. W. Rice, **1999**, Comparison of Escherichia coli, total coliform, and fecal coliform populations as indicators of wastewater treatment efficiency. *Water Environ. Res*, *71* (3), 332-339.

Emerson, D., E. J. Fleming, and J. M. McBeth, **2010**, Iron-oxidizing bacteria: an environmental and genomic perspective. *Annu. Rev. Microbiol.*, *64*, 561-583.

Evershed, R. P., I. D. Bull, L. T. Corr, Z. M. Crossman, B. E. van Dongen, C. J. Evans, S. Jim, H. R. Mottram, A. J. Mukherjee, and R. D. Pancost, **2007**, Compound-specific stable isotope analysis in ecology and paleoecology. *Stable isotopes in ecology and environmental science*, *480*.

Ferrer, I., and E. M. Thurman, **2010**, Analysis of sucralose and other sweeteners in water and beverage samples by liquid chromatography/time-of-flight mass spectrometry. *J. Chromatogr. A*, *1217* (25), 4127-4134.

Ferrer, I., J. A. Zweigenbaum, and E. M. Thurman, **2013**, Analytical methodologies for the detection of sucralose in water. *Anal. Chem.*, *85* (20), 9581-9587.

Florida Statute, **2020**, §403.708(12)(c). United States.

Fu, Q.-L., M. Fujii, and E. Kwon, **2020**, Development and Application of a High-Precision Algorithm for Nontarget Identification of Organohalogens Based on Ultrahigh-Resolution Mass Spectrometry. *Anal. Chem.*, *92* (20), 13989-13996.

Gabbanini, S., E. Lucchi, F. Guidugli, R. Matera, and L. Valgimigli, **2010**, Anomeric discrimination and rapid analysis of underivatized lactose, maltose, and sucrose in vegetable matrices by U-HPLC–ESI-MS/MS using porous graphitic carbon. *J. Mass Spectrom.*, *45* (9), 1012-1018.

Gabelica, V., and E. D. Pauw, **2005**, Internal energy and fragmentation of ions produced in electrospray sources. *Mass Spectrom. Rev.*, *24* (4), 566-587.

Games, L. M., and J. Hayes, **1977**, Carbon isotopic study of the fate of landfill leachate in groundwater. *J. Water Pollut. Control Fed.*, 668-677.

Gan, Z., H. Sun, R. Wang, and B. Feng, **2013**, A novel solid-phase extraction for the concentration of sweeteners in water and analysis by ion-pair liquid chromatography–triple quadrupole mass spectrometry. *J. Chromatogr. A*, *1274*, 87-96.

Gannes, L. Z., C. M. Del Rio, and P. Koch, **1998**, Natural abundance variations in stable isotopes and their potential uses in animal physiological ecology. *Comp. Biochem. Physiol. A: Physiol.*, *119* (3), 725-737.

García-Galán, M. J., M. S. Díaz-Cruz, and D. Barceló, **2008**, Identification and determination of metabolites and degradation products of sulfonamide antibiotics. *TrAC, Trends Anal. Chem.*, *27* (11), 1008-1022.

Gaytán, I., A. Sánchez-Reyes, M. Burelo, M. Vargas-Suárez, I. Liachko, M. Press, S. Sullivan, M. J. Cruz-Gómez, and H. Loza-Tavera, **2020**, Degradation of recalcitrant polyurethane and xenobiotic additives by a selected landfill microbial community and its biodegradative potential revealed by proximity ligation-based metagenomic analysis. *Front. Microbiol.*, *10*, 2986.

Gomi, R., T. Matsuda, Y. Matsui, and M. Yoneda, **2014**, Fecal source tracking in water by next-generation sequencing technologies using host-specific Escherichia coli genetic markers. *Environ. Sci. Technol.*, *48* (16), 9616-9623.

Gonsior, M., **2019**, FT-ICR MS and Orbitrap mass spectrometry approaches in environmental chemistry. In *Fundamentals and Applications of Fourier Transform Mass Spectrometry*, Elsevier: pp 407-423.

Gonsior, M., M. Zwartjes, W. J. Cooper, W. Song, K. P. Ishida, L. Y. Tseng, M. K. Jeung, D. Rosso, N. Hertkorn, and P. Schmitt-Kopplin, **2011**, Molecular characterization of effluent organic matter identified by ultrahigh resolution mass spectrometry. *Water Res.*, *45* (9), 2943-2953.

Green, N. W., D. McInnis, N. Hertkorn, P. A. Maurice, and E. M. Perdue, **2015**, Suwannee River natural organic matter: isolation of the 2R101N reference sample by reverse osmosis. *Environ. Eng. Sci.*, *32* (1), 38-44.

Grøn, C., J. B. Christensen, D. L. Jensen, P. Kjeldsen, and P. Østfeldt, **2000**, Organic halogens in landfill leachates. *Water, Air, Soil Pollut.*, *120* (3-4), 331-345.

Guan, B., and R. B. Cole, **2008**, MALDI linear-field reflectron TOF post-source decay analysis of underivatized oligosaccharides: determination of glycosidic linkages and anomeric configurations using anion attachment. *J. Am. Soc. Mass. Spectrom.*, *19* (8), 1119-1131.

Hadwen, W. L., and A. H. Arthington, **2007**, Food webs of two intermittently open estuaries receiving 15N-enriched sewage effluent. *Estuar. Coast. Shelf Sci.*, *71* (1-2), 347-358.

Hale, R. L., J. H. Hoover, W. M. Wollheim, and C. J. Vörösmarty, **2013**, History of nutrient inputs to the northeastern United States, 1930–2000. *Global Biogeochem. Cycles*, *27* (2), 578-591.

Hamilton, J., K. Reinert, J. Hagan, and W. Lord, **1995**, Polymers as solid waste in municipal landfills. *J. Air Waste Manag. Assoc.*, *45* (4), 247-251.

Harvey, D. J., **2005**, Fragmentation of negative ions from carbohydrates: part 1. Use of nitrate and other anionic adducts for the production of negative ion electrospray spectra from N-linked carbohydrates. *J. Am. Soc. Mass. Spectrom., 16* (5), 622-630.

Hecht, E. S., M. Scigelova, S. Eliuk, and A. Makarov, **2006**, Fundamentals and Advances of Orbitrap Mass Spectrometry. *Encyclopedia of Analytical Chemistry: Applications, Theory and Instrumentation*, 1-40.

Herzsprung, P., N. Hertkorn, W. von Tümpling, M. Harir, K. Friese, and P. Schmitt-Kopplin, **2014**, Understanding molecular formula assignment of Fourier transform ion cyclotron resonance mass spectrometry data of natural organic matter from a chemical point of view. *Anal. Bioanal. Chem., 406* (30), 7977-7987.

Hider, R. C., and X. Kong, **2010**, Chemistry and biology of siderophores. *Nat. Prod. Rep., 27* (5), 637-657.

Huang, N., M. M. Siegel, G. H. Kruppa, and F. H. Laukien, **1999**, Automation of a Fourier transform ion cyclotron resonance mass spectrometer for acquisition, analysis, and e-mailing of high-resolution exact-mass electrospray ionization mass spectral data. *J. Am. Soc. Mass. Spectrom., 10* (11), 1166-1173.

Hudson, N., A. Baker, and D. Reynolds, **2007**, Fluorescence analysis of dissolved organic matter in natural, waste and polluted waters—a review. *River Res. Appl., 23* (6), 631-649.

Hughes, B., D. Beale, P. Dennis, S. Cook, and W. Ahmed, **2017**, Cross-comparison of human wastewater-associated molecular markers in relation to fecal indicator bacteria and enteric viruses in recreational beach waters. *Applied and Environmental Microbiology, 83* (8), e00028-17.

Iavarone, A. T., and E. R. Williams, **2003**, Mechanism of charging and supercharging molecules in electrospray ionization. *J. Am. Chem. Soc., 125* (8), 2319-2327.

Ichou, F., A. Schwarzenberg, D. Lesage, S. Alves, C. Junot, X. Machuron-Mandard, and J. C. Tabet, **2014**, Comparison of the activation time effects and the internal energy distributions for the CID, PQD and HCD excitation modes. *J. Mass Spectrom., 49* (6), 498-508.

Iverson, G., M. A. O'Driscoll, C. P. Humphrey, A. K. Manda, and E. Anderson-Evans, **2015**, Wastewater nitrogen contributions to coastal plain watersheds, NC, USA. *Water, Air, Soil Pollut., 226* (10), 1-17.

Jambon, I., S. Thijs, G. Torres-Farada, F. Rineau, N. Weyens, P. Samyn, and J. Vangronsveld, **2019**, Fenton-mediated biodegradation of chlorendic acid-a highly

chlorinated organic pollutant-by fungi isolated from a polluted site. *Front. Microbiol.*, *10*, 1892.

James, C. A., J. P. Miller-Schulze, S. Ultican, A. D. Gipe, and J. E. Baker, **2016**, Evaluating contaminants of emerging concern as tracers of wastewater from septic systems. *Water Res.*, *101*, 241-251.

Jensen, D. L., J. K. Boddum, S. Redemann, and T. H. Christensen, **1998**, Speciation of dissolved iron (II) and manganese (II) in a groundwater pollution plume. *Environ. Sci. Technol.*, *32* (18), 2657-2664.

Jiang, Y., and R. B. Cole, **2005**, Oligosaccharide analysis using anion attachment in negative mode electrospray mass spectrometry. *J. Am. Soc. Mass. Spectrom.*, *16* (1), 60-70.

Johnson, J., L. Schewel, and T. Graedel, **2006**, The contemporary anthropogenic chromium cycle. *Environ. Sci. Technol.*, *40* (22), 7060-7069.

Jones, D. L., D. Shannon, D. V. Murphy, and J. Farrar, **2004**, Role of dissolved organic nitrogen (DON) in soil N cycling in grassland soils. *Soil Biol. Biochem.*, *36* (5), 749-756.

Jordan, T. E., D. L. Correll, and D. E. Weller, **1997a**, Effects of agriculture on discharges of nutrients from coastal plain watersheds of Chesapeake Bay. *J. Environ. Qual.*, *26*, 836-848.

Jordan, T. E., D. L. Correll, and D. E. Weller, **1997b**, Relating nutrient discharges from watersheds to land use and streamflow variability. *Water Resour. Res.*, *33* (11), 2579-2590.

Kahl, S., S. Kleinsteuber, J. Nivala, M. van Afferden, and T. Reemtsma, **2018**, Emerging biodegradation of the previously persistent artificial sweetener acesulfame in biological wastewater treatment. *Environ. Sci. Technol.*, *52* (5), 2717-2725.

Kahle, D., and H. Wickham, **2013**, ggmap: Spatial Visualization with ggplot2. *The R journal*, *5* (1), 144-161.

Kanazawa, A., and S.-l. Teshima, **1978**, Occurrence of coprostanol, an indicator of fecal pollution, in sea-water and sediments. *Oceanologica Acta*, *1* (1), 39-44.

Kapelewska, J., U. Kotowska, and K. Wiśniewska, **2016**, Determination of personal care products and hormones in leachate and groundwater from Polish MSW landfills by ultrasound-assisted emulsification microextraction and GC-MS. *Environ. Sci. Pollut. Res.*, *23* (2), 1642-1652.

Katz, B. G., S. M. Eberts, and L. J. Kauffman, **2011**, Using Cl/Br ratios and other indicators to assess potential impacts on groundwater quality from septic systems: a review and examples from principal aquifers in the United States. *J. Hydrol.*, *397* (3-4), 151-166.

Kaushal, S. S., P. M. Groffman, L. E. Band, E. M. Elliott, C. A. Shields, and C. Kendall, **2011**, Tracking nonpoint source nitrogen pollution in human-impacted watersheds. *Environ. Sci. Technol.*, *45* (19), 8225-8232.

Kendall, C., E. M. Elliott, and S. D. Wankel, **2007**, Tracing anthropogenic inputs of nitrogen to ecosystems. *Stable isotopes in ecology and environmental science*, *2* (1), 375-449.

Kim, M. S., E. Piggott, N. Zrinyi, C. Lee, and A. L.-T. Pham, **2020**, Reduction of chlorendic acid by zero-valent iron: Kinetics, products, and pathways. *J. Hazard. Mater.*, *384*, 121269.

Kim, S., D. Kim, M. J. Jung, and S. Kim, **2021**, Analysis of environmental organic matters by Ultrahigh-Resolution mass spectrometry—A review on the development of analytical methods. *Mass Spectrom. Rev.*

Kind, T., and O. Fiehn, **2007**, Seven Golden Rules for heuristic filtering of molecular formulas obtained by accurate mass spectrometry. *BMC Bioinform.*, *8* (1), 105.

Kjeldsen, P., M. A. Barlaz, A. P. Rooker, A. Baun, A. Ledin, and T. H. Christensen, **2002**, Present and long-term composition of MSW landfill leachate: a review. *Crit. Rev. Environ. Sci. Technol.*, *32* (4), 297-336.

Kleinsteuber, S., T. Rohwerder, U. Lohse, B. Seiwert, and T. Reemtsma, **2019**, Sated by a Zero-Calorie Sweetener: Wastewater Bacteria Can Feed on Acesulfame. *Front. Microbiol.*, *10*, 2606.

Koch, B. P., T. Dittmar, M. Witt, and G. Kattner, **2007**, Fundamentals of molecular formula assignment to ultrahigh resolution mass data of natural organic matter. *Anal. Chem.*, *79* (4), 1758-1763.

Koch, W., S. Forcisi, R. Lehmann, and P. Schmitt-Kopplin, **2014**, Sensitivity improvement in hydrophilic interaction chromatography negative mode electrospray ionization mass spectrometry using 2-(2-methoxyethoxy) ethanol as a post-column modifier for non-targeted metabolomics. *J. Chromatogr. A*, *1361*, 209-216.

Kokotou, M. G., and N. S. Thomaidis, **2013**, Determination of eight artificial sweeteners in wastewater by hydrophilic interaction liquid chromatography-tandem mass spectrometry. *Anal. Methods*, *5* (16), 3825-3833.

Kolpin, D. W., E. T. Furlong, M. T. Meyer, E. M. Thurman, S. D. Zaugg, L. B. Barber, and H. T. Buxton, **2002**, Pharmaceuticals, hormones, and other organic wastewater contaminants in US streams, 1999− 2000: A national reconnaissance. *Environ. Sci. Technol.*, *36* (6), 1202-1211.

Krook, J., N. Svensson, and M. Eklund, **2012**, Landfill mining: A critical review of two decades of research. *Waste Manage.*, *32* (3), 513-520.

Kümmerer, K., and E. Helmers, **2000**, Hospital effluents as a source of gadolinium in the aquatic environment. *Environ. Sci. Technol.*, *34* (4), 573-577.

Lam, J. C., J. Lyu, K. Y. Kwok, and P. K. Lam, **2016**, Perfluoroalkyl substances (PFASs) in marine mammals from the South China Sea and their temporal changes 2002–2014: concern for alternatives of PFOS? *Environ. Sci. Technol.*, *50* (13), 6728-6736.

Lang, J. R., B. M. Allred, J. A. Field, J. W. Levis, and M. A. Barlaz, **2017**, National estimate of per-and polyfluoroalkyl substance (PFAS) release to US municipal landfill leachate. *Environ. Sci. Technol.*, *51* (4), 2197-2205.

LeBlanc, L. A., J. S. Latimer, J. T. Ellis, and J. G. Quinn, **1992**, The geochemistry of coprostanol in waters and surface sediments from Narragansett Bay. *Estuar. Coast. Shelf Sci.*, *34* (5), 439-458.

Li, D., J. W. O'Brien, B. J. Tscharke, P. M. Choi, Q. Zheng, F. Ahmed, J. Thompson, J. Li, J. F. Mueller, and H. Sun, **2020**, National wastewater reconnaissance of artificial sweetener consumption and emission in Australia. *Environ. Int.*, *143*, 105963.

Li, J., Q. Ye, and J. Gan, **2014**, Degradation and transformation products of acetaminophen in soil. *Water Res.*, *49*, 44-52.

Li, Y., M. Harir, M. Lucio, B. Kanawati, K. Smirnov, R. Flerus, B. P. Koch, P. Schmitt-Kopplin, and N. Hertkorn, **2016**, Proposed guidelines for solid phase extraction of Suwannee River dissolved organic matter. *Anal. Chem.*, *88* (13), 6680-6688.

Lim, F. Y., S. L. Ong, and J. Hu, **2017**, Recent advances in the use of chemical markers for tracing wastewater contamination in aquatic environment: a review. *Water*, *9* (2), 143.

Liu, J., and S. M. Avendaño, **2013**, Microbial degradation of polyfluoroalkyl chemicals in the environment: a review. *Environ. Int.*, *61*, 98-114.

Liu, Y., and E. B. Kujawinski, **2015**, Chemical composition and potential environmental impacts of water-soluble polar crude oil components inferred from ESI FT-ICR MS. *PloS one, 10* (9), e0136376.

Longnecker, K., and E. B. Kujawinski, **2011**, Composition of dissolved organic matter in groundwater. *Geochim. Cosmochim. Acta, 75* (10), 2752-2761.

Loos, M., C. Gerber, F. Corona, J. Hollender, and H. Singer, **2015**, Accelerated isotope fine structure calculation using pruned transition trees. *Anal. Chem., 87* (11), 5738-5744.

Loos, R., R. Carvalho, D. C. António, S. Comero, G. Locoro, S. Tavazzi, B. Paracchini, M. Ghiani, T. Lettieri, and L. Blaha, **2013**, EU-wide monitoring survey on emerging polar organic contaminants in wastewater treatment plant effluents. *Water Res., 47* (17), 6475-6487.

Loos, R., B. M. Gawlik, K. Boettcher, G. Locoro, S. Contini, and G. Bidoglio, **2009**, Sucralose screening in European surface waters using a solid-phase extraction-liquid chromatography–triple quadrupole mass spectrometry method. *J. Chromatogr. A, 1216* (7), 1126-1131.

Loos, R., G. Locoro, T. Huber, J. Wollgast, E. H. Christoph, A. De Jager, B. M. Gawlik, G. Hanke, G. Umlauf, and J.-M. Zaldívar, **2008**, Analysis of perfluorooctanoate (PFOA) and other perfluorinated compounds (PFCs) in the River Po watershed in N-Italy. *Chemosphere, 71* (2), 306-313.

Lucio, M. Datamining metabolomics: the convergence point of non-target approach and statistical investigation. Technische Universität München, 2009.

Luek, J. L. Characterization of Organic Compounds in Hydraulic Fracturing Fluid. 2017.

Lusk, M. G., and G. S. Toor, **2016**, Dissolved organic nitrogen in urban streams: Biodegradability and molecular composition studies. *Water Res., 96*, 225-235.

Maizel, A. C., and C. K. Remucal, **2017**, The effect of advanced secondary municipal wastewater treatment on the molecular composition of dissolved organic matter. *Water Res., 122*, 42-52.

Marschall, H. R., and G. L. Foster, **2018**, Boron isotopes in the earth and planetary sciences—a short history and introduction. In *Boron Isotopes*, Springer: pp 1-11.

Maryland Department of the Environment, **2009**, Maryland Historic Landfill Initiative, Available from: https://mde.maryland.gov/programs/LAND/MarylandBrownfieldVCP/Pages/HistoricLandfillInitiative.aspx.

Maryland Senate Bill 236, **2012**, Legislation by Session. Available from: http://mlis.state.md.us/2012rs/billfile/sb0236.htm.

Maryland Senate Bill 320, **2004**, Legislation by Session. Available from: http://mlis.state.md.us/2004rs/billfile/sb0320.htm.

Masoner, J. R., D. W. Kolpin, I. M. Cozzarelli, K. L. Smalling, S. C. Bolyard, J. A. Field, E. T. Furlong, J. L. Gray, D. Lozinski, and D. Reinhart, **2020**, Landfill leachate contributes per-/poly-fluoroalkyl substances (PFAS) and pharmaceuticals to municipal wastewater. *Environ. Sci. Water Res. Technol.*, *6* (5), 1300-1311.

Masoner, J. R., D. W. Kolpin, E. T. Furlong, I. M. Cozzarelli, and J. L. Gray, **2016**, Landfill leachate as a mirror of today's disposable society: pharmaceuticals and other contaminants of emerging concern in final leachate from landfills in the conterminous United States. *Environ. Toxicol. Chem.*, *35* (4), 906-918.

Masoner, J. R., D. W. Kolpin, E. T. Furlong, I. M. Cozzarelli, J. L. Gray, and E. A. Schwab, **2014**, Contaminants of emerging concern in fresh leachate from landfills in the conterminous United States. *Environ. Sci. Process. Impacts*, *16* (10), 2335-2354.

Mawhinney, D. B., R. B. Young, B. J. Vanderford, T. Borch, and S. A. Snyder, **2011**, Artificial sweetener sucralose in US drinking water systems. *Environ. Sci. Technol.*, *45* (20), 8716-8722.

McMillan, A., J. B. Renaud, G. B. Gloor, G. Reid, and M. W. Sumarah, **2016**, Post-acquisition filtering of salt cluster artefacts for LC-MS based human metabolomic studies. *J. Cheminformatics*, *8* (1), 1-5.

Mead, R. N., J. B. Morgan, G. B. Avery Jr, R. J. Kieber, A. M. Kirk, S. A. Skrabal, and J. D. Willey, **2009**, Occurrence of the artificial sweetener sucralose in coastal and marine waters of the United States. *Mar. Chem.*, *116* (1-4), 13-17.

Meyer, C., S. Perez, C. Herve du Penhoat, and V. Michon, **1993**, Conformational analysis of 4, 1', 6'-trichloro-4, 1', 6'-trideoxy-galacto-sucrose (Sucralose) by a combined molecular-modeling and NMR spectroscopy approach. *J. Am. Chem. Soc.*, *115* (22), 10300-10310.

Michalski, G., T. Meixner, M. Fenn, L. Hernandez, A. Sirulnik, E. Allen, and M. Thiemens, **2004**, Tracing atmospheric nitrate deposition in a complex semiarid ecosystem using $\Delta^{17}O$. *Environ. Sci. Technol.*, *38* (7), 2175-2181.

Michalski, G., Z. Scott, M. Kabiling, and M. H. Thiemens, **2003**, First measurements and modeling of $\Delta^{17}O$ in atmospheric nitrate. *Geophys. Res. Lett.*, *30* (16).

Mitchelmore, C. L., K. He, M. Gonsior, E. Hain, A. Heyes, C. Clark, R. Younger, P. Schmitt-Kopplin, A. Feerick, and A. Conway, **2019**, Occurrence and distribution of UV-filters and other anthropogenic contaminants in coastal surface water, sediment, and coral tissue from Hawaii. *Sci. Total Environ.*, *670*, 398-410.

Mohammadzadeh, H., and I. Clark, **2008**, Degradation pathways of dissolved carbon in landfill leachate traced with compound-specific ^{13}C analysis of DOC. *Isotopes Environ. Health Stud.*, *44* (3), 267-294.

Mohammadzadeh, H., and I. Clark, **2011**, Bioattenuation in groundwater impacted by landfill leachate traced with $\delta^{13}C$. *Groundwater*, *49* (6), 880-890.

Montoya, J. P., **2007**, Natural abundance of 15N in marine planktonic ecosystems. *Stable isotopes in ecology and environmental science*, 176-201.

Moskalyk, R., and A. Alfantazi, **2003**, Processing of vanadium: a review. *Miner. Eng.*, *16* (9), 793-805.

Murphy, K. R., A. Hambly, S. Singh, R. K. Henderson, A. Baker, R. Stuetz, and S. J. Khan, **2011**, Organic matter fluorescence in municipal water recycling schemes: toward a unified PARAFAC model. *Environ. Sci. Technol.*, *45* (7), 2909-2916.

Murphy, K. R., C. A. Stedmon, D. Graeber, and R. Bro, **2013**, Fluorescence spectroscopy and multi-way techniques. PARAFAC. *Anal. Methods*, *5* (23), 6557-6566.

Murphy, K. R., C. A. Stedmon, P. Wenig, and R. Bro, **2014**, OpenFluor–an online spectral library of auto-fluorescence by organic compounds in the environment. *Anal. Methods*, *6* (3), 658-661.

mzCloud: Advanced Mass Spectral Database, **2018**, Chlorendic acid, Available from: https://www.mzcloud.org/compound/reference/2993.

Neset, T.-S. S., H. Singer, P. Longrée, H.-P. Bader, R. Scheidegger, A. Wittmer, and J. C. M. Andersson, **2010**, Understanding consumption-related sucralose emissions—A conceptual approach combining substance-flow analysis with sampling analysis. *Sci. Total Environ.*, *408* (16), 3261-3269.

NTP (National Toxicology Program), **2016**, Report on Carcinogens, Fourteenth Edition: Chlorendic Acid. U.S. Department of Health and Human Services: Research Triangle Park.

Oakley, S. M., A. J. Gold, and A. J. Oczkowski, **2010**, Nitrogen control through decentralized wastewater treatment: Process performance and alternative management strategies. *Ecol. Eng.*, *36* (11), 1520-1531.

Oloibiri, V., S. De Coninck, M. Chys, K. Demeestere, and S. W. Van Hulle, **2017**, Characterisation of landfill leachate by EEM-PARAFAC-SOM during physical-chemical treatment by coagulation-flocculation, activated carbon adsorption and ion exchange. *Chemosphere*, *186*, 873-883.

Öman, C., and P.-Å. Hynning, **1993**, Identification of organic compounds in municipal landfill leachates. *Environ. Pollut.*, *80* (3), 265-271.

Oppenheimer, J., A. Eaton, M. Badruzzaman, A. W. Haghani, and J. G. Jacangelo, **2011**, Occurrence and suitability of sucralose as an indicator compound of wastewater loading to surface waters in urbanized regions. *Water Res.*, *45* (13), 4019-4027.

Oppenheimer, J. A., M. Badruzzaman, and J. G. Jacangelo, **2012**, Differentiating sources of anthropogenic loading to impaired water bodies utilizing ratios of sucralose and other microconstituents. *Water Res.*, *46* (18), 5904-5916.

Ordoñez, E. Y., J. B. Quintana, R. Rodil, and R. Cela, **2013**, Determination of artificial sweeteners in sewage sludge samples using pressurised liquid extraction and liquid chromatography–tandem mass spectrometry. *J. Chromatogr. A*, *1320*, 10-16.

Ordóñez, E. Y., J. B. Quintana, R. Rodil, and R. Cela, **2012**, Determination of artificial sweeteners in water samples by solid-phase extraction and liquid chromatography–tandem mass spectrometry. *J. Chromatogr. A*, *1256*, 197-205.

Ottmar, K. J., L. M. Colosi, and J. A. Smith, **2012**, Fate and transport of atorvastatin and simvastatin drugs during conventional wastewater treatment. *Chemosphere*, *88* (10), 1184-1189.

Palmer, M., A. Spivack, and J. Edmond, **1987**, Temperature and pH controls over isotopic fractionation during adsorption of boron on marine clay. *Geochim. Cosmochim. Acta*, *51* (9), 2319-2323.

Panno, S., K. C. Hackley, H. Hwang, S. Greenberg, I. Krapac, S. Landsberger, and D. O'kelly, **2006**, Characterization and identification of Na-Cl sources in ground water. *Groundwater*, *44* (2), 176-187.

Pastén-Zapata, E., R. Ledesma-Ruiz, T. Harter, A. I. Ramírez, and J. Mahlknecht, **2014**, Assessment of sources and fate of nitrate in shallow groundwater of an agricultural area by using a multi-tracer approach. *Sci. Total Environ.*, *470*, 855-864.

Paxéus, N., **2000**, Organic compounds in municipal landfill leachates. *Water Sci. Technol.*, *42* (7-8), 323-333.

Pehlivanoglu-Mantas, E., and D. L. Sedlak, **2006**, Wastewater-derived dissolved organic nitrogen: analytical methods, characterization, and effects—a review. *Crit. Rev. Environ. Sci. Technol.*, *36* (3), 261-285.

Phillips, P., A. Chalmers, J. Gray, D. Kolpin, W. Foreman, and G. Wall, **2012**, Combined sewer overflows: an environmental source of hormones and wastewater micropollutants. *Environ. Sci. Technol.*, *46* (10), 5336-5343.

Poiger, T., J. A. Field, T. M. Field, H. Siegrist, and W. Giger, **1998**, Behavior of fluorescent whitening agents during sewage treatment. *Water Res.*, *32* (6), 1939-1947.

Poulin, B. A., J. N. Ryan, and G. R. Aiken, **2014**, Effects of iron on optical properties of dissolved organic matter. *Environ. Sci. Technol.*, *48* (17), 10098-10106.

Powers, L. C., J. L. Luek, P. Schmitt-Kopplin, B. J. Campbell, C. Magen, L. W. Cooper, and M. Gonsior, **2018**, Seasonal changes in dissolved organic matter composition in Delaware Bay, USA in March and August 2014. *Org. Geochem.*, *122*, 87-97.

Ptacek, C. J., **1998**, Geochemistry of a septic-system plume in a coastal barrier bar, Point Pelee, Ontario, Canada. *J. Contam. Hydrol.*, *33* (3-4), 293-312.

Radke, M., C. Lauwigi, G. Heinkele, T. E. Mürdter, and M. Letzel, **2009**, Fate of the antibiotic sulfamethoxazole and its two major human metabolites in a water sediment test. *Environ. Sci. Technol.*, *43* (9), 3135-3141.

Raeke, J., O. J. Lechtenfeld, M. Wagner, P. Herzsprung, and T. Reemtsma, **2016**, Selectivity of solid phase extraction of freshwater dissolved organic matter and its effect on ultrahigh resolution mass spectra. *Environ. Sci. Process. Impacts*, *18* (7), 918-927.

Raymond, P. A., and J. E. Bauer, **2001**, Use of ^{14}C and ^{13}C natural abundances for evaluating riverine, estuarine, and coastal DOC and POC sources and cycling: a review and synthesis. *Org. Geochem.*, *32* (4), 469-485.

Reinhart, D. R., and T. G. Townsend, **1997**, *Landfill bioreactor design & operation*. CRC press.

Reinhart, D. R., and T. G. Townsend, **2007**, Design and Operational Issues Related to the Co-Disposal of Sludges and Biosolids in Class I Landfills-Phase III. *report to the Florida Center for Solid and Hazardous Waste Management*.

Renou, S., J. Givaudan, S. Poulain, F. Dirassouyan, and P. Moulin, **2008**, Landfill leachate treatment: Review and opportunity. *J. Hazard. Mater.*, *150* (3), 468-493.

Reynolds, G. W., J. T. Hoff, and R. W. Gillham, **1990**, Sampling bias caused by materials used to monitor halocarbons in groundwater. *Environ. Sci. Technol.*, *24* (1), 135-142.

Ribbers, K., L. Breuer, and R.-A. Düring, **2019**, Detection of artificial sweeteners and iodinated X-ray contrast media in wastewater via LC-MS/MS and their potential use as anthropogenic tracers in flowing waters. *Chemosphere, 218*, 189-196.

Richards, S., E. Paterson, P. J. Withers, and M. Stutter, **2016**, Septic tank discharges as multi-pollutant hotspots in catchments. *Sci. Total Environ., 542*, 854-863.

Richards, S., P. J. Withers, E. Paterson, C. W. McRoberts, and M. Stutter, **2017**, Potential tracers for tracking septic tank effluent discharges in watercourses. *Environ. Pollut., 228*, 245-255.

Richardson, S. D., and S. Y. Kimura, **2020**, Water analysis: emerging contaminants and current issues. *Anal. Chem., 92* (1), 473-505.

Roberts, A., A. Renwick, J. Sims, and D. Snodin, **2000**, Sucralose metabolism and pharmacokinetics in man. *Food Chem. Toxicol., 38*, 31-41.

Robertson, W., **2008**, Irreversible phosphorus sorption in septic system plumes? *Groundwater, 46* (1), 51-60.

Robertson, W., and D. Blowes, **1995**, Major ion and trace metal geochemistry of an acidic septic-system plume in silt. *Groundwater, 33* (2), 275-283.

Robertson, W., T. Moore, J. Spoelstra, L. Li, R. Elgood, I. Clark, S. Schiff, R. Aravena, and J. Neufeld, **2012**, Natural attenuation of septic system nitrogen by anammox. *Groundwater, 50* (4), 541-553.

Robertson, W., D. Van Stempvoort, D. Solomon, J. Homewood, S. Brown, J. Spoelstra, and S. Schiff, **2013**, Persistence of artificial sweeteners in a 15-year-old septic system plume. *J. Hydrol., 477*, 43-54.

Robertson, W., D. Van Stempvoort, J. Spoelstra, S. Brown, and S. Schiff, **2016**, Degradation of sucralose in groundwater and implications for age dating contaminated groundwater. *Water Res., 88*, 653-660.

Robertson, W. D., and D. L. Garda, **2020**, Pyrite oxidation halts migration of a phosphorus plume. *Groundwater, 58* (1), 27-34.

Robertson, W. D., S. Schiff, and C. Ptacek, **1998**, Review of phosphate mobility and persistence in 10 septic system plumes. *Groundwater, 36* (6), 1000-1010.

Robertson, W. D., D. R. Van Stempvoort, and S. L. Schiff, **2019**, Review of phosphorus attenuation in groundwater plumes from 24 septic systems. *Sci. Total Environ., 692*, 640-652.

Rodríguez-Escales, P., and X. Sanchez-Vila, **2016**, Fate of sulfamethoxazole in groundwater: Conceptualizing and modeling metabolite formation under different redox conditions. *Water Res., 105,* 540-550.

Rogers, J. D., E. M. Thurman, I. Ferrer, J. S. Rosenblum, M. V. Evans, P. J. Mouser, and J. N. Ryan, **2019**, Degradation of polyethylene glycols and polypropylene glycols in microcosms simulating a spill of produced water in shallow groundwater. *Environ. Sci. Process. Impacts, 21* (2), 256-268.

Roy, J. W., D. R. Van Stempvoort, and G. Bickerton, **2014**, Artificial sweeteners as potential tracers of municipal landfill leachate. *Environ. Pollut., 184,* 89-93.

Ruf, A. Enhancing detection sensitivity in mass spectrometry by anionic dopants, M.S. Thesis. Technische Universität München, 2013.

Sauvé, S., and M. Desrosiers, **2014**, A review of what is an emerging contaminant. *Chem. Cent. J., 8* (1), 1-7.

Schaedler, F., C. Lockwood, U. Lueder, C. Glombitza, A. Kappler, and C. Schmidt, **2018**, Microbially mediated coupling of Fe and N cycles by nitrate-reducing Fe (II)-oxidizing bacteria in littoral freshwater sediments. *Appl. Environ. Microbiol., 84* (2), e02013-17.

Schaider, L. A., J. M. Ackerman, and R. A. Rudel, **2016**, Septic systems as sources of organic wastewater compounds in domestic drinking water wells in a shallow sand and gravel aquifer. *Sci. Total Environ., 547,* 470-481.

Schaider, L. A., S. A. Balan, A. Blum, D. Q. Andrews, M. J. Strynar, M. E. Dickinson, D. M. Lunderberg, J. R. Lang, and G. F. Peaslee, **2017**, Fluorinated compounds in US fast food packaging. *Environ. Sci. Technol., 4* (3), 105-111.

Scheurer, M., H.-J. Brauch, and F. T. Lange, **2009**, Analysis and occurrence of seven artificial sweeteners in German waste water and surface water and in soil aquifer treatment (SAT). *Anal. Bioanal. Chem., 394* (6), 1585-1594.

Scheurer, M., F. R. Storck, H.-J. Brauch, and F. T. Lange, **2010**, Performance of conventional multi-barrier drinking water treatment plants for the removal of four artificial sweeteners. *Water Res., 44* (12), 3573-3584.

Schmitt-Kopplin, P., Z. Gabelica, R. D. Gougeon, A. Fekete, B. Kanawati, M. Harir, I. Gebefuegi, G. Eckel, and N. Hertkorn, **2010**, High molecular diversity of extraterrestrial organic matter in Murchison meteorite revealed 40 years after its fall. *Proc. Natl. Acad. Sci. U.S.A., 107* (7), 2763-2768.

Seiler, R. L., **2005**, Combined use of ^{15}N and ^{18}O of nitrate and ^{11}B to evaluate nitrate contamination in groundwater. *Appl. Geochem., 20* (9), 1626-1636.

Seurinck, S., T. Defoirdt, W. Verstraete, and S. D. Siciliano, **2005**, Detection and quantification of the human-specific HF183 Bacteroides 16S rRNA genetic marker with real-time PCR for assessment of human faecal pollution in freshwater. *Environ. Microbiol., 7* (2), 249-259.

Sharpless, C. M., and N. V. Blough, **2014**, The importance of charge-transfer interactions in determining chromophoric dissolved organic matter (CDOM) optical and photochemical properties. *Environ. Sci. Process. Impacts*, *16* (4), 654-671.

Shen, L., E. J. Reiner, K. A. MacPherson, T. M. Kolic, P. A. Helm, L. A. Richman, C. H. Marvin, D. A. Burniston, B. Hill, and I. D. Brindle, **2011**, Dechloranes 602, 603, 604, Dechlorane Plus, and Chlordene Plus, a newly detected analogue, in tributary sediments of the Laurentian Great Lakes. *Environ. Sci. Technol., 45* (2), 693-699.

Showers, W. J., B. Genna, T. McDade, R. Bolich, and J. C. Fountain, **2008**, Nitrate contamination in groundwater on an urbanized dairy farm. *Environ. Sci. Technol., 42* (13), 4683-4688.

Singer, H., S. Müller, C. Tixier, and L. Pillonel, **2002**, Triclosan: occurrence and fate of a widely used biocide in the aquatic environment: field measurements in wastewater treatment plants, surface waters, and lake sediments. *Environ. Sci. Technol., 36* (23), 4998-5004.

Singh, S. P., A. Azua, A. Chaudhary, S. Khan, K. L. Willett, and P. R. Gardinali, **2010**, Occurrence and distribution of steroids, hormones and selected pharmaceuticals in South Florida coastal environments. *Ecotoxicology*, *19* (2), 338-350.

Singh, S. P., and P. Bose, **2017**, Reductive dechlorination of endosulfan isomers and its metabolites by zero-valent metals: reaction mechanism and degradation products. *RSC Adv., 7* (44), 27668-27677.

Slack, R., J. Gronow, and N. Voulvoulis, **2005**, Household hazardous waste in municipal landfills: contaminants in leachate. *Sci. Total Environ., 337* (1-3), 119-137.

Smirnov, K. Ultra-High Resolution Mass Spectrometry in Characterizing the Impact of Whole Grain Diet on Human Gut Meta-Metabolome. Technische Universität München, 2018.

Smith, J. P., S. D. Oktay, J. Kada, and C. R. Olsen, **2008**, Iodine-131: a potential short-lived, wastewater-specific particle tracer in an urbanized estuarine system. *Environ. Sci. Technol., 42* (15), 5435-5440.

Snider, D. M., J. W. Roy, W. D. Robertson, D. I. Garda, and J. Spoelstra, **2017**, Concentrations of artificial sweeteners and their ratios with nutrients in septic system wastewater. *Ground Water Monit. Rem., 37* (3), 94-102.

Soh, L., K. A. Connors, B. W. Brooks, and J. Zimmerman, **2011**, Fate of sucralose through environmental and water treatment processes and impact on plant indicator species. *Environ. Sci. Technol., 45* (4), 1363-1369.

Song, F., **2011**, "Cross-talk" in scheduled multiple reaction monitoring caused by in-source fragmentation in herbicide screening with liquid chromatography electrospray tandem mass spectrometry. *J. Agric. Food. Chem., 59* (9), 4361-4364.

Standley, L. J., R. A. Rudel, C. H. Swartz, K. R. Attfield, J. Christian, M. Erickson, and J. G. Brody, **2008**, Wastewater-contaminated groundwater as a source of endogenous hormones and pharmaceuticals to surface water ecosystems. *Environ. Toxicol. Chem., 27* (12), 2457-2468.

Stanley, E. H., and J. T. Maxted, **2008**, Changes in the dissolved nitrogen pool across land cover gradients in Wisconsin streams. *Ecol. Appl., 18* (7), 1579-1590.

Statom, R., G. Thyne, and J. McCray, **2004**, Temporal changes in leachate chemistry of a municipal solid waste landfill cell in Florida, USA. *Environ. Geol., 45* (7), 982-991.

Stedmon, C. A., and R. Bro, **2008**, Characterizing dissolved organic matter fluorescence with parallel factor analysis: a tutorial. *Limnol. Oceanogr. Methods, 6* (11), 572-579.

Stefania, G. A., M. Rotiroti, I. J. Buerge, C. Zanotti, V. Nava, B. Leoni, L. Fumagalli, and T. Bonomi, **2019**, Identification of groundwater pollution sources in a landfill site using artificial sweeteners, multivariate analysis and transport modeling. *Waste Manage., 95*, 116-128.

Stenson, A. C., A. G. Marshall, and W. T. Cooper, **2003**, Exact masses and chemical formulas of individual Suwannee River fulvic acids from ultrahigh resolution electrospray ionization Fourier transform ion cyclotron resonance mass spectra. *Anal. Chem., 75* (6), 1275-1284.

Stockholm Convention, **2017**, Stockholm Convention on persistent organic pollutions (POPs).

Stookey, L. L., **1970**, Ferrozine—a new spectrophotometric reagent for iron. *Anal. Chem., 42* (7), 779-781.

Stubbins, A., J.-F. Lapierre, M. Berggren, Y. T. Prairie, T. Dittmar, and P. A. del Giorgio, **2014**, What's in an EEM? Molecular signatures associated with dissolved organic fluorescence in boreal Canada. *Environ. Sci. Technol., 48* (18), 10598-10606.

Subedi, B., N. Codru, D. M. Dziewulski, L. R. Wilson, J. Xue, S. Yun, E. Braun-Howland, C. Minihane, and K. Kannan, **2015**, A pilot study on the assessment of trace organic contaminants including pharmaceuticals and personal care products from on-site wastewater treatment systems along Skaneateles Lake in New York State, USA. *Water Res., 72*, 28-39.

Subedi, B., and K. Kannan, **2014**, Fate of artificial sweeteners in wastewater treatment plants in New York State, USA. *Environ. Sci. Technol., 48* (23), 13668-13674.

Swaney, D. P., B. Hong, C. Ti, R. W. Howarth, and C. Humborg, **2012**, Net anthropogenic nitrogen inputs to watersheds and riverine N export to coastal waters: a brief overview. *Curr. Opin. Environ. Sustain., 4* (2), 203-211.

Sylvetsky, A. C., and K. I. Rother, **2016**, Trends in the consumption of low-calorie sweeteners. *Physiol. Behav., 164*, 446-450.

Thiemens, M. H., and J. E. Heidenreich, **1983**, The mass-independent fractionation of oxygen: A novel isotope effect and its possible cosmochemical implications. *Science, 219* (4588), 1073-1075.

Torres, C. I., S. Ramakrishna, C.-A. Chiu, K. G. Nelson, P. Westerhoff, and R. Krajmalnik-Brown, **2011**, Fate of sucralose during wastewater treatment. *Environ. Eng. Sci., 28* (5), 325-331.

Trudel, D., L. Horowitz, M. Wormuth, M. Scheringer, I. T. Cousins, and K. Hungerbühler, **2008**, Estimating consumer exposure to PFOS and PFOA. *Risk Anal., 28* (2), 251-269.

Tseng, L. Y., M. Gonsior, P. Schmitt-Kopplin, W. J. Cooper, P. Pitt, and D. Rosso, **2013**, Molecular characteristics and differences of effluent organic matter from parallel activated sludge and integrated fixed-film activated sludge (IFAS) processes. *Environ. Sci. Technol., 47* (18), 10277-10284.

Twardowski, M. S., E. Boss, J. M. Sullivan, and P. L. Donaghay, **2004**, Modeling the spectral shape of absorption by chromophoric dissolved organic matter. *Mar. Chem., 89* (1-4), 69-88.

Tziotis, D., N. Hertkorn, and P. Schmitt-Kopplin, **2011**, Kendrick-analogous network visualisation of ion cyclotron resonance Fourier transform mass spectra: improved options for the assignment of elemental compositions and the classification of organic molecular complexity. *Eur. J. Mass Spectrom., 17* (4), 415-421.

United States Census Bureau, **1992**, Maryland: 1990, Population and Housing Unit Counts. *1990 United States Census*.

United States Census Bureau, **2012**, Maryland: 2010, Population and Housing Unit Counts. *2010 United States Census*.

United States Environmental Protection Agency, **1988**, Federal Register: August 30, 1988, Part III. 40 CFR Parts 257 and 258. Solid Waste Disposal Facility Criteria; Proposed Rule. Vol. 53, p 33345.

United States Environmental Protection Agency, **1991**, Federal Register: October 9, 1991, Part II. 40 CFR Parts 257 and 258. Solid Waste Disposal Facility Criteria; Final Rule. Vol. 56, pp 51011-51012.

United States Environmental Protection Agency, **1993**, Method 410.4, Revision 2.0: The Determination of Chemical Oxygen Demand by SemiAutomated Colorimetry.

United States Environmental Protection Agency, **2002**, Onsite wastewater treatment systems manual.

United States Environmental Protection Agency, **2007**, EPA Method 1694: Pharmaceuticals and personal care products in water, soil, sediment, and biosolids by HPLC/MS/MS, December 2007.

United States Environmental Protection Agency, **2008a**, Municipal Solid Waste in The United States: 2007 Facts and Figures.

United States Environmental Protection Agency, **2008b**, Septic Systems Fact Sheet. United States Environmental Protection Agency Washington, DC.

United States Environmental Protection Agency, **2016**, Aquatic Life Ambient Water Quality Criteria Update for Cadmium-2016

United States Environmental Protection Agency, **2020a**, Advancing Sustainable Materials Management: 2018 Fact Sheet, Assessing Trends in Materials Generation and Management in the United States.

United States Environmental Protection Agency, **2020b**, Landfill Methane Outreach Program Landfill and Landfill Gas Energy Project Database https://www.epa.gov/lmop/landfill-technical-data.

United States Food and Drug Administration, **1988**, Federal Register: July 28, 1988, 21 CFR Part 172. Food Additives Permitted For Direct Addition To Food For Human Consumption; Acesulfame Potassium; Final Rule. Vol. 53, pp 28379-28383.

United States Food and Drug Administration, **2016**, Federal Register: August 30, 2016, 21 CFR Part 310. Safety and Effectiveness of Consumer Antiseptics; Topical Antimicrobial Drug Products for Over-the-Counter Human Use; Final Rule. Vol. 81, pp 61106-61130.

United States Geological Survey, **2017**, StreamStats: Streamflow Statistics and Spatial Analysis Tools for Water-Resources Applications, Available from: http://streamstats.usgs.gov.

United States Geological Survey, **2019**, Chesapeake Bay Phase 6 Land Use Viewer, Available from: https://chesapeake.usgs.gov/phase6/map.

van Breukelen, B. M., W. F. Röling, J. Groen, J. Griffioen, and H. W. van Verseveld, **2003**, Biogeochemistry and isotope geochemistry of a landfill leachate plume. *J. Contam. Hydrol.*, *65* (3-4), 245-268.

Van Drecht, G., A. Bouwman, J. Harrison, and J. Knoop, **2009**, Global nitrogen and phosphate in urban wastewater for the period 1970 to 2050. *Global Biogeochem. Cycles*, *23* (4).

van Krevelen, D., **1950**, Graphical-statistical method for the study of structure and reaction processes of coal. *Fuel*, *29*, 269-284.

Van Stempvoort, D. R., J. W. Roy, S. J. Brown, and G. Bickerton, **2011**, Artificial sweeteners as potential tracers in groundwater in urban environments. *J. Hydrol.*, *401* (1-2), 126-133.

Vengosh, A., **1998**, The isotopic composition of anthropogenic boron and its potential impact on the environment. *Biol. Trace Elem. Res.*, *66* (1), 145-151.

Vengosh, A., K. Heumann, S. Juraske, and R. Kasher, **1994**, Boron isotope application for tracing sources of contamination in groundwater. *Environ. Sci. Technol.*, *28* (11), 1968-1974.

Vengosh, A., and I. Pankratov, **1998**, Chloride/bromide and chloride/fluoride ratios of domestic sewage effluents and associated contaminated ground water. *Groundwater*, *36* (5), 815-824.

Venkiteswaran, J., P. Boeckx, and D. Gooddy, **2019**, Towards a global interpretation of dual nitrate isotopes in surface waters. *J. Hydrol. X*, *4*, 100037.

Vogel, T. M., C. S. Criddle, and P. L. McCarty, **1987**, ES&T critical reviews: transformations of halogenated aliphatic compounds. *Environ. Sci. Technol.*, *21* (8), 722-736.

Wang, M., J. Li, H. Shi, D. Miao, Y. Yang, L. Qian, and S. Gao, **2018**, Photolysis of atorvastatin in aquatic environment: Influencing factors, products, and pathways. *Chemosphere*, *212*, 467-475.

Wang, S., M. Matt, B. L. Murphy, M. Perkins, D. A. Matthews, S. D. Moran, and T. Zeng, **2020**, Organic micropollutants in New York lakes: a statewide citizen science occurrence study. *Environ. Sci. Technol.*, *54* (21), 13759-13770.

Wasik, A., J. McCourt, and M. Buchgraber, **2007**, Simultaneous determination of nine intense sweeteners in foodstuffs by high performance liquid chromatography and evaporative light scattering detection—development and single-laboratory validation. *J. Chromatogr. A*, *1157* (1-2), 187-196.

Waska, H., A. Koschinsky, M. J. R. Chancho, and T. Dittmar, **2015**, Investigating the potential of solid-phase extraction and Fourier-transform ion cyclotron resonance mass spectrometry (FT-ICR-MS) for the isolation and identification of dissolved metal–organic complexes from natural waters. *Mar. Chem.*, *173*, 78-92.

Wei, Z., T. Xu, and D. Zhao, **2019**, Treatment of per-and polyfluoroalkyl substances in landfill leachate: status, chemistry and prospects. *Environ. Sci. Water Res. Technol.*, *5* (11), 1814-1835.

Weishaar, J. L., G. R. Aiken, B. A. Bergamaschi, M. S. Fram, R. Fujii, and K. Mopper, **2003**, Evaluation of specific ultraviolet absorbance as an indicator of the chemical composition and reactivity of dissolved organic carbon. *Environ. Sci. Technol.*, *37* (20), 4702-4708.

Weller, D. E., M. E. Baker, and T. E. Jordan, **2011**, Effects of riparian buffers on nitrate concentrations in watershed discharges: new models and management implications. *Ecol. Appl.*, *21* (5), 1679-1695.

Weller, D. E., T. E. Jordan, D. L. Correll, and Z.-J. Liu, **2003**, Effects of land-use change on nutrient discharges from the Patuxent River watershed. *Estuaries*, *26* (2), 244-266.

Wickham, H., **2016**, *ggplot2: elegant graphics for data analysis*. Springer-Verlag: New York.

Wilhelm, S. R., S. L. Schiff, and J. A. Cherry, **1994**, Biogeochemical evolution of domestic waste water in septic systems: 1. Conceptual model. *Groundwater*, *32* (6), 905-916.

Wilhelm, S. R., S. L. Schiff, and W. D. Robertson, **1996**, Biogeochemical evolution of domestic waste water in septic systems: 2. Application of conceptual model in sandy aquifers. *Groundwater*, *34* (5), 853-864.

Williams, C., and D. David, **1976**, The accumulation in soil of cadmium residues from phosphate fertilizers and their effect on the cadmium content of plants. *Soil Sci.*, *121* (2), 86-93.

Wolf, L., C. Zwiener, and M. Zemann, **2012**, Tracking artificial sweeteners and pharmaceuticals introduced into urban groundwater by leaking sewer networks. *Sci. Total Environ.*, *430*, 8-19.

Wong, A. W., H. Wang, and C. B. Lebrilla, **2000**, Selection of anionic dopant for quantifying desialylation reactions with MALDI-FTMS. *Anal. Chem.*, *72* (7), 1419-1425.

Wood, S., B. John, and D. Hawkins, **2000**, The pharmacokinetics and metabolism of sucralose in the dog. *Food Chem. Toxicol.*, *38*, 99-106.

Wu, M., Y. Qian, J. M. Boyd, S. E. Hrudey, X. C. Le, and X.-F. Li, **2014**, Direct large volume injection ultra-high performance liquid chromatography-tandem mass spectrometry determination of artificial sweeteners sucralose and acesulfame in well water. *J. Chromatogr. A*, *1359*, 156-161.

Xu, Y.-F., W. Lu, and J. D. Rabinowitz, **2015**, Avoiding misannotation of in-source fragmentation products as cellular metabolites in liquid chromatography–mass spectrometry-based metabolomics. *Anal. Chem.*, *87* (4), 2273-2281.

Yang, L., J. Hur, and W. Zhuang, **2015**, Occurrence and behaviors of fluorescence EEM-PARAFAC components in drinking water and wastewater treatment systems and their applications: a review. *Environ. Sci. Pollut. Res.*, *22* (9), 6500-6510.

Yang, Y.-Y., G. S. Toor, P. C. Wilson, and C. F. Williams, **2016**, Septic systems as hot-spots of pollutants in the environment: Fate and mass balance of micropollutants in septic drainfields. *Sci. Total Environ.*, *566*, 1535-1544.

Yasuhara, A., H. Shiraishi, M. Nishikawa, T. Yamamoto, O. Nakasugi, T. Okumura, K. Kenmotsu, H. Fukui, M. Nagase, and Y. Kawagoshi, **1999**, Organic components in leachates from hazardous waste disposal sites. *Waste Manage. Res.*, *17* (3), 186-197.

Ying, G.-G., X.-Y. Yu, and R. S. Kookana, **2007**, Biological degradation of triclocarban and triclosan in a soil under aerobic and anaerobic conditions and comparison with environmental fate modelling. *Environ. Pollut.*, *150* (3), 300-305.

Yuan, Z., C. He, Q. Shi, C. Xu, Z. Li, C. Wang, H. Zhao, and J. Ni, **2017**, Molecular insights into the transformation of dissolved organic matter in landfill leachate concentrate during biodegradation and coagulation processes using ESI FT-ICR MS. *Environ. Sci. Technol.*, *51* (14), 8110-8118.

Zanini, L., W. Robertson, C. Ptacek, S. Schiff, and T. Mayer, **1998**, Phosphorus characterization in sediments impacted by septic effluent at four sites in central Canada. *J. Contam. Hydrol.*, *33* (3-4), 405-429.

Zepp, R. G., W. M. Sheldon, and M. A. Moran, **2004**, Dissolved organic fluorophores in southeastern US coastal waters: correction method for eliminating Rayleigh and Raman scattering peaks in excitation–emission matrices. *Mar. Chem.*, *89* (1-4), 15-36.

Zhang, T., H. Sun, X. Qin, Z. Gan, and K. Kannan, **2015**, PFOS and PFOA in paired urine and blood from general adults and pregnant women: assessment of urinary elimination. *Environ. Sci. Pollut. Res.*, *22* (7), 5572-5579.

Zhu, J., and R. B. Cole, **2000**, Formation and decompositions of chloride adduct ions,[M+ Cl]−, in negative ion electrospray ionization mass spectrometry. *J. Am. Soc. Mass. Spectrom.*, *11* (11), 932-941.

Zhu, J., and R. B. Cole, **2001**, Ranking of gas-phase acidities and chloride affinities of monosaccharides and linkage specificity in collision-induced decompositions of negative ion electrospray-generated chloride adducts of oligosaccharides. *J. Am. Soc. Mass. Spectrom.*, *12* (11), 1193-1204.